Synthesis and Characterisation of Electrochemically-derived Graphene Oxide

Pei Yu

B.Eng. (Hons)

A thesis submitted for the degree of Doctor of Philosophy at

Monash University in 2019

Department of Materials Science and Engineering

Monash University

Copyright notice

I certify that I have made all reasonable efforts to secure copyright permissions for third-party content included in this thesis and have not knowingly added copyright content to my work without the owner's permission.

Abstract

Graphene oxide (GO) and its derivatives, have been widely used in various applications such as energy storage devices, sensors, nanofiltration, and desalination. With regards the production of GO, chemical oxidation of graphite (CGO) has been the most popular route due to its low cost, high yield and good dispersibility of CGO in water. However, this method has certain drawbacks. Typically, this production procedure is dangerous, with a high risk of explosion by forming manganese heptoxide. In addition, the need for additional purification steps to remove residual metal ions and the introduction of irreparable hole defects further limit its applications. In this work electrochemical oxidation and exfoliation of graphite have been explored due to the greener and simpler processes they represent, along with fewer defects in the electrochemically-derived graphene oxide (EGO). Nonetheless, there are still many challenges to be solved to accelerate its development. Conventional electrochemical methods often show discontinuous electrochemical oxidation processes due to graphite pieces peeling off from the electrode before complete oxidation and exfoliation. There is still a lack of rational design of electrochemical cells to improve exfoliation and oxidation levels for industrial productions. In addition, previously reported EGO normally shows poor aqueous dispersibility, which significantly restricts its processability into larger quantities and structures in practical applications. Another challenge is the lack of understanding of the structure, chemistry, and properties of EGO such as its dispersibility, ability to be reduced, ion or molecule permeability, and the relationships between its structure and properties.

This thesis reports on a new electrochemical oxidation method to produce graphene oxide with improved exfoliation and oxidation levels, improves the aqueous dispersibility with optimized electrochemical methods, characterises the structure, chemistry and properties of EGO, and investigates how EGO differs from CGO in terms of microwave reduction ability and the properties of resultant multilayered membranes. The research is this divided in to four parts.

The first part introduces a mechanically-assisted electrochemical exfoliation process to produce EGO directly from graphite flakes, which is promising for large-scale production of graphene oxide. The mechanical stirring allows continuous physical contact of graphite flakes with the electrode, which improves oxidation and exfoliation levels of the graphite. The resultant EGO shows less defects, better long-term stability in ethanol, and more facile thermal reduction ability than conventional CGO. To increase the aqueous dispersibility of EGO for better processability, a more controllable electrochemical oxidation process is studied in the next section with an investigation of various factors influencing the dispersibility including electrochemical oxidation

time, graphite sources and electrolyte concentrations. With the optimized conditions, aqueous dispersible EGO was produced with long-term stability and good processability. In the third part, one intriguing property of graphene oxide, microwave reduction ability, was investigated for EGO and it was demonstrated how it differs from CGO in terms reduction efficiency by the microwave. EGO could be rapidly reduced by microwave irradiation within seconds to produce very high-quality graphene with a large aromatic domain size of 102.8 nm and a high C/O ratio of 33.6, which shows much higher microwave reduction efficiency than conventional CGO. The fourth part is aimed at understanding the properties of EGO membranes including stability in water and ionic sieving properties. It was found that EGO membranes exhibit higher stability in aqueous solution and better rejections to ions and molecules than CGO membranes. The structures and chemistry of the material were also studied in this section, which provides a deep understanding on their relationships with the properties of EGO membranes.

In summary, the thesis represents a comprehensive investigation of EGO relating to synthesis and characterisation of structure, chemistry, and properties, which shows the great potential of electrochemical methods to produce graphene oxide and its utility in applications.

Declaration

This thesis contains no material which has been accepted for the award of any other degree or diploma at any university or equivalent institution and that, to the best of my knowledge and belief, this thesis contains no material previously published or written by another person, except where due reference is made in the text of the thesis.

Signature:

Print Name: Pei Yu

Date: 07/03/2019

Publications during candidature

1. **Yu, P.**; Lowe, S. E.; Simon, G. P.; Zhong, Y. L., Electrochemical exfoliation of graphite and production of functional graphene. *Current Opinion in Colloid & Interface Science* **2015,** *20* (5–6), 329-338.
2. **Yu, P.**; Tian, Z.; Lowe, S. E.; Song, J.; Ma, Z.; Wang, X.; Han, Z. J.; Bao, Q.; Simon, G. P.; Li, D.; Zhong, Y. L., Mechanically-Assisted Electrochemical Production of Graphene Oxide. *Chemistry of Materials* **2016,** *28* (22), 8429-8438.
3. Tian, Z.; **Yu, P.**; Lowe, S. E.; Pandolfo, A. G.; Gengenbach, T. R.; Nairn, K. M.; Song, J.; Wang, X.; Zhong, Y. L.; Li, D., Facile electrochemical approach for the production of graphite oxide with tunable chemistry. *Carbon* **2017,** *112*, 185-191.

Thesis including published works declaration

I hereby declare that this thesis contains no material which has been accepted for the award of any other degree or diploma at any university or equivalent institution and that, to the best of my knowledge and belief, this thesis contains no material previously published or written by another person, except where due reference is made in the text of the thesis.

This thesis includes 1 original paper published in peer reviewed journals. The core theme of the thesis is Synthesis and characterisation of electrochemically-derived graphene oxide. The ideas, development and writing up of all the papers in the thesis were the principal responsibility of myself, the student, working within the Department of Materials and Engineering, Monash University, under the supervision of Prof. Dan Li, Prof. George P. Simon, Dr. Yulin Zhong.

The inclusion of co-authors reflects the fact that the work came from active collaboration between researchers and acknowledges input into team-based research.

In the case of Chapter 3, my contribution to the work involved the following:

Thesis Chapter	**Publication Title**	**Status** *(published, in press, accepted or returned for revision, submitted)*	**Nature and % of student contribution**	**Co-author name(s) Nature and % of Co-author's contribution***	**Co-author(s), Monash student Y/N***
3	*Mechanically-Assisted Electrochemical Production of Graphene Oxide*	*Published*	*60%. Key ideas, experimental works, results analysis and writing up*	*1) Zhiming Tian, experimental works and analysis of results, input into manuscript 5%* *2) Sean E. Lowe, analysis of results and writing up, input into manuscript 4%* *3) Jingchao Song, experimental works, input into manuscript 3%* *4) Zhirui Ma, experimental works, input into manuscript 3%* *5) Xin Wang, experimental works, input into manuscript 3%* *6) Zhao Jun Han, writing up, input into manuscript 3%* *7) Qiaoliang Bao, writing up, input into manuscript 3%*	*Yes* *No* *Yes* *Yes* *Yes* *No* *No*

				8) George P. Simon, analysis of results and writing up, input into manuscript 4% *9) Dan Li, analysis of results and writing up, input into manuscript 4%* *10) Yu Lin Zhong*, key ideas, analysis of results and writing up, input into manuscript 8%*	*No* *No* *No*

I have / have not renumbered sections of submitted or published papers in order to generate a consistent presentation within the thesis.

Student signature: Date: 07/03/2019

The undersigned hereby certify that the above declaration correctly reflects the nature and extent of the student's and co-authors' contributions to this work. In instances where I am not the responsible author I have consulted with the responsible author to agree on the respective contributions of the authors.

Main Supervisor signature: Date: 14/03/2019

Acknowledgements

I would like to express my sincere gratitude and appreciation to my supervisors Prof. Dan Li and Prof. George P. Simon, for their conscientious guidance and support. Their professional knowledge and experience have provided me with valuable advice and comments during my PhD research and the writing up of this thesis. I would like to sincerely thank my former supervisor Dr. Yulin Zhong, for his guidance and valuable comments on my writing. His kind encouragement assisted me through the first stage of my PhD research.

Next, I would like to express my thankfulness to Dr. Zhiyuan Xiong for his advice and inspiration, which help a lot in my research and writing. I also thank Dr. Zhiming Tian for his guidance in experiments and assistance in my research. I would like to thank Dr. Hualin Zhan, Dr. Ke Xie, and Dr. Jingchao Song for their help in Raman and XPS characterizations. I would like to thank Mr. Sean E. Lowe, Mr. Zhirui Ma, Mr. Xin Wang, Dr. Zhaojun Han for their help and comments in my research and writing-up of my first paper. I acknowledge Monash Centre for Electron Microscopy (MCEM) and the assistance from Dr. Xiya Fang for using Nova SEM. I acknowledge the Monash X-ray Platform (MXP) and assistance from Dr. Jisheng Ma for the use of D2 Phaser XRD. I also acknowledge Melbourne Centre for Nanofabrication (MCN) for the use of Dimension iCon AFM. I acknowledge the Australian Synchrotron for the use of the soft X-ray beamline.

I would like to thank Dr. Jing Xiao for sharing her valuable advice and research experience with me. Her encouragements helped me a lot during my PhD research. Also, I would like to express my thanks to other friends and group members including Ms. Zijun He, Ms. Jingying Liu, Ms. Qi Zhang, Dr. Diyan Liu, Mr. Longbing Qu, Ms. Peiyao Wang, Dr. Mengyang Zhang, Dr. Ashley Robert, Dr. Ling Qiu, Dr Chi Cheng, Dr. Yufei Wang, Ms. Yang Cao, Mr. Kangyan Wang, Ms. Xingyue Qian, and Mr. Xiao Wang for their help in research, sharing of experience, and emotional support.

Finally, I wish to express my great thanks to my family, my parents and my sister, for their endless love, emotional and financial support. I would like to express my special thanks to my fiancé, Mr. Ke Zhang, for his great support and company throughout this study.

Table of Contents

List of Figures

Chapter 2

Chapter 3

Chapter 4

Chapter 5

Chapter 6

List of abbreviation

AAO	Anodic aluminium oxide
AFM	Atomic force microscope
CGO	Chemically-derived graphene oxide
CrCGO	Chemically-reduced CGO
CrEGO	Chemically-reduced EGO
DMF	Dimethylformamide
EGO	Electrochemically-exfoliated graphene oxide
EIS	Electrochemical impedance spectroscopy
FTIR	Fourier-transform infrared spectroscopy
FWHM	Full width at half maximum
GIC	Graphite intercalation compounds
GO	Graphene oxide
MB	Methylene blue
HOPG	Highly orientated pyrolytic graphite
MwEGO	Microwave-irradiated EGO
MwCGO	Microwave-irradiated CGO
MwTrEGO	Microwave-irradiated TrEGO
MwTrCGO	Microwave-irradiated TrCGO
PGO	Pristine graphite oxide
RB	Rhodamine B
RGO	Reduced graphene oxide
SEM	Scanning electron microscopy
TEM	Transmission electron microscopy
TGA	Thermogravimetric analysis
TrEGO	Thermally-reduced EGO
TrCGO	Thermally-reduced CGO
XPS	X-ray photoelectron spectroscopy
XRD	X-ray diffraction

Chapter 1. Introduction

Graphene oxide (GO) has gained increasing interest, with extensive studies of GO-based materials recently reported due to its potential significance in various applications. With the development of graphene-based materials in many applications such as energy-storage devices[1], sensors[2], transparent conductive films[3] or graphene-polymer nanocomposites[4], graphene oxide has been regarded as a promising precursor for bulk synthesis of graphene by various reduction processes. With its special two-dimensional structure and abundant oxygenated functional groups on its surface, graphene oxide has also been used in many fields such as nanofiltration and separation[5-6], electrochemical sensors, electrocatalysis[7], polymer nanocomposites[8] and functional dispersing agents[9].

The most common method to produce graphene oxide is chemical oxidation of graphite with subsequent exfoliation into chemically-derived graphene oxide (CGO). With a long history tracing back to 150 years ago, chemical oxidation of graphite experienced some important developments and improvements. In 1859, Brodie first described oxidation of graphite in nitric acid and potassium chlorate[10]. Staudenmaier optimised the method in 1898 to reduce the possibilities of explosion[11]. Following this, Charpy first used potassium permanganate as an oxidant to oxidise graphite. In 1958 Hummers and Offeman developed the protocol with the same procedure to oxidise graphite with potassium permanganate, sodium nitrate, and sulphuric acid[12]. The Hummers method has now become the most used method to produce graphene oxide with several optimizations later[13]. Graphene oxide produced by chemical oxidation shows many oxygen functional groups on its surface, including hydroxyl, carboxyl, and epoxy moieties, all of which render graphene oxide highly dispersible and processable.

Structures, chemistry and properties of CGO have been comprehensively investigated. It is known that the structure of CGO sheets consists of nanoscale graphitic sp^2 domains with disordered sp^3 oxygen domain or defects surrounding them. Chemical analysis CGO has large amounts of carboxylic acid groups at the edge of sheets and hydroxyl and epoxy groups at the basal plane of sheets[9]. In addition to the characterisations of structure and chemistry, various properties of CGO have also been extensively studied. CGO is found to show very good dispersibility in water. The factors influencing the aqueous dispersibility and chemistry underlying the phenomena have been reported widely, which is important for processability of CGO[9, 14-15]. Another important property of graphene oxide is its ability to be reduced. In

addition to widely investigated reduction methods including thermal reduction and chemical reduction, microwave reduction of graphene oxide also appears to be a promising and rapid reduction method to produce highly conductive graphene with good qualities[16]. When assembled into laminated membranes, graphene oxide membranes show excellent water permeation and molecular sieving properties, another intriguing aspect of graphene oxide[5].

The past decade has witnessed the growth of graphene oxide field in its property studies and application developments. While graphene oxide related studies have been reported at an increasing rate, the studies of graphene oxide are mainly based on chemical oxidation methods due to their advantages of high oxidation, good dispersibility, and processability. However, chemical oxidation methods have some problematic issues. One common issue is the use of strong oxidants which will raise safety issues, especially on an industrial scale. In the Hummers method, the use of sodium nitrate produces toxic and hazardous gases. Another common risk comes from potassium permanganate that reacts to form manganese heptoxide, which can readily explode at high temperature[17]. In addition, the use of strong oxidants will also introduce metal ion impurities into final graphene oxide products such as K^+, Na^+, Mn^{2+} and Fe^{3+}. Complicated and time-consuming purification steps including filtration, centrifugation, and dialysis are required to reduce the impurities. The wastewater after the washing steps will also contaminate the environment with heavy metal ions. Apart from the issues in the production process, there are also some disadvantages with the quality of the GO products by chemical oxidation methods. The traditional Hummers method can produce hole defects within the lattice of graphene oxide by the formation of CO_2 that removes carbon atoms from the lattice. Therefore, developing alternative oxidation methods which avoid the above issues are highly in demand to produce graphene oxide.

In addition to chemical oxidation of graphite, another promising wet chemical method to produce graphene oxide is the electrochemical oxidation of graphite which is green and simple. Increasing attention has been drawn to electrochemical oxidation and exfoliation of graphite over the last several years, although it has been a long history to use electrochemical intercalation of graphite to produce graphite intercalation compounds (GIC)[18]. The production of graphene oxide normally involves applying a positive current or voltage to the graphite electrode to attract anions and molecules to co-intercalate between graphite sheets with subsequent oxidation within the graphite. Although electrochemical methods have been developed increasingly in the last decade, most of the studies aimed to produce less defective

few-layer graphene/graphene oxide sheets with a low level of oxidation by a quick electrochemical exfoliation process[19]. The electrochemically-exfoliated graphene/graphene oxide (EGO) sheets normally show high conductivities with low oxidation and few defects[20-23], which are promising in applications that require high conductivities such as transparent conductive films or supercapacitors.

Without the need of strong oxidants, electrochemical methods can achieve oxidation of graphite by a controlled positive current on graphite electrode which is immersed in an aqueous electrolyte such as H_2SO_4. Since the electrochemical oxidation method is still nascent, many challenges need to be solved to drive its development. One challenge is the discontinuous electrochemical oxidation process since graphite often falls into pieces and lose contact with electrode before complete oxidation process is achieved. As a result, oxidation and exfoliation degree will be very low, with mainly few-layer graphene flakes produced[20-25]. In addition, with few oxygen groups generated on their surface, they can only disperse in organic solvents such as dimethylformamide instead of water, which limits their processability and applications. Therefore, achieving production of graphene oxide with a high oxidation degree would be an important step forward for electrochemical methods. Another challenge is the current, limited understanding of electrochemically-produced graphene oxide (EGO) including its structure, chemistry as well as important properties. Previous studies mainly focus on the production of graphene oxide by electrochemical oxidation process without in-depth characterizations and analysis of its properties[20-22, 26-27]. Important properties about graphene oxide such as dispersibility, reduction property, and ion or molecule permeability need to be investigated to obtain a comprehensive understanding about EGO. With limited applications reported for electrochemically-derived graphene oxide, it is important to make a thorough investigation about its properties and determine its key properties that differentiate it from CGO.

This work will be aimed at developing a new, scalable approach for the synthesis of graphene oxide by electrochemical oxidation method, and particularly to study the chemical structure, colloidal chemistry of EGO, and investigate how aqueous dispersible EGO could be produced with optimized electrochemical conditions, and how EGO could differ from CGO in terms of ability of microwave reduction and the properties of multilayered membranes based on EGO. Specifically, we firstly developed a novel electrochemical exfoliation process with the assistance of mechanical stirring to produce EGO directly from graphite flakes, which is different from the conventional electrochemical methods. Furthermore, we synthesized

aqueous-dispersible EGO by a controllable anodic oxidation of graphite foil and studied the influence of electrochemical conditions on the dispersibility. Next, we found the rapid microwave reduction properties of EGO to produce high-quality graphene, which is much more efficient than microwave reduction of CGO. Finally, we investigated the stability and nanofiltration properties of EGO laminated membranes.

The study will thus be a comprehensive investigation of EGO in terms of its synthesis, structure, chemistry, and properties. It is expected that electrochemical oxidation method will be further developed, and that electrochemically-derived graphene oxide can be widely studied and used in more applications based on this study.

In **Chapter 2**, a literature review will be presented about synthesis, characterisation, properties, and applications of graphene oxide. Firstly, the recent progress and challenges of graphene oxide production methods will be reviewed including chemical oxidation routes and electrochemical oxidation methods. Dispersibility of graphene oxide in aqueous and organic solvents will then be discussed, including progress and significance. Next is a review about the reduction of graphene oxide and its change in properties. Finally, applications of graphene oxide as permeation membranes will be reviewed in terms of their development and remaining challenges.

Chapter 3 is aimed at developing a new, continuous electrochemical oxidation and exfoliation process to solve the problems of premature peeling of graphite pieces. A novel mechanically-assisted electrochemical method is reported to produce graphene oxide directly from graphite flakes. With mechanical stirring as assistance, graphite flakes in the electrolyte can be directly used instead of using the single bulk graphite electrode reported in previous electrochemical methods[20-22]. Mechanical stirring allows continuous contact into electrode and oxidation of graphite flakes. Exfoliation is also achieved and graphene oxide sheets result, with most of them less than 3 layers. This method avoids the use of hazardous chemical oxidants and shows a simple purification process, whilst the electrolyte can also be readily recycled. These advantages make the method promising for large-scale and cost-effective production of graphene oxide. In addition to such advantages of the process, the resultant EGO produced by this method shows distinct favourable properties: fewer physical defects than CGO, facile reduction ability, high conductivity of thermally-reduced EGO, and long-term stability in ethanol when compared with CGO.

Chapter 4 is aimed at increasing the aqueous dispersibility of EGO, which is important for its processability and further assembly for various applications. This chapter studies the aqueous dispersibility of EGO by using a more controllable electrochemical oxidation process. Different factors affecting the electrochemical oxidation process are, for the first time, investigated for their influence on the dispersibility of EGO. With optimized conditions, the electrochemical oxidation process could achieve high dispersibility of EGO in water. Long-term stability of EGO dispersion is also studied, which found that EGO aqueous dispersion can remain stable for at least 19 days. The chemistry underlying such good dispersibility is also investigated by using some necessary characterisations such as zeta-potential. This work paves the way for further processing of EGO and application of the material.

Chapter 5 focuses on another intriguing property of graphene oxide: its ability to be reduced by microwave radiation, with the aim of investigating how EGO differs from CGO in this property for the first time. In this chapter, the microwave reduction process of EGO is studied and compared with CGO. It was found that the EGO membrane can be significantly reduced in a rapid microwave treatment of just 3 sec. Microwave-reduced EGO exhibits a high conductivity of about 49140 S/m. In comparison, CGO could not be directly reduced by microwave treatment without a thermal treatment in advance. Factors including microwave time, microwave power, membrane thickness, and microwave atmosphere was also investigated. Microwave-reduced EGO is also found to be of high quality, with few defects and oxygen groups remaining within the structure. By extensive characterisation of EGO before and after microwave treatment, structure and chemistry of the materials are also studied to explain the mechanism of quick microwave reduction properties of EGO. The rapid microwave reduction of EGO makes it a promising method to produce highly conductive graphene.

In **Chapter 6**, the aim is to understand the properties of EGO assembled membrane structure and the differences it shows from CGO membrane. In this study, we first investigated aqueous stability of EGO membranes produced by electrochemical oxidation method for nanofiltration since traditional CGO membranes have poor stability in the aqueous solution that makes it easy to swell and disintegrate. In this the study, it was found that EGO membrane exhibits limited swelling and keeps integrated in water. Ion and molecule permeation about EGO membranes were also investigated and good ion sieving properties for EGO membrane demonstrated. These membranes nanofiltration performance were also studied, and it is found that EGO membranes also show good aqueous solution permeance and good rejection of ions and/or

molecules. The structures of EGO and its membranes were also characterised to determine its sieving and permeation properties. The work in this chapter shows that EGO can be considered as a good candidate for nanofiltration applications.

Chapter 7 will outline the main conclusions of this thesis and summarize the contributions that this project made in the field of graphene oxide. The opportunities and challenges in future work will also be discussed to facilitate the possible development of the electrochemical production of graphene and applications of electrochemically-derived graphene oxide.

Reference

1. Yang, X.; Cheng, C.; Wang, Y.; Qiu, L.; Li, D., Liquid-Mediated Dense Integration of Graphene Materials for Compact Capacitive Energy Storage. *Science* **2013,** *341* (6145), 534-537.

2. Robinson, J. T.; Perkins, F. K.; Snow, E. S.; Wei, Z.; Sheehan, P. E., Reduced Graphene Oxide Molecular Sensors. *Nano Letters* **2008,** *8* (10), 3137-3140.

3. Eda, G.; Fanchini, G.; Chhowalla, M., Large-area ultrathin films of reduced graphene oxide as a transparent and flexible electronic material. *Nature Nanotechnology* **2008,** *3*, 270.

4. Huang, X.; Qi, X.; Boey, F.; Zhang, H., Graphene-based composites. *Chemical Society Reviews* **2012,** *41* (2), 666-686.

5. Joshi, R. K.; Carbone, P.; Wang, F. C.; Kravets, V. G.; Su, Y.; Grigorieva, I. V.; Wu, H. A.; Geim, A. K.; Nair, R. R., Precise and Ultrafast Molecular Sieving Through Graphene Oxide Membranes. *Science* **2014,** *343* (6172), 752-754.

6. Abraham, J.; Vasu, K. S.; Williams, C. D.; Gopinadhan, K.; Su, Y.; Cherian, C. T.; Dix, J.; Prestat, E.; Haigh, S. J.; Grigorieva, I. V.; Carbone, P.; Geim, A. K.; Nair, R. R., Tunable sieving of ions using graphene oxide membranes. *Nat Nano* **2017,** *12* (6), 546-550.

7. Chen, D.; Feng, H.; Li, J., Graphene Oxide: Preparation, Functionalization, and Electrochemical Applications. *Chemical Reviews* **2012,** *112* (11), 6027-6053.

8. Zhu, Y.; Murali, S.; Cai, W.; Li, X.; Suk, J. W.; Potts, J. R.; Ruoff, R. S., Graphene and Graphene Oxide: Synthesis, Properties, and Applications. *Advanced Materials* **2010,** *22* (35), 3906-3924.

9. Kim, J.; Cote, L. J.; Huang, J., Two Dimensional Soft Material: New Faces of Graphene Oxide. *Accounts of Chemical Research* **2012,** *45* (8), 1356-1364.

10. Brodie, B. C., On the atomic weight of graphite. *Philosophical Transactions of the Royal Society of London* **1859,** *149*, 249-259.

11. Staudenmaier, L., Verfahren zur Darstellung der Graphitsäure. *Berichte der deutschen chemischen Gesellschaft* **1898,** *31* (2), 1481-1487.

12. Hummers, W. S.; Offeman, R. E., Preparation of Graphitic Oxide. *Journal of the American Chemical Society* **1958,** *80* (6), 1339-1339.

13. Marcano, D. C.; Kosynkin, D. V.; Berlin, J. M.; Sinitskii, A.; Sun, Z.; Slesarev, A.; Alemany, L. B.; Lu, W.; Tour, J. M., Improved Synthesis of Graphene Oxide. *ACS Nano* **2010,** *4* (8), 4806-4814.

14. Konkena, B.; Vasudevan, S., Understanding Aqueous Dispersibility of Graphene Oxide and Reduced Graphene Oxide through pKa Measurements. *The Journal of Physical Chemistry Letters* **2012,** *3* (7), 867-872.

15. Chi, C.; Dan, L., Solvated Graphenes: An Emerging Class of Functional Soft Materials. *Advanced Materials* **2013,** *25* (1), 13-30.

16. Voiry, D.; Yang, J.; Kupferberg, J.; Fullon, R.; Lee, C.; Jeong, H. Y.; Shin, H. S.; Chhowalla, M., High-quality graphene via microwave reduction of solution-exfoliated graphene oxide. *Science* **2016**.

17. Lowe, S. E.; Zhong, Y. L., Challenges of Industrial-Scale Graphene Oxide Production. In *Graphene Oxide*, John Wiley & Sons, Ltd: 2016; pp 410-431.

18. Yu, P.; Lowe, S. E.; Simon, G. P.; Zhong, Y. L., Electrochemical exfoliation of graphite and production of functional graphene. *Current Opinion in Colloid & Interface Science* **2015,** *20* (5–6), 329-338.

19. Yang, S.; Lohe, M. R.; Müllen, K.; Feng, X., New-Generation Graphene from Electrochemical Approaches: Production and Applications. *Advanced Materials* **2016,** *28* (29), 6213-6221.

20. Su, C.-Y.; Lu, A.-Y.; Xu, Y.; Chen, F.-R.; Khlobystov, A. N.; Li, L.-J., High-Quality Thin Graphene Films from Fast Electrochemical Exfoliation. *ACS Nano* **2011,** *5* (3), 2332-2339.

21. Parvez, K.; Li, R.; Puniredd, S. R.; Hernandez, Y.; Hinkel, F.; Wang, S.; Feng, X.; Müllen, K., Electrochemically Exfoliated Graphene as Solution-Processable, Highly Conductive Electrodes for Organic Electronics. *ACS Nano* **2013,** *7* (4), 3598-3606.

22. Parvez, K.; Wu, Z.-S.; Li, R.; Liu, X.; Graf, R.; Feng, X.; Müllen, K., Exfoliation of Graphite into Graphene in Aqueous Solutions of Inorganic Salts. *Journal of the American Chemical Society* **2014,** *136* (16), 6083-6091.

23. Rao, K. S.; Senthilnathan, J.; Liu, Y.-F.; Yoshimura, M., Role of Peroxide Ions in Formation of Graphene Nanosheets by Electrochemical Exfoliation of Graphite. *Scientific Reports* **2014,** *4*, 4237.

24. Liu, J.; Yang, H.; Zhen, S. G.; Poh, C. K.; Chaurasia, A.; Luo, J.; Wu, X.; Yeow, E. K. L.; Sahoo, N. G.; Lin, J.; Shen, Z., A green approach to the synthesis of high-quality graphene oxide flakes via electrochemical exfoliation of pencil core. *RSC Advances* **2013,** *3* (29), 11745-11750.

25. Wu, L.; Li, W.; Li, P.; Liao, S.; Qiu, S.; Chen, M.; Guo, Y.; Li, Q.; Zhu, C.; Liu, L., Powder, Paper and Foam of Few-Layer Graphene Prepared in High Yield by Electrochemical Intercalation Exfoliation of Expanded Graphite. *Small* **2014,** *10* (7), 1421-1429.

26. Tian, Z.; Yu, P.; Lowe, S. E.; Pandolfo, A. G.; Gengenbach, T. R.; Nairn, K. M.; Song, J.; Wang, X.; Zhong, Y. L.; Li, D., Facile electrochemical approach for the production of graphite oxide with tunable chemistry. *Carbon* **2017,** *112*, 185-191.

27. Pei, S.; Wei, Q.; Huang, K.; Cheng, H.-M.; Ren, W., Green synthesis of graphene oxide by seconds timescale water electrolytic oxidation. *Nature Communications* **2018,** *9* (1), 145.

Chapter 2. Literature review

2.1 Background

Graphene is a two-dimensional material consisting of sp^2-bonded carbon atoms and has attracted increasing attention from academia and industry in the last 15 years or so. Ever since 2004 when Novoselov and Geim[28] discovered the unique electronic properties of the two-dimensional monocrystalline, the amount of research about graphene started its exponential growth, which was further boosted by the Nobel Prize awarded to Novoselov and Geim for their discovery in 2010 (**Figure 1**). With a greater number of scientists focusing on studies of graphene, more remarkable properties were discovered including high carrier mobilities (200,000 $cm^2\ V^{-1}\ s^{-1}$)[29], high Young's modulus (~ 1 TPa)[30], superior thermal conductivity (~5000 $Wm^{-1}K^{-1}$)[31], and high specific surface area (2630 m^2g^{-1})[32].

The development of graphene facilitated research of graphene oxide (GO), which also shows rapid growth in the last decade (**Figure 1**), even though its discovery can be traced back to 1859 when Brodie first produced graphite oxide by chemical oxidation of graphite and then dispersed it in water[10]. GO is disordered and of an insulating nature, with excellent dispersibility and processability in solution. Despite reducing interests on GO from physicists, more chemists are focusing on it due to its oxygen-containing chemical structures which provides high processability to fabricate macrostructures or composites, tunability of sp^3 fraction to tune its properties and functionality to form hybrid groups[7, 9, 33-34].

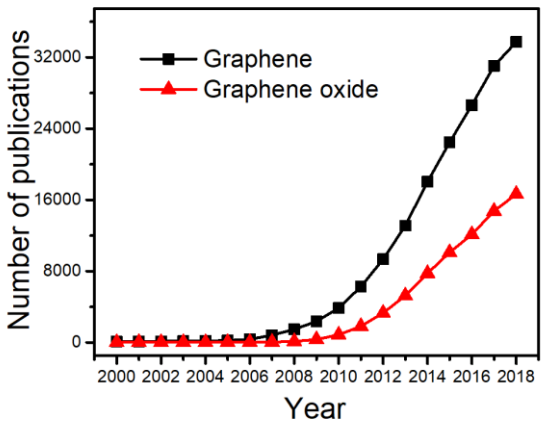

Figure 1. The number of publications in "graphene" and "graphene oxide" related topics from the year 2000 – 2018.

Within the graphene family, there are several types of graphene-based materials that are similar but show different structures, which makes it important to clarify the concepts. Pristine graphene is an "ideal" graphene without defects on its plane, showing perfectly aligned carbon atoms in a honeycomb structure, as shown in **Figure 2a**. It is very hard to achieve pristine graphene, even with relatively delicate production methods such as mechanical exfoliation e.g. scotch tape, molecular assembly, or chemical vapor deposition which normally result in high quality graphene in comparisons to other methods. These production methods are suitable for the theoretical research of graphene which requires nearly perfect graphene and applications that require a small amount of graphene such as touch screens or solar cells. However, for large scale production of graphene for applications such as energy storage electrode or conducting fillers in composite, these methods have low advantage in terms of cost. To produce graphene at high yield and low cost, research has tended to put more emphasis on graphene oxide which is a cheap and scalable precursor to graphene. GO is an oxidised form of graphene, which is composed not only sp^2 bonded carbon atoms but also large amounts of sp^3 hybridised carbon-oxygen functional groups, as shown in **Figure 2b**. The oxygen groups are heterogeneously distributed on the surface of GO, providing excellent dispersibility in aqueous solution but disrupting conjugated honeycomb structures and electrical conductivities. Thus, GO needs to be reduced to remove its oxygen groups and recover its conjugated networks to produce conductivity.

Nevertheless, reduced graphene oxide (RGO) is not a perfect honeycomb carbon structure like pristine graphene and contains some remaining oxygen groups that are difficult to remove and some defects such as holes on its basal plane, as shown in **Figure 2c**[15]. As another member in the graphene family, graphite is intrinsically made up of many layers of graphene (**Figure 2d**) and can be used as a cheap and abundant source to produce GO. To increase the interlayer distance and reduce attractive forces between graphite layers, it can be oxidised to form oxygen groups on each layer. The resultant graphite oxide is a stack of graphene oxide layers (**Figure 2e**), which can be easily exfoliated from each other when dispersed in water due to repulsive forces between oxygen units.

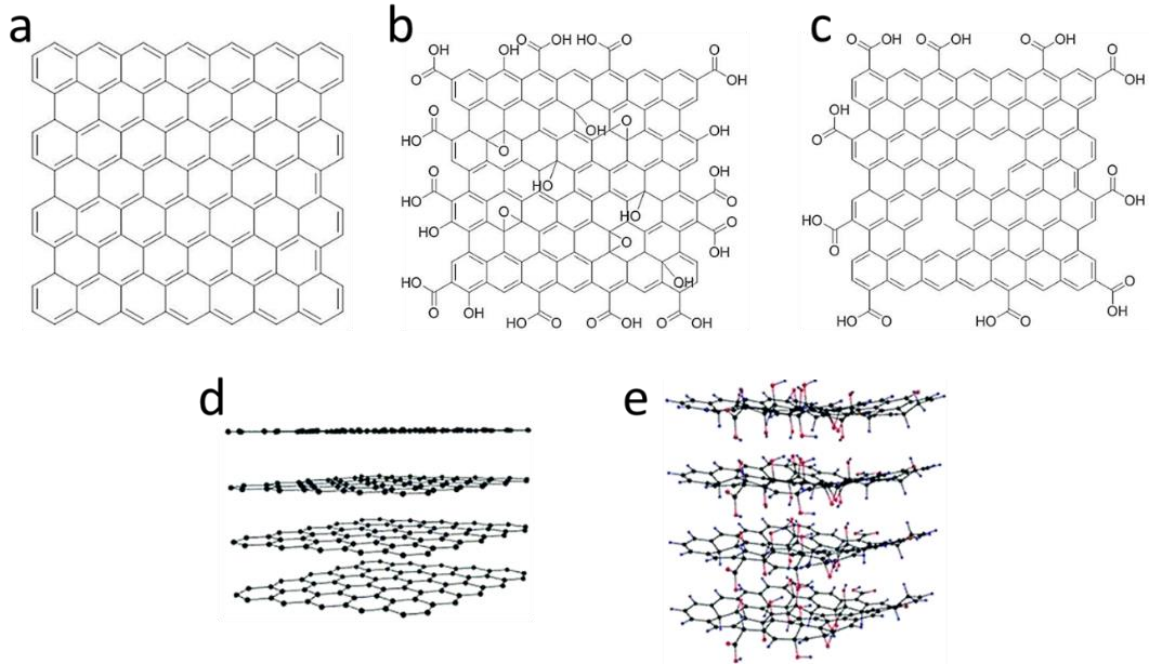

Figure 2. Schematic of (a) pristine graphene[15] (b) graphene oxide[15] (c) reduced graphene oxide[15] (d) graphite and (e) graphite oxide.

Graphene oxide has shown its importance in producing graphene for applications such as supercapacitors[35], transparent conductive films[3] and conducting polymer composites[36]. Moreover, GO itself can also be utilised in various applications with its oxygen moieties which yield functionality. For example, GO-laminated membranes show well-defined nanochannels between the layers, which can be used for nanofiltration or desalination[37]. GO can also be used as sensors for detecting humidity due to the presence of abundant oxygen groups[38]. In addition, with excellent dispersibility, GO can act as surfactants for carbon nanotubes[39]. It was also found that GO can be used in biomedical applications such as drug delivery[40]. These promising and potential applications present an enormous practical value of the research study on GO. Research of GO is currently devoted to following fields: synthesis, characterisation of atomic or chemical structure, properties, processing and the study of macrostructure and performance[7-9, 17, 33-34, 41]. An overview of the research fields of graphene oxide is given in **Figure 3**. For synthesis of GO, many efforts have been put on the chemical oxidation of graphite such as Hummer's method, with several later modifications[7-8, 33, 41].

Despite of high oxidation degree and good dispersibility and processability of produced GO, chemical methods shows drawbacks of using harsh oxidants, high risk of explosion, complex steps and large amounts of defects. As an alternative oxidation method, electrochemical

oxidation of graphite is drawing more attention due to it being a greener and simpler process[42]. Previous research on electrochemical methods put more emphases on synthesizing graphene with the purpose of minimising oxidation degree. While the resultant graphene shows a high electrical conductivity with limited defects, the exfoliation degree, dispersibility, and processability have previously been largely disregarded[20-23].

Characterisation of the structure and properties have already been extensively studied for chemically-derived GO (CGO), which reveals large amounts of structural information and a range of properties such as dispersibility, electrical conductivity, reduction ability and so on. However, there has been much less research on properties and characterisation of electrochemically-derived GO (EGO), which is necessary for working towards applications of EGO. As for further processing of GO into macrostructures for various applications, work to date have shown good processability and uniform macrostructure of CGO such as CGO membrane, which presented good ionic sieving properties[5]. Despite the fact that CGO has been widely explored for its properties and performance, many studies also show challenges to be resolved for CGO such as poor reduction efficiency of CGO[16] and structural instability of CGO membrane when used in aqueous solutions[43]. Therefore, the exploration of EGO with regards to its structure, properties, processing and performance in applications is significant for both improvement of current CGO-based applications, and for the development of electrochemical methods and EGO as an alternative graphene oxide.

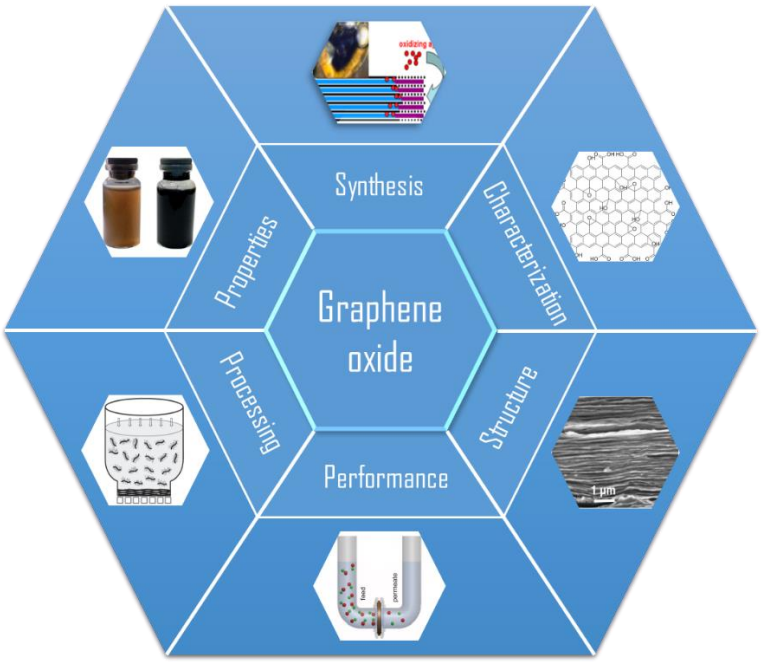

Figure 3. An overview of the research fields of graphene oxide.

This literature review will introduce the great progress of graphene oxide research in terms of the synthesis, characterisations, properties and graphene oxide membrane. A detailed description will be given for developments and current challenges of chemical and electrochemical synthesis to demonstrate the usefulness of studying electrochemical methods as the next generation GO-synthesis method that makes clear the possibility of replacing traditional chemical methods. The structural and chemical characterisation will then be introduced to give a comprehensive overlook for atomic and chemical structures of graphene oxide. In the review, given the broad aspects in the field, only dispersibility and the reducing ability of graphene oxide will be discussed, also being the two main research components of this thesis. Moreover, the final part will be devoted to graphene oxide membranes which can be used in applications of ionic sieving and nanofiltration.

2.2 Synthesis of graphene oxide

2.2.1 Chemical methods

2.2.1.1 Progress of chemical synthesis

The history of chemical production of graphite oxide can be traced back to the 19th century when the first pioneers explored the reactivity of graphite with strong oxidant chemicals. In 1859, Brodie tried oxidising graphite with oxidising agents by mixing graphite with three times its weights of "chlorate of potash" (i.e. potassium chlorate or $KClO_3$) and sufficient nitric acid (HNO_3) at 60 °C for 3 - 4 days[10]. After washing to remove the acid and salts and drying, the whole oxidation process was repeated four times until no further change of the product was found. Finally, light yellow products with increased weight resulted. On the application of heat, the product decomposed with the evolution of gases, leaving a black residue similar to original graphite. By analysing the elements in the products, it was found to be a mixture of carbon, hydrogen, and oxygen with a composition of C: H: O = 61.04: 1.85: 37.11. It was also found that the products were soluble in pure water but insoluble in acid or saline water. Brodie named the products as "graphic acid"[10]. This well-known study was the beginning of graphene oxide scientific research. Much later research about graphene oxide are based on modifications of Brodie's method. His finding of insolubility of "graphic acid" in acid or saline water became an important research topic in the application of graphene oxide for more than 100 years.

However, the rudimentary exploration of graphite oxidation by Brodie represented just the start. In 1898, Staudenmaier realised the high risk of explosion by Brodie's method and

developed a modified Brodie's method to oxidise graphite[11]. He reduced the percentage of fuming nitric acid (HNO_3) by replacing two-thirds with concentrated sulfuric acid for the purpose of improving the acidity of the reagents. He also added potassium perchlorate in aliquots over the four-day reaction, instead of by a single addition. The improvements reduced the risk of explosion. The modification also allows the whole oxidation process in a single reaction vessel with similar oxidation degree (C: O ≈ 2:1) to Brodie's multiple oxidation processes.

Subsequently Charpy proposed the use of potassium permanganate ($KMnO_4$) as the oxidizing agent[44]. Nearly 50 years later, Hummers and Offeman developed the famous Hummers method to oxidise graphite based on potassium permanganate[12]. They pointed out the Staudenmaier method and modified methods based on it were time-consuming and hazardous, with a high risk of explosion. Therefore, they developed an oxidative method by using a mixture of concentrated sulfuric acid (H_2SO_4), sodium nitrate ($NaNO_3$) and potassium permanganate ($KMnO_4$) within two hours at a low temperature to avoid hazards. Graphite flakes and $NaNO_3$ were added into H_2SO_4 whilst stirring. The mixture was then cooled to the temperature of 0 °C by an ice-bath, and $KMnO_4$ was then slowly added into the mixture by vigorous agitation. After that, the mixture was kept at around 35 °C for 30 minutes, during which the mixture became increasingly thickened with gradually decreased evolution of gas. Next, some of water was added into the mixture and maintained for 15 minutes at 98 °C. Finally, a large amount of water was used to dilute the mixture and 3% hydrogen peroxide (H_2O_2) was added to reduce excess permanganate and manganese dioxide (MnO_2). There were some purification processes used, such as filtration and dialysis to remove manganese and other ions after the oxidation process. The produced graphene oxide showed a bright yellow color with a high oxidation degree (C: O = 2.1 – 2.9). Currently Hummers method is the most widely used method to produce graphite oxide with several optimisations later based on it. It is much safer than the Brodie and Staudenmaier methods if the temperature during the procedures is carefully maintained. The shorter oxidation time required also makes it widely accepted.

In the last 20 years, with the increasing applications of graphene oxide and breakthrough discovery of graphene by Novoselov and Geim[28, 45], the production of graphene oxide attracts more and more attention. Many works have studied or reported modification and optimisation of the Hummers method. Kovtyukhaova and colleagues have reported a modified Hummers method by adding a peroxidation procedure before the normal Hummers method[46]. The pre-

oxidation of graphite powder was achieved by mixing with concentrated H_2SO_4, $K_2S_2O_8$, and P_2O_5 for 6 h. This pre-oxidation process allows complete oxidation of the graphite source and tackled the issue of incompletely oxidised graphite in the final product. This procedure has been recently used by many other workers in their preparation of graphene oxide[1, 26, 47-48]. Other work by Hirata and co-workers reported a modified Hummers method[49]. In their work, the oxidation period was prolonged to five days and a multi-step purification process was employed to achieve high purity. Longer oxidation times were used to achieve a high-yield of thin-film particles of graphite oxide since increased oxidation degree will enhance electrostatic repulsion between graphene oxide layers. By examination of products using atomic force microscopy (AFM), they found the thin particles of graphite oxide they produced had, on average, a thickness of several nanometers. Their work also provided a tentative category of graphene-family in terms of layer number and oxidation state, including graphene, graphite, graphite oxide and graphene oxide.

Later in 2010, the efficiency of Hummers' method was further improved by removing $NaNO_3$ whilst using more $KMnO_4$ and replacing H_2SO_4 electrolyte with a mixture of H_2SO_4 and H_3PO_4 with a ratio of 9:1, as shown in **Figure 4**. The advantages of the improved method over Hummers' method are the elimination of exotherm and toxic gas during production, higher oxidation degree with the more hydrophilic carbon material, and more isolated aromatic rings[13]. Another study has found that oxidation conditions could influence the area of GO sheets. By modifying the Hummers' method to use a milder condition with less $KMnO_4$ and lower reaction temperature, the area of the GO sheets can exhibit a maximum value of around 40000 μm^2 [50]. Later, further research has tried to optimise the method, and the quality of GO by adjusting the amounts of oxidants and electrolyte[51], and/or controlling the temperatures[52]. The above modified Hummers' methods pushed the process towards a much more well-studied system by varying the conditions, but the ingredients were not significantly changed.

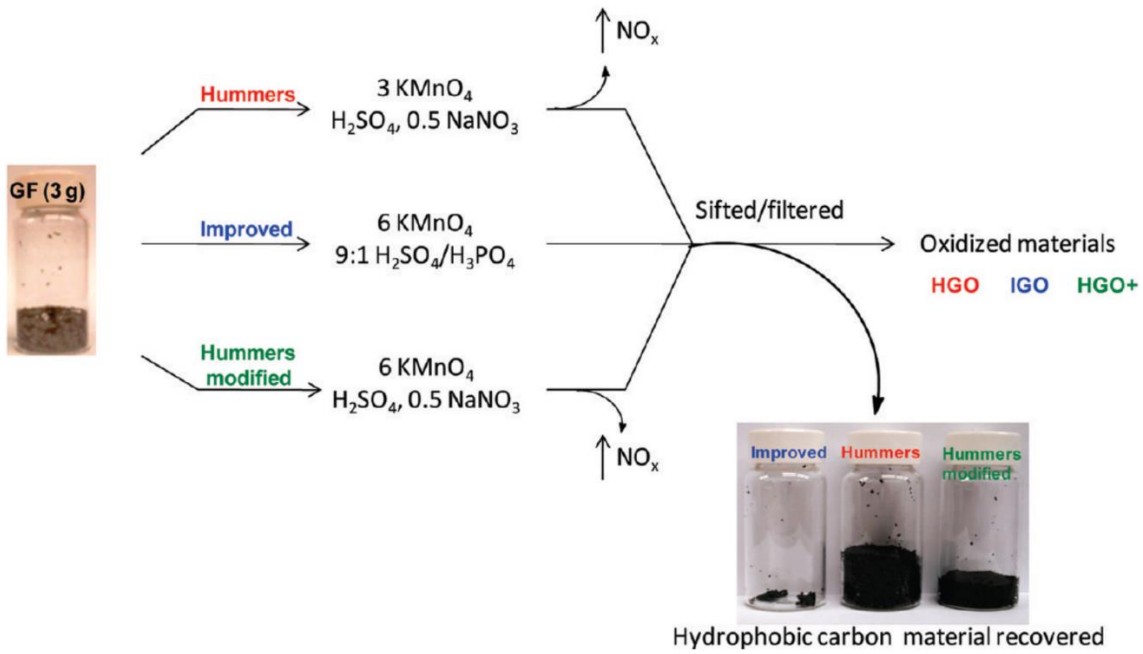

Figure 4. Schematic of the procedures of improved Hummers' method, in comparison with Hummers' method and a modified Hummers' method[13].

Recently, a novel oxidant, K_2FeO_4, has been proposed for green chemical oxidation of graphite[53]. The chemical process is much simpler than Hummers' method and only involves the reaction among three ingredients: K_2FeO_4, H_2SO_4, and graphite, for 1 h at room temperature. The produced GO shows excellent dispersibility in water and similar chemical compositions to GO produced by Hummers' method. This chemical oxidation method significantly simplifies the processes, reduces the reaction time and uses a much safer oxidant K_2FeO_4 than $KMnO_4$ and $NaNO_3$, which builds a new route for chemical oxidation of graphite. Another work demonstrated the possibility of using graphite sulfate as a precursor, which could react with water to form oxidised graphene with the carbon content of 86%, indicating a low oxidation degree[54].

2.2.1.2 Oxidation Mechanism

Early explorations about chemical oxidation of graphite mainly involve the development and improvement of the methods such as Brodie-based methods or Hummers-based methods, with little report of studies of the oxidation mechanisms involved. In recent years, work has started to appear relating to the studies of the chemical oxidation processes and mechanisms of the formed groups or defects. One such work studied the progressive formation of the functional groups in graphene oxide, by applying successive oxidising treatments with the Brodie

method[55]. The analysis of functional groups at different steps showed the increase of oxidation degree with more treatments. By applying higher oxidation levels, the unoxidised aromatic domains were oxidised, and the already-oxidised region will further oxidise the hydroxyl or ether groups to ketones or carboxylic acid groups[55]. Another work studied the evolution of oxygen groups with increasing oxidation degree by using the modified Hummers' method. However, this work states that hydroxyl and carboxyl groups are formed in the initial stage of the oxidation process, and are transformed into epoxide groups when the oxidation level increases. Moreover, the zeta potential of GO will also be increased with a higher oxidation degree, indicating the formation of more electronegative functional groups[56]. Even though the oxygen groups have been examined at various oxidation levels, the evolution of the functional groups is still not a very clear process, with a lack of investigation into the reaction mechanisms. In addition, the different analyses from the above two works demonstrate the complexity of the graphite oxidation process, which may be influenced by various factors and makes it difficult to provide a definite group evolution process.

The oxidation processes within graphite flakes with modified Hummers' method were studied by Dimiev et al.[57], who provided the mechanism of graphene oxide formation in the scale of a graphite piece (with a size of around 300 μm), as shown in **Figure 5**. Formation of GO involves three steps: formation of H_2SO_4-GIC, conversion of GIC into graphite oxide, and exfoliation of graphite oxide into graphene oxide. The conversion of GIC shows an edge-to-center oxidation process, which is limited by the diffusion rate of oxidants in to the narrow galleries between layers to replace intercalant molecules. Therefore, the size of the graphite flakes is an important factors affecting the degree of oxidation, with smaller flakes exhibiting faster oxidation process[57]. This work gives a very detailed analysis in the second oxidation process, which provides greater understanding for progressive formation process within a single graphite flake or grain.

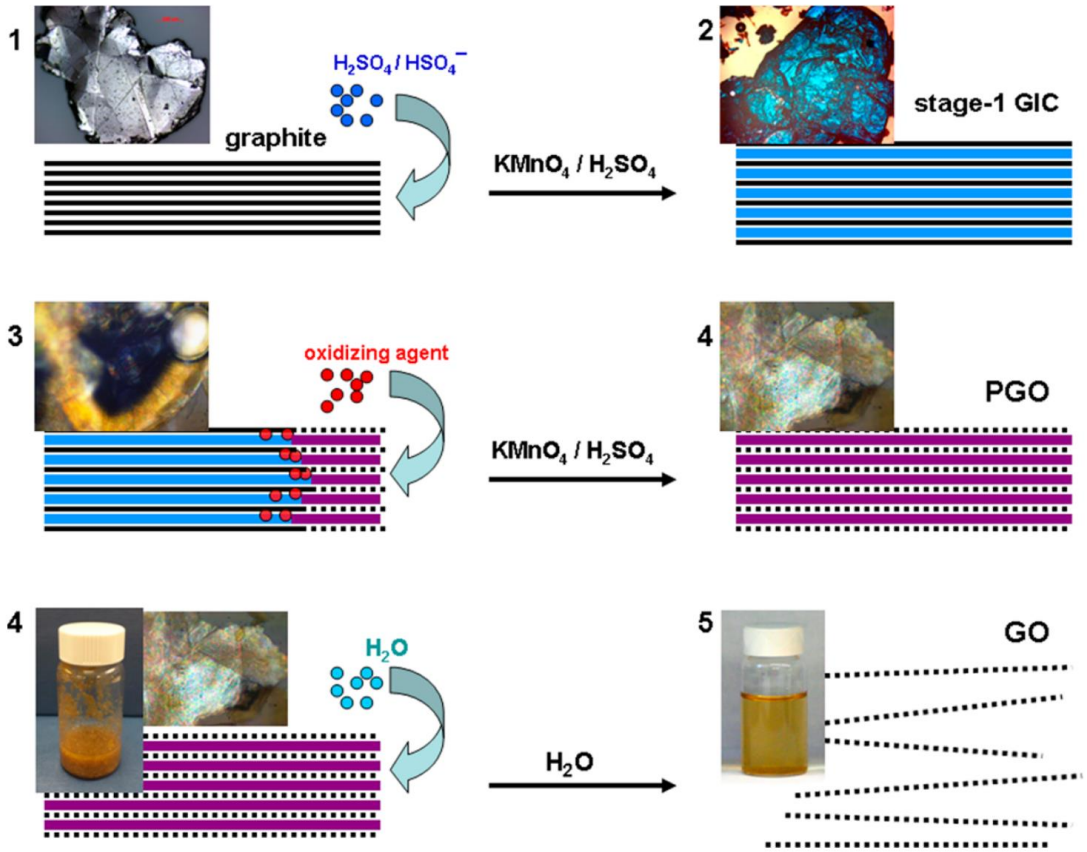

Figure 5. A schematic of GO formation from graphite with three steps: formation of H2SO4-GIC from graphite, conversion of GIC into pristine graphite oxide (PGO), and exfoliation of PGO into GO[57].

During the oxidation process, line defects or cracks are formed within the basal plane of graphene (**Figure 5a**), reducing the size of GO sheetsproduced[58]. To explain this, phenomena an unzipping mechanism has been proposed, which suggests epoxy groups tend to be formed and locked in opposite positions of a hexagonal ring, arranging themselves in a strained line, as shown in **Figure 5b**[58]. Another study shows that with further oxidation, the epoxy chain can be easily transformed into epoxy pairs, which then tends to be converted to more stable carbonyl pairs at room temperature. The carbonyl pairs will, therefore, cut the sheet in to two parts[59]. Research has been undertaken to better understand the cutting process during the oxidation process in the scale of the molecule. One study has used density functional theory to study the positions of 1,2-ether groups and hydroxyl groups in GO structure at different oxidation levels[60]. It showed that the hydroxyl group tends to sit on the adjacent carbon atoms to the 1,2-ether group, but on the opposite side of the plane, as shown in **Figure 6a**. The skeleton also shows a wrinkling of ~0.5 Å, which is mainly caused by the deformation of hydroxyl groups. With higher degree of oxidation, the positions of hydroxyl groups relative to

1,2-ether groups are the same, but all ether groups tend to reside on one side, with all the hydroxyl groups located on the other side (**Figure 6b**). GO with higher oxidation levels also showed a larger band gap, which leads to insulating behaviour[60].

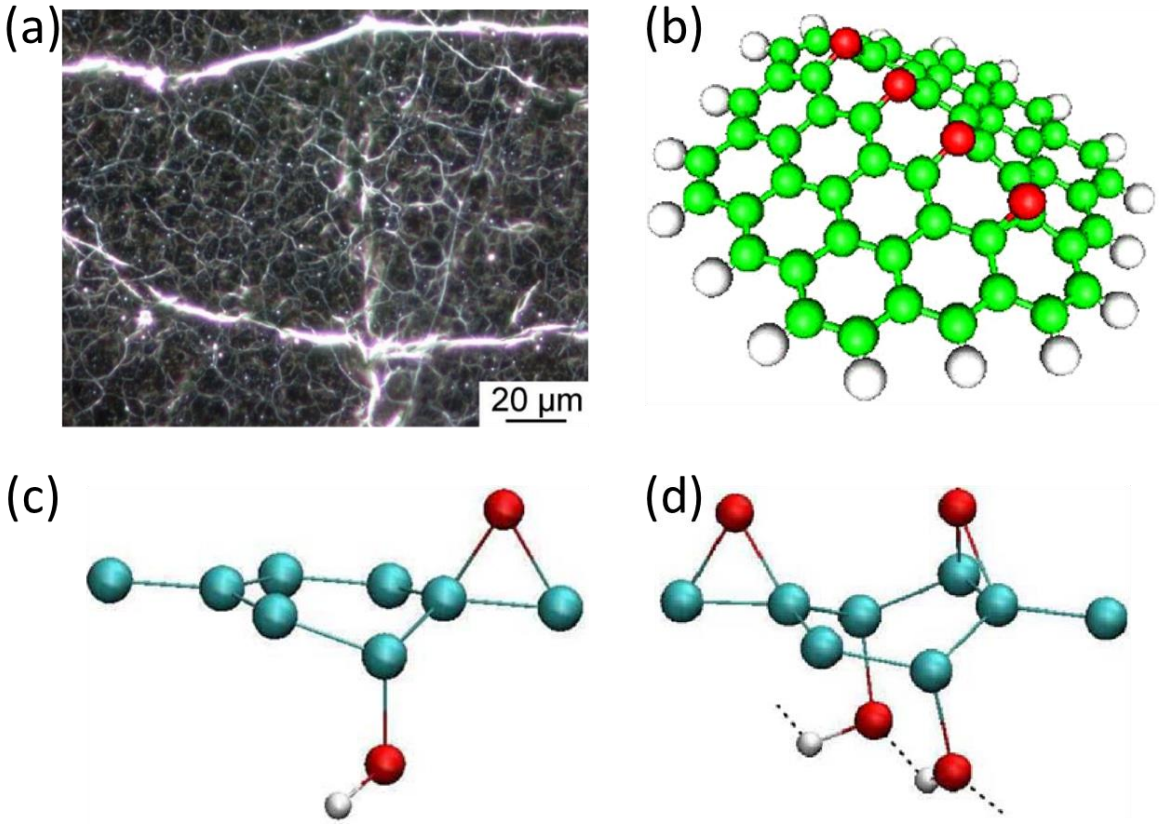

Figure 6. (a) Optical microscope image of oxidised graphite with line defects. (b) Schematic of graphene plane with aligned epoxy groups[58]. Configuration of GO (c) with one 1,2-ether oxygen and one hydroxyl at low oxidation level. (d) with two 1,2-ether oxygen and two hydroxyl groups at high oxidation level[60].

2.2.1.3 Drawbacks and Challenges

There are some drawbacks and challenges for chemical oxidation methods. The major problems arise from the use of oxidants such as $NaNO_3$, $KMnO_4$, or K_2FeO_4, which brought issues of safety and challenges in the cost of chemicals, quality of GO products and complexity of processes.

The Hummers' method involves the use of two harsh oxidants: $NaNO_3$ and $KMnO_4$, which make the method hazardous. The addition of $NaNO_3$ in the chemical reactions will cause the formation of NO_2 and N_2O_4, which are two hazardous and toxic gases. Due to the health issues,

some work further developed modified Hummers' methods and removed the $NaNO_3$ in the oxidation process, making it a much safer method[13, 51]. Although the $NaNO_3$ has been removed in some work, all modified Hummers' method work still makes the use of $KMnO_4$, which is another source of hazards. $KMnO_4$ can react with the H_2SO_4 electrolyte, producing a dangerous side-product: manganese heptoxide (Mn_2O_7)[61]. Mn_2O_7 has the oxidising property and can react with organics when the temperature exceeds 55 °C or explode by itself when temperature is higher than 95 °C[62]. During the oxidation reactions, the temperature can easily rise to 60 °C if cooling water is not used making it highly dangerous to do the production.

A recent, novel chemical oxidation method eliminated the use of $NaNO_3$ and $KMnO_4$ and replaced them with K_2FeO_4 as the oxidant[53]. Even though it is a much safer oxidant without a high risk of explosion, it has the drawbacks of high cost and rapid decomposition in water, preventing it becoming an attractive oxidant for chemical methods[17]. Another big challenge for chemical oxidation methods is the quality of the GO products. GO produced by chemical methods often show large amounts of hole defects in the carbon lattice, which has been reported to be caused by the formation of carbon dioxide (CO_2) during the oxidation reactions. Some work has tried to minimise the defects by increasing oxidation time at lower temperatures (<10 °C), which would produce issues for scalability due to increasing costs[52]. In addition to the above challenges, chemical oxidation methods also show problems of complex reaction process with multi-steps. The use of oxidants also increases the purification steps including stirring, centrifugation, sonication, filtration, and dialysis, which are essential to remove the metal ions and the acids[17]. The complex process not only increases the whole production time but also results in higher costs, which is less favorable in industrial production.

The above drawbacks and challenges make it important to continuously modify the current chemical methods or develop new chemical methods, such as looking for alternative chemical oxidants and simplifying the processes. In addition, alternative techniques are appearing to oxidise the graphite in a greener and the simpler way such as electrochemical oxidation methods, which will be introduced in the next section.

2.2.2 Electrochemical methods

2.2.2.1 Graphite intercalation chemistry

Electrochemical methods are part of a growing number of graphene production routes. Unlike chemical methods, which often rely on harsh oxidants, electrochemical methods take advantage

of graphite's conductive properties to intercalate molecules between graphene layers. By using graphite as an electrode, a positive or negative charge can be imparted in to the material, encouraging the intercalation of oppositely charged ions and facilitating exfoliation. Even though the method can be performed as a single electrochemical process, it normally involves several reaction steps during the whole process, including graphite intercalation of ions to form graphite intercalation compound (GIC), oxidation or functionalisation of the GIC, exfoliation of the oxidised/functionalised graphite.

Graphite intercalation of ions is the first step of the electrochemical process, making it an essential foundation for further producing graphene oxide or exfoliating graphite to produce graphene. Even though the electrochemical synthesis of graphene or graphene oxide does not have a very long history, the study of graphite intercalation chemistry can be traced to the first GIC produced by Schafhautl in 1841[63], which laid a solid foundation for the development of electrochemical methods. More methods have been developed to produce GIC including chemical intercalation methods, electrochemical intercalation or even photochemical methods. Besides, there are many types of species that can be intercalated into the graphite such as acids, alkali metals, halogens, and metal halides. The first electrochemical intercalation process was developed by Rudorff and Hofmann in 1938, which used sulphuric acid to intercalate into graphite by electrochemical control[64]. In the 1970s and 1980s, there is highly increased interests in electrochemical intercalation methods to produce GIC due to findings of unique properties of GIC and developments of applications such as lithium/graphite fluoride batteries[65-66]. Lithium-ion intercalated graphite was well-studied for the production of batteries, which is still under enormous study today due to the commercial applications of batteries. With regards electrochemical production of graphene, lithium was also used as a intercalant to exfoliate the graphite by applying negative current/voltage, which was inspired by the battery system[67].

As one of the most widely used GIC precursors, the graphite-acid compound has been produced electrochemically and extensively studied from the 1960s to 2000s[68-77]. The acids such as sulphuric acids, perchloric acids, and nitric acids can intercalate into graphite layers by the convenient electrochemical methods with the fixed current or voltages[68]. During the electrochemical formation process of GIC-H_2SO_4, a positive current is applied to the graphite, attracting the negative bisulphate ions. When the potential on graphite reaches the threshold potential, the bisulphate ions will start to intercalate between the sheets, which is accompanied

by the intercalation of neutral H_2SO_4 molecules[71]. During the intercalation process, GIC with various stage numbers will be formed at different stages, as shown in **Figure 7**. A stage 1 GIC represents that one layer of graphene is between two adjacent intercalant layers, which indicates a saturated status of intercalation. Stage 2 GIC means there are two graphene layers between two intercalant layers. Stage 4 GIC has four layers of graphene between intercalating molecules. The intercalation is a transition process from high stage GIC to lower stage GIC. The final GIC products by electrochemical methods are normally Stage 1 or 2 GIC, depending on the concentrations of the electrolyte.

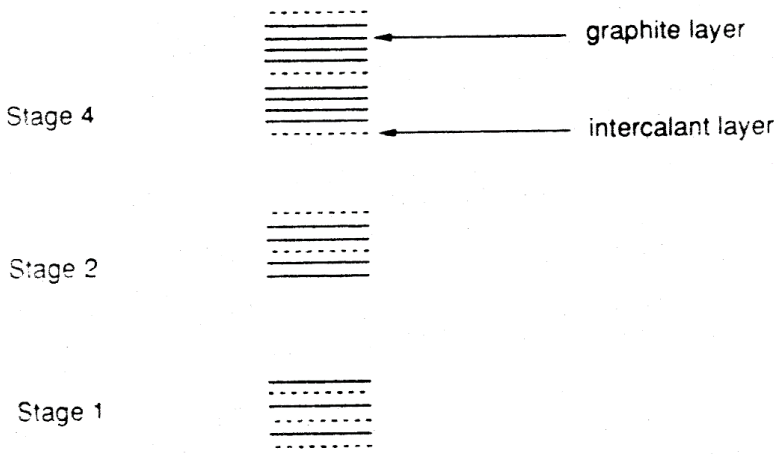

Figure 7. Schematic of GIC: stage 1, stage 2, stage 4[76].

Intercalation of ions or molecules will increase the interlayer distance between two graphene layers and reduce the attractive forces between them, making it much easier to exfoliated graphene layers from the graphite bulk. Many electrochemical methods utilise this to exfoliate graphite to produce graphene or further oxidise the GIC by more easily inserting water molecules to the lattice for electrochemical oxidation. Moreover, the electrochemical intercalation of graphite can be monitored by measuring the potential, making it a good method to theoretical studies of the intercalation process.

2.2.2.2 Electrochemical setup

There are several essential components in electrochemical setups including a working electrode connected to a bulk graphite, a counter electrode, electrolyte soaking all components, and a power supply connecting the working and counter electrodes. As for graphite sources, there are various forms including the bulk graphite such as highly orientated pyrolytic graphite (HOPG) graphite foil and graphite rod, and graphite pieces such as graphite flakes or graphite powders with various mesh sizes. For bulk graphite, they can directly adhere to a working electrode and

include platinum wire by conductive carbon tapes. For graphite flakes or powders, they normally require preformation into a plate or pad by compressions, which will introduce extra costs. As for the counter electrode, Pt or graphite are mostly used. A typical electrochemical setup is shown in **Figure** 8, with a positive current applied to the graphite through the working electrode. The counter electrode is on the opposite side of the reaction container, with a certain distance to the graphite to void the short circuit. Sometimes, a negative current will be applied to the working electrode for a cathodic exfoliation, which will produce graphene but not graphene oxide.

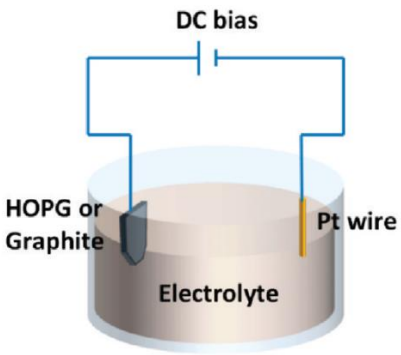

Figure 8. A typical schematic of the electrochemical setup[20].

In addition to the common setups, more novel setups have been provided to improve the efficiency and exfoliation rates. For example, Liu et al. came up with a novel vertical electrochemical cell, as shown in **Figure 9a**[78]. The vertical configuration put the graphite rod at the bottom of an electrochemical cell, on top of which are electrolyte and counter electrode. This configuration allows multiple electrochemical exfoliation processes, because the exfoliated graphite pieces during the electrochemical process will not leave the graphite bulk, as occurs in conventional setups. Therefore, this setup improves the exfoliation rate and efficiency compared to conventional setups[78]. Work by Abdelkader et al. reported a continuous electrochemical exfoliation setup, as shown in **Figure 9b**[79]. In this setup, the graphite electrode is located at the bottom of a reaction vessel which is fully filled with electrolyte. During the electrochemical process, the graphite electrode will be slowly inserted into the electrolyte and the graphite surface that is in contact with the electrolyte will be exfoliated, which then float to the top of the vessel and out of the cell through the channel[79]. This setup avoids the exfoliation of large pieces of graphite into the electrolyte that would reduce the exfoliation percentage. Another method to enhance the efficiency of electrochemical exfoliation is the addition of a shear field in the process, proposed by Shinde et al[80]. They designed a customised microfluidic reaction, as shown in **Figure 9c**. Within the reactor, there is the working electrode located at

the bottom of the reactor and the counter electrode locating at the top, with the electrolyte flowing from one side to another. The shear forces within the reactor would help with the exfoliation of the graphite during the electrochemical exfoliation process, which minimises the fragmentation and oxidation of graphene, and provides possibilities of the automated and continuous reaction sequence[80]. In other work by Tian et al., a Tee-cell setup was able to control the oxidation level of the electrochemical process, which avoided the detachment of the graphite pieces by clamping the working and counter electrode tightly, as shown in **Figure 9d**[26]. Moreover, graphite was also able to be confined by a paraffin coating to prevent the peeling off of graphite pieces from the graphite bulk (**Figure 9e**), which is proposed by Wang et al[81]. A recent work shows a continuous electrochemical setup (**Figure 9f**) with continuous insertion of the pre-intercalated graphite into the electrolyte, which allowed for the full oxidation of the GIC in contact with the electrolyte, which paved the way for scalable production in industry[27].

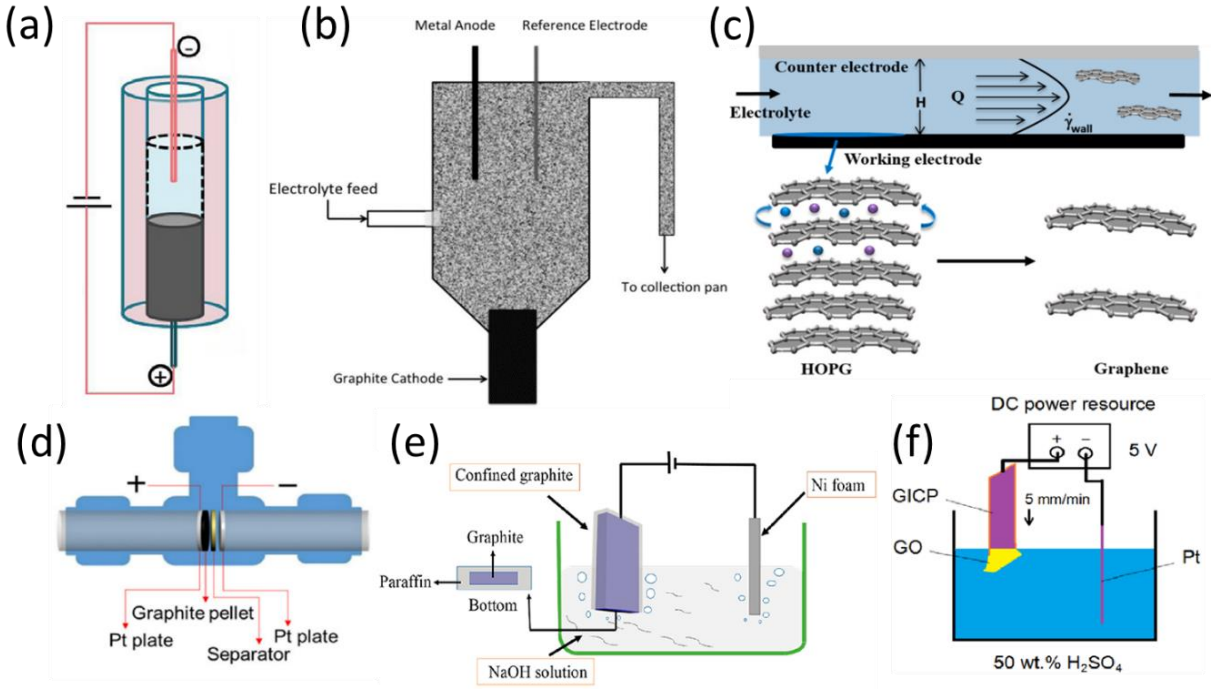

Figure 9. (a) Schematic of a multiple electrochemical exfoliation setup with a graphite rod[78]. (b) A schematic of a continuous electrochemical exfoliation setup[79]. (c) Schematic of a shear-assisted electrochemical micro-reactor[80]. (d) A schematic of a Tee-cell setup for electrochemical oxidation of graphite[26]. (e) A schematic of electrochemical exfoliation of a confined graphite by paraffin[81]. and (f) Continuous electrochemical oxidation of intercalated graphite by inserting the electrode slowly into electrolyte[27].

2.2.2.3 Mechanisms of electrochemical methods

The general mechanisms of electrochemical methods are different for anodic production of oxidised graphene and cathodic production of non-oxidised graphene flakes. For anodic exfoliation (**Figure 10a**), a positive current is applied to the graphite electrode, attracting negative ions to intercalate into the graphite layers[42]. The intercalation of the ions will increase the interlayer distance of the graphite sheets and cause the expansion of the graphite layers. In addition to the intercalating ions, there are sometimes other co-intercalating species such as solvent molecules to intercalate together with ions into the graphite lattice. The co-intercalating species can demonstrate electrochemical reactions under the positive potentials, and form gases such as oxygen gas to further expand the graphite. When water is used as the solvent of the electrolyte, oxidation of the graphite will also occur on the graphite. The expansion of the graphite reduces the π-π attracting forces between the graphene sheets and makes it much easier to exfoliate the graphite. The oxidation of the graphite will introduce oxygen groups, forming repulsive forces between the sheets and pushing the graphene sheets away from each other. Therefore, the oxidised and expanded graphite can be easily exfoliated into monolayer graphene oxide or few-layer graphene oxide sheets. The cathodic electrochemical production uses a negative bias to attract ions with positive charges from the electrolyte such as Li^+ ions, which also causes the expansion of graphite by increasing interlayer spacings. However, graphene flakes will not be oxidised in this process due to the negative current.

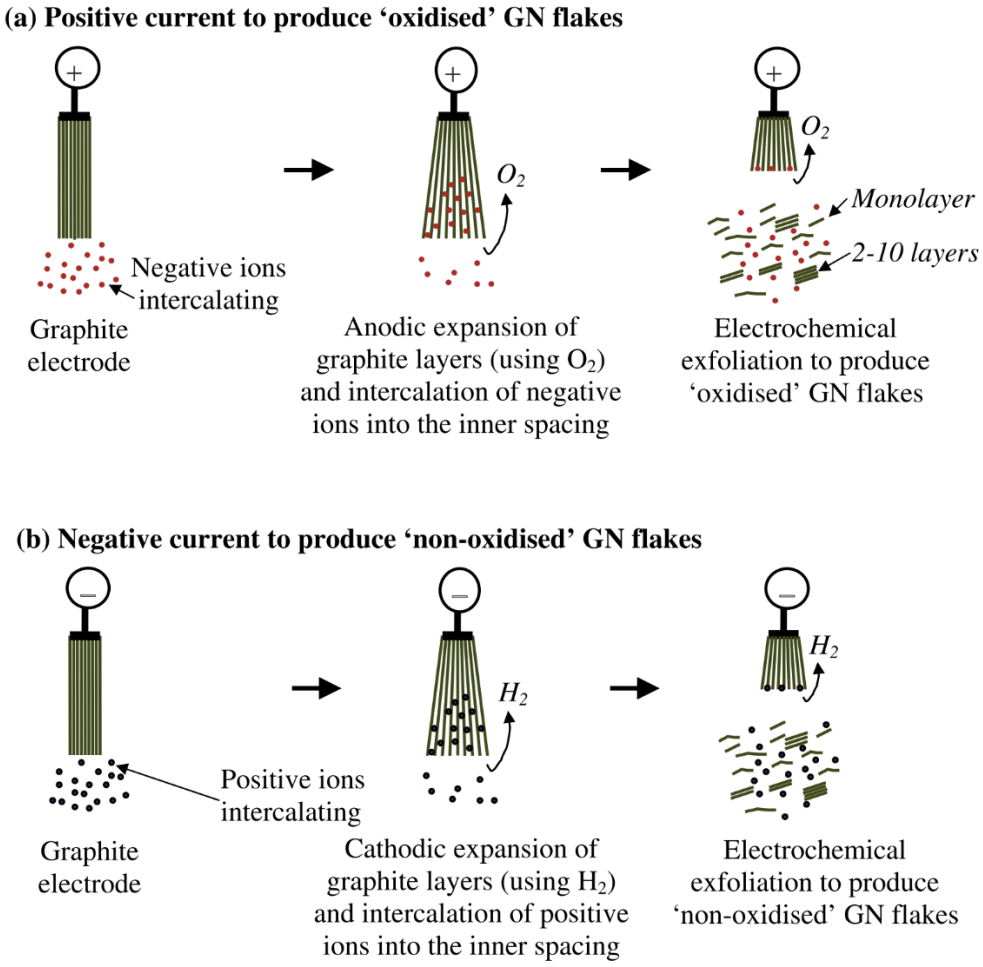

Figure 10. Schematic of the mechanism of electrochemical methods for (a) positive current to produce oxidised graphene flakes and (b) negative current to produce non-oxidised graphene flakes[42].

In addition to the polarity of the potential which determines the major mechanism, the specific mechanisms for electrochemical methods are also affected by other conditions such as the nature of the electrolytes. Both organic solvents and aqueous solvents have been used as the electrolytes, but the use of organic solvents in the electrochemical methods has limited the oxidation levels. To produce oxidised graphene or graphite, aqueous solutions are most frequently used due to the oxidation effect of H_2O under positive potentials. A mechanism about electrochemical oxidation, intercalation, and exfoliation in aqueous solution has been proposed by Parvez et al., as shown in **Figure 11**[22]. In their proposed theory, the hydrolysis of water during the electrochemical process will create hydroxyl ions (OH^-), which is a strong nucleophile, to attack the edges or grain boundaries of the graphite. The oxidised edges or grain boundaries will expand the graphite to allow intercalations of negatively charged sulphate ions (SO_4^{2-}), which will be co-intercalated with more water molecules in to the graphite layers. The

oxidation will continue through the graphite layer structures, and more gases from hydrolysis of water or others will exfoliate the graphite sheets. The oxidation mechanism in the electrochemical processes was also presented, as shown in **Figure 11b**[22]. The hydroxyl ions (OH^-) attacking the graphite will produce two vicinal OH groups, which will then react to form epoxide rings or two carbonyl groups. These formed oxygen groups make the graphite hydrophilic, attracting more waters to the vicinity of the oxidised area. In addition, carbon atoms may also react with water to produce CO_2 gases, which can help with the exfoliation, together with the O_2 gases from hydrolysis of water.

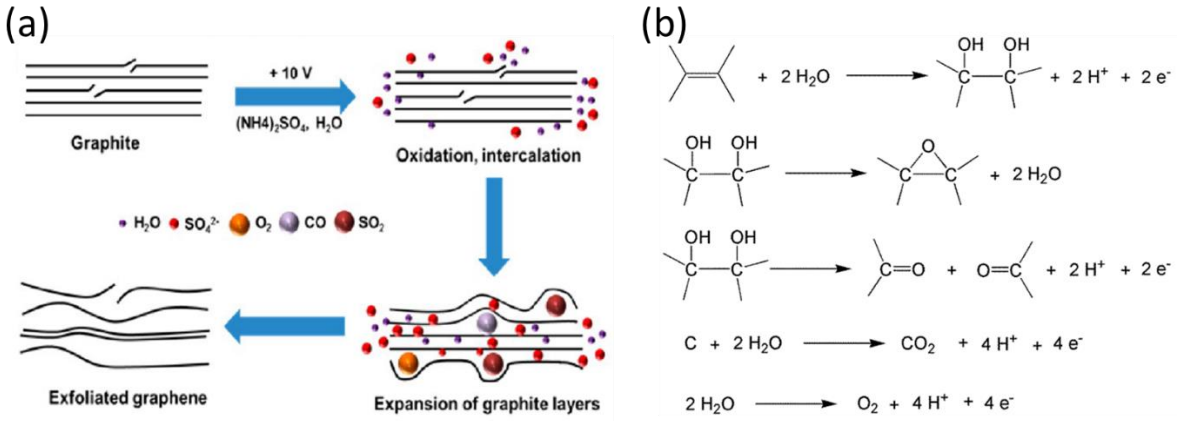

Figure 11. (a) Schematic of an electrochemical mechanism in (NH4)2SO4 aqueous solution. (b) Electrochemical oxidation reactions of graphite in aqueous solution[22].

2.2.2.4 Research progress on electrochemically-derived graphene oxide

This section will introduce recent research progress of electrochemical methods to produce graphene oxide, with the emphasis on the development of electrochemical methods, the study of electrochemical conditions, and quality of produced graphene oxide. Electrochemical methods of producing graphene oxide have only attracted interests from researchers in recent ten years, despite the long history of the electrochemical intercalations. The early research about electrochemical productions was almost entirely aimed to produce high-quality graphene sheets with minimal oxygen groups. However, the use of the anodic production and the use of aqueous electrolytes does not mean an avoidance the oxidation process. A certain degree of oxidation in the produced graphene sheets still occurs.

In one of the first works reported by Su et al. in 2011[20], an electrochemical exfoliation method was reported with the use of H_2SO_4 and KOH aqueous solution. In this method, an initial low

voltage was applied to wet the surface of the graphite electrode, which can assist with intercalation of anions. Subsequently, an alternating voltage of +10 V and -10 V will be applied to the electrode, with the +10 V for oxidising and exfoliating the graphite and the -10 V for reducing the oxygen groups. The resultant graphene sheets show superior electrical properties and larger lateral sizes. However, a small level of oxidation was still found from the observation of the D peak of Raman spectra and oxygen groups from FTIR and XPS spectrum.

In 2013, Parvez et al. studied the impact of H_2SO_4 concentration on the efficiency of electrochemical exfoliation[21]. They demonstrated that 0.1 M H_2SO_4 had a higher exfoliation efficiency than 1 M and 5 M H_2SO_4, which may be caused by the large graphite fragments generated by H_2SO_4 with higher concentrations. However, the efficiency of exfoliated will be compromised, with too low concentrations due to fewer anions for intercalation. Moreover, pure H_2SO_4 electrolyte and a mixed electrolyte of H_2SO_4/acetic (1:1) show no exfoliations of graphite, which indicates water are important elements in the electrochemical process to form oxygen and hydroxyl radicals for oxidation. The resultant GO by 0.1 M H_2SO_4 contains 7.5 wt% of oxygen content, which indicates a certain but low degree of oxidation happens. The sheet resistance of a single sheet is 4.8 kΩ/□, which is low and shows the high quality of the produced graphene sheet.

Another work of Parvez et al. to highlight is the detailed study of aqueous electrolyte of inorganic salts in the electrochemical exfoliation of graphite, which emphasises the importance of electrolytes[22]. Electrolytes including $(NH_4)_2SO_4$, Na_2SO_4, K_2SO_4, et al. were examined for their exfoliation effects, with the results showing that SO_4^{2-} ions have the best exfoliation efficiency among other anions. The concentrations of $(NH_4)_2SO_4$ also show significant influences on the exfoliation yields. With a concentration of < 0.01 M, the exfoliation yield is less than 5 wt%, which increases to >75 wt% at a concentration of 1 M. However, when the concentration further increases to 3 M and 5 M, the yield reduces to 50 wt% due to less water for oxidation. The resultant graphene sheets made under optimised conditions show 5.5 at. wt% of oxygen content, which is very low. More than 80 % of the graphene sheets have a lateral size of larger than 5 µm. Moreover, most of the graphene sheets (>85 %) are less than 3 layers. The D and G peak ratio I_D/I_G from Raman analysis is 0.25, indicating much fewer defects than chemically reduced graphene oxide (~ 1.0).

Rao et al. developed another aqueous electrolyte system, which is composed of NaOH, H_2O_2, and H_2O[23]. The addition of H_2O_2 into this system greatly increases the exfoliation efficiency,

which indicates the important role of H_2O_2 in the electrochemical exfoliation processes. With optimised conditions of 3 M NaOH and 130 mM H_2O_2 with +1 V applied for 10 min and +3 V for 10 min, high-quality graphene sheets could be produced with a high yield of 95% (3-6 layers). The oxidation degree is even further minimised to a C/O ratio of 17.2. The I_D/I_G ratio is 0.67 due to relatively high I_D/I_G ratio of graphite which is 0.54.

As can be seen from the above studies, many focus on producing graphene sheets with minimised oxidation degree. In the last three or four years, more work has tried to emphasise the production of graphene oxide with higher oxidation degree via electrochemical oxidation of graphite[26-27, 82-84]. The transition of the purposes may be due to the poor aqueous dispersibility of electrochemically-exfoliated graphene sheets, which are normally dispersed in organic solvents such as DMF. Moreover, it was realised that oxygen groups on graphene sheets are not a problem, but rather an advantage for better dispersibility, processability and functionalisation.

In the work reported by Cao et al. a two-step electrochemical processes was used to produce GO[84]. The first step is intercalation of graphite in concentrated H_2SO_4 to form Stage 1 GIC. The second step is the oxidation and exfoliation of the GIC in $(NH_4)_2SO_4$ aqueous solution. The produced GO shows more than 90% of monolayers and oxygen content of 17.7 at. %. Tian et al. reported a Tee-cell setup for electrochemical oxidation of graphite, which produced GO with the highest oxygen content of 25.1 at.%[26]. In recent work by Pei et al., a continuous and controlled electrochemical synthesis of graphene oxide was undertaken, with the setup shown in **Figure 9f**[27]. This work has achieved the highest oxygen content of 29.2 at.%, compared with other reported electrochemical methods of producing GO, which places the electrochemical methods on a par with the chemical methods.

2.2.2.5 Perspective

The recent works of employing electrochemical methods to produce graphene oxide open the routes for future work about electrochemical methods and show the possibilities of producing GO with relatively high oxidation degrees by this green, simple and controllable oxidation methods. Great potential has been shown by replacing the currently-employed chemical oxidation methods in industry, with the electrochemical oxidation methods being one. In addition, the potentially different properties of electrochemically-derived graphene oxide from

chemically-derived graphene oxide may bring more novel applications of GO or improve the current performances of GO-based applications.

There remain many challenges in electrochemical oxidation methods that need to be resolved for further development of the method. Firstly, there are still some limitations for the employment of the electrochemical methods in industries. The traditional electrochemical setups include a bulk graphite electrode directly inserted in the electrolytes, which can easily fall into pieces during the electrochemical processes and lose electrical contact before complete oxidation. As a result, the GO produced by traditional setups shows low oxidation and exfoliation degree. Although some novel setups have been proposed to avoid the undesired facts, the graphite sources used are normally bulk graphite such as graphite rod, plate, and foil or pre-formed graphite, which normally requires high cost or extra efforts. In addition, the characterisations and study of properties of electrochemically-derived graphene oxide are still limited in current researches. For example, dispersibility has been rarely studied due to the mostly poor aqueous dispersible GO produced from electrochemical methods. There is also no study about how electrochemical conditions affect the dispersibility of the products. Another important property of EGO was also not widely studied in previous research, is its ability to be thermally reduced and also by microwaves, and the subsequent properties of such reduced EGO. Due to the limited aqueous dispersibility of EGO in previous studies, EGO has been rarely assembled into the macrostructure such as membranes, which could be used in a variety of applications such as nanofiltration or desalination. There is no understanding of the properties of the assembled macrostructures and related applications, as well as how the properties of EGO are related to the performance of the macro-structures. Therefore, it is necessary to develop novel setups for potentially industrial production of graphene oxide, produce aqueous dispersible EGO, as well as to study the properties of the EGO such as dispersibility and reduction ability, assemble the aqueous dispersible EGO into macrostructure for investigation for potential applications and understand the relationships between the structures and performances.

2.3 Characterisations and properties of graphene oxide

2.3.1 Characterisations of structure and chemistry

Characterisations is an important way for studying the structure and chemistry of graphene oxide, as well as for exploring the relationships between the structure and properties of GO or

performance of the GO-based applications. In this section, a variety of reported characterisation methods for studying the graphene oxide or graphene will be introduced as important guidance for investigating structures, chemistry, and morphologies of EGO or EGO assembled structures.

Raman spectroscopy is a widely-used and powerful tool to study the structures of graphene or graphene oxide, which provides extensive information about the atomic structures, defects, and functionalisation degree. A typical Raman spectrum normally contains D (~1350 cm^{-1}), G (~1580 cm^{-1}) and 2D (~2700 cm^{-1}) peaks for carbon-based materials, with the intensity, width, and positions reflecting structure information. The G peak is indicative of the sp^2 structures within the graphene-based materials, while the D peak reflects the intensity of the aromatic rings around the defective regions. The 2D peak is dependent on the highly ordered aromatic regions and a number of the stacked layers in an assembly. Tuinstra and Koenig in 1970 reported that the intensity of the D peak is inversely proportional to the aromatic size of the graphite materials[85]. Based on Tuinstra and Koenig (TK) theory, an equation (2.1) has been proposed by Cancado et al[86]. to calculate the aromatic domain size.

$$L_a(nm) = (2.4 \times 10^{-10})\, \lambda^4 (I_D/I_G)^{-1} \qquad 2.1$$

It has been extensively used later in the study of graphene structures. However, this equation only applies to the graphene with a small number of defects.

As for more disordered graphene-based materials such as graphene oxide, Ferrari et al. proposed a three-stage model about the variation of G peak position and I(D)/I(G) ratio with the amorphisation degree, as shown in **Figure 12**[87-88]. Stage 1 is the transformation of graphite to nanocrystalline graphite, when the G position and I(D)/I(G) increase with smaller crystalline size, corresponding to the TK theory. In Stage 2, when amorphisation increases with increasing sp^3 bonds, the G peak position and I(D)/I(G) ratio decrease. In Stage 3, the G peak position increases and I(D)/I(G) decreases with larger amounts of sp^3 bonds. The decreased I(D)/I(G) at Stages 2 and 3 result from the decreased amounts of aromatic sixfold rings when the defective region increased to a certain amount, causing the decreased signal for the intensity of D peaks[89]. It was found that when the average distances between the defects L_D are smaller than 5 nm, the relationship between I(D)/I(G) and L_D will be at Stage 2 or 3. Equations have been proposed to calculate aromatic domain size from I(D)/I(G) in the disordered graphene materials[89]. The above theories provide a comprehensive understanding of the Raman spectrum

of graphene oxide materials and act as a useful tool for explaining the aromatic structure within it. In addition, the D and G peaks can also be fitted with D* (1150 – 1200 cm^{-1}), D'' (1500 – 1550 cm^{-1}) and D' (~1620 cm^{-1}) peaks, which provide more information about disorders, functionalisation, and type of defects[90]. Currently, Raman spectroscopy has been extensively employed as an analysing tool to explain the qualities of the produced graphene oxide[13, 51, 53, 56]. However, the misleading use of TK theories to calculate the aromatic domain size of graphene oxide or graphene result in some misinterpretations of structures. Care must be taken by choosing the correct theories and equations in future Raman characterisations.

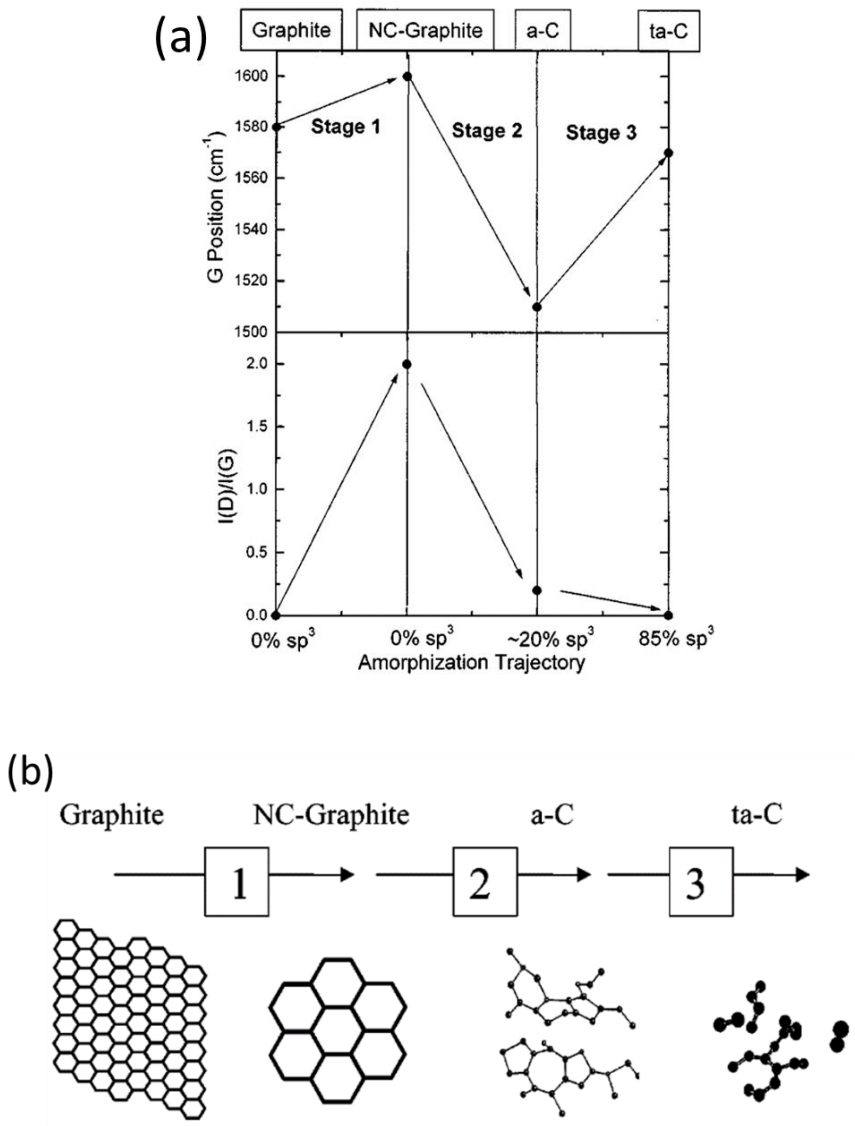

Figure 12. (a) Three-stage model: G position and I(D)/I(G) ratio change with the amorphization and disorder[87]. (b) The change of the sp2 and sp3 configurations in three amorphization stages[88].

X-ray diffraction (XRD) is another widely-used characterisation tool for investigating the structures of materials. Unlike Raman spectroscopy which can directly reflect the atomic structure information, XRD is used to examine the crystalline structure of an assembled graphene or graphene oxide macrostructures, which can be further analysed to reflect the atomic structure information. The XRD peak positions of graphene oxide or graphene assemblies reflect the interlayer spacing between the stacking layers. For example, graphene oxide assembly normally shows a peak at around 12°, while graphite has a sharp peak at around 26.7°. According to the Bragg equation (2.2):

$$\lambda = 2d\sin\theta \qquad 2.2$$

where λ is wavelength and d is interlayer spacings, the interlayer spacings of graphene oxide and graphite are 0.37 nm and 0.17 nm respectively. In addition to the peak positions, the broadening or width of the peak could also reflect some structural information. The Scherrer equation (2.3) can be used to measure the coherent domain size along the axis of the peak,

$$\beta(2\theta) = K\lambda/(L_{(2\theta)}\cos\theta) \qquad 2.3$$

where $\beta(2\theta)$ is widths of peak and $L_{(2\theta)}$ is the coherent domain size[91]. XRD spectra are often used as an examination tool for the transformation of graphite to graphene oxide, which can be directly observed from the change of peak positions[26-27]. In addition, XRD is also widely used in the structure investigation of graphene oxide membranes, such as the change of the XRD peaks in a variety of solvents, which shows the information about the interlayer distance of GO in different solvents[92]. However, XRD is mainly limited to the study of crystalline structures instead of porous structure, as it will not show much information about the structures of the porous assemblies.

X-ray photoelectron spectroscopy (XPS) can be used to characterise the chemistry of the graphene-based material in the surface with a penetration depth of about 10 nm. The XPS spectra can reveal the information about the percentage of elements such as carbon, oxygen, nitrogen, and sulfur which are mostly detected from the graphene or graphene oxide. In addition, the high-resolution scanning for an element can show the specific carbon or oxygen, functional groups. XPS has the advantages of quantitative analysis of the elements, which can be used as a general tool to assess the oxidation degree of the produced graphene oxide. It can also quantitatively measure the amounts of different oxygen functional groups. This direct tool for measurement of chemical compositions is significantly useful in the study of graphene

oxide such as assessing the oxidation degree of the produced GO or evaluating the remaining oxygen groups after reduction of GO. In addition to XPS, thermogravimetric analysis (TGA) and Fourier-transform infrared spectroscopy (FTIR) are another two commonly used methods to characterise the chemistry of graphene-related materials. TGA shows the weight loss of the materials with the gradually increasing temperature in a specific atmosphere such as air or nitrogen. For graphene oxide, the weight losses during elevated temperature is mainly due to the removal of a variety of oxygen functional groups. Therefore, the TGA curves are good reflections of the composition of oxygen groups, as well as the information about the reduction temperatures of them. FTIR can also be used to examine the oxygen functional groups in graphene oxide but it is not a quantitative method.

In addition to characterisation for structure and chemistry, there are some common techniques to characterise the morphology of the graphene materials. Due to the two-dimensional morphology of graphene, it shows hundreds of nanometers to tens of micrometers of lateral sizes, while being less than 1 nanometre in the thickness dimension. The lateral structures of graphene or graphene oxide can be easily imaged by scanning electron microscopy (SEM) or transmission electron microscopy (TEM). As for thickness information, the graphene or GO sheets needs to be measured by atomic force microscopy (AFM), which can show the thickness and flatness of the sheets.

2.3.2 Dispersibility

In this section, one of the most important properties of graphene-based materials will be introduced: its dispersibility, which determines the processability of the material for further applications. It is widely accepted that graphene is a hydrophobic 2D material, which can easily aggregate and restack into graphite in polar solvents. As a comparison, graphene oxide with abundant oxygen groups normally shows good dispersibility in aqueous solutions. To understand the dispersibility of graphene or graphene oxide, it is important to illustrate the colloidal interactions which lay a foundation for colloidal stability. The Derjaguin–Landon–Verwey–Overbeek theory introduces the interactions between two particles in a liquid with two force contributions: the attractive van der Waals forces and the repulsive electrical double layer forces (or electrostatic repulsive forces)[93]. There are three classical cases of the overall interactions of the two forces with the separation distances between two colloidal particles, as shown in **Figure 13**[94]. When the electrostatic repulsive forces dominate, the dispersion will be stable. In the opposite case, the dispersion will form irreversible coagulation if attractive van

der Waals forces dominate. The third type is the reversible flocculation which is caused by the state at a secondary minimum of the sum of the forces. Graphene oxide contains large amounts of carboxylic acid and hydroxyl groups, which can be ionised in water, forming electrostatic repulsive forces. Therefore, the stability of the graphene oxide dispersion is determined by the overall interactions between the van der Waals forces and electrostatic repulsive forces. It has been demonstrated that two interacting GO particles could be face-to-face and edge-to-edge[94]. When two flat GO sheets are edge-to-edge, the electrostatic repulsive forces will dominate due to the rapid decay of van der Waals forces with distance. As a result, the GO dispersion will be stable in a confined 2D space. However, the dispersion of GO in water is in a 3D space, where the two particles may show face-to-face interactions. In this case, the van der Waals forces and π-π interactions will form an energy minimum on the curve. The reversible flocculation will be formed at this time, which is often observed in the storage of graphene oxide for a long time.

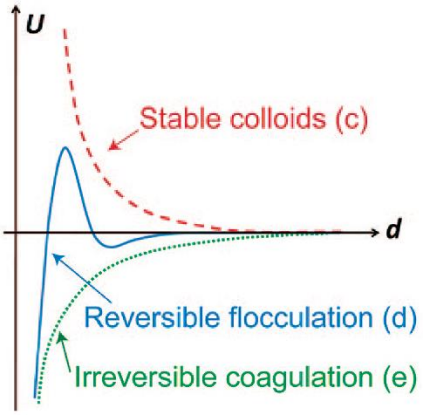

Figure 13. Total energy U versus particles separation profiles[94].

In recent years, there are many studies about the dispersibility of graphene oxide or reduced graphene. Paredes et al. reported the dispersibility of graphene oxide in a variety of solvents including water and 13 organic solvents, as shown in **Figure 14**[95]. It was found that chemically-derived graphene oxide (by the Hummers method) showed long-term stability in water, ethylene glycol, DMF, NMP and THF solvents, which provide a basis for further processing of the GO in various applications. One important factor that influences the colloidal stability is the size of graphene oxide sheets. When the GO sheets are reduced to nanosheets with lateral sizes smaller than 100 nm, the GO dispersion is found to be much more stable, which results from higher charge density due to more edge -COOH groups and more uniform distributions of sizes[96]. In addition to the sizes of GO sheets, the types of oxygen groups also have an important influence on the stability of GO dispersion at various pHs[14]. The phenolic groups

mainly ionise at basic pH, providing the electrostatic forces for GO. In neutral water, the carboxylic groups play an important role by becoming ionised to form charge species. However, in acidic environments, most of the phenolic groups and carboxylic groups will not ionise. In such cases, the carboxylic groups with phenolic OH groups ortho to them will ionise and form stable aqueous dispersions. This work demonstrated the influence of oxygen groups and their locations on the aqueous dispersibility of GO.

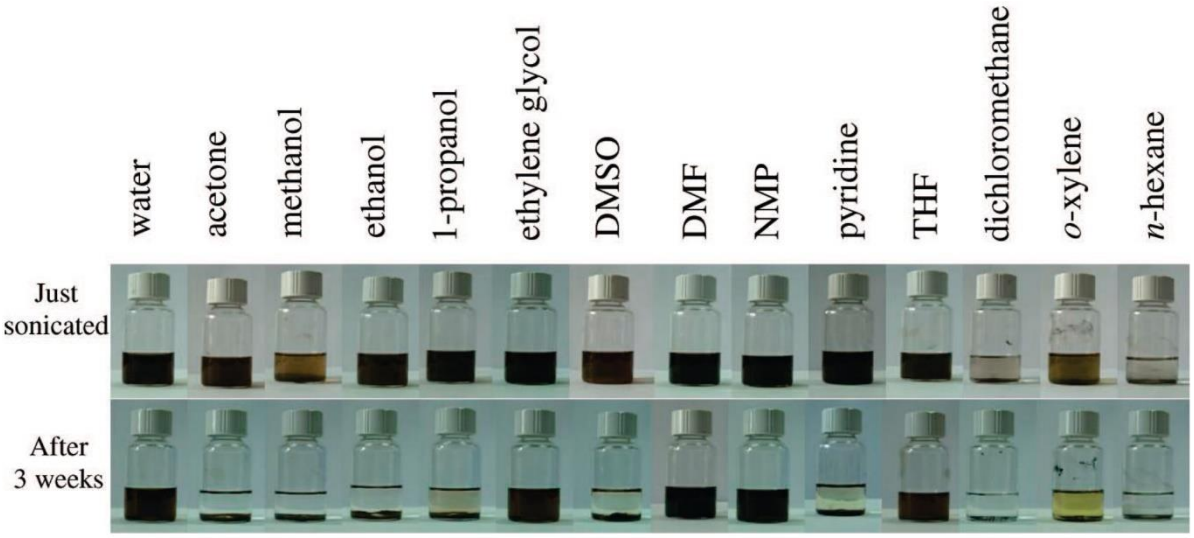

Figure 14. The dispersion of chemically-derived graphene oxide (by the Hummers method) in water and 13 organic solvents[95].

The electrostatic repulsive forces can come from two types of charge: one is by ionisation of surface groups to form charged surface, another is by adsorption of external ions on to the previously uncharged surface. Therefore, the production of aqueous dispersible graphene or graphene oxide normally involves functionalisation of graphene to form covalently bonded groups or stabilisation of graphene with extra stabilisers or additives. Work has been tried to oxidise the edge of graphene to form carboxylic groups[97] or reduce the graphene oxide with the preservation of carboxylic groups[98]. However, the oxidation of only the edge area produces mostly few-layer graphene sheets with only a small amount of single-layer graphene[97]. Other work functionalises the graphene with negatively charged $-SO_3H$ groups, which causes repulsive forces between the sheets. However, the conductivity is limited by the $-SO_3H$ groups, which cannot be removed by normal reduction[99].

One intriguing property of colloidal particles and indicator of colloidal stability is their capability to form liquid crystalline phases[100]. Colloidal particles normally show an isotropic

phase in a diluted concentration. With increasing concentration, a combination of isotropic phase and nematic phases coexist, which transform into a complete liquid crystalline phase above a critical concentration. In 2009, Kim et al.[101] first discovered the graphene oxide liquid crystals (GOLC) with nematic ordering, which paved the way of relevant research in GOLC[100, 102-104]. Graphene oxide colloidals show discotic shape with a large aspect ratio. This shape anisotropy makes graphene oxide colloidals tend to form liquid crystals in the stable, exfoliated dispersions. Even though graphene oxide has been found to show liquid crystallinity above a critical concentration, various graphene oxide may show different critical concentrations due to their differences in aspect ratio, lateral size, thickness, polydispersity, ionic impurities and pH[100]. Graphene oxide sheets with a larger aspect ratio tend to form GOLC at a lower critical concentration, while it is not easy for smaller and thicker graphene oxide sheets to form liquid crystals[105]. Polydispersity also shows influence on the GOLC with a broader polydispersity causing a broader isotropic to nematic phase transition[106-107]. With the development of GOLC, many promising applications areas such as GOLC-based fibers, papers, supercapacitors, batteries, catalysts are being developed[100].

2.3.3 Reduction of graphene oxide

Due to the excellent electrical conductivity of pristine graphene, reduction of graphene oxide has been widely performed to produce reduced graphene oxide with relatively high electrical conductivity. With the prevalence of graphene in various applications, it is important to study the reduction abilities of graphene oxide. Currently, there are several types of methods for reduction of graphene oxide, including thermal reduction, chemical reduction, microwave reduction, etc. Among them, thermal reduction and chemical reduction are the two most frequently-used methods for reducing graphene oxide to graphene. The thermal reduction has the advantages of simplicity, only requiring high-temperature annealing, reliability with the temperature adjustable to change the reduction degree, and high yield with large amounts of materials reduced at the same time[108]. Chemical reduction methods eliminate the need for an oven, which is a cheaper and more readily available way to reduce graphene oxide. However, both methods show drawbacks including energy- and time-consuming issues for thermal reductions and toxic agents used for chemical reductions.

Microwave reduction is a novel method to reduce graphene oxide by providing microwave irradiations on the materials. The method has the advantages of uniform and rapid heating compared to conventional reduction methods. In addition, it is a simple and convenient way

for manipulation, which can be easily performed in a commercial microwave oven. The development of microwave reduction has only come to the fore in the last decade. Chen et al. utilised microwave to reduce the graphene oxide in the solutions[109]. The combination of N, N-dimethylacetamide, and water can control the temperature up to 165 °C. The conductivity of the microwave-reduced GO shows 10^4 times higher conductivity than GO and reaches to 200 S/m. Later, CGO powders have been reduced by microwave irradiation, which can show sparking and even burning within 1 min[110]. The resultant GO shows an electrical conductivity of 274 S/m but a high I_D/I_G ratio of around 1[110]. The efficiency of pure graphene oxide is poor, as found from the above research. To improve the efficiency, more research has involved adding conductive graphene powders or graphite flakes or reduced graphene oxide paper to make a contact with the original graphene oxide[111-114]. The conductivities of the microwave reduced graphene oxide have been improved overall, with a much-enhanced carbon to oxygen ratio C/O (~15 – 20). Voiry et al. reported the microwave reduction of a thermally annealed graphene oxide, which exhibits significantly high efficiency with great improvement in the aromatic domain size from Raman spectroscopy, as shown in **Figure 15**[16]. By comparing it with other graphene, it shows much higher quality than graphene oxide and chemically reduced GO, and a similar quality to CVD-graphene. This greatly improved efficiency represents the efficient microwave reaction in the partially reduced domains which are conductive and reactive to microwaves. Despite progress, the microwave reduction of chemically-produced graphene oxide is still limited due to its low efficiency.

The addition of graphene or graphite may change the original structures. The pre-treatment of thermal annealing requires extra energy and time, which reduces the attractiverapid and energy-saving advantages of the microwave. Moreover, there are no studies about the microwave reductions of electrochemically-derived graphene oxide, which may show different reduction abilities and properties compared to chemically-derived graphene oxide.

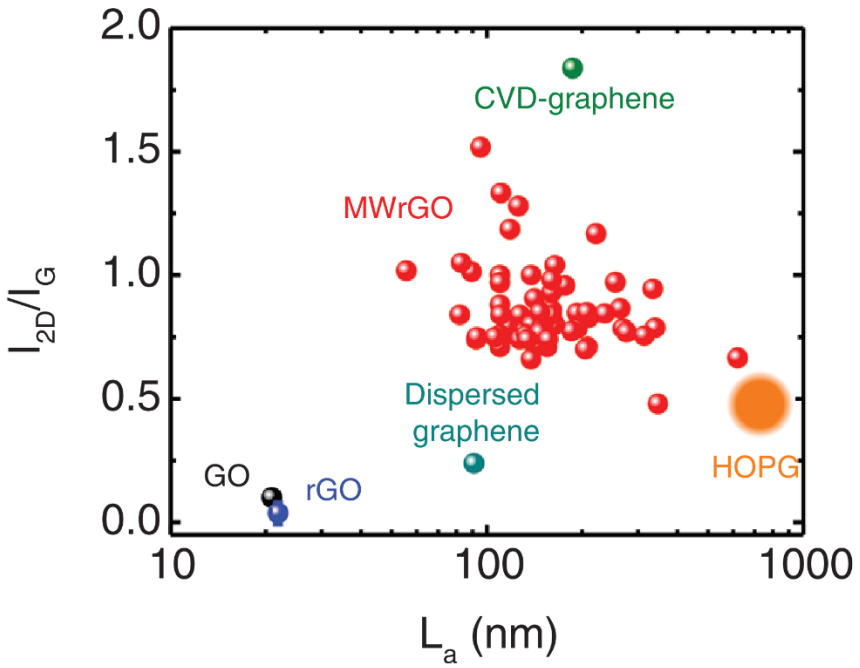

Figure 15. I_{2D}/I_G ratio versus the crystal size (La) for microwave-reduced GO (MWrGO), CVD-graphene, HOPG, dispersed graphene, rGO, and GO[16].

2.4 Graphene oxide membrane

Chemically-derived graphene oxide shows excellent aqueous dispersibility and processability, which encourages the use of the sheets as nano-building blocks for assembling into laminar membranes through filtration or coating. The resultant GO membranes show flexibility and good mechanical strength, with hydrogen bonds holding the GO sheets together[37]. The laminated GO membranes contain 2D nano-channels determined by the interlayer spacing between the GO layers, which can be used to transport molecules with sizes smaller than that of nanochannels. With the characteristic of tuneable chemistry, the sizes of the nanochannels can be adjusted by functionalisation of the GO building blocks with macromolecules or polymers. The advantages of GO laminated membrane make it a promising candidate for mass transport. The past several years have witnessed the progress of chemically-derived GO membranes, which can be used as separation membranes for nanofiltration or desalination. The transport properties of molecules or ions have also been extensively studied.

Initially, Nair and co-workers[115] have investigated the permeation properties of GO membranes for gas molecules and solvent vapor molecules. The important findings of impermeability of GO membrane to all gases and solvent molecules, except for water molecules, have led to the GO-based membranes emerging as a hot topic. This pioneering work shows that water

molecules can transport 10^{10} times faster than He molecules. They proposed that the fast transport of water resulted from the pristine-graphene capillaries within GO membranes, which allow the low-friction flow of one layer of water molecules. This work indicates GO laminated membranes are promising in water separation applications based on the favorable mass-transport properties. In addition to the molecular sieving properties in the dry state, the GO membranes also show selective ion permeation when they are utilised in water. For the studies of ion transport in GO membranes, it was initially reported by Raidongia and Huang[116], which demonstrated the ionic transport behaviors of KCl in the 2D nanochannels of the GO membranes. Later, Sun et al.[117] studied permeation properties of a variety of salts including $NaHSO_4$, NaCl, NaOH, $NaHCO_3$, $CuSO_4$, $MnSO_4$, and $CdSO_4$. They found sodium salts showed much quicker permeation rates than heavy-metal salts, which indicates the potential applications of GO membrane in ions separation.

Joshi et al. examined the permeation rates of a broader range of ions through GO membranes, as shown in **Figure 16**[5]. To test the permeation behaviors, they used a U-shape setup which is separated into two parts: feed and permeation compartments. It was found that GO laminates could block all the ions or molecules with a hydrated radius larger than 4.5 Å but allowed the permeation of ions smaller than 4.5 Å such as K^+, Na^+, and Mg^{2+} ions. This work emphasises the importance of physical size effect of the nanochannels in GO membranes. In addition, the much higher permeation rates of small ions can result from the capillary-like high pressures of the nanocapillaries[5].

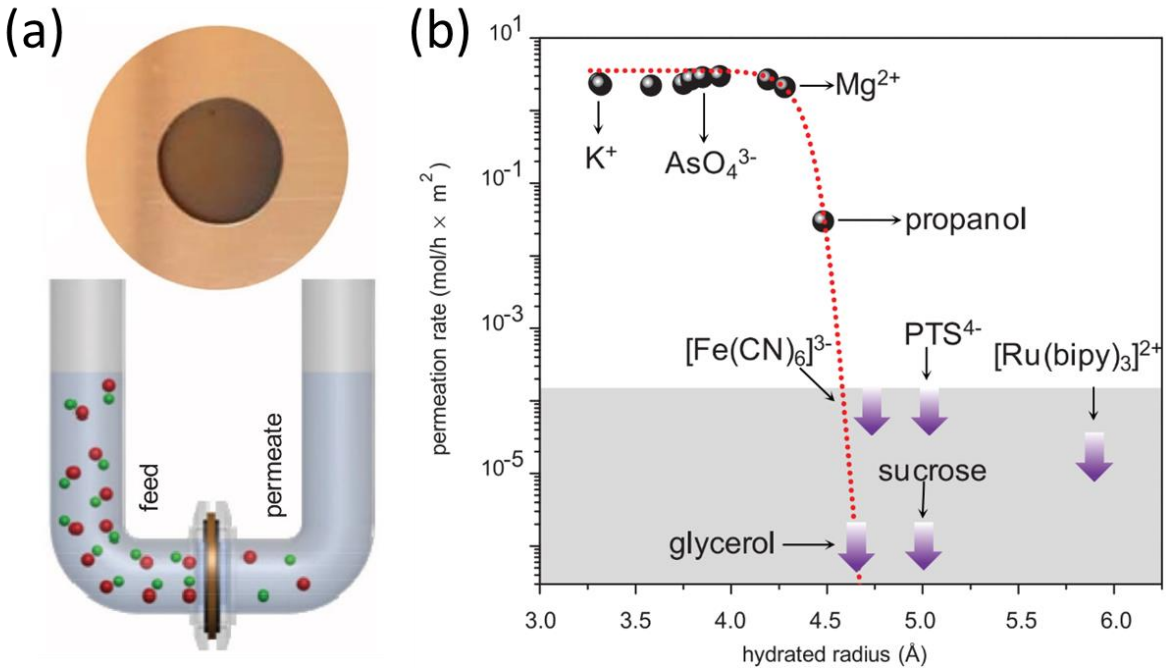

Figure 16. Ionic permeation of GO membranes: (a) Schematic of ion permeation setup, top: photograph of a GO membrane with a copper foil. (b) Permeations rates versus hydrated radius of a variety of ions[5].

Some research has tried to improve the water permeance by adding other materials into the structure as the spacers between the graphene oxide sheets. One such work reported the use of multi-walled carbon nanotubes in to the reduced graphene oxide sheets to increase the water permeability 4.8 times higher than the pristine rGO membrane[118]. In other work positively charged copper hydroxide nanostrands were mixed with negatively charged GO sheets, which were filtered to form membranes[119]. The nanostrands were then dissolved to form nanochannels within the GO membranes and demonstrated a ten times enhancements of the solution permeance.

Although graphene oxide membranes show promising applications in molecule or ion separations, there are still challenges for the chemically-derived GO membranes. With the high oxidation degree and abundant oxygen groups on GO sheets surface, GO membranes show poor stability in aqueous solutions, which exhibit a gradual enlargement of the interlayer distance when soaked in water. This progressive increase of interlayer distance will enlarge the nanochannels between the GO sheets, which will show decreased rejection for ions. This challenge impeded the further applications of graphene oxide membranes in nanofiltrations or desalination in industries. Some research has proposed methods to solve this problem. For

example, one paper reported using the physical confinement of GO membranes with epoxy in a certain humidity as a way to keep the size of the nanochannels unchanged when soaked in water[6]. However, this method increases the complexity of the manipulation, which is not a suitable method for industrial applications. Another work reported adjusted the interlayer distance of GO membrane with ions, but the membrane had to be soaked in the same ions solution to prevent escaping of the ions[120]. Both methods are not suitable for real applications in industry. More work in the future is required to resolve the instability problems of graphene oxide membranes.

2.5 Conclusions

This literature review gives a comprehensive background of graphene oxide in terms of its progress in synthesis methods, characterisations, properties, and one promising application in graphene oxide membranes. A detailed introduction of synthesis methods including chemical oxidation methods and electrochemical oxidation methods has been given, which has laid the groundwork for developing electrochemical methods and studying the properties of the electrochemically-derived graphene oxide. Characterisation and properties of graphene oxide was also discussed, with an emphasis on the dispersibility and reduced properties, which provide a basic understanding for further investigations of properties of EGO in the following experimental chapters. The final part of the chapter introduced current developments of GO membranes, as well as the challenges and limitations for current chemically-derived GO membranes, which builds a background for the development and characterisations of EGO membranes.

As discussed in this literature review, there are some limitation and challenges in current chemical oxidation and electrochemical oxidation methods. The first aim of this research is to develop a new electrochemical method with improved setups, which is potentially suitable for the industrial productions of graphene oxide with more complete exfoliation and oxidation. Due to poor aqueous dispersibility and very few studies about the properties of EGO, exploring its aqueous dispersibility and how the electrochemical methods conditions influence the property are the second aim of the thesis. In addition to dispersibility, another interesting property of EGO, reduction ability, is also not well understood. In the following chapters, the microwave reduction abilities of EGO will be reported. The final experimental chapter will be aimed at producing assembled EGO membranes, characterising the properties and structure, as well as studying the relationships between the structures and performances for the first time.

2.6 References

1. Novoselov, K. S.; Geim, A. K.; Morozov, S. V.; Jiang, D.; Zhang, Y.; Dubonos, S. V.; Grigorieva, I. V.; Firsov, A. A., Electric Field Effect in Atomically Thin Carbon Films. *Science* **2004,** *306* (5696), 666-669.

2. Bolotin, K. I.; Sikes, K. J.; Jiang, Z.; Klima, M.; Fudenberg, G.; Hone, J.; Kim, P.; Stormer, H. L., Ultrahigh electron mobility in suspended graphene. *Solid State Communications* **2008,** *146* (9), 351-355.

3. Lee, C.; Wei, X.; Kysar, J. W.; Hone, J., Measurement of the Elastic Properties and Intrinsic Strength of Monolayer Graphene. *Science* **2008,** *321* (5887), 385-388.

4. Balandin, A. A.; Ghosh, S.; Bao, W.; Calizo, I.; Teweldebrhan, D.; Miao, F.; Lau, C. N., Superior Thermal Conductivity of Single-Layer Graphene. *Nano Letters* **2008,** *8* (3), 902-907.

5. Stoller, M. D.; Park, S.; Zhu, Y.; An, J.; Ruoff, R. S., Graphene-Based Ultracapacitors. *Nano Letters* **2008,** *8* (10), 3498-3502.

6. Brodie, B. C., On the atomic weight of graphite. *Philosophical Transactions of the Royal Society of London* **1859,** *149*, 249-259.

7. Dreyer, D. R.; Park, S.; Bielawski, C. W.; Ruoff, R. S., The chemistry of graphene oxide. *Chemical Society Reviews* **2010,** *39* (1), 228-240.

8. Loh, K. P.; Bao, Q.; Eda, G.; Chhowalla, M., Graphene oxide as a chemically tunable platform for optical applications. *Nat Chem* **2010,** *2* (12), 1015-1024.

9. Chen, D.; Feng, H.; Li, J., Graphene Oxide: Preparation, Functionalization, and Electrochemical Applications. *Chemical Reviews* **2012,** *112* (11), 6027-6053.

10. Kim, J.; Cote, L. J.; Huang, J., Two Dimensional Soft Material: New Faces of Graphene Oxide. *Accounts of Chemical Research* **2012,** *45* (8), 1356-1364.

11. Chi, C.; Dan, L., Solvated Graphenes: An Emerging Class of Functional Soft Materials. *Advanced Materials* **2013,** *25* (1), 13-30.

12. Yang, X.; Zhu, J.; Qiu, L.; Li, D., Bioinspired Effective Prevention of Restacking in Multilayered Graphene Films: Towards the Next Generation of High-Performance Supercapacitors. *Advanced Materials* **2011,** *23* (25), 2833-2838.

13. Eda, G.; Fanchini, G.; Chhowalla, M., Large-area ultrathin films of reduced graphene oxide as a transparent and flexible electronic material. *Nature Nanotechnology* **2008,** *3*, 270.

14. Wang, M.; Duan, X.; Xu, Y.; Duan, X., Functional Three-Dimensional Graphene/Polymer Composites. *ACS Nano* **2016,** *10* (8), 7231-7247.

15. Sun, P.; Wang, K.; Zhu, H., Recent Developments in Graphene-Based Membranes: Structure, Mass-Transport Mechanism and Potential Applications. *Advanced Materials* **2016,** *28* (12), 2287-2310.

16. Borini, S.; White, R.; Wei, D.; Astley, M.; Haque, S.; Spigone, E.; Harris, N.; Kivioja, J.; Ryhänen, T., Ultrafast Graphene Oxide Humidity Sensors. *ACS Nano* **2013,** *7* (12), 11166-11173.

17. Cote Laura, J.; Kim, J.; Tung Vincent, C.; Luo, J.; Kim, F.; Huang, J., Graphene oxide as surfactant sheets. In *Pure and Applied Chemistry*, 2010; Vol. 83, p 95.

18. Liu, Z.; Robinson, J. T.; Sun, X.; Dai, H., PEGylated Nanographene Oxide for Delivery of Water-Insoluble Cancer Drugs. *Journal of the American Chemical Society* **2008,** *130* (33), 10876-10877.

19. Zhu, Y.; Murali, S.; Cai, W.; Li, X.; Suk, J. W.; Potts, J. R.; Ruoff, R. S., Graphene and Graphene Oxide: Synthesis, Properties, and Applications. *Advanced Materials* **2010,** *22* (35), 3906-3924.

20. Eigler, S.; Hirsch, A., Chemistry with Graphene and Graphene Oxide—Challenges for Synthetic Chemists. *Angewandte Chemie International Edition* **2014,** *53* (30), 7720-7738.

21. Lowe, S. E.; Zhong, Y. L., Challenges of Industrial-Scale Graphene Oxide Production. In *Graphene Oxide*, John Wiley & Sons, Ltd: 2016; pp 410-431.

22. Low, C. T. J.; Walsh, F. C.; Chakrabarti, M. H.; Hashim, M. A.; Hussain, M. A., Electrochemical approaches to the production of graphene flakes and their potential applications. *Carbon* **2013,** *54*, 1-21.

23. Su, C.-Y.; Lu, A.-Y.; Xu, Y.; Chen, F.-R.; Khlobystov, A. N.; Li, L.-J., High-Quality Thin Graphene Films from Fast Electrochemical Exfoliation. *ACS Nano* **2011,** *5* (3), 2332-2339.

24. Parvez, K.; Li, R.; Puniredd, S. R.; Hernandez, Y.; Hinkel, F.; Wang, S.; Feng, X.; Müllen, K., Electrochemically Exfoliated Graphene as Solution-Processable, Highly Conductive Electrodes for Organic Electronics. *ACS Nano* **2013,** *7* (4), 3598-3606.

25. Parvez, K.; Wu, Z.-S.; Li, R.; Liu, X.; Graf, R.; Feng, X.; Müllen, K., Exfoliation of Graphite into Graphene in Aqueous Solutions of Inorganic Salts. *Journal of the American Chemical Society* **2014,** *136* (16), 6083-6091.

26. Rao, K. S.; Senthilnathan, J.; Liu, Y.-F.; Yoshimura, M., Role of Peroxide Ions in Formation of Graphene Nanosheets by Electrochemical Exfoliation of Graphite. *Scientific Reports* **2014,** *4*, 4237.

27. Joshi, R. K.; Carbone, P.; Wang, F. C.; Kravets, V. G.; Su, Y.; Grigorieva, I. V.; Wu, H. A.; Geim, A. K.; Nair, R. R., Precise and Ultrafast Molecular Sieving Through Graphene Oxide Membranes. *Science* **2014,** *343* (6172), 752-754.

28. Voiry, D.; Yang, J.; Kupferberg, J.; Fullon, R.; Lee, C.; Jeong, H. Y.; Shin, H. S.; Chhowalla, M., High-quality graphene via microwave reduction of solution-exfoliated graphene oxide. *Science* **2016**.

29. Zheng, S.; Tu, Q.; Urban, J. J.; Li, S.; Mi, B., Swelling of Graphene Oxide Membranes in Aqueous Solution: Characterization of Interlayer Spacing and Insight into Water Transport Mechanisms. *ACS Nano* **2017,** *11* (6), 6440-6450.

30. Staudenmaier, L., Verfahren zur Darstellung der Graphitsäure. *Berichte der deutschen chemischen Gesellschaft* **1898,** *31* (2), 1481-1487.

31. Charpy, G., Sur la Formation de L'oxyde Graphitique et la Définition du Graphite. *C. R. Hebd. Séances Acad. Sci.* **1909,** *148*, 920− 923.

32. Hummers, W. S.; Offeman, R. E., Preparation of Graphitic Oxide. *Journal of the American Chemical Society* **1958,** *80* (6), 1339-1339.

33. Novoselov, K. S.; Geim, A. K.; Morozov, S. V.; Jiang, D.; Katsnelson, M. I.; Grigorieva, I. V.; Dubonos, S. V.; Firsov, A. A., Two-dimensional gas of massless Dirac fermions in graphene. *Nature* **2005,** *438*, 197.

34. Kovtyukhova, N. I.; Ollivier, P. J.; Martin, B. R.; Mallouk, T. E.; Chizhik, S. A.; Buzaneva, E. V.; Gorchinskiy, A. D., Layer-by-Layer Assembly of Ultrathin Composite Films from Micron-Sized Graphite Oxide Sheets and Polycations. *Chemistry of Materials* **1999,** *11* (3), 771-778.

35. Li, D.; Muller, M. B.; Gilje, S.; Kaner, R. B.; Wallace, G. G., Processable aqueous dispersions of graphene nanosheets. *Nat Nano* **2008,** *3* (2), 101-105.

36. Tian, Z.; Yu, P.; Lowe, S. E.; Pandolfo, A. G.; Gengenbach, T. R.; Nairn, K. M.; Song, J.; Wang, X.; Zhong, Y. L.; Li, D., Facile electrochemical approach for the production of graphite oxide with tunable chemistry. *Carbon* **2017,** *112*, 185-191.

37. Yang, X.; Cheng, C.; Wang, Y.; Qiu, L.; Li, D., Liquid-Mediated Dense Integration of Graphene Materials for Compact Capacitive Energy Storage. *Science* **2013,** *341* (6145), 534-537.

38. Kim, F.; Luo, J.; Cruz-Silva, R.; Cote, L. J.; Sohn, K.; Huang, J., Self-Propagating Domino-like Reactions in Oxidized Graphite. *Advanced Functional Materials* **2010,** *20* (17), 2867-2873.

39. Hirata, M.; Gotou, T.; Horiuchi, S.; Fujiwara, M.; Ohba, M., Thin-film particles of graphite oxide 1:: High-yield synthesis and flexibility of the particles. *Carbon* **2004,** *42* (14), 2929-2937.

40. Marcano, D. C.; Kosynkin, D. V.; Berlin, J. M.; Sinitskii, A.; Sun, Z.; Slesarev, A.; Alemany, L. B.; Lu, W.; Tour, J. M., Improved Synthesis of Graphene Oxide. *ACS Nano* **2010,** *4* (8), 4806-4814.

41. Zhao, J.; Pei, S.; Ren, W.; Gao, L.; Cheng, H.-M., Efficient Preparation of Large-Area Graphene Oxide Sheets for Transparent Conductive Films. *ACS Nano* **2010,** *4* (9), 5245-5252.

42. Chen, J.; Yao, B.; Li, C.; Shi, G., An improved Hummers method for eco-friendly synthesis of graphene oxide. *Carbon* **2013,** *64*, 225-229.

43. Eigler, S.; Enzelberger-Heim, M.; Grimm, S.; Hofmann, P.; Kroener, W.; Geworski, A.; Dotzer, C.; Röckert, M.; Xiao, J.; Papp, C.; Lytken, O.; Steinrück, H.-P.; Müller, P.; Hirsch, A., Wet Chemical Synthesis of Graphene. *Advanced Materials* **2013,** *25* (26), 3583-3587.

44. Peng, L.; Xu, Z.; Liu, Z.; Wei, Y.; Sun, H.; Li, Z.; Zhao, X.; Gao, C., An iron-based green approach to 1-h production of single-layer graphene oxide. *Nature Communications* **2015,** *6*, 5716.

45. Eigler, S., Graphite sulphate - a precursor to graphene. *Chemical Communications* **2015,** *51* (15), 3162-3165.

46. Szabó, T.; Berkesi, O.; Forgó, P.; Josepovits, K.; Sanakis, Y.; Petridis, D.; Dékány, I., Evolution of Surface Functional Groups in a Series of Progressively Oxidized Graphite Oxides. *Chemistry of Materials* **2006,** *18* (11), 2740-2749.

47. Krishnamoorthy, K.; Veerapandian, M.; Yun, K.; Kim, S. J., The chemical and structural analysis of graphene oxide with different degrees of oxidation. *Carbon* **2013,** *53*, 38-49.

48. Dimiev, A. M.; Tour, J. M., Mechanism of Graphene Oxide Formation. *ACS Nano* **2014,** *8* (3), 3060-3068.

49. Li, J.-L.; Kudin, K. N.; McAllister, M. J.; Prud'homme, R. K.; Aksay, I. A.; Car, R., Oxygen-Driven Unzipping of Graphitic Materials. *Physical Review Letters* **2006,** *96* (17), 176101.

50. Li, Z.; Zhang, W.; Luo, Y.; Yang, J.; Hou, J. G., How Graphene Is Cut upon Oxidation? *Journal of the American Chemical Society* **2009,** *131* (18), 6320-6321.

51. Lahaye, R. J. W. E.; Jeong, H. K.; Park, C. Y.; Lee, Y. H., Density functional theory study of graphite oxide for different oxidation levels. *Physical Review B* **2009,** *79* (12), 125435.

52. Koch, K. R., Oxidation by Mn207: An impressive demonstration of the powerful oxidizing property of dimanganeseheptoxide. *Journal of Chemical Education* **1982,** *59* (11), 973.

53. Simon, A.; Dronskowski, R.; Krebs, B.; Hettich, B., The Crystal Structure of Mn2O7. *Angewandte Chemie International Edition in English* **1987,** *26* (2), 139-140.

54. Schafhaeutl, C., Ueber die Verbindungen des Kohlenstoffes mit Silicium, Eisen und anderen Metallen, welche die verschiedenen Gattungen von Roheisen, Stahl und Schmiedeeisen bilden. *Journal für Praktische Chemie* **1840,** *20* (1), 465-485.

55. Rüdorff, W.; Hofmann, U., Über Graphitsalze. *Zeitschrift für anorganische und allgemeine Chemie* **1938,** *238* (1), 1-50.

56. Eichinger, G.; Besenhard, J. O., High energy density lithium cells: Part II. Cathodes and complete cells. *Journal of Electroanalytical Chemistry and Interfacial Electrochemistry* **1976,** *72* (1), 1-31.

57. Inagaki, M., Applications of graphite intercalation compounds. *Journal of Materials Research* **1989,** *4* (6), 1560-1568.

58. Wang, J.; Manga, K. K.; Bao, Q.; Loh, K. P., High-Yield Synthesis of Few-Layer Graphene Flakes through Electrochemical Expansion of Graphite in Propylene Carbonate Electrolyte. *Journal of the American Chemical Society* **2011,** *133* (23), 8888-8891.

59. Bottomley, M. J.; Parry, G. S.; Ubbelohde, A. R.; Young, D. A., 1083. Electrochemical preparation of salts from well-oriented graphite. *Journal of the Chemical Society (Resumed)* **1963,** (0), 5674-5680.

60. Aronson, S.; Frishberg, C.; Frankl, G., Thermodynamic properties of the graphite-bisulfate lamellar compounds. *Carbon* **1971,** *9* (6), 715-723.

61. Jnioui, A.; Metrot, A.; Storck, A., Electrochemical production of graphite salts using a three-dimensional electrode of graphite particles. *Electrochimica Acta* **1982,** *27* (9), 1247-1252.

62. Inagaki, M.; Iwashita, N.; Kouno, E., Potential change with intercalation of sulfuric acid into graphite by chemical oxidation. *Carbon* **1990,** *28* (1), 49-55.

63. Alsmeyer, D. C.; McCreery, R. L., In situ Raman monitoring of electrochemical graphite intercalation and lattice damage in mild aqueous acids. *Analytical Chemistry* **1992,** *64* (14), 1528-1533.

64. Fiang, J.; Beck, F., Thermodynamic data for anodic solid state graphite oxidation products in 96% sulphuric acid. *Carbon* **1992,** *30* (2), 223-228.

65. Beck, F.; Jiang, J.; Krohn, H., Potential oscillations during galvanostatic overoxidation of graphite in aqueous sulphuric acids. *Journal of Electroanalytical Chemistry* **1995,** *389* (1), 161-165.

66. Hathcock, K. W.; Brumfield, J. C.; Goss, C. A.; Irene, E. A.; Murray, R. W., Incipient Electrochemical Oxidation of Highly Oriented Pyrolytic Graphite: Correlation between Surface Blistering and Electrolyte Anion Intercalation. *Analytical Chemistry* **1995,** *67* (13), 2201-2206.

67. Noel, M.; Santhanam, R., Electrochemistry of graphite intercalation compounds. *Journal of Power Sources* **1998,** *72* (1), 53-65.

68. Choo, H.-S.; Kinumoto, T.; Jeong, S.-K.; Iriyama, Y.; Abe, T.; Ogumi, Z., Mechanism for Electrochemical Oxidation of Highly Oriented Pyrolytic Graphite in Sulfuric Acid Solution. *Journal of The Electrochemical Society* **2007,** *154* (10), B1017-B1023.

69. Liu, J.; Poh, C. K.; Zhan, D.; Lai, L.; Lim, S. H.; Wang, L.; Liu, X.; Gopal Sahoo, N.; Li, C.; Shen, Z.; Lin, J., Improved synthesis of graphene flakes from the multiple electrochemical exfoliation of graphite rod. *Nano Energy* **2013,** *2* (3), 377-386.

70. Abdelkader, A. M.; Kinloch, I. A.; Dryfe, R. A. W., Continuous Electrochemical Exfoliation of Micrometer-Sized Graphene Using Synergistic Ion Intercalations and Organic Solvents. *ACS Applied Materials & Interfaces* **2014,** *6* (3), 1632-1639.

71. Shinde, D. B.; Brenker, J.; Easton, C. D.; Tabor, R. F.; Neild, A.; Majumder, M., Shear Assisted Electrochemical Exfoliation of Graphite to Graphene. *Langmuir* **2016,** *32* (14), 3552-3559.

72. Wang, H.; Wei, C.; Zhu, K.; Zhang, Y.; Gong, C.; Guo, J.; Zhang, J.; Yu, L.; Zhang, J., Preparation of Graphene Sheets by Electrochemical Exfoliation of Graphite in Confined Space and Their Application in Transparent Conductive Films. *ACS Applied Materials & Interfaces* **2017,** *9* (39), 34456-34466.

73. Pei, S.; Wei, Q.; Huang, K.; Cheng, H.-M.; Ren, W., Green synthesis of graphene oxide by seconds timescale water electrolytic oxidation. *Nature Communications* **2018,** *9* (1), 145.

74. Ambrosi, A.; Pumera, M., Electrochemically Exfoliated Graphene and Graphene Oxide for Energy Storage and Electrochemistry Applications. *Chemistry – A European Journal* **2016,** *22* (1), 153-159.

75. Gurzęda, B.; Florczak, P.; Kempiński, M.; Peplińska, B.; Krawczyk, P.; Jurga, S., Synthesis of graphite oxide by electrochemical oxidation in aqueous perchloric acid. *Carbon* **2016,** *100*, 540-545.

76. Cao, J.; He, P.; Mohammed, M. A.; Zhao, X.; Young, R. J.; Derby, B.; Kinloch, I. A.; Dryfe, R. A. W., Two-Step Electrochemical Intercalation and Oxidation of Graphite for the Mass Production of Graphene Oxide. *Journal of the American Chemical Society* **2017,** *139* (48), 17446-17456.

77. Tuinstra, F.; Koenig, J. L., Raman Spectrum of Graphite. *The Journal of Chemical Physics* **1970,** *53* (3), 1126-1130.

78. Cançado, L. G.; Takai, K.; Enoki, T.; Endo, M.; Kim, Y. A.; Mizusaki, H.; Jorio, A.; Coelho, L. N.; Magalhães-Paniago, R.; Pimenta, M. A., General equation for the determination of the crystallite size La of nanographite by Raman spectroscopy. *Applied Physics Letters* **2006,** *88* (16), 163106.

79. Ferrari, A. C.; Robertson, J., Interpretation of Raman spectra of disordered and amorphous carbon. *Physical Review B* **2000,** *61* (20), 14095-14107.

80. Ferrari, A. C.; Rodil, S. E.; Robertson, J., Interpretation of infrared and Raman spectra of amorphous carbon nitrides. *Physical Review B* **2003,** *67* (15), 155306.

81. Lucchese, M. M.; Stavale, F.; Ferreira, E. H. M.; Vilani, C.; Moutinho, M. V. O.; Capaz, R. B.; Achete, C. A.; Jorio, A., Quantifying ion-induced defects and Raman relaxation length in graphene. *Carbon* **2010,** *48* (5), 1592-1597.

82. Claramunt, S.; Varea, A.; López-Díaz, D.; Velázquez, M. M.; Cornet, A.; Cirera, A., The Importance of Interbands on the Interpretation of the Raman Spectrum of Graphene Oxide. *The Journal of Physical Chemistry C* **2015,** *119* (18), 10123-10129.

83. Langford, J. I.; Wilson, A. J. C., Scherrer after sixty years: A survey and some new results in the determination of crystallite size. *Journal of Applied Crystallography* **1978,** *11* (2), 102-113.

84. Yang, Q.; Su, Y.; Chi, C.; Cherian, C. T.; Huang, K.; Kravets, V. G.; Wang, F. C.; Zhang, J. C.; Pratt, A.; Grigorenko, A. N.; Guinea, F.; Geim, A. K.; Nair, R. R., Ultrathin graphene-based membrane with precise molecular sieving and ultrafast solvent permeation. *Nature Materials* **2017**.

85. Liang, Y.; Hilal, N.; Langston, P.; Starov, V., Interaction forces between colloidal particles in liquid: Theory and experiment. *Advances in Colloid and Interface Science* **2007,** *134-135*, 151-166.

86. Cote, L. J.; Kim, F.; Huang, J., Langmuir−Blodgett Assembly of Graphite Oxide Single Layers. *Journal of the American Chemical Society* **2009,** *131* (3), 1043-1049.

87. Paredes, J. I.; Villar-Rodil, S.; Martínez-Alonso, A.; Tascón, J. M. D., Graphene Oxide Dispersions in Organic Solvents. *Langmuir* **2008,** *24* (19), 10560-10564.

88. Luo, J.; Cote, L. J.; Tung, V. C.; Tan, A. T. L.; Goins, P. E.; Wu, J.; Huang, J., Graphene Oxide Nanocolloids. *Journal of the American Chemical Society* **2010,** *132* (50), 17667-17669.

89. Konkena, B.; Vasudevan, S., Understanding Aqueous Dispersibility of Graphene Oxide and Reduced Graphene Oxide through pKa Measurements. *The Journal of Physical Chemistry Letters* **2012,** *3* (7), 867-872.

90. Tian, S.; Sun, J.; Yang, S.; He, P.; Wang, G.; Di, Z.; Ding, G.; Xie, X.; Jiang, M., Controllable Edge Oxidation and Bubbling Exfoliation Enable the Fabrication of High Quality Water Dispersible Graphene. *Scientific Reports* **2016,** *6*, 34127.

91. Konkena, B.; Vasudevan, S., Engineering a Water-Dispersible, Conducting, Photoreduced Graphene Oxide. *The Journal of Physical Chemistry C* **2015,** *119* (11), 6356-6362.

92. Si, Y.; Samulski, E. T., Synthesis of Water Soluble Graphene. *Nano Letters* **2008,** *8* (6), 1679-1682.

93. Ganguly, A.; Sharma, S.; Papakonstantinou, P.; Hamilton, J., Probing the Thermal Deoxygenation of Graphene Oxide Using High-Resolution In Situ X-ray-Based Spectroscopies. *The Journal of Physical Chemistry C* **2011,** *115* (34), 17009-17019.

94. Chen, W.; Yan, L.; Bangal, P. R., Preparation of graphene by the rapid and mild thermal reduction of graphene oxide induced by microwaves. *Carbon* **2010,** *48* (4), 1146-1152.

95. Zhu, Y.; Murali, S.; Stoller, M. D.; Velamakanni, A.; Piner, R. D.; Ruoff, R. S., Microwave assisted exfoliation and reduction of graphite oxide for ultracapacitors. *Carbon* **2010,** *48* (7), 2118-2122.

96. Park, S.-H.; Bak, S.-M.; Kim, K.-H.; Jegal, J.-P.; Lee, S.-I.; Lee, J.; Kim, K.-B., Solid-state microwave irradiation synthesis of high quality graphene nanosheets under hydrogen containing atmosphere. *Journal of Materials Chemistry* **2011,** *21* (3), 680-686.

97. Hu, H.; Zhao, Z.; Zhou, Q.; Gogotsi, Y.; Qiu, J., The role of microwave absorption on formation of graphene from graphite oxide. *Carbon* **2012,** *50* (9), 3267-3273.

98. Liu, R.; Zhang, Y.; Ning, Z.; Xu, Y., A Catalytic Microwave Process for Superfast Preparation of High-Quality Reduced Graphene Oxide. *Angewandte Chemie* **2017,** *129* (49), 15883-15888.

99. Jiang, W.; Yang, C.; Chen, G.-X.; Yan, X.-Q.; Chen, S.-N.; Su, B.-W.; Liu, Z.; Tian, J., Preparation of High-Quality Graphene Using Triggered Microwave Reduction Under Air Atmosphere. *Journal of Materials Chemistry C* **2018**.

100. Nair, R. R.; Wu, H. A.; Jayaram, P. N.; Grigorieva, I. V.; Geim, A. K., Unimpeded Permeation of Water Through Helium-Leak–Tight Graphene-Based Membranes. *Science* **2012,** *335* (6067), 442-444.

101. Raidongia, K.; Huang, J., Nanofluidic Ion Transport through Reconstructed Layered Materials. *Journal of the American Chemical Society* **2012,** *134* (40), 16528-16531.

102. Sun, P.; Zhu, M.; Wang, K.; Zhong, M.; Wei, J.; Wu, D.; Xu, Z.; Zhu, H., Selective Ion Penetration of Graphene Oxide Membranes. *ACS Nano* **2013,** *7* (1), 428-437.

103. Goh, K.; Jiang, W.; Karahan, H. E.; Zhai, S.; Wei, L.; Yu, D.; Fane, A. G.; Wang, R.; Chen, Y., All-Carbon Nanoarchitectures as High-Performance Separation Membranes with Superior Stability. *Advanced Functional Materials* **2015,** *25* (47), 7348-7359.

104. Huang, H.; Song, Z.; Wei, N.; Shi, L.; Mao, Y.; Ying, Y.; Sun, L.; Xu, Z.; Peng, X., Ultrafast viscous water flow through nanostrand-channelled graphene oxide membranes. *Nature Communications* **2013,** *4*, 2979.

105. Abraham, J.; Vasu, K. S.; Williams, C. D.; Gopinadhan, K.; Su, Y.; Cherian, C. T.; Dix, J.; Prestat, E.; Haigh, S. J.; Grigorieva, I. V.; Carbone, P.; Geim, A. K.; Nair, R. R., Tunable sieving of ions using graphene oxide membranes. *Nat Nano* **2017,** *12* (6), 546-550.

106. Chen, L.; Shi, G.; Shen, J.; Peng, B.; Zhang, B.; Wang, Y.; Bian, F.; Wang, J.; Li, D.; Qian, Z.; Xu, G.; Liu, G.; Zeng, J.; Zhang, L.; Yang, Y.; Zhou, G.; Wu, M.; Jin, W.; Li, J.; Fang, H., Ion sieving in graphene oxide membranes via cationic control of interlayer spacing. *Nature* **2017,** *550*, 380-383.

Chapter 3. Mechanically-Assisted Electrochemical Production of Graphene Oxide

This chapter is aimed to develop a new electrochemical method to produce graphene oxide. Chemical oxidation methods to synthesize graphene oxide have the drawbacks of using explosive oxidizing agents, contaminations by residual metal ions, and the formation of hole defects on graphene oxide sheets. Conventional electrochemical methods show problems of incomplete oxidation and exfoliation due to premature peeling of graphite pieces from the electrode. In this chapter, a novel mechanically-assisted electrochemical method is developed to produce graphene oxide. Mechanical stirring has been used as assistance to the electrochemical oxidation and exfoliation process, which allows the continuous physical contact between graphite flakes and working electrode for oxidation and exfoliation. The electrochemically-derived graphene oxide has been characterized and shows good oxidation degree and less physical defects than CGO. It also shows facile reduction ability and long-term stability in ethanol when compared with CGO.

CHEMISTRY OF MATERIALS

Article

pubs.acs.org/cm

Mechanically-Assisted Electrochemical Production of Graphene Oxide

Pei Yu,[†] Zhiming Tian,[†] Sean E. Lowe,[‡] Jingchao Song,[†] Zhirui Ma,[†] Xin Wang,[†] Zhao Jun Han,[§,#] Qiaoliang Bao,[†] George P. Simon,[†] Dan Li,[†] and Yu Lin Zhong*[,‡]

[†]Department of Materials Science and Engineering, Monash University, Clayton, Victoria 3800, Australia

[‡]Centre for Clean Environment and Energy, Gold Coast Campus, Griffith University, Gold Coast, Queensland 4222, Australia

[§]CSIRO Manufacturing, 36 Bradfield Road, Lindfield, New South Wales 2070, Australia

[#]Department of Materials, University of Oxford, Parks Road, Oxford, OX1 3PH, United Kingdom

Supporting Information

ABSTRACT: Graphene oxide (GO) is promising for a variety of applications due to its excellent dispersibility and processability. However, current chemical oxidation routes have several drawbacks, including the use of explosive oxidizing agents, residual metal ions contaminations, and the creation of irreparable hole defects on the GO sheet. The electrochemical exfoliation and oxidation of graphite is a potentially greener approach without the need for extensive purification steps. Most reported electrochemical methods employ a single preformed bulk graphite as electrode, which limits their scalability, reproducibility, and degree of oxidation. Herein, we reported a novel mechanically assisted electrochemical method to produce graphene oxide directly from graphite flakes. The electrochemically derived graphene oxide (EGO) shows a good degree of oxidation but with less physical defects than chemically derived graphene oxide (CGO). EGO has good dispersibility in water and various solvents and, in particular, displays better long-term stability in ethanol when compared with CGO. Notably, unlike conventional CGO, EGO can undergo facile thermal conversion at 200 °C in air to conductive thermally processed EGO, which is highly desirable for heat/chemical-sensitive applications.

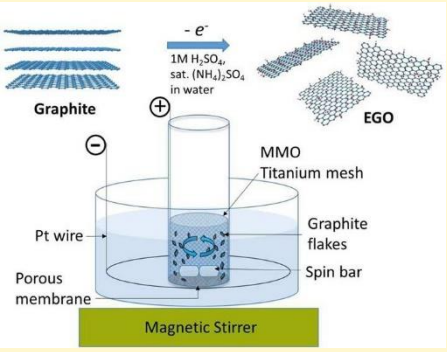

INTRODUCTION

Graphene oxide (GO), an oxidized form of graphene, and its reduced form, reduced graphene oxide (rGO), are graphene-like materials which have attracted significant research and commercial interest.[1−3] GO has been widely used due to the presence of oxygen functionalities which impart good dispersibility in water and organic solvents.[4−7] Reactive oxygen groups also allow the material to be functionalized through covalent attachment of small molecules or polymers.[1,8,9] These advantages of GO and more typically, the conductivity of its reduced form, rGO, are highly sought after for transparent conductive films,[10] lithium ion battery,[11,12] ultracapacitor electrodes,[13−17] dye-sensitized solar cell electrodes,[18] sensors to detect gases and biomolecules,[19,20] or as a filler in polymers for better mechanical strength, electrical conductivity, and thermal stability.[21,22]

Graphene oxide is usually exfoliated from graphite oxide, which is produced by chemical oxidation of graphite. In the late 1800s, Brodie and Staudenmaier demonstrated the oxidation of graphite by $KClO_3$, HNO_3, and H_2SO_4.[23,24] In 1909, Charpy oxidized graphite in sulfuric acid by potassium permanganate.[25] In 1958, Hummers and Offeman developed the protocol introduced by Charpy for oxidizing graphite with $KMnO_4$, $NaNO_3$, and H_2SO_4.[25,26] The Hummers method has become the most widely used approach for production of graphene oxide, and it has since undergone several optimizations.[27−30] In 2013, Eigler et al. synthesized low defect GO via the modified Hummers method by using only a low reaction temperature.[30] Recently, Voiry et al. employed a similar approach to produce graphene oxide, which was reported to exhibit high quality after simple microwave reduction.[31] Although the low-temperature chemical oxidation can achieve low defect GO, the low-temperature process has to be controlled for a long period. Apart from the frequently employed modified Hummers' method, Peng et al. employed a promising novel oxidant, K_2FeO_4, to replace the hazardous oxidants used in previous methods.[32] Eigler yielded graphene with a low density of defects from graphite sulfate by its reaction with water.[33] The main advantages of the chemical oxidation routes are high yield and good dispersibility of graphene oxide, but there are some inherent issues and limitations. Apart from the generation of toxic gases (such as NO_2 and N_2O_4 or ClO_2) in most of the traditional oxidation routes, the main concern is the risk of explosion such as the formation of manganese heptoxide

Received: October 16, 2016
Revised: October 30, 2016
Published: October 31, 2016

DOI: 10.1021/acs.chemmater.6b04415
Chem. Mater. 2016, 28, 8429−8438

(Mn_2O_7) in Hummers method.[34] Furthermore, the residual metal ions from the chemical oxidants, such as $KMnO_4$, K_2FeO_4, and $KClO_3$, require additional purification steps, typically involving the use of H_2O_2 and HCl.[35] The use of strong oxidizing agents also tend to introduce irreparable hole defects to GO sheet,[32,36] limiting the electrical conductivity of the subsequent rGO.[37,38] In contrast, the electrochemical exfoliation of graphite may present a greener, simpler, and capable way of producing less defective graphene.[39]

Electrochemical approaches achieve exfoliation of graphite by intercalation of molecules or ions between graphite layers through electrochemical activation.[40] In most previously reported electrochemical exfoliation methods, the graphite sources were in the single bulk form such as graphite rod, graphite foil, and highly orientated pyrolytic graphite (HOPG).[40−46] The need to preform these types of graphite electrodes introduces extra cost, and the reproducibility of electrochemical exfoliation will be affected by batch variation of graphite electrodes. Moreover, the electrochemical exfoliation efficiency will be affected by the size of the graphite electrodes. In addition, it is difficult to achieve uniform and good oxidation of the graphene product, as the preformed graphite electrodes often exfoliate into few or multilayer graphene and lose electrical contact before a sufficient degree of oxidation can occur. All of these factors will limit the scalability of electrochemical exfoliation with preformed graphite electrodes.

In this work, we developed a novel electrochemical exfoliation method which employs mechanical stirring to assist the electrochemical exfoliation and oxidation of graphite flakes to graphene oxide sheets. With mechanical assistance, graphite flakes in the electrolyte can be directly used instead of using a single bulk graphite electrode. We have investigated several parameters affecting the efficiency of the electrochemical process and characterized the as-produced electrochemically derived graphene oxide (EGO) in details.

■ EXPERIMENTAL SECTION

Materials. The graphite source used throughout the experiments was graphite flakes purchased from Sigma-Aldrich (product no. 332461, particle size: +100 mesh). Reagent grade $(NH_4)_2SO_4$ (99.0%), concentrated H_2SO_4 (98%), and solvents—dimethylformamide (DMF) (99.8%), isopropyl alcohol (IPA) (99.5%), absolute ethanol (100%), tetrahydrofuran (THF) (99.9%), acetone (99.5%), toluene (99.5%) and hexane (99%)—were purchased and used as received from Sigma-Aldrich. Ultrapure water (Millipore system) was used for the preparation of electrolyte and all other experimental procedures that required water. The working electrode used in the electrochemical exfoliation process was a mixed metal oxide (MMO) coated titanium mesh ribbon (mesh size: 3 mm × 2 mm, ribbon width: 2 cm) purchased from Savcor Products Australia Pty Ltd. Platinum wire (0.25 mm diameter, product no. PT005121) was purchased from Goodfellow Cambridge Ltd. (U.K.) and used as the counter electrode. For comparison, chemically derived graphene oxide (CGO) synthesized by the modified Hummers method was purchased from Sixth Element (Changzhou, China) Materials Technology Co., Ltd. CGO was also synthesized in our lab (CGO-lab) via the modified Hummers method[47] with the graphite flakes from Sigma-Aldrich (product no. 332461, particle size: +100 mesh). In brief, 20 g of graphite flakes was preoxidized in an 80 °C solution of concentrated H_2SO_4 (30 mL), $K_2S_2O_8$ (10 g), and P_2O_5 (10 g), which was then washed and dried. The preoxidized graphite was added to concentrated H_2SO_4 (460 mL) at 0 °C with $KMnO_4$ (60 g) added gradually. After stirring at 35 °C for 2 h, 920 mL of water was slowly added. After 15 min, more water (2.8 L) and 30% H_2O_2 solution (50 mL) was added to terminate the reaction. Finally, the oxidized graphite was washed with 1:10 HCl and dialyzed to remove metal ions and acids.

Synthesis of Electrochemically Derived Graphene Oxide (EGO). Typically, 100 mg of graphite flakes were placed inside a cylindrical glass tube (diameter = 3 cm, the graphite-containing vessel), which was capped at the bottom end with a polyvinylidene fluoride (PVDF) membrane (Durapore membrane, 0.65 μm diameter pore size, Millipore) as shown in Figure 1. The MMO-coated titanium mesh was placed around the inner wall of the graphite-containing tube such that the working electrode was flush with the tube wall. A magnetic Teflon spin bar was placed inside the tube. The capped end of the tube holding the graphite and working electrode was suspended in the electrolyte bath held in a second vessel, a 250 mL beaker. The membrane kept the graphite and graphene oxide product inside the tube, while allowing ions and electrolytes to pass through. The height of the tube relative to the beaker was adjusted such that the electrolyte would diffuse through the membrane and reach the top of the working electrode. A platinum wire loop was used as counter electrode and was placed around the inner wall of the outer beaker. A second magnetic stirrer (∼1 mm diameter) was placed at the bottom of the outer beaker to agitate the electrolyte. A typical laboratory magnetic stirrer was used to control the revolution of the magnetic spin bars. Typically, 150 mL of 1 M H_2SO_4 in saturated $(NH_4)_2SO_4$ aqueous solution (with excess $(NH_4)_2SO_4$ salt crystals) was used as electrolyte. To minimize evaporation of the electrolyte, parafilm was placed over the annulus surrounding the reaction tube.

During the electrochemical process, a positive constant current (e.g., 0.6 A) was applied to the working electrode for a certain period (e.g., 24 h) using a DC power supply (Atten PPS3205T-3S). At the same time, the graphite slurry was stirred with a spin bar at a fixed rotation rate. Following the electrochemical charging, the slurry was removed from the apparatus and repeatedly washed with water and recovered via centrifugation (Ample Scientific Champion S-50D centrifuge) for at least three times until the pH of the EGO dispersion was higher than 6.0. The washed slurry was redispersed in 200 mL of water via a sonication bath (Bransonic CPX2800H-E) for 15 min, followed by centrifugation at 1000 rpm for 2 h. After centrifugation, the supernatant containing EGO was carefully drawn out and used for further characterization. When required, the final EGO dispersion was filtered onto a PVDF membrane by vacuum filtration and peeled off the membrane to form a freestanding EGO film. The film was further dried overnight at room temperature in a vacuum oven (Sumsung DZG-6020). Similarly, CGO films were produced by vacuum filtration of aqueous CGO dispersions and dried overnight at room temperature in a vacuum oven. Thermal reduction of freestanding EGO or CGO film was carried out in a typical laboratory oven in air (Kenton 101-0AS). For the preparation of EGO or CGO dispersion in different solvents, vacuum-dried EGO or CGO films were added into different solvents to make 0.1 mg/mL dispersion and sonicated in an ultrasonic bath for 30 min.

Characterization. Transmission electron microscopy (TEM) images were obtained using FEI Tecnai G2 T20

TWIN TEM with an accelerating voltage of 200 kV. TEM samples were prepared by dipping holey carbon grids into aqueous EGO dispersion (~0.1 mg/mL) and dried in air. Atomic force microscopy (AFM) images were taken by Bruker Dimension Icon AFM under tapping mode. AFM samples were prepared by spin-coating aqueous EGO dispersion (~0.1 mg/mL) at 3000 rpm on Si (100) wafer, previously cleaned in Piranha solution. Raman characterization was performed directly on individual EGO or CGO sheet, drop-casted on 300 nm SiO_2/Si wafer, using a confocal Raman microscope (WITec, alpha300 R) with 532 nm laser as excitation source. X-ray diffraction (XRD) characterization was also performed on EGO or CGO film with a Bruker D2 Phaser diffractometer (Cu Kα radiation, λ = 1.5418 Å) at room temperature. The XRD patterns were collected from 2Θ of 6° to 30° with a step size of 0.05° and at a rate of 1 s/step. X-ray photoelectron spectroscopy (XPS) was performed on the soft X-ray beamline at the Australian Synchrotron with a SPECS Phoibos 150 hemispheric analyzer, with typical energy resolution of better than 100 meV. Thermogravimetric analysis (TGA) of EGO or CGO film samples was performed on a Thermo thermogravimetry/differential thermal analyzer (TG/DTA) 6300. The sample (typically 5 mg) was heated under argon atmosphere from 30 to 700 °C at 2 °C min^{-1}. Attenuated total reflectance (ATR) FTIR measurements were carried out on a PerkinElmer Spectrum 100 system coupled with a universal ATR accessory (diamond/ZnSe ATR crystal). The electrical conductivity measurements for EGO and CGO films of similar weight (around 6 mg) were carried out on a Jandel 4-point probe system with a linear arrayed head (probe spacing of 1 mm). The thicknesses of film samples and lateral size of EGO sheet, drop-casted on Si wafer, were obtained from scanning electron microscopy (SEM) images using FEI Nova NanoSEM 450 FEGSEM with an accelerating voltage of 5 kV. Zeta potentials of EGO and CGO dispersion (0.1 mg/mL) were measured by a Malvern Zetasizer Nano ZS analyzer.

■ RESULTS AND DISCUSSION

Electrochemical Production of EGO. An apparatus shown in Figure 1 was designed to produce EGO from graphite flakes. Various key parameters of the electrochemical process were studied, shown in Table 1, including stirring speed, initial graphite amount, current applied to the working electrode, and total electrochemical reaction time. After the samples were washed, the yield of EGO (in weight percentage) and XRD peak ratio of GO to graphite (vide infra) were measured and tabulated in Table 1. These two measurements indicate the exfoliation efficiency and oxidation degree, respectively. Baseline conditions of 1200 rpm stirring speed, 100 mg of graphite flakes, 0.6 A current, and 24 h of reaction time were established. Each parameter was then varied while the remaining baseline conditions were held constant.

The efficacy of mechanical assistance in our electrochemical method was studied with various stirring speeds (400, 600, 800, 1000, 1200 rpm) of the spin bar under the baseline conditions (100 mg of graphite flakes, 0.6 A current, 24 h of reaction time). It was found that a higher stirring speed resulted in a higher yield of EGO and a higher XRD peak ratio, which correlates to a higher exfoliation efficiency and degree of oxidation. In addition to higher shear stresses, the higher stirring speeds provide more centrifugal force to graphite flakes, allowing better contact with the MMO-coated titanium electrode. Four batches of 50, 100, 200, and 400 mg were

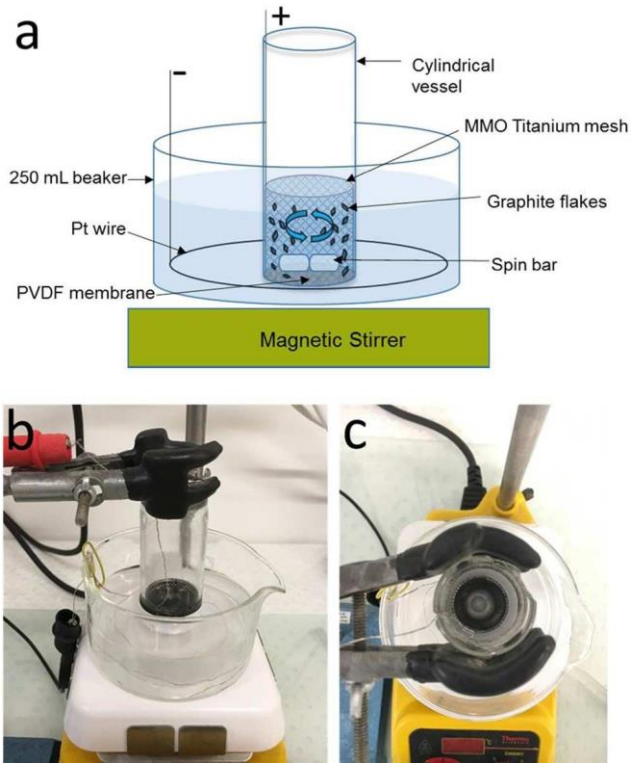

Figure 1. (a) Schematic drawing of the mechanically assisted electrochemical exfoliation setup. (b) Photograph of the setup (side view). (c) Photograph of the setup (top view).

Table 1. Influence of Different Parameters on Yield of EGO and XRD Peak Ratio

parameters	samples	yield of EGO (wt %)	XRD peak ratio
stirring speed	400 rpm	10	0.66
	600 rpm	14.4	1.15
	800 rpm	18.0	1.73
	1000 rpm	25.6	1.81
	1200 rpm	37.6	2.08
initial graphite amount	50 mg	31.2	1.04
	100 mg	37.6	2.08
	200 mg	31.2	1.36
	400 mg	25.6	0.76
current	0.3 A	33.6	1.92
	0.6 A	37.6	2.08
time	6 h	11.6	0.87
	12 h	24.0	1.61
	24 h	37.6	2.08
	48 h	38.8	2.92

studied under the baseline conditions to understand the effect of initial graphite loading. The yield of EGO increased from a graphite loading of 50 mg to 100 mg, but decreased from 100 mg to 400 mg. We surmised that an optimum graphite loading (around 100 mg in the current set up) allows for effective distribution of electrical current among the graphite flakes. With regards to the applied current and reaction time, we found that the higher current density and longer reaction period contributed to higher yield and higher XRD peak ratio. Although the maximum yield of EGO was about 40 wt % in the current setup, there is the possibility of recycling and reuse of

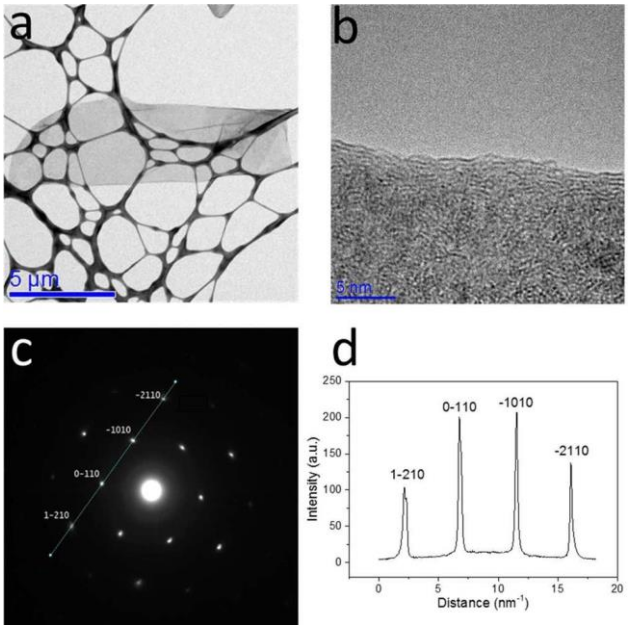

Figure 2. (a) TEM image of a typical EGO sheet. (b) High-resolution TEM image showing edge of EGO sheet from (a). (c) Electron diffraction pattern taken from EGO sheet from (a). (d) Diffracted intensity taken along the 1−210 to −2110 axis for patterns shown in (c).

the remaining flakes. Hence, there is still much room for improvement.

The mechanisms for the mechanically assisted electrochemical exfoliation and oxidation of graphite are proposed to be the following: centrifugal force, from the stirring, pushes the graphite flakes toward MMO-coated titanium mesh, creating physical contact between the flakes and the mesh. The positive current/voltage applied to the MMO-coated titanium mesh, positively charges the graphite flakes that come in contact with the mesh and encourages the intercalation of anions (e.g., SO_4^{2-} ions). Concurrently, it is suggested that the electrolysis of water at the anode/positively charged graphite flakes produces oxygen and ozone, in which the latter can decompose to hydroxyl radicals (·OH). These oxidizing radicals can attack the sp^2 carbons at graphite edges and grain boundaries first, producing oxygen functional groups (Scheme S1).[42] The oxygen functional groups at edges open up graphite flakes, which facilitates further intercalation of SO_4^{2-} ions and water molecules for further oxidation on the basal planes. The electrolysis of intercalated water to oxygen gas in the expanded graphite can also contribute to the graphite exfoliation process. Apart from electrochemical exfoliation, the stirring spin bar creates shear forces between graphite layers, assisting in the exfoliation of graphite flakes. Continuous stirring allows repeated physical contact between the incompletely exfoliated graphite and MMO-coated titanium mesh electrode for continual oxidation and exfoliation.

Microscopy Characterization of EGO. EGO was produced under the baseline conditions for further characterization and studies. The morphology of EGO was investigated by transmission electron microscopy (TEM), and Figure 2a shows a typical EGO sheet with lateral size of about a few micrometers. The high-magnification image of the edge of EGO sheet in Figure 2b shows a single fringe which is consistent with the presence of a single layer EGO. From the selected area diffraction pattern shown in Figure 2c, a typical 6-fold symmetric diffraction pattern is observed. The intensity of diffraction spot from the (0−110) plane is more intense than

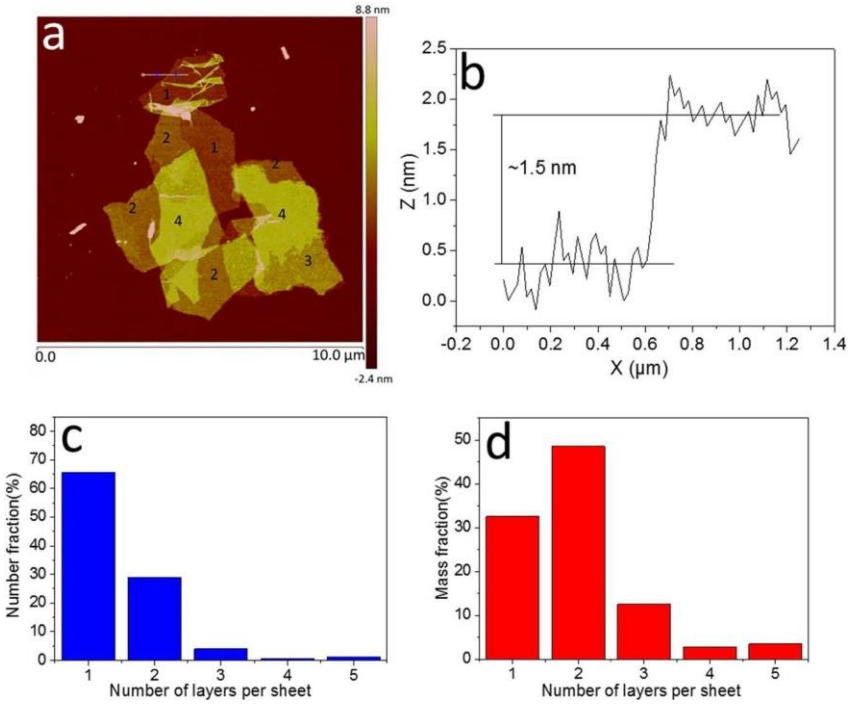

Figure 3. (a) AFM image of several stacked EGO sheets. The thickness was measured at several points, and based on a layer height of 1.5 nm, the number of graphene oxide layers in different regions of the image was inferred and is shown on the image. (b) Line profile of topmost EGO sheet in (a). (c) Frequency distribution of the number of layers in the product. (d) Mass distribution of the number of layers in the product.

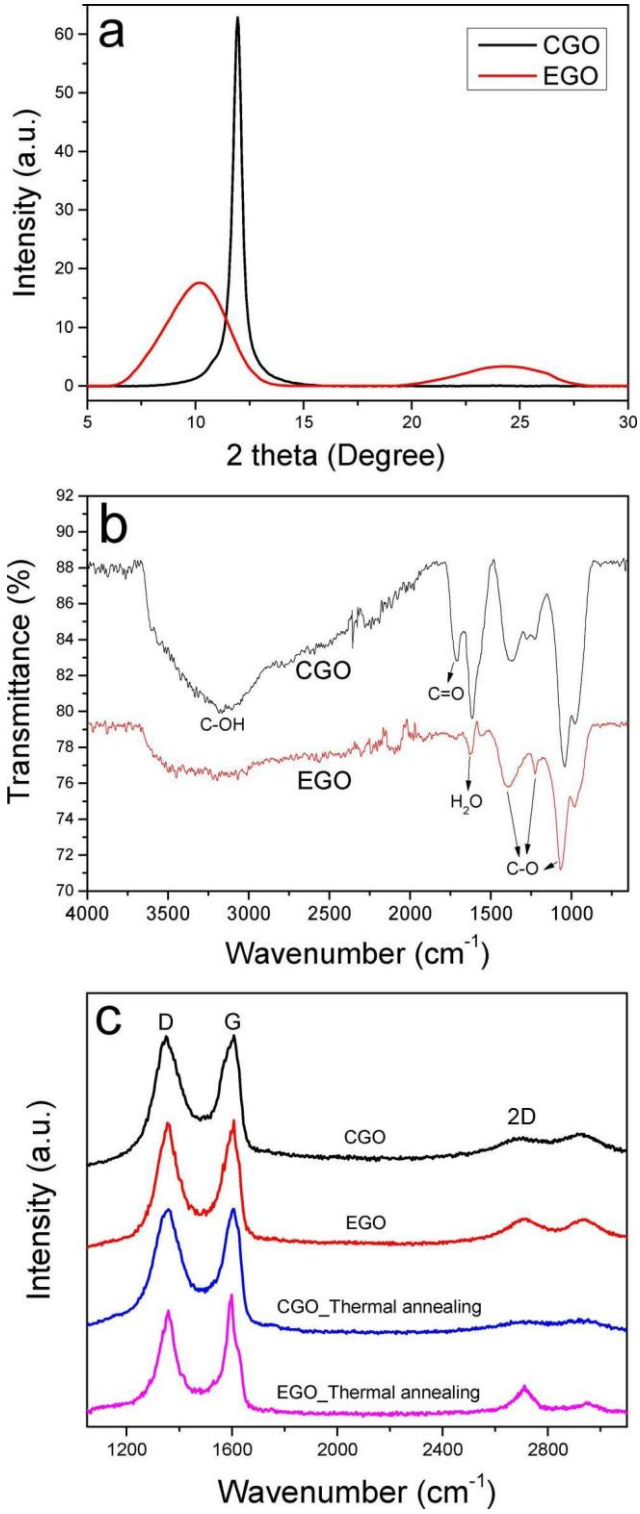

Figure 4. (a) XRD patterns and (b) ATR-FTIR spectrum of CGO and EGO film; and (c) Raman spectrum of individual CGO and EGO sheet before and after thermal annealing at 200 °C for 1 h.

that from the (1−210) plane (Figure 2d), further confirming that the observed EGO was single layer.[48] More low-magnification TEM images are shown in Figure S1, revealing folded and crumpled structures of EGO sheets. SEM images of the EGO sheets (Figure S2), drop-casted on Si wafer, show that the lateral size of EGO sheets were about 1 to 10 μm.

Atomic force microscopy (AFM) was employed to examine the thickness of the EGO sheets. Figure 3a shows several stacked EGO sheets with a folded and crumpled EGO sheet morphology, which is the characteristic of single-layered EGO. By drawing a line profile across the EGO sheet as shown in Figure 3b, the thickness of the EGO sheet was found to be 1.5 nm which was due to the presence of oxygen functional groups on the EGO sheet. Another typical AFM image of a single-layer EGO sheet is shown in Figure S3a and its corresponding AFM height profile (Figure S3b) again shows a thickness of 1.5 nm. To estimate the fraction of single layer EGO in the products, several AFM images (Figure S4) were analyzed and their corresponding line profiles were recorded for statistical analysis of the thickness. The number fractions of EGO sheet are shown in Figure 3c. The number fraction of monolayer EGO in the product was about 66%. To calculate the mass fraction, the areas of all the graphene sheets were measured and calculated according to the equation:[48]

$$\frac{M_{\mathrm{Ind}}}{M_{\mathrm{T}}} = \frac{\sum_{\mathrm{Individuals}} A_{\mathrm{monolayer}}}{\sum_{\mathrm{Allflakes}} N_{\mathrm{monolayer}} A_{\mathrm{monolayer}}}$$

where M_{Ind} is the mass of all monolayer graphene, M_{T} is the mass of all EGO sheets, $A_{\mathrm{monolayer}}$ is the area of a monolayer, and $N_{\mathrm{monolayer}}$ represents the number of monolayers in a given flake. The mass fraction (Figure 3d) of a single-layer EGO sheet in product was calculated to be about 33 wt %. It is important to note that the thicknesses of few-layered EGO were multiples of 1.5 nm (i.e., the thickness of single sheet EGO), and this indicates that the EGO products were predominantly oxidized, despite being stacked. The observed few-layered EGO may be due to incomplete exfoliation to single layer EGO or restacking during the drying step.

Chemical Properties of EGO. XRD was utilized to confirm the conversion of graphite to graphite oxide. XRD patterns of EGO and CGO produced by the Hummers method are shown in Figure 4a. EGO exhibited a broad, main peak at around 10.1°, indicating an interlayer distance of 8.75 Å. This expanded interlayer distance is due to the oxidation of graphite to EGO. At about 24.1° (d = 3.69 Å), there is a small broad peak which is attributed to randomly stacked single or few layer graphene sheets which were not oxidized. In comparison, CGO exhibited a single sharp peak at 11.5°, which corresponds to the interlayer distance of 7.64 Å. The attenuated total reflection Fourier transform infrared (ATR-FTIR) spectra for CGO and EGO films are shown in Figure 4b. For CGO, the spectrum shows the presence of C═O (at 1706 cm^{-1}), various types of C−O (at 1370 cm^{-1}, 1278−1230 cm^{-1}, 1042 cm^{-1}), O−H (at 2850−3600 cm^{-1}), and water bending modes (at 1614 cm^{-1}).[27,49−51] EGO also exhibits peaks of various types of C−O (at 1388 cm^{-1}, 1226 cm^{-1}, 1066 cm^{-1}), O−H (at 2850−3600 cm^{-1}) and water bending modes (at 1630 cm^{-1}), suggesting oxidation of graphite during the process. However, the very weak peak at about 1716 cm^{-1} for EGO indicated that a lower concentration of C═O groups was presented in EGO, compared with CGO. Figure 4c shows the Raman spectra of individual EGO and CGO sheet before and after thermal annealing at 200 °C in air for 1 h. Both CGO and EGO showed a prominent D peak with intensity comparable to the G peak, indicating a structural disorder due to oxidation. After thermal annealing at 200 °C in air for 1 h, there was no obvious change in intensity of D peak for CGO. Whereas, EGO clearly displayed a decrease in D peak intensity after thermal annealing, which is due to increase in

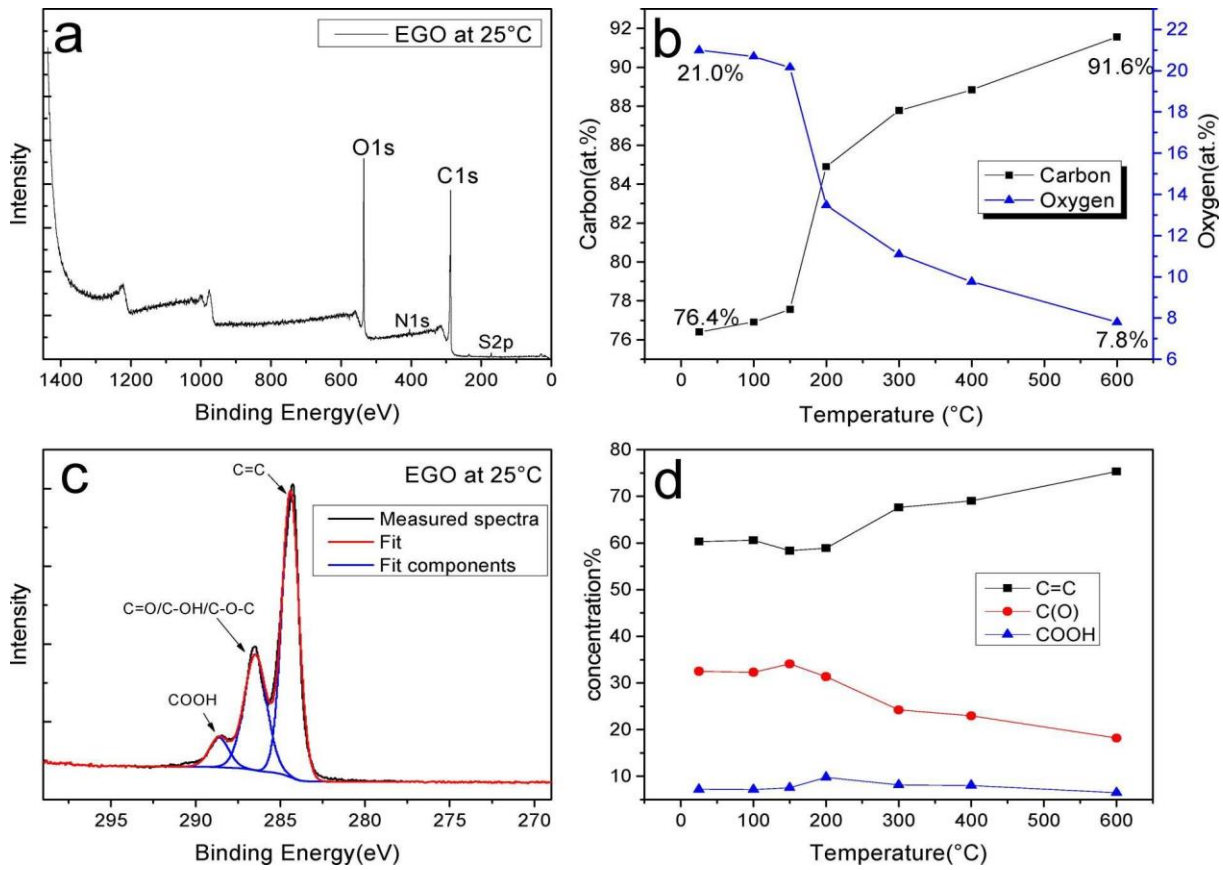

Figure 5. (a) XPS survey spectra of EGO at room temperature. (b) Carbon and oxygen content of EGO after heating at different temperatures. (c) XPS C 1s spectra of EGO. (d) C═C, C(O), and COOH concentration in EGO after heating at different temperatures.

size of in-plane sp^2 domains. In addition, G peak of EGO shifted to lower frequency and became sharper after heat treatment, indicating less disorder.[52] The low and broad 2D peaks of CGO and EGO are attributed to steric effects of oxygen moieties and reduction in sp^2 domains.[53,54] After thermal annealing, the 2D peak of EGO increased and sharpened, which also supports the fact of less disorder. Together, these results indicate more oxygen functional groups and smaller in-plane sp^2 domains in CGO than EGO, which is due to harsher oxidation conditions during CGO synthesis.[38] After thermal annealing, EGO showed larger sp^2 domains and recovered to a more graphitic structure than CGO.

Figure 5a shows X-ray photoelectron spectroscopy (XPS) survey scan of as-produced EGO with predominately carbon and oxygen signal, and little residual electrolyte ($(NH_4)_2SO_4$). As-produced EGO contained approximately 21.0 at. % oxygen content and 76.4 at. % carbon content (correction for their atomic sensitivity factors) with C/O ratio of 3.64, which is larger than typical C/O ratios of CGO (approximately 2−2.6).[55−58] The high-resolution XPS C 1s spectrum (Figure 5c) can be fitted into three components attributed to the graphitic carbon (C═C, 284.4 eV, 60.3%), carbon bonded to single oxygen (C═O/C−OH/C−O−C, 286.5 eV, 32.5%), and carboxyl carbon (COOH, 288.7 eV, 7.2%). In comparison to previously reported CGO produced using the Hummer's method, the as-produced EGO appears to contain relatively less oxygen-containing moieties, in particular a lower carboxyl content.[59,54]

Incremental heating of EGO was carried out in an ultrahigh vacuum preparation chamber and the changes in carbon, oxygen, nitrogen, and sulfur contents were monitored, with the results shown in Table S1. The content changes of carbon and oxygen with temperature were plotted in Figure 5b. There was a sharp decrease in oxygen content (accompanied by increase in carbon content) after heating of the sample to 200 °C, and this was reflected in the changes of the three C 1s components, as shown in Figure 5d. The graphitic carbon component increased while the functionalized carbon components decreased, showing the temperature-dependent elimination of oxygen functional groups (thermal reduction process). Figure S5 shows the thermal gravimetric analysis (TGA) of EGO and CGO, which shows that EGO (34.5 wt %) experienced less total weight loss percentage than CGO (46 wt %) at 600 °C. This is consistent with EGO having less oxygen functional groups susceptible to thermal reduction. The most dramatic weight loss occurred at around 137−176 °C for EGO and 164−195 °C for CGO. This implies that the oxygen functional groups in EGO can be removed at lower temperature than those of CGO.

Electrical Properties of EGO. Thermal reduction of freestanding EGO and CGO films was carried out at 200 °C in air and their sheet resistances were measured after 0, 2, 5, 10, 15, 30, and 60 min of thermal reduction using four point probe measurement. Their corresponding conductivities were calculated taking account of their respective thicknesses (measured by scanning electron microscope), and the results are shown in Figure 6a. The initial conductivity of EGO (before thermal

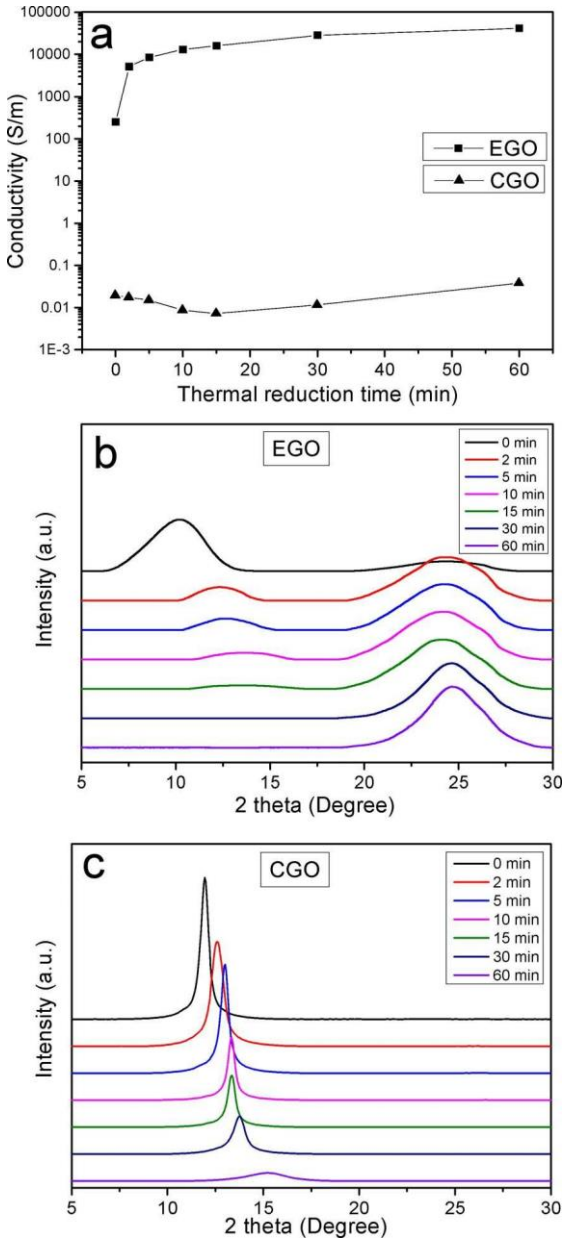

Figure 6. (a) Conductivity change of EGO and CGO films after various thermal reduction time at 200 °C in an oven (air atmosphere). (b) XRD spectrum of EGO film after various thermal reduction times. (c) XRD spectrum of CGO film after various thermal reduction times.

reduction) was about 250 S/m which rapidly increased to about 10 000 S/m after heating for 5 min, saturating at about 41 000 S/m after 60 min. In comparison, there was no considerable increase in conductivity for CGO film after heating at 200 °C for 60 min. Similar thermal behavior was observed on the CGO synthesized (CGO-lab) with the same graphite source (as used in EGO), as shown in Figure S6. The thermally induced structural change in the EGO and CGO film was monitored by XRD, and the XRD patterns of EGO and CGO films after different thermal reduction times are shown in Figure 6b,c, respectively. With increased thermal reduction time, the EGO peak (10.1°) in the XRD spectrum of EGO became smaller and shifted toward higher 2Θ, while the graphite peak (24.1°) grew larger and sharper. This is associated with a decrease in the

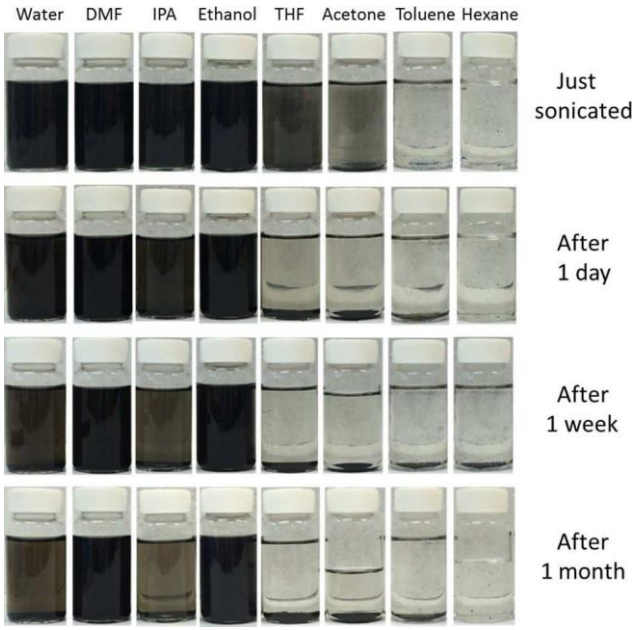

Figure 7. EGO dispersion in solvents: water, DMF, IPA, ethanol, THF, acetone, toluene, hexane after just sonicated, 1 day, 1 week, and 1 month.

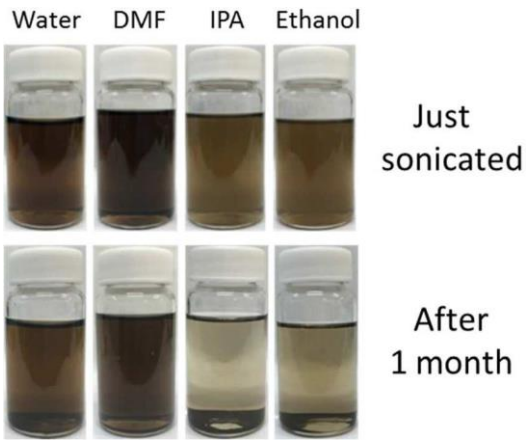

Figure 8. GO dispersion in solvents: water, DMF, IPA, ethanol after just sonicated and 1 month.

interlayer distance as oxygen functionalities were removed and indicates that the facile thermal reduction of the EGO to highly pristine graphene layers which could effectively and orderly restacked to the graphitic form. On the other hand, the GO peak (11.5°) of CGO film decreased gradually with a shift to higher 2Θ but with no observable graphite peak even after 60 min of heating. In fact, the reported XRD patterns of fully reduced CGO, via various chemical or physical methods, only showed a weak and broad graphite peak due to the disordered restacking of crumpled or structurally defective rGO sheets.[54,60−64]

Dispersibility of EGO. EGO was dispersed by sonication (30 min) in different solvents (water, DMF, IPA, ethanol, THF, acetone, toluene, and hexane) to a fixed concentration of 0.1 mg/mL for all of the solvents. Figure 7 shows the photographs of all the EGO dispersions immediately after sonication, after standing for 1 day, 1 week, and 1 month. For the "just sonicated" samples, it was observed that EGO could be well-

dispersed in water, DMF, IPA, and ethanol but not in THF, acetone, toluene, and hexane. After 1 month, sedimentation of EGO was observed in IPA and water but not in DMF or ethanol, which demonstrates the long-term stability of EGO in DMF and ethanol. To explain the long term stability of EGO in DMF and ethanol, zeta potentials of EGO in water, DMF, and ethanol were measured, shown in Table S2. Zeta potentials of EGO in DMF, ethanol, and water were −53.1, −41.9, and −33.3 mV respectively, which were all more negative than −30 mV and hence had sufficient electrostatic repulsion for long-term stability.[7] For comparison, CGO dispersions of the same concentration were prepared in water, DMF, IPA, and ethanol (Figure 8), and it was obvious that CGO showed sedimentation in ethanol after standing for 1 month. As described by Paredes et al., CGO prepared by the Hummers method displayed long-term stability in water, DMF, and THF but short-term stability in IPA, ethanol, acetone.[5] The dispersibility of EGO was further tested at a higher starting concentration (3 mg/mL) in water, DMF, and ethanol. EGO concentration of 2.1, 2.5, and 2.6 mg/mL was retained in water, DMF, and ethanol, respectively, after 24 h of sedimentation (Table S3).

Recycling of Electrolyte. Solvent and electrolyte can constitute a significant cost and waste generation in most chemical processes. We investigated the possibility of recycling of the electrolyte in our electrochemical process because the EGO product could be easily extracted from the electrolytic bath. Three sequential batches (EGO-1, EGO-2 and EGO-3) were produced under the same conditions with recycled electrolytic bath: 1 M H_2SO_4 in saturated $(NH_4)_2SO_4$ aqueous solution (with excess $(NH_4)_2SO_4$ salt crystals in the bath). After each batch, there was a small loss of electrolyte volume due to evaporation and the electrolytic decomposition of water, and hence, water was added to make up similar electrolyte volume for all batches. Across all batches, the reaction yield and quality of EGO were similar as indicated by the consistent percentage yield of EGO and their XRD peaks ratios (Table S4). This demonstrates the feasibility of electrolyte recycling and possibility of conversion to a continuous production process.

■ CONCLUSIONS

In conclusion, we have developed a novel mechanically assisted electrochemical method to produce graphene oxide directly from loose graphite flakes, which avoids the need to preform a graphite electrode. The stirring effect enabled repeated physical contact between the incompletely exfoliated graphite and the working electrode, facilitating further oxidation and exfoliation. With this greener electrochemical method, hazardous chemical oxidants are not required; a simple purification process (water rinsing) is sufficient and the electrolyte can be easily recycled. From an industrial perspective, these advantages are highly desirable for the large-scale and cost-effective production of GO.

Moreover, the method can produce a new type of GO with distinct properties. The produced EGO has a lower oxidation degree and less physical defects than the conventional CGO; yet interestingly, it shows better long-term stability in ethanol. While CGO requires chemical or high thermal treatment for complete reduction, EGO was effectively converted at 200 °C and ambient condition to its highly conductive form. The good dispersibility of EGO and excellent conductivity of thermally processed EGO, coupled with the facile reduction ability, make it an ideal conductive nanofiller in heat-sensitive matrices. For future work, the development of this mechanically assisted electrochemical approach will be pursued and the unique properties of EGO will be capitalized in niche applications.

■ ASSOCIATED CONTENT

Supporting Information

The Supporting Information is available free of charge on the ACS Publications website at DOI: 10.1021/acs.chemmater.6b04415.

Additional experimental data on the following topics are available: TEM images of EGO, SEM images of EGO, AFM images of EGO, XPS elemental composition analysis of EGO, TGA curves of EGO and CGO, Zeta potentials of EGO in various solvent, concentrations of EGO in various solvent, reaction yield of EGO with recycled electrolyte, and reaction schemes of electrochemical oxidation of graphite (PDF)

■ AUTHOR INFORMATION

Corresponding Author

* (Y.L.Z.) E-mail: y.zhong@griffith.edu.au.

Notes

The authors declare no competing financial interest.

■ ACKNOWLEDGMENTS

The authors acknowledge the funding support from Australian Research Council (DE 140101662, DP140101501 and FT150100450), Baosteel-Australia Joint Research and Development Centre (BA11006) and the use of the SEM and TEM facilities at the Monash Centre for Electron Microscopy. Part of this research was undertaken on the soft X-ray beamline at the Australian Synchrotron, Victoria, Australia (beam time awards AS152/SXR/R9389).

■ REFERENCES

(1) Dreyer, D. R.; Park, S.; Bielawski, C. W.; Ruoff, R. S. The Chemistry of Graphene Oxide. *Chem. Soc. Rev.* **2010**, *39*, 228−240.

(2) Loh, K. P.; Bao, Q.; Ang, P. K.; Yang, J. The Chemistry of Graphene. *J. Mater. Chem.* **2010**, *20*, 2277−2289.

(3) Allen, M. J.; Tung, V. C.; Kaner, R. B. Honeycomb Carbon: A Review of Graphene. *Chem. Rev.* **2010**, *110*, 132−145.

(4) Li, D.; Kaner, R. B. Graphene-Based Materials. *Science* **2008**, *320*, 1170−1171.

(5) Paredes, J. I.; Villar-Rodil, S.; Martínez-Alonso, A.; Tascón, J. M. D. Graphene Oxide Dispersions in Organic Solvents. *Langmuir* **2008**, *24*, 10560−10564.

(6) Texter, J. Graphene Dispersions. *Curr. Opin. Colloid Interface Sci.* **2014**, *19*, 163−174.

(7) Li, D.; Muller, M. B.; Gilje, S.; Kaner, R. B.; Wallace, G. G. Processable Aqueous Dispersions of Graphene Nanosheets. *Nat. Nanotechnol.* **2008**, *3*, 101−105.

(8) Eigler, S.; Hirsch, A. Chemistry with Graphene and Graphene Oxide—Challenges for Synthetic Chemists. *Angew. Chem., Int. Ed.* **2014**, *53*, 7720−7738.

(9) Sun, Z.; James, D. K.; Tour, J. M. Graphene Chemistry: Synthesis and Manipulation. *J. Phys. Chem. Lett.* **2011**, *2*, 2425−2432.

(10) Becerril, H. A.; Mao, J.; Liu, Z.; Stoltenberg, R. M.; Bao, Z.; Chen, Y. Evaluation of Solution-Processed Reduced Graphene Oxide Films as Transparent Conductors. *ACS Nano* **2008**, *2*, 463−470.

(11) Kucinskis, G.; Bajars, G.; Kleperis, J. Graphene in Lithium Ion Battery Cathode Materials: A review. *J. Power Sources* **2013**, *240*, 66−79.

(12) Yang, Y.; Wang, C.; Yue, B.; Gambhir, S.; Too, C. O.; Wallace, G. G. Electrochemically Synthesized Polypyrrole/Graphene Composite Film for Lithium Batteries. *Adv. Energy Mater.* **2012**, *2*, 266−272.
(13) Stoller, M. D.; Park, S.; Zhu, Y.; An, J.; Ruoff, R. S. Graphene-Based Ultracapacitors. *Nano Lett.* **2008**, *8*, 3498−3502.
(14) Antiohos, D.; Pingmuang, K.; Romano, M. S.; Beirne, S.; Romeo, T.; Aitchison, P.; Minett, A.; Wallace, G.; Phanichphant, S.; Chen, J. Manganosite−Microwave Exfoliated Graphene Oxide Composites for Asymmetric Supercapacitor Device Applications. *Electrochim. Acta* **2013**, *101*, 99−108.
(15) Yang, X.; Zhu, J.; Qiu, L.; Li, D. Bioinspired Effective Prevention of Restacking in Multilayered Graphene Films: Towards the Next Generation of High-Performance Supercapacitors. *Adv. Mater.* **2011**, *23*, 2833−2838.
(16) Vivekchand, S. R. C.; Rout, C. S.; Subrahmanyam, K. S.; Govindaraj, A.; Rao, C. N. R. Graphene-Based Electrochemical Supercapacitors. *Proc. - Indian Acad. Sci., Chem. Sci.* **2008**, *120*, 9−13.
(17) Wang, Y.; Shi, Z.; Huang, Y.; Ma, Y.; Wang, C.; Chen, M.; Chen, Y. Supercapacitor Devices Based on Graphene Materials. *J. Phys. Chem. C* **2009**, *113*, 13103−13107.
(18) Velten, J.; Mozer, A. J.; Li, D.; Officer, D.; Wallace, G.; Baughman, R.; Zakhidov, A. Carbon Nanotube/Graphene Nanocomposite as Efficient Counter Electrodes in Dye-Sensitized Solar Cells. *Nanotechnology* **2012**, *23*, 085201.
(19) Robinson, J. T.; Perkins, F. K.; Snow, E. S.; Wei, Z.; Sheehan, P. E. Reduced Graphene Oxide Molecular Sensors. *Nano Lett.* **2008**, *8*, 3137−3140.
(20) Mohanty, N.; Berry, V. Graphene-Based Single-Bacterium Resolution Biodevice and DNA Transistor: Interfacing Graphene Derivatives with Nanoscale and Microscale Biocomponents. *Nano Lett.* **2008**, *8*, 4469−4476.
(21) Zhu, Y.; Murali, S.; Cai, W.; Li, X.; Suk, J. W.; Potts, J. R.; Ruoff, R. S. Graphene and Graphene Oxide: Synthesis, Properties, and Applications. *Adv. Mater.* **2010**, *22*, 3906−3924.
(22) Sayyar, S.; Murray, E.; Thompson, B. C.; Gambhir, S.; Officer, D. L.; Wallace, G. G. Covalently Linked Biocompatible Graphene/Polycaprolactone Composites for Tissue Engineering. *Carbon* **2013**, *52*, 296−304.
(23) Brodie, B. C. On the Atomic Weight of Graphite. *Philos. Trans. R. Soc.* **1859**, *149*, 249−259.
(24) Staudenmaier, L. Verfahren zur Darstellung der Graphitsäure. *Ber. Dtsch. Chem. Ges.* **1898**, *31*, 1481−1487.
(25) Charpy, G. Sur la Formation de L'oxyde Graphitique et la Définition du Graphite. *C. R. Hebd. Séances Acad. Sci.* **1909**, *148*, 920−923.
(26) Hummers, W. S.; Offeman, R. E. Preparation of Graphitic Oxide. *J. Am. Chem. Soc.* **1958**, *80*, 1339−1339.
(27) Marcano, D. C.; Kosynkin, D. V.; Berlin, J. M.; Sinitskii, A.; Sun, Z.; Slesarev, A.; Alemany, L. B.; Lu, W.; Tour, J. M. Improved Synthesis of Graphene Oxide. *ACS Nano* **2010**, *4*, 4806−4814.
(28) Chen, J.; Yao, B.; Li, C.; Shi, G. An Improved Hummers Method for Eco-Friendly Synthesis of Graphene Oxide. *Carbon* **2013**, *64*, 225−229.
(29) Hirata, M.; Gotou, T.; Horiuchi, S.; Fujiwara, M.; Ohba, M. Thin-Film Particles of Graphite Oxide: High-Yield Synthesis and Flexibility of the Particles. *Carbon* **2004**, *42*, 2929−2937.
(30) Eigler, S.; Enzelberger-Heim, M.; Grimm, S.; Hofmann, P.; Kroener, W.; Geworski, A.; Dotzer, C.; Röckert, M.; Xiao, J.; Papp, C.; Lytken, O.; Steinrück, H.-P.; Müller, P.; Hirsch, A. Wet Chemical Synthesis of Graphene. *Adv. Mater.* **2013**, *25*, 3583−3587.
(31) Voiry, D.; Yang, J.; Kupferberg, J.; Fullon, R.; Lee, C.; Jeong, H. Y.; Shin, H. S.; Chhowalla, M. High-quality Graphene via Microwave Reduction of Solution-Exfoliated Graphene Oxide. *Science* **2016**, *353*, 1413−1416.
(32) Peng, L.; Xu, Z.; Liu, Z.; Wei, Y.; Sun, H.; Li, Z.; Zhao, X.; Gao, C. An Iron-Based Green Approach to 1-h Production of Single-Layer Graphene Oxide. *Nat. Commun.* **2015**, *6*, 5716.
(33) Eigler, S. Graphite Sulphate - A Precursor to Graphene. *Chem. Commun.* **2015**, *51*, 3162−3165.
(34) Koch, K. R. Oxidation by Mn_2O_7: An Impressive Demonstration of the Powerful Oxidizing Property of Dimanganeseheptoxide. *J. Chem. Educ.* **1982**, *59*, 973.
(35) Yeh, C.-N.; Raidongia, K.; Shao, J.; Yang, Q.-H.; Huang, J. On the Origin of the Stability of Graphene Oxide Membranes in Water. *Nat. Chem.* **2015**, *7*, 166−170.
(36) Eigler, S.; Dotzer, C.; Hirsch, A. Visualization of Defect Densities in Reduced Graphene Oxide. *Carbon* **2012**, *50*, 3666−3673.
(37) Eda, G.; Fanchini, G.; Chhowalla, M. Large-Area Ultrathin Films of Reduced Graphene Oxide as a Transparent and Flexible Electronic Material. *Nat. Nanotechnol.* **2008**, *3*, 270−274.
(38) Stankovich, S.; Dikin, D. A.; Piner, R. D.; Kohlhaas, K. A.; Kleinhammes, A.; Jia, Y.; Wu, Y.; Nguyen, S. T.; Ruoff, R. S. Synthesis of Graphene-Based Nanosheets via Chemical Reduction of Exfoliated Graphite Oxide. *Carbon* **2007**, *45*, 1558−1565.
(39) Low, C. T. J.; Walsh, F. C.; Chakrabarti, M. H.; Hashim, M. A.; Hussain, M. A. Electrochemical Approaches to the Production of Graphene Flakes and their Potential Applications. *Carbon* **2013**, *54*, 1−21.
(40) Yu, P.; Lowe, S. E.; Simon, G. P.; Zhong, Y. L. Electrochemical Exfoliation of Graphite and Production of Functional Graphene. *Curr. Opin. Colloid Interface Sci.* **2015**, *20*, 329−338.
(41) Wang, J.; Manga, K. K.; Bao, Q.; Loh, K. P. High-Yield Synthesis of Few-Layer Graphene Flakes through Electrochemical Expansion of Graphite in Propylene Carbonate Electrolyte. *J. Am. Chem. Soc.* **2011**, *133*, 8888−8891.
(42) Parvez, K.; Wu, Z.-S.; Li, R.; Liu, X.; Graf, R.; Feng, X.; Müllen, K. Exfoliation of Graphite into Graphene in Aqueous Solutions of Inorganic Salts. *J. Am. Chem. Soc.* **2014**, *136*, 6083−6091.
(43) Liu, J.; Yang, H.; Zhen, S. G.; Poh, C. K.; Chaurasia, A.; Luo, J.; Wu, X.; Yeow, E. K. L.; Sahoo, N. G.; Lin, J.; Shen, Z. A Green Approach to the Synthesis of High-Quality Graphene Oxide Flakes via Electrochemical Exfoliation of Pencil Core. *RSC Adv.* **2013**, *3*, 11745−11750.
(44) Su, C.-Y.; Lu, A.-Y.; Xu, Y.; Chen, F.-R.; Khlobystov, A. N.; Li, L.-J. High-Quality Thin Graphene Films from Fast Electrochemical Exfoliation. *ACS Nano* **2011**, *5*, 2332−2339.
(45) Zhong, Y. L.; Swager, T. M. Enhanced Electrochemical Expansion of Graphite for in Situ Electrochemical Functionalization. *J. Am. Chem. Soc.* **2012**, *134*, 17896−17899.
(46) Yang, S.; Lohe, M. R.; Müllen, K.; Feng, X. New-Generation Graphene from Electrochemical Approaches: Production and Applications. *Adv. Mater.* **2016**, *28*, 6213−6221.
(47) Kovtyukhova, N. I.; Ollivier, P. J.; Martin, B. R.; Mallouk, T. E.; Chizhik, S. A.; Buzaneva, E. V.; Gorchinskiy, A. D. Layer-by-Layer Assembly of Ultrathin Composite Films from Micron-Sized Graphite Oxide Sheets and Polycations. *Chem. Mater.* **1999**, *11*, 771−778.
(48) Hernandez, Y.; Nicolosi, V.; Lotya, M.; Blighe, F. M.; Sun, Z.; De, S.; McGovern, I. T.; Holland, B.; Byrne, M.; Gun'Ko, Y. K.; Boland, J. J.; Niraj, P.; Duesberg, G.; Krishnamurthy, S.; Goodhue, R.; Hutchison, J.; Scardaci, V.; Ferrari, A. C.; Coleman, J. N. High-Yield Production of Graphene by Liquid-Phase Exfoliation of Graphite. *Nat. Nanotechnol.* **2008**, *3*, 563−568.
(49) Xu, Y.; Bai, H.; Lu, G.; Li, C.; Shi, G. Flexible Graphene Films via the Filtration of Water-Soluble Noncovalent Functionalized Graphene Sheets. *J. Am. Chem. Soc.* **2008**, *130*, 5856−5857.
(50) Stankovich, S.; Piner, R. D.; Nguyen, S. T.; Ruoff, R. S. Synthesis and Exfoliation of Isocyanate-Treated Graphene Oxide Nanoplatelets. *Carbon* **2006**, *44*, 3342−3347.
(51) Dimiev, A. M.; Alemany, L. B.; Tour, J. M. Graphene Oxide. Origin of Acidity, Its Instability in Water, and a New Dynamic Structural Model. *ACS Nano* **2013**, *7*, 576−588.
(52) Kudin, K. N.; Ozbas, B.; Schniepp, H. C.; Prud'homme, R. K.; Aksay, I. A.; Car, R. Raman Spectra of Graphite Oxide and Functionalized Graphene Sheets. *Nano Lett.* **2008**, *8*, 36−41.
(53) Dresselhaus, M. S.; Jorio, A.; Hofmann, M.; Dresselhaus, G.; Saito, R. Perspectives on Carbon Nanotubes and Graphene Raman Spectroscopy. *Nano Lett.* **2010**, *10*, 751−758.

(54) Ganguly, A.; Sharma, S.; Papakonstantinou, P.; Hamilton, J. Probing the Thermal Deoxygenation of Graphene Oxide Using High-Resolution In Situ X-ray-Based Spectroscopies. *J. Phys. Chem. C* **2011**, *115*, 17009−17019.
(55) Jeong, H.-K.; Lee, Y. P.; Lahaye, R. J. W. E.; Park, M.-H.; An, K. H.; Kim, I. J.; Yang, C.-W.; Park, C. Y.; Ruoff, R. S.; Lee, Y. H. Evidence of Graphitic AB Stacking Order of Graphite Oxides. *J. Am. Chem. Soc.* **2008**, *130*, 1362−1366.
(56) Hontoria-Lucas, C.; López-Peinado, A. J.; López-González, J. d. D.; Rojas-Cervantes, M. L.; Martín-Aranda, R. M. Study of Oxygen-Containing Groups in a Series of Graphite Oxides: Physical and Chemical Characterization. *Carbon* **1995**, *33*, 1585−1592.
(57) Szabó, T.; Berkesi, O.; Forgó, P.; Josepovits, K.; Sanakis, Y.; Petridis, D.; Dékány, I. Evolution of Surface Functional Groups in a Series of Progressively Oxidized Graphite Oxides. *Chem. Mater.* **2006**, *18*, 2740−2749.
(58) Schniepp, H. C.; Li, J.-L.; McAllister, M. J.; Sai, H.; Herrera-Alonso, M.; Adamson, D. H.; Prud'homme, R. K.; Car, R.; Saville, D. A.; Aksay, I. A. Functionalized Single Graphene Sheets Derived from Splitting Graphite Oxide. *J. Phys. Chem. B* **2006**, *110*, 8535−8539.
(59) Mattevi, C.; Eda, G.; Agnoli, S.; Miller, S.; Mkhoyan, K. A.; Celik, O.; Mastrogiovanni, D.; Granozzi, G.; Garfunkel, E.; Chhowalla, M. Evolution of Electrical, Chemical, and Structural Properties of Transparent and Conducting Chemically Derived Graphene Thin Films. *Adv. Funct. Mater.* **2009**, *19*, 2577−2583.
(60) Chen, H.; Müller, M. B.; Gilmore, K. J.; Wallace, G. G.; Li, D. Mechanically Strong, Electrically Conductive, and Biocompatible Graphene Paper. *Adv. Mater.* **2008**, *20*, 3557−3561.
(61) Abouimrane, A.; Compton, O. C.; Amine, K.; Nguyen, S. T. Non-Annealed Graphene Paper as a Binder-Free Anode for Lithium-Ion Batteries. *J. Phys. Chem. C* **2010**, *114*, 12800−12804.
(62) Zhang, K.; Zhang, Y.; Wang, S. Enhancing Thermoelectric Properties of Organic Composites through Hierarchical Nanostructures. *Sci. Rep.* **2013**, *3*, 3448.
(63) Hsiao, M.-C.; Ma, C.-C. M.; Chiang, J.-C.; Ho, K.-K.; Chou, T.-Y.; Xie, X.; Tsai, C.-H.; Chang, L.-H.; Hsieh, C.-K. Thermally Conductive and Electrically Insulating Epoxy Nanocomposites with Thermally Reduced Graphene Oxide-Silica Hybrid Nanosheets. *Nanoscale* **2013**, *5*, 5863−5871.
(64) Wang, Z.-L.; Xu, D.; Huang, Y.; Wu, Z.; Wang, L.-M.; Zhang, X.-B. Facile, Mild and Fast Thermal-Decomposition Reduction of Graphene Oxide in Air and its Application in High-Performance Lithium Batteries. *Chem. Commun.* **2012**, *48*, 976−978.

Supporting Information

Mechanically-assisted Electrochemical Production of Graphene Oxide

Pei Yu,† Zhiming Tian,† Sean E. Lowe,‡ Jingchao Song,† Zhirui Ma,† Xin Wang,† Zhao Jun Han,§,# Qiaoliang Bao,† George P. Simon,† Dan Li,† Yu Lin Zhong*,‡

†Department of Materials Science and Engineering, Monash University, Clayton, Victoria 3800, Australia

‡Centre for Clean Environment and Energy, Gold Coast Campus, Griffith University, Gold Coast, Queensland 4222, Australia

§CSIRO Manufacturing, 36 Bradfield Road, Lindfield, New South Wales 2070, Australia

#Department of Materials, University of Oxford, Parks Road, Oxford, OX1 3PH, United Kingdom

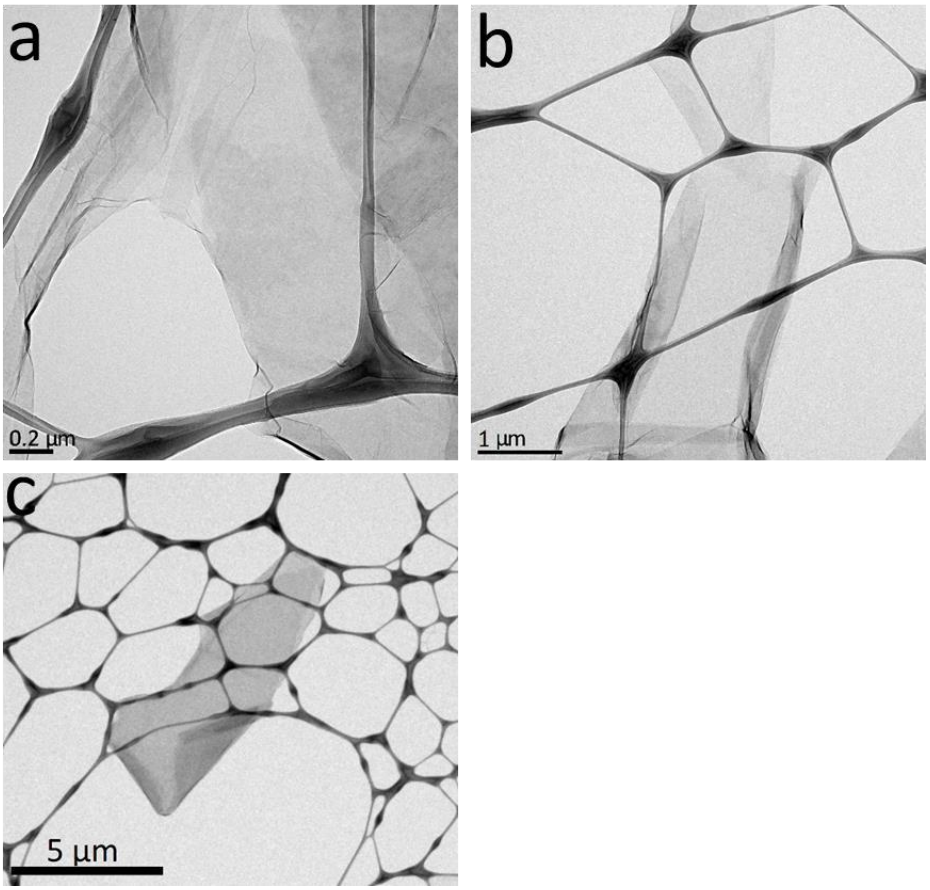

Figure S1. Low-magnification TEM images of EGO sheets with scale bar of (a) 0.2 µm, (b) 1 µm and (c) 5 µm.

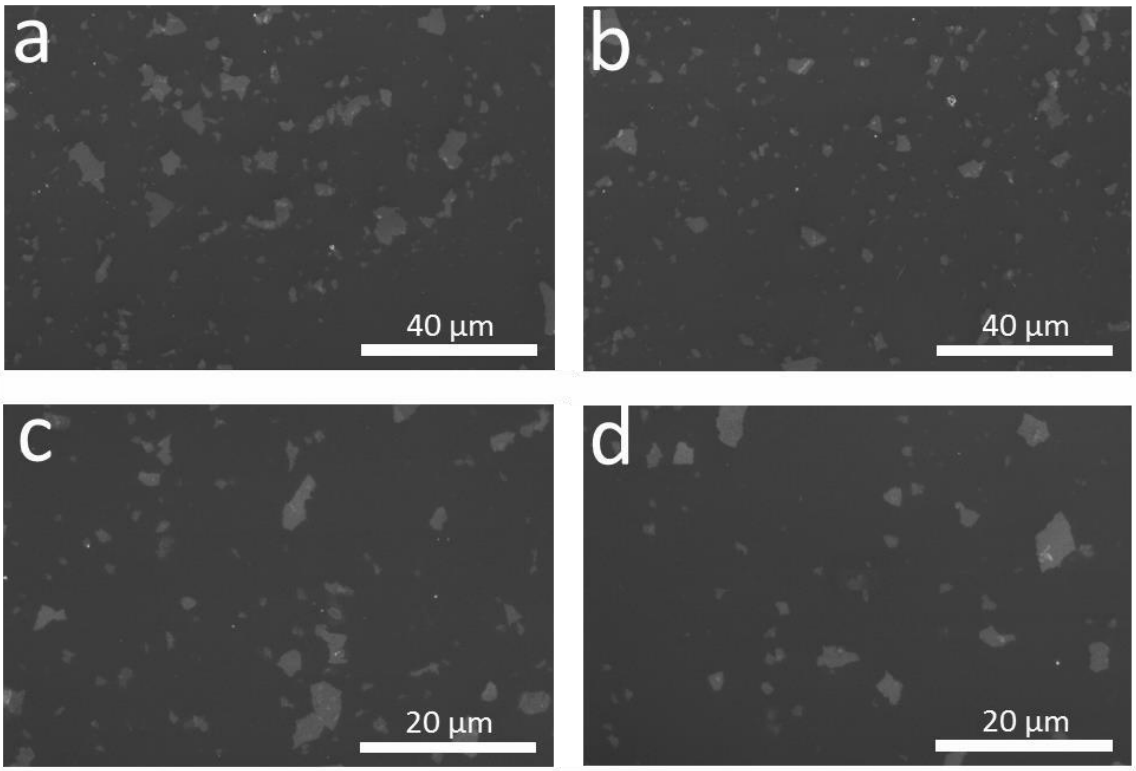

Figure S2. SEM images of EGO sheets on Si wafer with scale bar of (a)(b) 40 µm and (c)(d) 20 µm.

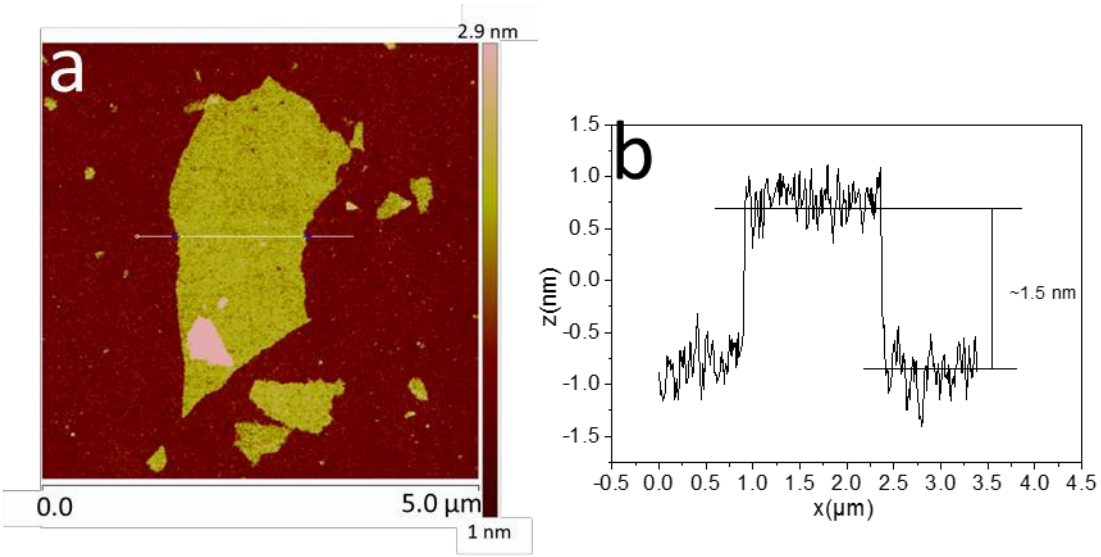

Figure S3. (a) AFM image of monolayer EGO sheets and (b) line profile of EGO sheet drawn in (a).

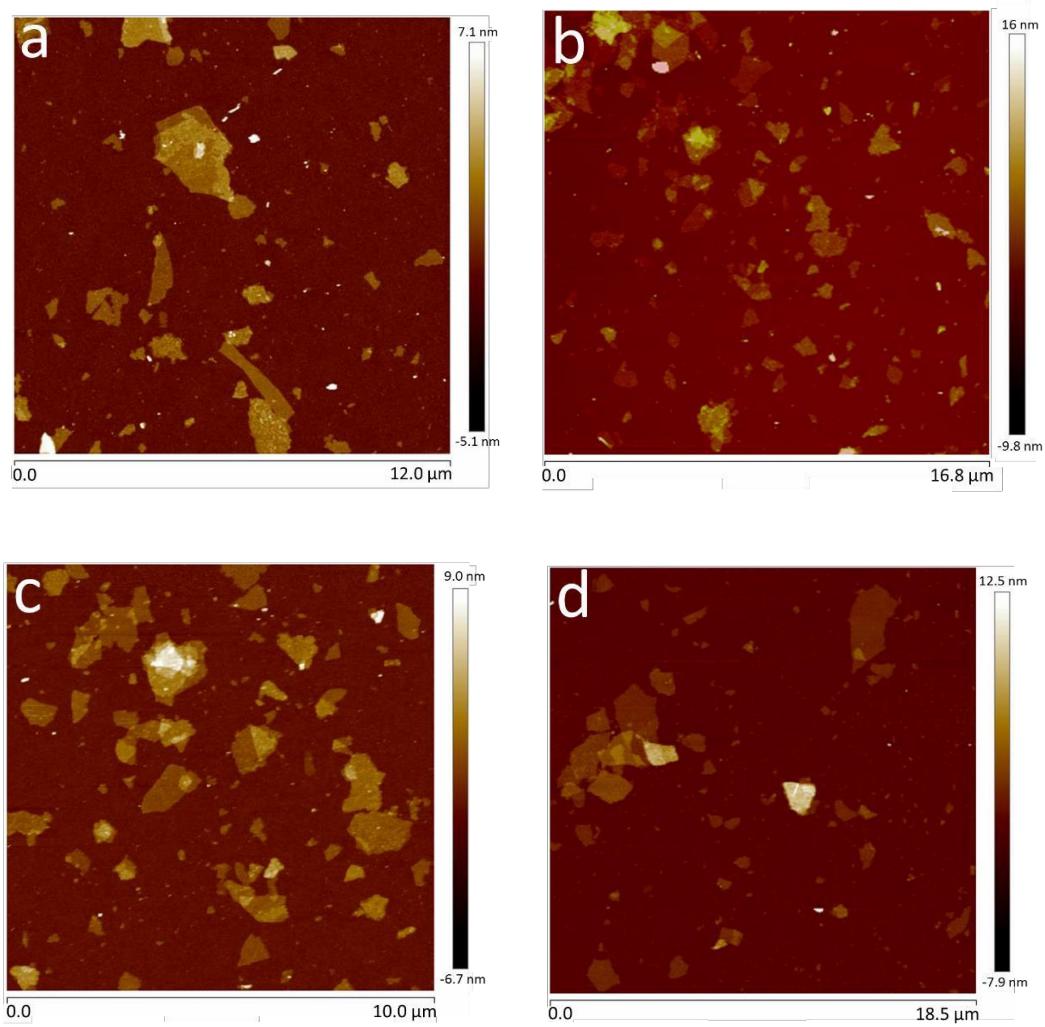

Figure S4. AFM images of EGO sheets for statistical calculation on the layer number distribution.

Table S1. Carbon, oxygen, nitrogen and sulphur element percentage (%) of EGO after annealing at different temperatures under UHV condition, from XPS.

Temperature (°C)	C1s	O1s	N1s	S2p
25	76.40	20.99	1.45	1.16
100	76.91	20.69	1.39	1.01
150	77.56	20.16	1.38	0.90
200	84.90	13.47	0.78	0.85
300	87.78	11.09	0.65	0.48
400	88.97	9.98	0.62	0.43
600	91.56	7.80	0.55	0.09

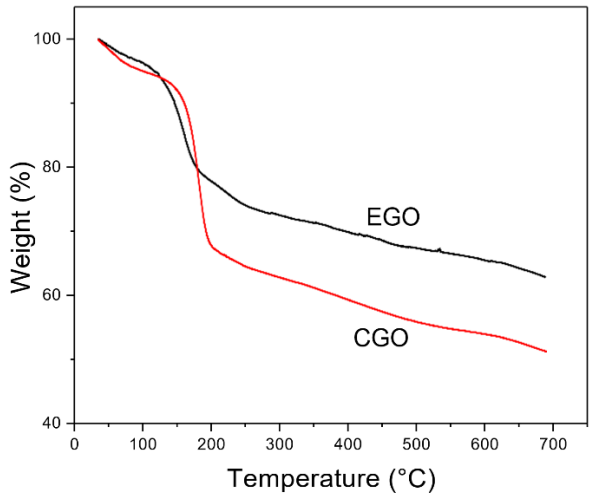

Figure S5. TGA curve of EGO (black) and CGO (red) performed at scan rate of 2 ºC/min in Argon.

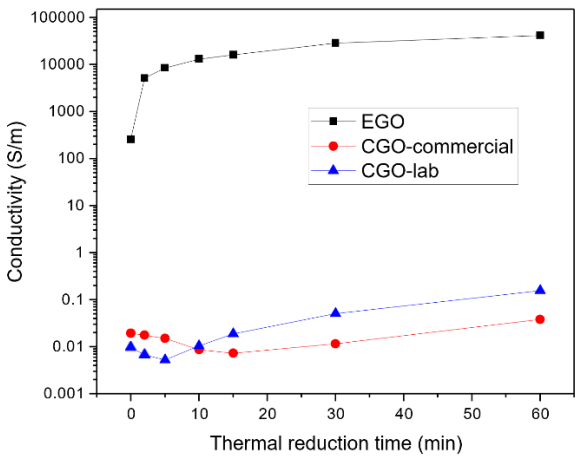

Figure S6. Comparison of CGO synthesized from lab with CGO purchased from commercial company and EGO for their conductivity change after various thermal reduction time at 200°C in an oven (air atmosphere).

Table S2. Zeta potential of EGO in water, DMF and ethanol.

	Water	DMF	Ethanol
Zeta potential (mV)	-33.3 ± 0.9	-53.1 ± 8.1	-41.9 ± 16.9

Table S3. Concentration change of EGO in water, DMF and ethanol after standing for 24 hours.

	EGO in water	EGO in DMF	EGO in ethanol
Initial concentration	3 mg/ml		
Concentration after 24 hours	2.1 mg/ml	2.5 mg/ml	2.6 mg/ml

Table S4. Yield and XRD peak ratio (graphene oxide peak/graphite peak) of EGO products from three batches with recycled electrolyte.

	Yield (wt.%)	XRD peak ratio
EGO-1	37.6	2.08
EGO-2	34.4	1.89
EGO-3	34.0	1.90

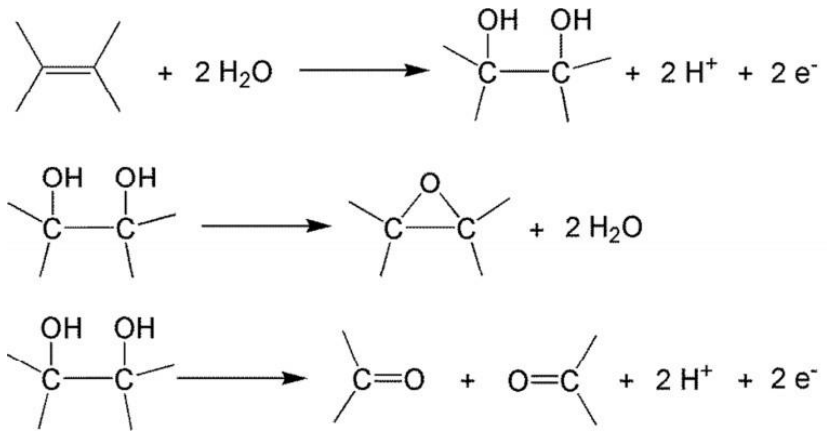

Scheme S1: Schematic representation of the electrochemical oxidation of graphite.[42]

Chapter 4. Electrochemical preparation of aqueous-dispersible graphene oxide

4.1 Introduction

4.1.1 Background of aqueous dispersible graphene oxide

As an important member of the graphene family, graphene oxide (GO) has attracted wide interest in both research and industry[7, 9, 17]. One of the most important reasons why GO is widely studied or used is due to its superior aqueous dispersibility[4, 14, 47]. As a general precursor of graphene that is frequently used in a wide range of applications such as energy storage devices, processable GO is often required in large quantities[35, 121]. In addition, GO sheets are often assembled into various macrostructures such as uniform membranes that are used in nanofiltration[5, 37], and ultra-elastic foams for sensors[122]. It requires homogeneous GO dispersions to form these uniform structures, resulting in fascinating properties. Moreover, GO sheets with tuneable chemistry also act as promising precursor fillers or templates for graphene-based polymer/inorganic composites to achieve enhanced properties such as enhanced electrical conductivity, increased strength, improved gas selectivity or electromagnetic interference shielding[4, 123]. For graphene-polymer composites, it is vital to form a uniform dispersion of GO within the polymer matrix for achieving the required properties. Good aqueous dispersibility of GO is critical for it to be homogeneously mixed with water-soluble polymers[124-125]. Some graphene-inorganic composites also require aqueous solution based fabrication processes[4]. If GO agglomerates are formed in the aqueous dispersion, it will be a great difficulty to form the desired structures and achieve effective properties for specific applications. Moreover, excellent and stable aqueous dispersibility of GO would also benefit its storage and transportation properties in industrial applications.

The basal plane of GO is bonded with abundant oxygen functional groups including hydroxyl, epoxy, carbonyl and carboxylic groups[33]. The colloidal stability of graphene oxide sheets in aqueous solutions is determined by a sum of interacting colloidal forces between the GO sheets[15]. The oxygen functional groups can introduce repulsive electrostatic forces and hydration forces which tend to push GO sheets apart from each other. The π-π domain in the non-oxidsed area will form attractive van der Waals forces and hydrophobic forces. A stable GO dispersion is maintained by the stronger repulsive forces being greater than the attractive forces. In the GO-water system, it has been noted that electrostatic forces are dominant due to

their strong long-range interactions caused by the ionisation of carboxylic and hydroxyl groups[15]. Therefore, the surface chemistry of graphene oxide needs to be considered to achieve a stable graphene oxide dispersion.

Graphene oxide is commonly produced by oxidation of graphite with chemical oxidants such as sodium hypochlorite or potassium permanganate[33]. The formation of oxygen groups breaks the original π-π conjugated region, which reduces the strong, attractive van der Waals forces between adjacent graphene sheets. With reduced attraction, exfoliation of the graphite oxide can be readily achieved by external forces such as ultra-sonication or agitation. Chemical oxidation of graphite such as Hummer's method is the most popular route to produce graphene oxide due to its scalability and high degree of oxidation degree[12-13, 46]. Due to strong oxidation, chemically-derived graphene oxide (CGO) shows remarkable dispersibility in water, which can achieve more than 10 mg/ml dispersions[46]. The chemistry of CGO contributing to the aqueous stability has been much studied. Electrostatic forces come not only from the ionisation of carboxylic groups but also are strengthened and stabilised by the phenolic and hydroxyl groups neighbouring the carboxylic groups[14]. Even though CGO shows superior aqueous dispersibility, the chemical oxidation methods and their products have some drawbacks. The use of strong oxidising agents increases the risk of explosion and produces hazardous gases[17]. The use of a large amount of water in the purification process and discharge of wastewater are also environmentally unfriendly processes[17]. Furthermore, products often contain some remaining heavy metal ions such as Mn^{2+}, which may affect the properties of graphene oxide in applications. Therefore, it is important to develop alternative methods to produce aqueous and dispersible graphene oxide.

4.1.2 Current challenges in electrochemically-derived graphene oxide-

As an environmentally-benign route, electrochemical oxidation of graphite has gained increasing popularity in producing graphene oxide[19, 126]. The electrochemical methods avoid the use of strong oxidising agents. Rather, a positive current is usually applied to the graphite electrode to oxidise it in an aqueous solution[19]. In previously reported works electrochemical methods are mainly used to exfoliate the graphite with minimum oxygen functional groups introduced into the structure[20-23, 82, 127]. These electrochemically-produced graphene/graphene oxide sheets contain limited oxygen functional groups and show poor dispersibility in water. They are normally dispersed in organic solvents such as dimethylformamide (DMF) which is hazardous. Therefore, the poor aqueous dispersibility of these electrochemically-derived

graphene/graphene oxide limits their further processability into macrostructures and applications. Producing aqueous dispersible graphene oxide by the electrochemical method is important to advance the widespread use of this route. Even though some recent works have been trying to synthesise a more oxidised graphene oxide via electrochemical routes[26-27, 82, 84], there is still a lack of research on the factors influencing the production of dispersible EGO.

In Chapter 3, a novel mechanically-assisted electrochemical method was outlined to produce graphene oxide with a good degree of oxidation. The resultant EGO showed a much-enhanced dispersibility in water compared to previously reported electrochemical methods. The EGO concentration of 2.1 mg/ml was reported in the previous chapter, but the dispersion contained large amounts of multi-layer graphene sheets. It is important to further enhance the dispersibility of the EGO sheets and explore how the electrochemical process conditions influences the dispersibility of EGO. In this chapter, an electrochemical Tee-cell setup was used, which has been previously reported[26], to electrochemically oxidise graphite with a well-controlled electrochemical program. It is a simpler and more controllable electrochemical oxidation method than the mechanically-assisted method, and provides a good platform for studying how electrochemical factors influence the produced EGO. The objectives of this chapter is to investigate how important parameters such as oxidation time/stages, graphite sources, and electrolyte concentrations impact the electrochemical processes and aqueous dispersibility of EGO products; and produce highly aqueous dispersible EGO by a controlled and optimised electrochemical process.

4.2 Experimental Section

4.2.1 Materials

Two types of graphite sources were used in this chapter: graphite flakes and graphite foils. Graphite flakes were the same graphite source as that in Chapter 3, which was purchased from Sigma-Aldrich (product no. 332461, particle size: +100 mesh). Graphite foils were purchased from Sigma-Aldrich (Product No. GF82433538, thickness 0.2 mm). Sulphuric acid (H_2SO_4) was used as electrolytes in the electrochemical method, which was purchased from Sigma-Aldrich (Product No. 435589). All the water used in the experiments was ultrapure water from the Millipore Direct-Q system. Aqueous solutions of various pH were prepared by adding appropriate amounts of hydrochloric acid (HCl) or (sodium hydroxide) NaOH into ultrapure water. HCl (ACS reagent, 37%) was purchased from Sigma-Aldrich (Product No. 320331).

NaOH (reagent grade, 97%, powder) was purchased from Sigma-Aldrich (Product No. 655104).

4.2.2 Electrochemical oxidation of graphite by Tee-cell setup

In this chapter, an electrochemical oxidation method reported previously was used[26]. Firstly, graphite foil was cut into a small pellet with a diameter of 12.7 mm (32 mg). If graphite flakes were used as the source, 32 mg were pressed into a pellet with a diameter of 12.7 mm under a pressure of 100 bar. Electrolytes used in the experiments were prepared by diluting concentrated H_2SO_4 into various concentrations: 18 M, 15 M, 12 M, 9 M, 6 M. The two-electrode Tee-cell setup used in the experiments was purchased from Swagelok Eastern Australia (product No. PFA-820-3). The schematic of the Tee-cell setup is shown in **Figure 1**, with a T-shape channel holding two electrodes. Graphite was attached to the left Pt working electrode with glass fibre separators put between graphite and right Pt counter electrode. The working and counter electrodes were pushed tightly towards each other to make a good electrical connection between graphite and working electrode. The electrolyte was then added from the top of the Tee-cell to soak the electrodes, graphite, and separators. The Pt working electrode and the counter electrode were connected to a VMP-300 potentiostat/galvanostat purchased from Bio-Logic. During the electrochemical process, a positive constant current (2 mA) was applied to the working electrode with the voltage change recorded. The charging time varied according to our investigations. In the study of the influence of oxidation time on dispersibility, charging time was set to be 3 h, 7 h, 11 h, 15 h, 19 h, and 22 h. In the study of graphite sources, the charging time was set to be 22 h. In the study of electrolyte concentration, the charging time was set to the beginning of the final stage when H_2O electrolysis began. After the electrochemical process, the modified/oxidised graphite pellet was taken out for further purifications. In terms of purification steps, the pellet was first placed into a centrifuge tube with 50 ml of water. After that, the tube was put in the sonication bath for 5 min to break up the pellet, which could be quickly reduced to pieces due to its oxidation degree. The tube was then centrifuged by a centrifugal device (Ample Scientific Champion S-50D centrifuge) at a speed of 4400 rpm. During this process, the modified/oxidized graphite pieces sink to the bottom of the centrifuge tube while the supernatant solution represented the remaining H_2SO_4 solution. Then the top solution was discarded, and ultrapure water was added to 50 ml. The sonication and centrifugation processes were repeated for twice until the supernatant solution reaches a neutral pH of 6 - 7. After the purification process, 50 ml dispersion of modified/oxidised graphite (30 ~ 50 mg, according to oxidation degree) sheets were obtained.

The dispersion was then exfoliated by ultrasonication via an ultrasonic probe (Branson Digital Sonifier S450D, 1/2" Horn, 500W, 30% amplitude, 30 min).

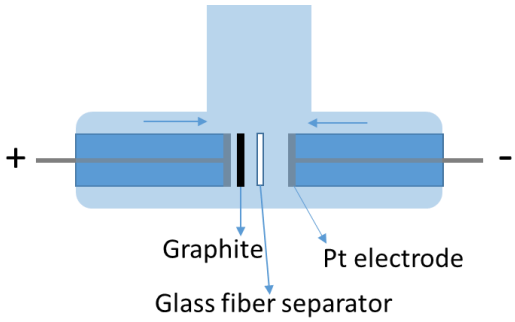

Figure 1. Schematic of a typical T-cell setup for electrochemical oxidation of graphite.

4.2.3 Dispersibility characterisation

To characterise the aqueous dispersibility of EGO produced at various conditions, the EGO dispersion after ultrasonication (30 min) was adjusted to a concentration of 0.7 mg/ml. The UV-Vis spectrum of the dispersion was then collected by a Varian Cary 300 UV/Visible spectrometer. The dispersion was diluted 20 times to ensure the intensity of the spectrum was in the range of the spectrometer. After recording the UV-Vis spectrum, the EGO dispersion was centrifuged for 30 min at 3000 rpm. The supernatant dispersion was taken out into another container and tested for its UV-Vis spectrum. The intensity of the maximum peak (~240 nm) for the supernatant dispersion divided by that for the original EGO dispersion was the percentage of the dispersed EGO in water solution. For long-term dispersibility test, the centrifuged dispersions were placed for a given amounts of time: 0, 1, 4, 6, 11, 19 days. The top dispersion was tested for its UV-Vis spectrum to calculate the concentration, which could also be expressed by the percentage of EGO dispersed, compared to its initial dispersion amount.

4.2.4 Other characterisations

Electrochemical impedance spectroscopy (EIS) was used to monitor the real-time graphite electrode resistance during the whole electrochemical process. Two platinum plates were placed on each side of the graphite working electrode and connected to the potentiostat. The impedance of the graphite working electrode was recorded during the electrochemical oxidation process.

X-ray Diffraction (XRD) was used to characterise EGO products for its compositions of graphene oxide and graphite, which showed different peak positions in XRD spectra. The XRD spectra were obtained from the Bruker D2 Phaser diffractometer (with Cu Kα radiation, λ = 1.5418 Å). EGO dispersions just after purification were filtered by vacuum to make EGO membranes. The membranes were placed in a 50°C oven overnight for complete dryness. The EGO membrane samples spectra were measured using XRD.

The zeta potential of EGO was measured in order to characterise its electrostatic repulsive forces to explain its dispersibility. A Malvern Zetasizer Nano ZS analyser was used to test 0.05 mg/ml EGO dispersion. As a comparison, CGO dispersion (0.05 mg/ml) was also tested by the analyser. CGO was produced by a modified Hummers method reported by Kovtyukhaova et al.[46] The process had several steps. Firstly, graphite (20 g) was added to 30 ml of concentrated H_2SO_4 which contained 10 g of $K_2S_2O_8$ and 10 g of P_2O_5 at 80 °C for 6 hours of pre-oxidation treatment. After washing, the preoxidised graphite was further oxidised in concentrated H_2SO_4 at 0 °C by gradually added $KMnO_4$ (60 g). The solution was then stirred for 2 h at 35 °C, after which time, water was slowly added to it. After 15 min, the reaction was terminated by adding more water and 50 ml of 30% H_2O_2 solution. A solution of 1:10 HCl was added to the solution to remove the metal ions. The resultant dispersion was repeatedly washed by centrifugation and dialysis. Finally, the CGO dispersion was ultrasonicated for 30 min.

Atomic force microscope (AFM) was used to characterise the EGO sheets. AFM images of EGO sheets were taken by Bruker Dimension Icon AFM (tapping mode). EGO dispersion with 0.01 mg/ml was dropped on top of a silicon wafer which was pre-treated by piranha solution (H_2SO_4: H_2O_2 = 3:1) to clean the surface and make the surface hydrophilic. When the EGO dispersion was dropped on the silicon surface, the droplets quickly spread due to the hydrophilicity of the surface. The silicon wafer was then placed on a hot plate (50°C) to evaporate the water. After drying, the silicon wafer with cast EGO sheets on top were taken to the AFM device.

4.2.5 Fabrication of EGO membrane

The EGO membrane was fabricated to demonstrate the processability of EGO aqueous dispersion. To produce the EGO membranes, 0.1 mg/ml EGO dispersion (10 ml) was filtrated through a filter by vacuum. The filter used was Anodisc alumina filters (Whatman® Anodisc inorganic filter membrane, supported, diameter 47 mm, pore size 0.1 μm). When the EGO

aqueous dispersion was filtered, the EGO sheets will stack layer-by-layer on top of the filter to form the EGO membrane. When all the water had been filtered, the membrane was dried by vacuum overnight. Following this procedure, the EGO membrane could be easily peeled from the alumina filter by tweezers.

4.3 Results and discussion

4.3.1 Electrochemical process

Electrochemical stages

A T-cell setup was used in this chapter to electrochemically oxidise graphite into graphite oxide. This setup has been previously reported, with the advantage of good controllability and batch-to-batch reproducibility[26]. More importantly, the electrochemical oxidation process could be well monitored by this setup which was connected to a potentiostat. Electrochemical oxidation of graphite was achieved by applying a constant current (I = 2 mA) on graphite in sulfuric acid solution (12 M). The galvanostatic charging curves were recorded during the whole electrochemical oxidation processes. A typical galvanostatic charging curve is shown in **Figure 2**. The process can be segmented into three characteristic stages: intercalation of graphite into graphite intercalation compound (GIC), oxidation of GIC and H_2O hydrolysis. Different electrochemical reactions thus happen in different stages.

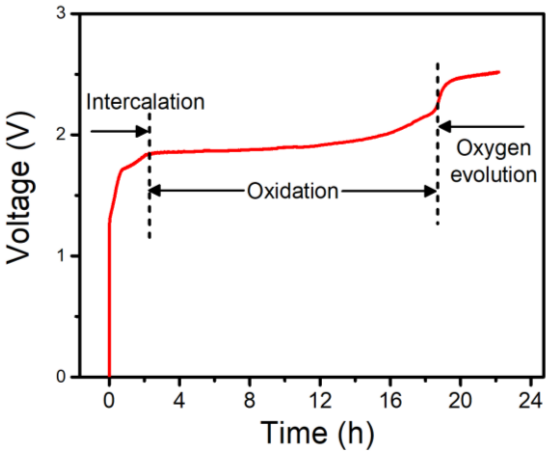

Figure 2. Galvanostatic charging curve of graphite foil with the voltage change at a constant current of 2 mA, with 12 M H_2SO_4.

In the initial stage, intercalation of graphite by H_2SO_4 electrolyte occurred to produce GIC. The intercalation stage shows two prominent slopes, representing different stages in GIC

production. As shown in **Figure 3a**, the first slope is the formation of Stage 3 and >3[76], where a layer of intercalants was formed between every three or more than three layers of graphene sheets. With increasing charging time, the stage number will decrease, indicating more H_2SO_4 intercalated into GIC, reaching a smaller stage number. With an electrolyte of 12 M H_2SO_4, Stage 2 could be formed in the final GIC because a further increase in voltage will activate the oxidation process. A schematic of the graphite intercalation process is shown in **Figure 3b**, showing the formation of a second-stage GIC. When the graphite is charged anodically, it will attract negatively charged HSO^{4-} ions together with H_2SO_4 and H_2O molecules to co-intercalate between the layers to form GIC.

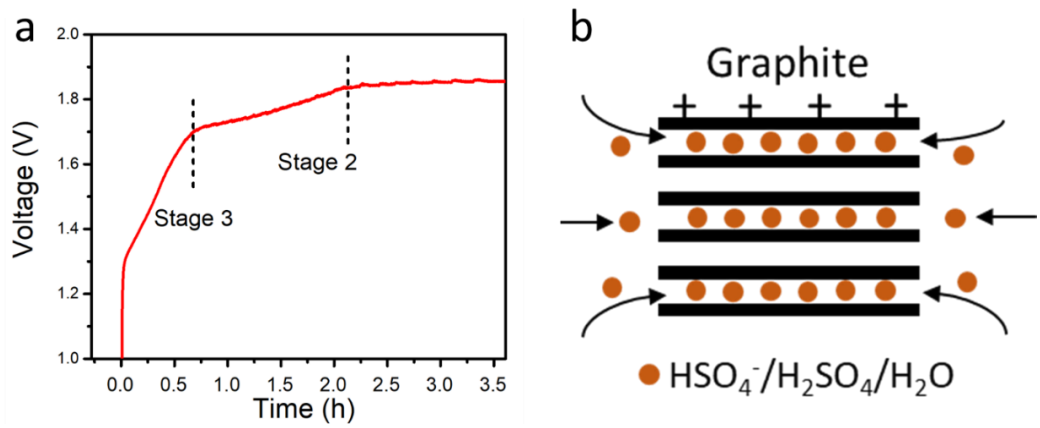

Figure 3. (a) Galvanostatic charging curve in the intercalation stage. (b) Schematic of intercalation of graphite with H_2SO_4 electrolyte.

When the voltage further increases, the galvanostatic charging curve is due to the second stage: oxidation of GIC. During the oxidation stage (**Figure 2**), an extended plateau can be observed due to the consumption of charge by the continuous oxidation process. During this stage, GIC will be converted into oxidised graphite by the reaction of graphite with H_2O molecules under the anodic charging. The oxidation process has been proposed in previous studies with the following equations (equation 4.1, 4.2 and 4.3)[74]. Firstly, water molecules react with carbon double bonds to form vicinal hydroxyl (-OH) groups. During further oxidation, the two vicinal -OH groups can react to form an epoxy ring, which can be further cleaved and oxidised into carbonyl groups.

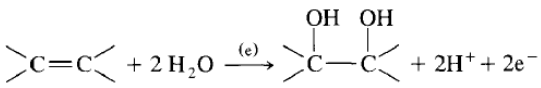

4.1

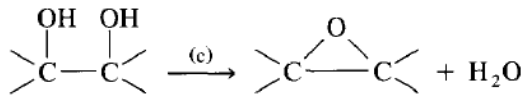

4.2

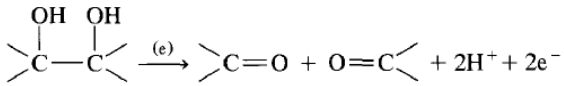

4.3

The real-time graphite electrode resistance was monitored by the EIS technique during the whole electrochemical process, as shown in **Figure 4a**. As can be observed, the resistance shows a slight increase within the first 15 h while it shows a huge increase from 15 h to 18.5 h. Then it fluctuates dramatically after 18.5 h. Within the first 15 hours, the re-scaled real-time graphite electrode resistance is shown in **Figure 4b**. The resistance shows a continuous development of this stage. Initially the resistance increases slowly, especially in the graphite intercalation stage. After 5 h, the slope of the resistance curve gradually increases due to further oxidation processes. The resistance begins to show a sharp increase from 12 h to 15 h, which indicates stronger oxidation process or destruction of the conductive pathway in this stage. After 15 h, a dramatic increase of resistance is also accompanied by noisy discontinuities, which may be caused by the formation of gas bubbles within the electrode. The gas bubbles lead to delamination of the oxidised graphite electrode, thus further reducing its conductive pathways between sheets and greatly increasing resistance. The formation of bubbles could also be confirmed by observations in experiments. It is not clear about the mechanism of the bubbles forming in this stage, but they may be due to H_2O hydrolysis within the electrode or oxidation process. After 18.5 h, the resistance shows great turbulence, which may be caused by the formation of gas bubbles on the Pt electrode.

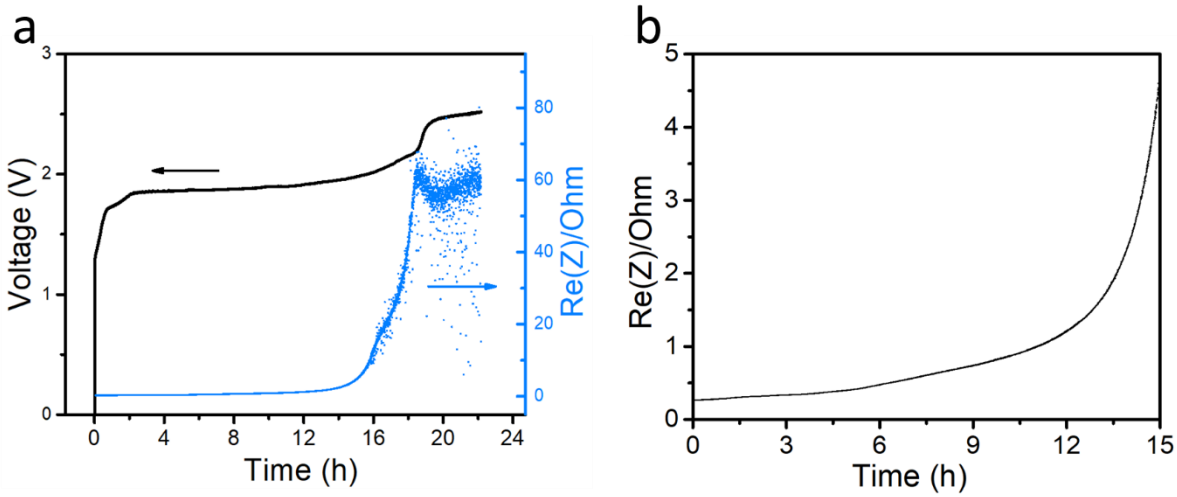

Figure 4. (a) Real-time graphite electrode resistance during the electrochemical process. (b) Re-scaled real-time graphite electrode resistance during 0 - 15 h.

Graphite sources

The electrochemical process above was performed on graphite foil. To investigate the influence of graphite sources, graphite flakes were also explored with the same electrochemical conditions (I = 2 mA, 12 M H_2SO_4). The galvanostatic charging curves of the two graphite sources are shown in **Figure 5**. The charging curve of graphite flakes also shows three main stages, similar to that of graphite foil. However, the oxidation stage of graphite flakes is much shorter than that of graphite foil, which may indicate a lower oxidation degree. The oscillations in the final period of oxidation stage of graphite flakes is another different characteristic to graphite foil. A zone model has been proposed in a previous study to explain the potential oscillations[74]. In each oscillation, the H_2O molecules oxidise a local zone into -OH groups, which will fill the space between graphene layers and lead to the formation of hydrogen bondings and block the movement of more H_2O molecules into the unoxidised region[74]. The anodic charge will result in further oxidation of the -OH groups into carbonyl groups, which will further increase the space between graphene sheets. As a result, H_2O molecules can further move into the unoxidised region and start the next oscillation process. The appearance of oscillations indicates that graphite flakes have more dense structures, with less free space between graphene sheets. The oscillations disappear in the charging curve of graphite foil, indicating that it contains more free space between graphene sheets, allowing continuous movement of H_2O into unoxidised regions.

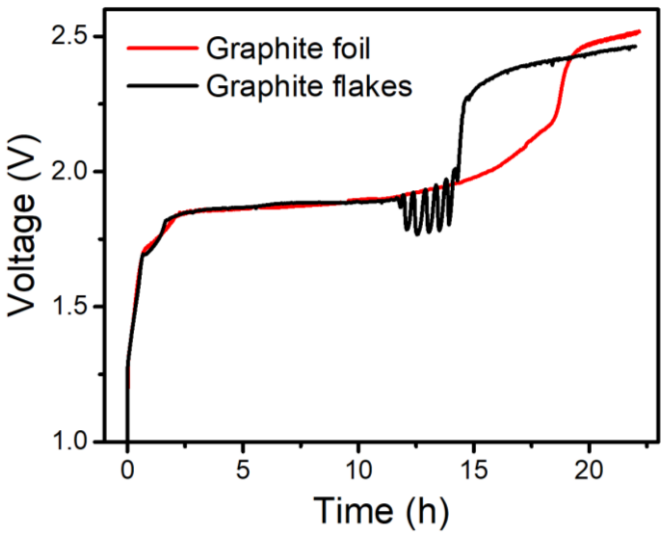

Figure 5. Galvanostatic charging curve during electrochemical oxidation of graphite foil and graphite flakes.

The denser and more ordered structures of graphite flakes can also be observed from the intercalation stages in its galvanostatic charging curve, as shown in **Figure 6a**. Dt/dV vs. time was plotted to clearly show the transition of intercalation stages in **Figure 6b**, with the peaks representing stage transition platforms. For graphite foil, dt/dV increased to the first plateau from the beginning, indicating the first intercalation stage: a transition from Stage 3+ to Stage 3. After a period of time, a significant peak rises at the time of about 1 h, which shows the second intercalation stage: a transition from Stage 3 to Stage 2. As a comparison, graphite flakes shows similar stages, but there is a much sharper peak observed in the second intercalation stage. The clearer transition between stages of graphite flakes shows a more ordered intercalation process due to less free space between graphene sheets. In comparison, graphite foil contains more free space between the sheets which leads to a less ordered intercalation process.

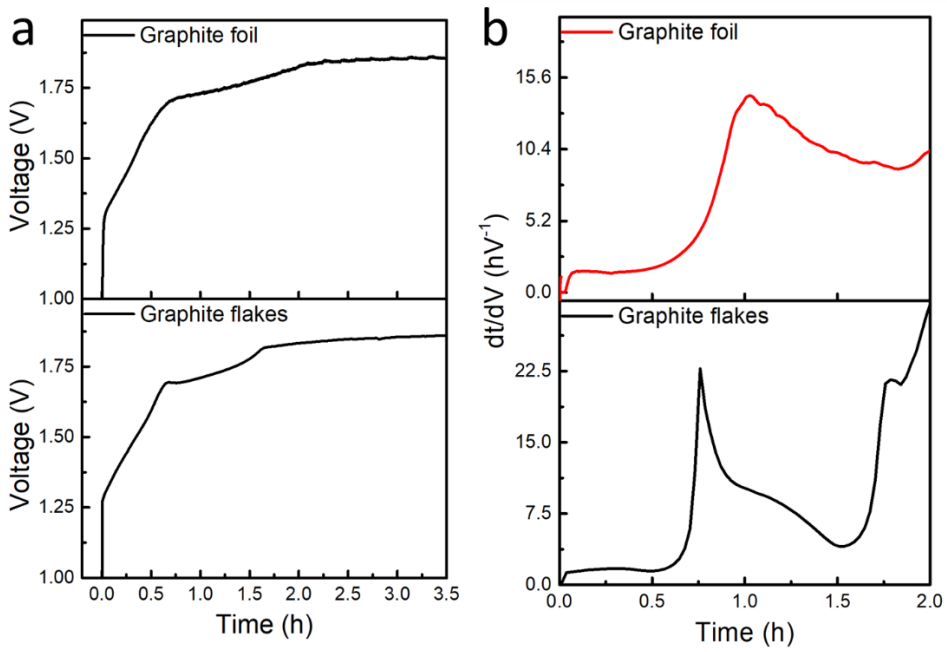

Figure 6. (a) Galvanostatic charging curve in the intercalation stage for graphite foil (top) and graphite flakes (bottom) with a constant current. (b) dt/dV derived from (a) vs. time.

Electrolyte concentrations

In addition to graphite source, electrolyte concentration is another important factor in the electrochemical oxidation of graphite. The galvanostatic charging curves (of graphite foil) with various concentrations of H_2SO_4 are shown in **Figure 7a**. The oxidation time (for the second stage) and voltage (at 5 h) with H_2SO_4 concentration were plotted in **Figure 7b**. With the

highest concentration of 18 M, the charging curve shows the shortest oxidation time of less than 10 h. When the concentration decreases, the oxidation time gradually increases with 6 M after almost 45 h. This shows that the oxidation process is related to the amount of H_2O in the H_2SO_4 electrolyte. Increasing amounts of H_2O in more diluted H_2SO_4 will contribute to longer oxidation times. It can be seen that different electrolyte concentrations show different oxidation voltages with 6 M H_2SO_4 exhibiting the greatest oxidation voltage. When the concentration increases, the oxidation voltage gradually decreases to its lowest value at 15 M H_2SO_4. The lower oxidation voltage shows that there is a lower voltage barrier for the graphite to be oxidised by H_2O. This may be because more intercalated graphite shows enlarged layer distances, which exhibites lower barrier for oxidation. Another possible cause is the formation of different oxygen groups in different H_2SO_4, which shows different oxidation voltages. The exact mechanism needs to be investigated in future work. When the concentration further increases to 18 M, the oxidation voltage increases again, which may be caused by the limited amount of H_2O molecules in the electrolyte or the lower conductivity of electrolyte at 18 M[128].

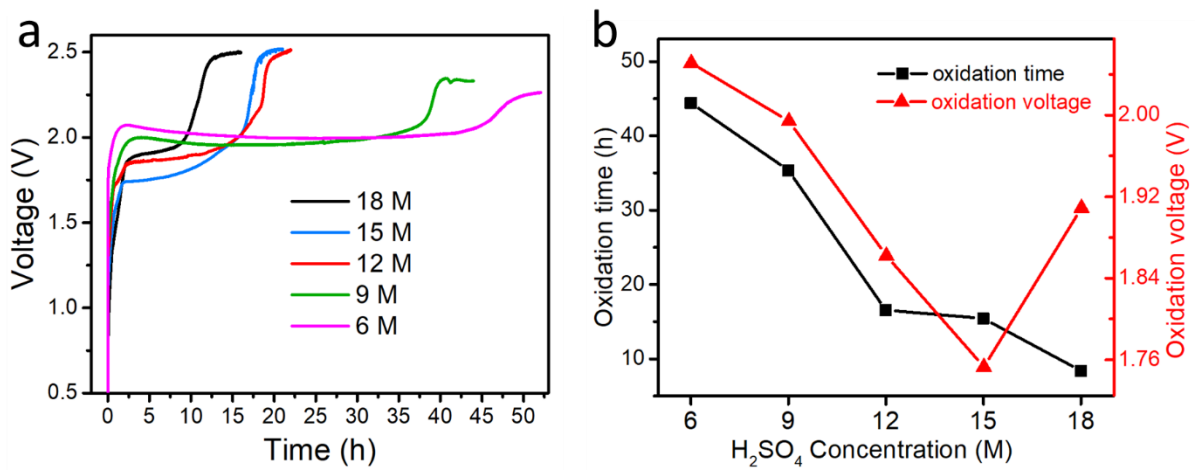

Figure 7. (a) Galvanostatic charging curves during electrochemical oxidation of graphite foil with electrolytes of 6 M, 9 M, 12 M, 15 M, 18 M H_2SO_4. (b) Oxidation time and voltage change with H_2SO_4 concentration.

The intercalation stages were analysed by deriving the charging curves to dt/dV vs. time, as shown in **Figure 8**. At the highest concentration of 18 M H_2SO_4, three peaks could be observed representing three main intercalation stages: Stage 3+ to Stage 3, Stage 3 to Stage 2, Stage 2 to Stage 1. When the concentration decreases, fewer and less distinct peaks were able to be observed in 15 M and 12 M H_2SO_4 , which shows fewer intercalation stages in diluted H_2SO_4 electrolyte. When H_2SO_4 is further diluted to 9 M and 6 M, the peak gradually diminishes and

disappears, which indicates less distinct intercalation stages in low concentrations. This result shows that a higher concentration of H_2SO_4 contributes to the intercalation process of graphite, while the lower concentrations show almost no intercalation process.

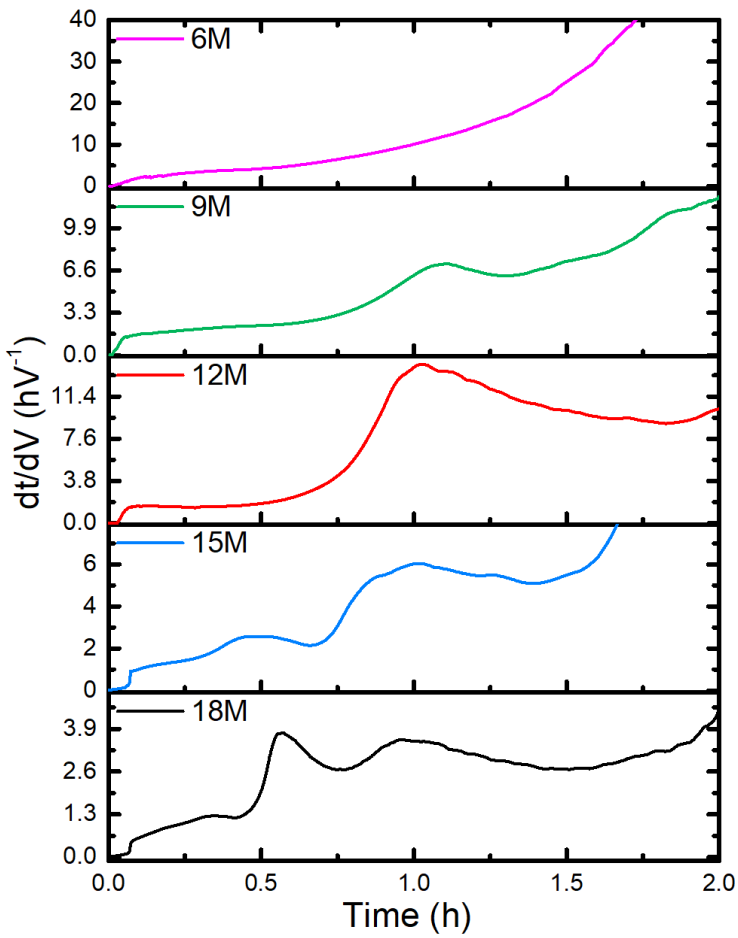

Figure 8. Dt/dV vs. time derived from Figure 7 at electrolytes of 6 M, 9 M, 12 M, 15 M, 18 M H_2SO_4.

4.3.2 Dispersibility of EGO

The dispersibility of EGO in water was examined for different oxidation times, graphite sources and electrolyte concentration. The EGO dispersions were centrifuged (3000 rpm, 30 min) to cause the non-dispersed EGO sheets to settle out. The weight percentages of remaining EGO were calculated to represent the dispersibility of EGO in water.

The percentages of dispersible EGO under different oxidation times are shown in **Figure 9a**. With 3 h of oxidation time, less than 10% of EGO is dispersible in water, which is due to the main graphite intercalation process with limited oxidation. When the oxidation time increases

to 7 h, the percentage of dispersible EGO increased dramatically to around 49%, with a subsequent moderate increase of 8% after 11 h. The percentage of dispersible EGO then shows a second dramatic increase to 76% after 15 h oxidation time. Finally, after 22 h, the percentage reaches a steady value of 82%. During the whole electrochemical process, the percentage shows two significant increases, at 3 – 7 h and at 11 – 15 h. During 3 – 7 h, it is speculated that oxygen groups are first formed on the edge of graphite, which transforms it from hydrophobic to hydrophilic. In the period of 7 – 11 h, oxidation continues towards the middle part of the basal plane that further increases the dispersibility but shows less influence than the oxidation process of 3 – 7 h. During 11 – 15 h, the dramatic increase of dispersibility may be due to a complete transformation of the remaining unoxidised area into the oxidised region, which greatly reduced π-π attractive forces. In addition, the formation of –COOH groups may also contribute to the progression of oxidation. After 15 h, the limited increase of dispersibility correlates with analysis shown in **Figure 4a** which shows the formation of gas bubbles within the electrode causing a significant increase of resistance. Therefore, during this period, most of the current is consumed for the electrolysis of H_2O into O_2, with only a small amount for further oxidation of graphite.

X-ray diffraction (XRD) was used to examine the composition of the products after the electrochemical process at various oxidation time and washing steps, as shown in **Figure 9b**. It can be observed that the XRD curves are composed of two main peaks in the 2θ scanning range of 6 - 32°. One peak is at around 12 - 13°, representing the formation of EGO with oxygen functional groups between the sheets. Another peak is at around 27°, indicating the existence of non-oxidised graphite in the product. The XRD curve of the product from 3 h of oxidation shows a significant peak at 27.0° but a weak peak at 13.1°, corresponding to the small amount of dispersible EGO in the product. With the increase of oxidation time, the XRD curves show gradually increased EGO peak, with a reducing graphite peak. After 15 h of oxidation, the graphite peak has been significantly diminished, indicating the majority of remaining graphite has been oxidised to EGO. Moreover, the positions of EGO peaks move to lower values of 2θ, corresponding to a larger interlayer spacing with longer oxidation time. This may result from the formation of an increased amount of oxygen functional groups increasing the interlayer distance.

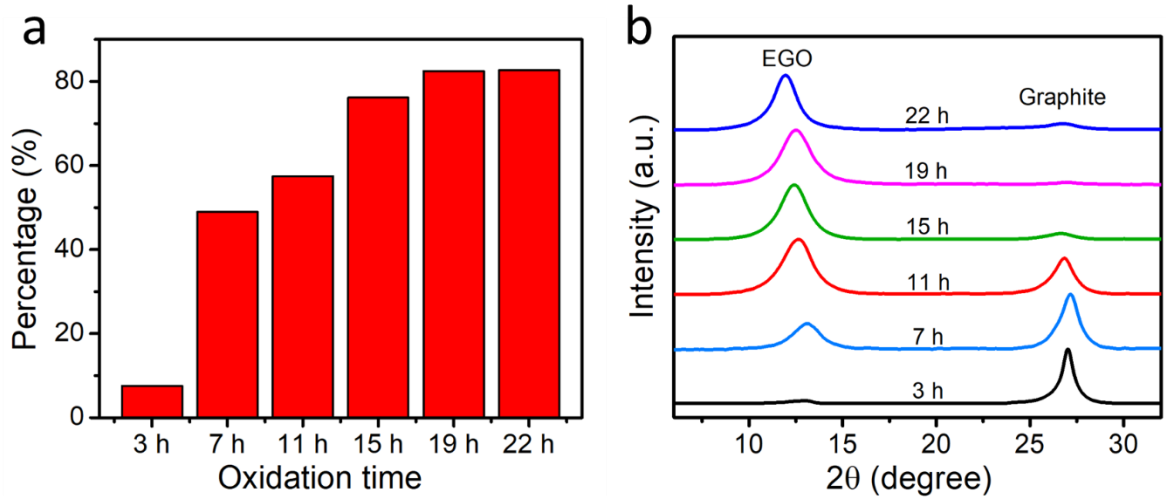

Figure 9. (a) Percentage of dispersible EGO after centrifuge (3000 rpm for 30 min) with different oxidation time by 12 M H_2SO_4. (b) XRD of electrochemically-oxidised graphite with different oxidation time.

The influences of graphite sources on aqueous dispersibility of produced EGO were also studied. The percentages of dispersible EGO after centrifugation produced from graphite foil and graphite flakes are shown in **Figure 10a**. EGO produced by graphite foil shows more than 80% of the product is dispersible in water at various initial concentrations. Even when the initial concentration reaches to 5 mg/ml, around 80% of EGO remained dispersible with a maximum concentration of 4 mg/ml achieved. This shows good dispersibility of EGO produced from graphite foil. In comparison, EGO produced from graphite flakes showed less dispersibility. The percentage of dispersible EGO by graphite flakes is greatest (84%) at the lowest initial concentration of 0.1 mg/ml. However, the percentage drops rapidly to about 42% when the initial concentration increases to 0.3 mg/ml. At an initial concentration of 0.5 mg/ml, the percentage retains a similar value (43%). The maximum concentration of dispersible EGO can reach 0.215 mg/ml at this point. For higher concentrations of 0.7 mg/ml, more than 80% of EGO sheets were precipitated to the bottom. For a more intuitive comparison, **Figure 10b** shows the images of EGO dispersions (0.7 mg/ml) produced from graphite foil and graphite flakes after 24 h. EGO dispersion by graphite foil is much more stable and homogeneous than EGO dispersion by graphite flakes, which aggregates after 24 h.

UV-vis spectroscopy of EGO by graphite foil and graphite flakes is shown in **Figure 10c**. The maximum peaks for EGO by graphite foil and graphite flakes are at 240 nm and 247 nm separately, which are due to the π-π* transitions of the aromatic C=C bonds. The higher peak

position of EGO produced by graphite flakes reflects a larger area of the aromatic region than that of EGO by graphite foil. It is likely that graphite foil has more pores and defects than graphite flakes because the production of it involves intercalation, expansion by heating and compression[129]. Graphite foil has a density of around 1.3 g/cm^3 while graphite flakes have a much higher density of about 2.2 g/cm^3. This explains the more ordered electrochemical intercalation process of graphite flakes. It has been regarded that electrochemical oxidation process starts from the edge of graphite towards the inner section[19, 74]. Therefore, more pores and defects could introduce more oxidation processes and reduce the barrier of oxidation into the inner part of graphite due to the shortening of each oxidation length. As a result, the oxidation could be completed more thoroughly with more oxygen functional groups introduced to the flakes.

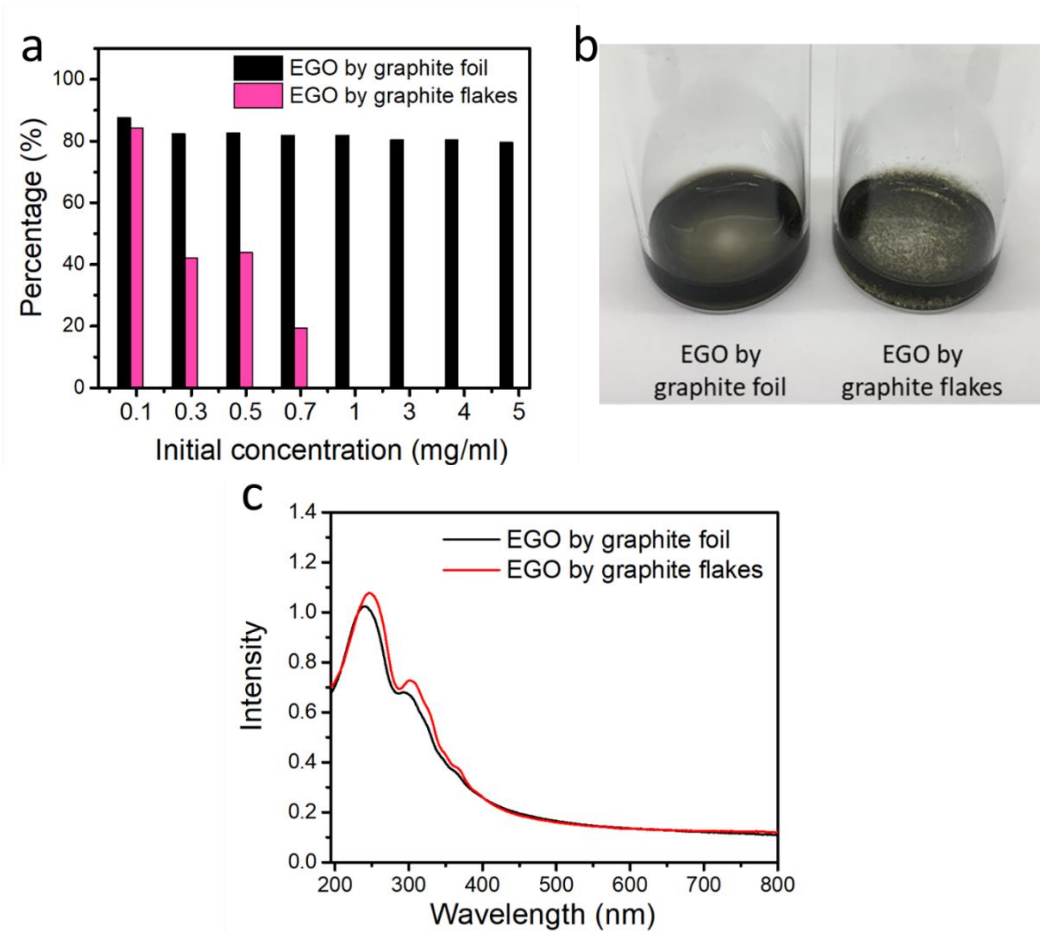

Figure 10. (a) Percentage of dispersible EGO after centrifuge (3000 rpm for 30 min) with different graphite source. (b) Picture of EGO produced from graphite foil and graphite flakes after placing for 24 h. (c) Uv-vis spectra of EGO produced from graphite foil and graphite flakes.

It has been shown in Section 4.3.1 that H_2SO_4 concentration has a large impact on the electrochemical processes including oxidation time, voltage and intercalation stages. Here, the influences of electrolyte concentrations on dispersibility of EGO were also studied. First, all the electrochemical processes were undertaken until they reach the 3rd stages (H_2O hydrolysis), when the 2nd stage of electrochemical oxidation is finished. As shown in **Figure 11a**, with the decrease of H_2SO_4 concentrations, the red bars (3rd stage) increase and reach to the maximum percentage at 12 M H_2SO_4. With the further decrease of concentration to 9 M and 6 M, the percentages of dispersible EGO show no much change. However, as shown in the previous section, the oxidation time will greatly increase when the H_2SO_4 concentration drop to 9 M and 6 M. The oxidation time required for 9 M and 6 M H_2SO_4 is about two or three times the oxidation time for 12 M H_2SO_4. Therefore, the electrochemical time (22 h) of 12 M H_2SO_4 was used as a standard time for attaining maximum dispersibility.

The electrochemical processes were then run for 22 h of charging time and tested their percentages of dispersible EGO again. As shown in **Figure 11a**, the black bars show similar percentage values to the red bars for 18 M, 15 M and 12 M H_2SO_4, while they are much lower than the red bars at 6 M and 9 M H_2SO_4. As a result, it can be observed that 12 M H_2SO_4 shows the highest percentage of dispersible EGO. The corresponding XRD curves of the electrochemically-modified products with 22 h of charging time were shown in **Figure 11b**. The product of 18 M H_2SO_4 shows a broad EGO peak and a broad graphite peak, indicating a weak amount of oxidation due to limited H_2O in the electrolyte. At 15 M H_2SO_4, the graphite peak greatly diminishes with a sharper EGO peak. When the concentration is diluted to 12 M H_2SO_4, the graphite peak is at a minimum among the samples, showing the highest level of oxidation. With a further diluted electrolyte to 9 M and 6 M H_2SO_4, the oxidation degree decreases again with an increase of graphite peaks and a decrease of EGO peaks. Therefore, considering the factors of oxidation time, 12 M H_2SO_4 is the optimal electrolyte concentration for producing the most dispersible EGO.

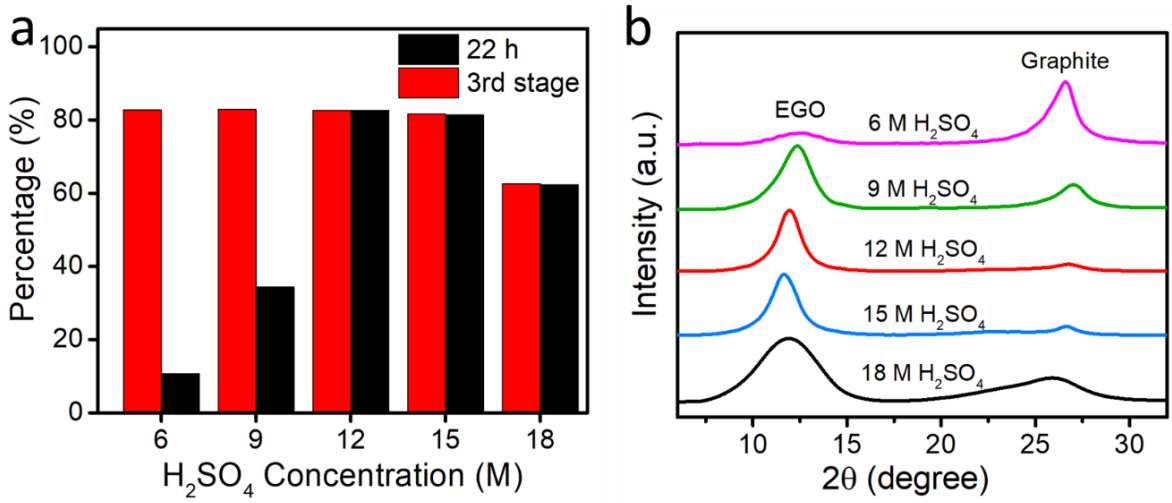

Figure 11. (a) Percentage of dispersible EGO after centrifugation (3000 rpm for 30 min) with different electrolyte concentrations after 22 h of oxidation, or reaching the 3rd stage. (b) XRD of electrochemically-oxidised graphite for different electrolyte concentrations after 22 h of oxidation.

4.3.3 Characterisation of dispersible EGO

As discussed above, dispersible EGO can be produced at optimised conditions (22 h, graphite foil, and 12 M H_2SO_4). In this section, the dispersible EGO was characterised for its stability, zeta-potential and sheet morphology.

To determine long-term stability, the concentration of EGO dispersions after standing for a certain time was tested. The concentrations were measured by UV-VIS spectroscopy. **Figure 12a** shows UV-VIS spectra of 0.3 mg/ml EGO dispersion placed for 0, 1, 6, and 19 days. The curves show little change after standing for 19 days. The corresponding percentage of dispersible EGO with time is shown in **Figure 12b**. It was found that percentages of dispersible EGO at various concentrations were higher than 80% at the initial time with 0.1 mg/ml EGO even reaching around 88%. After standing for more days, the concentrations fluctuate without any clear decrease. The fluctuations may be due to errors in the UV-VIS measurements. After 19 days, the lowest percentage of dispersible EGO still shows 79%. This shows the good long-term stability of EGO dispersions at a concentration of 0.1 – 1 mg/ml.

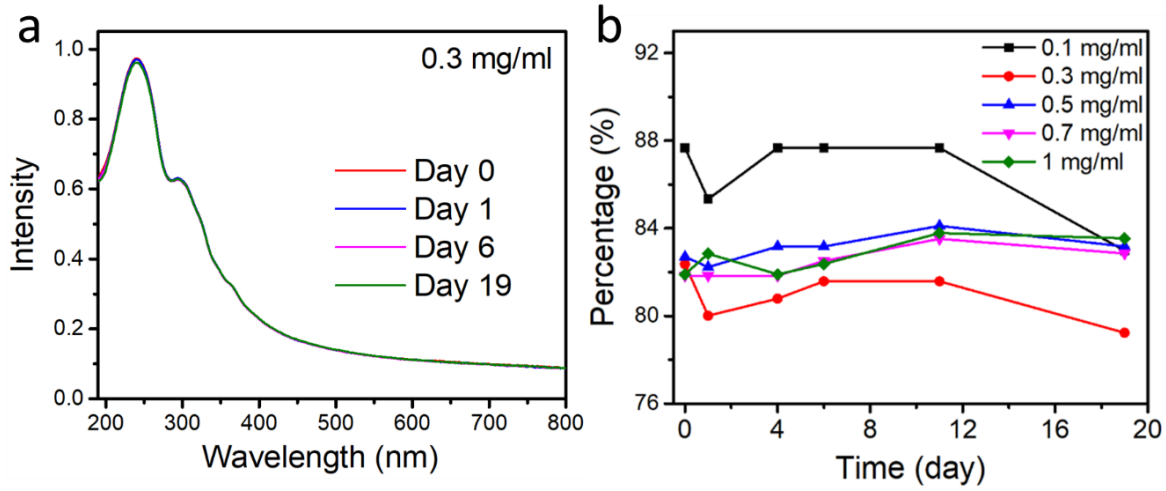

Figure 12. (a) UV-VIS change of 0.3 mg/ml EGO dispersion for 0, 1, 6 and 19 days. (b) Percentage of dispersible EGO with time at various concentrations (0.1, 0.3, 0.5, 0.7, 1 mg/ml).

As shown in the previous section, 4 mg/ml EGO dispersion is the maximum concentration that could be achieved. **Figure 13a** shows the picture of 4 mg/ml EGO dispersion, which is uniformly dispersed without any observable agglomerates. The dispersion was also tested for its stability of 7 days, with the concentration changes shown in **Figure 13b**. The concentration of the dispersion remains at around 4 mg/ml and shows almost no change after standing for 7 days.

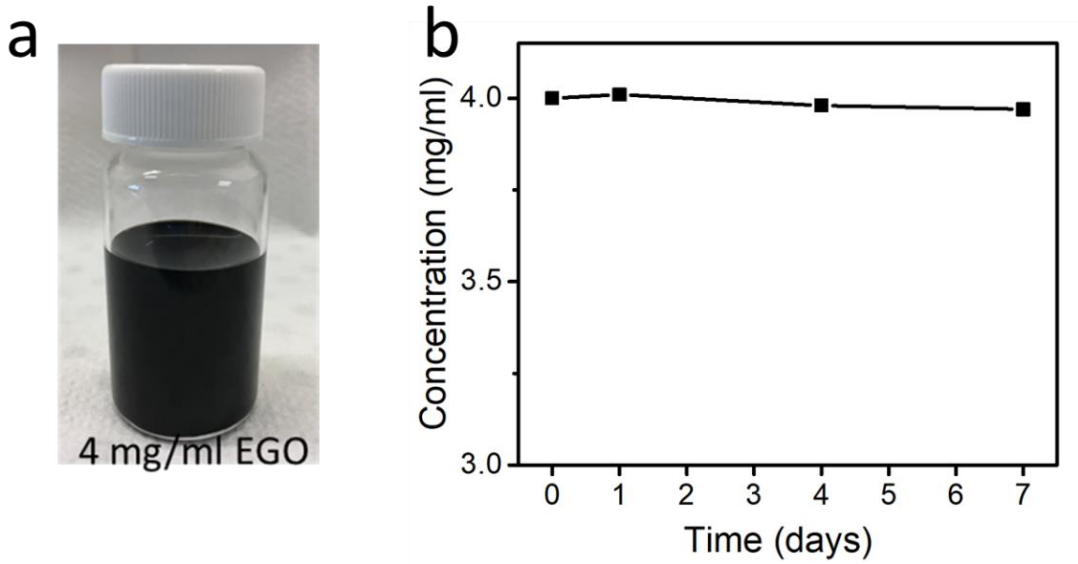

Figure 13. (a) Picture of 4 mg/ml EGO dispersion. (b) Concentration change of 4 mg/ml EGO dispersion.

The zeta potential has been used as a useful tool to characterise electrostatic charges on the surface of nanoparticles. Negative values of zeta potential represent negative charges on the surface. The more negative zeta potential is, the stronger repulsive forces between the nanoparticles. Zeta potentials of EGO dispersion (0.05 mg/ml) were measured at various pH, the results shown in **Figure 14**. In comparison, the zeta potentials of CGO dispersion were also measured. As can be observed, the absolute zeta potentials for both EGO and CGO increase with the increase of pH values. At pH less than about 2.2, the absolute zeta potential is less than 30 mV. When pH is greater than about 2.2, the value will be larger than 30 mV. Even though the absolute zeta potential of EGO dispersion is smaller than that of CGO dispersion, its zeta potential values of below -30 mV are sufficiently great enough to maintain repulsive forces between EGO sheets and thus retain good stability.

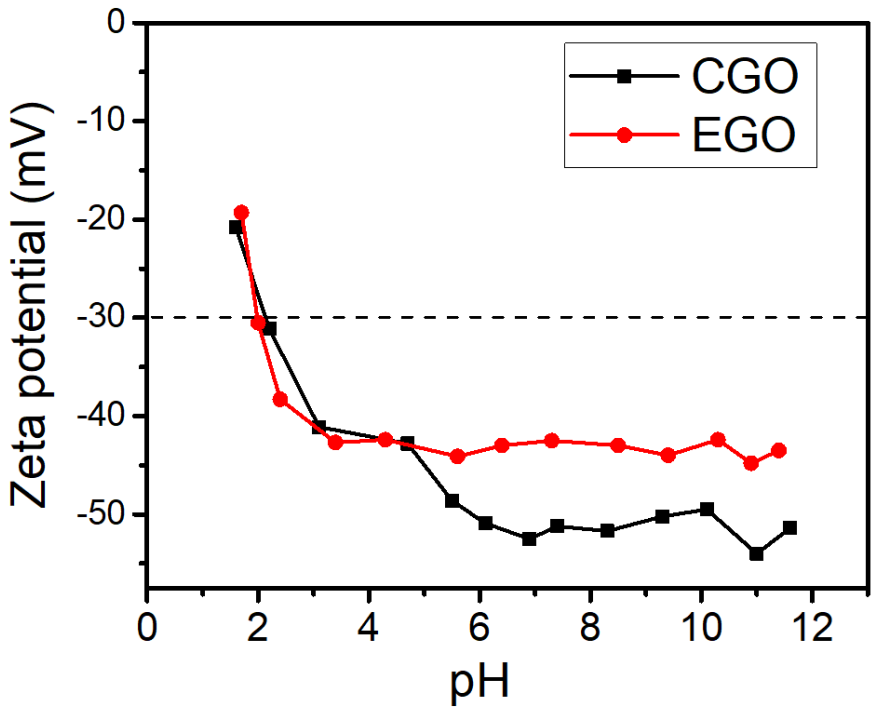

Figure 14. Zeta potential of EGO dispersion and CGO dispersion for various pH.

To characterise the thickness and the sheet size of EGO sheets, atomic force microscope (AFM) was used to examine the EGO sheets which were uniformly deposited on a Si wafer. **Figure 15** shows a typical EGO monolayer and its thickness. It can be observed that the EGO sheet shows a uniform thickness of about 1.2 nm, which is around the size of an oxidised graphene sheet. Several AFM images with larger scale were taken to statistically analyse the EGO sheets, which are shown in **Figure 16a**. As can be observed, most of the sheets (> 95%) are single-layer EGO sheets, which are much greater than the percentage (66%) of single-layer EGO sheets produced by the mechanically-assisted method in Chapter 3. **Figure 16b** shows the size distribution of single-layer EGO sheets. It can be seen that the EGO sheets are mainly distributed in the range of 100 nm – 1 μm. The relatively small size is due to th 30 min of sonication, which can simultaneously reduce layer numbers and lateral size of EGO sheets.

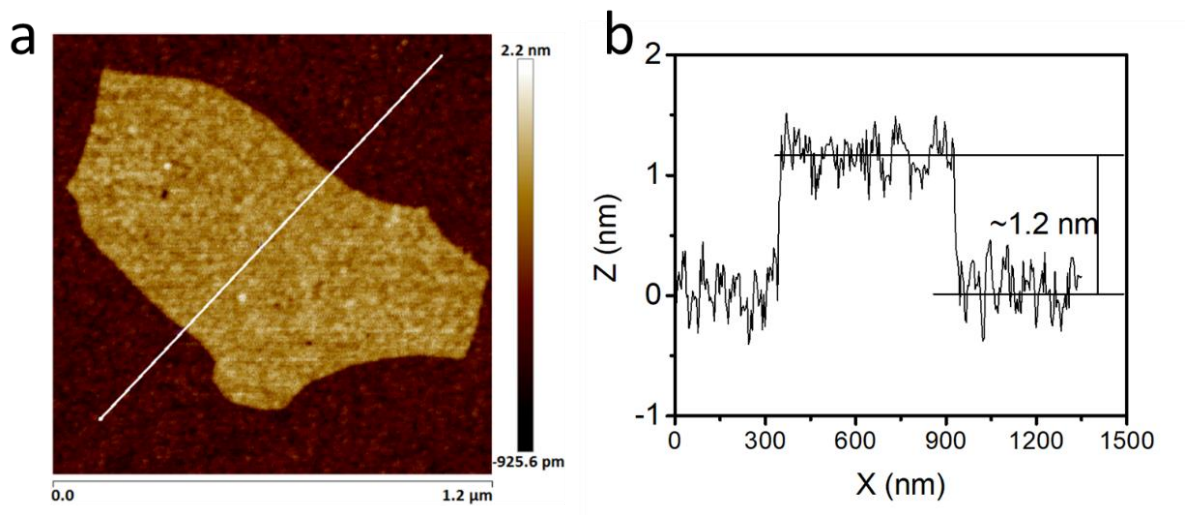

Figure 15. (a) A typical EGO monolayer and (b) its thickness measurement.

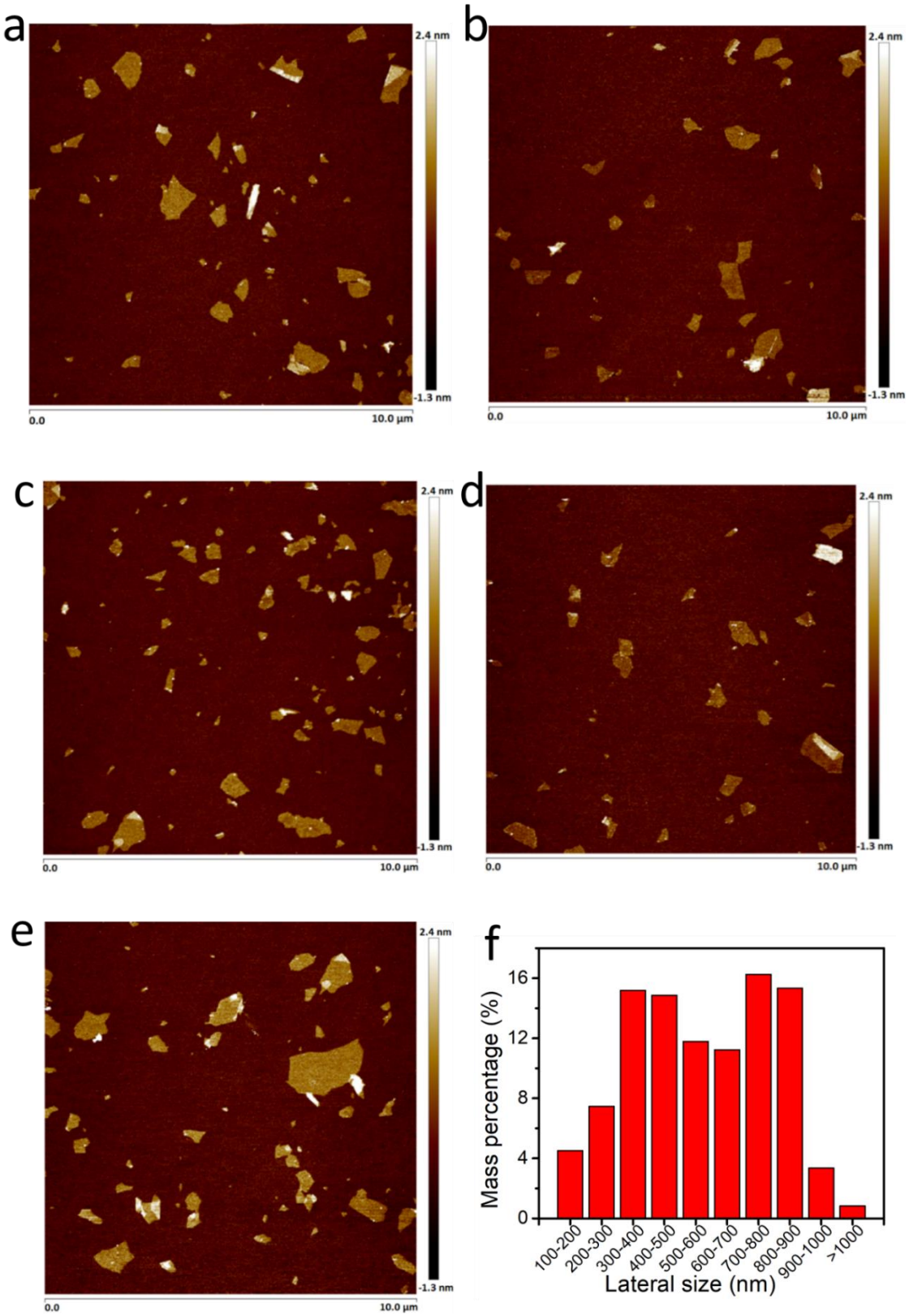

Figure 16. (a – e) AFM images of EGO sheets deposited on Si wafer. (f) Lateral size distribution of monolayer EGO sheets with the mass percentage.

The processability of the EGO dispersion was further tested by forming a membrane using vacuum filtration. A thin and free-standing EGO membrane with mass loading of 0.1 mg/cm^2 was fabricated and shown in **Figure 17**. During vacuum filtration, 0.1 mg/ml EGO dispersion is filtered through the filter. After drying in air for overnight, the EGO membrane could be readily peeled off. The membrane is also strong enough to withstand normal physical manipulation. As can be seen in the picture, the EGO membrane is uniform on a macro scale, with no obvious aggregations. This indicates good processability and formability of the EGO dispersion produced by the optimised electrochemical method.

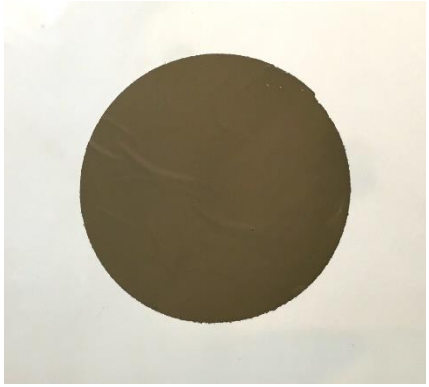

Figure 17. Picture of the free-standing EGO membrane (mass loading: 0.1 mg/cm^2)

4.4 Conclusions

In summary, the influences of important factors including electrochemical oxidation time, graphite sources and electrolyte concentrations on the electrochemical process and aqueous dispersibility of EGO by employing a controllable Tee-cell electrochemical oxidation method have been explored. With increasing oxidation time, the electrochemical process shows three sequential stages: intercalation, oxidation, and water hydrolysis. In the intercalation stage, the products show limited aqueous dispersibility due to limited oxidation. During the oxidation stage, the aqueous dispersibility of EGO increases with longer oxidation time but shows two significant increases in periods of 3 – 7 h and 11 – 15 h, which are due to the initial formation of oxygen functional groups and complete transformation of non-oxidized region separately.

The influence of graphite sources: graphite flakes and graphite foil, was also examined. Graphite flakes show a more ordered electrochemical process with shorter oxidation time than graphite foil due to denser structures of graphite flakes. EGO produced from graphite foil shows a much higher aqueous dispersibility than that produced from graphite flakes, which

indicates the importance of graphite source in producing graphene oxide. In addition to oxidation time and graphite sources, electrolyte concentrations also play an important role in the electrochemical process and aqueous dispersibility of the produced EGO. H_2SO_4 electrolyte with high concentrations can produce higher-stage GIC but exhibit limited oxidation level due to small amount of H_2O. H_2SO_4 electrolyte with low concentrations show an increased oxidation level but the small amount of H_2SO_4 restricted the intercalation process which causes a long oxidation time. The aqueous dispersibility of EGO reaches the maximum at around 12 M H_2SO_4. Overall, EGO dispersion with maximum aqueous dispersibility could be produced at optimised conditions: 22 h oxidation time, graphite foil source and 12 M H_2SO_4. The EGO dispersion produced at such optimised conditions was further characterised, and the long-term stability at various concentrations was demonstrated. The zeta potential of EGO dispersion is shown to be less than -30 mV, which indicates sufficient repulsive forces between EGO sheets. The AFM images of EGO sheets show a thickness of around 1.2 nm and lateral size of 100 nm – 1 µm. Moreover, an EGO membrane was fabricated to demonstrate the good processability of the EGO dispersion.

The results in this chapter assist in drawing a clear relationship between important factors in electrochemical process and aqueous dispersibility of the EGO products. By controlling and optimising the electrochemical conditions, highly aqueous dispersible EGO was produced, which could further enable the processability of EGO in to membranes for a range of applications.

4.5 References

1. Chen, D.; Feng, H.; Li, J., Graphene Oxide: Preparation, Functionalization, and Electrochemical Applications. *Chemical Reviews* **2012,** *112* (11), 6027-6053.
2. Kim, J.; Cote, L. J.; Huang, J., Two Dimensional Soft Material: New Faces of Graphene Oxide. *Accounts of Chemical Research* **2012,** *45* (8), 1356-1364.
3. Lowe, S. E.; Zhong, Y. L., Challenges of Industrial-Scale Graphene Oxide Production. In *Graphene Oxide*, John Wiley & Sons, Ltd: 2016; pp 410-431.
4. Huang, X.; Qi, X.; Boey, F.; Zhang, H., Graphene-based composites. *Chemical Society Reviews* **2012,** *41* (2), 666-686.
5. Konkena, B.; Vasudevan, S., Understanding Aqueous Dispersibility of Graphene Oxide and Reduced Graphene Oxide through pKa Measurements. *The Journal of Physical Chemistry Letters* **2012,** *3* (7), 867-872.

6. Li, D.; Muller, M. B.; Gilje, S.; Kaner, R. B.; Wallace, G. G., Processable aqueous dispersions of graphene nanosheets. *Nat Nano* **2008,** *3* (2), 101-105.

7. Yang, X.; Zhu, J.; Qiu, L.; Li, D., Bioinspired Effective Prevention of Restacking in Multilayered Graphene Films: Towards the Next Generation of High-Performance Supercapacitors. *Advanced Materials* **2011,** *23* (25), 2833-2838.

8. Qiu, L.; Zhang, X.; Yang, W.; Wang, Y.; Simon, G. P.; Li, D., Controllable corrugation of chemically converted graphene sheets in water and potential application for nanofiltration. *Chemical Communications* **2011,** *47* (20), 5810-5812.

9. Joshi, R. K.; Carbone, P.; Wang, F. C.; Kravets, V. G.; Su, Y.; Grigorieva, I. V.; Wu, H. A.; Geim, A. K.; Nair, R. R., Precise and Ultrafast Molecular Sieving Through Graphene Oxide Membranes. *Science* **2014,** *343* (6172), 752-754.

10. Sun, P.; Wang, K.; Zhu, H., Recent Developments in Graphene-Based Membranes: Structure, Mass-Transport Mechanism and Potential Applications. *Advanced Materials* **2016,** *28* (12), 2287-2310.

11. Qiu, L.; Liu, J. Z.; Chang, S. L. Y.; Wu, Y.; Li, D., Biomimetic superelastic graphene-based cellular monoliths. *Nature Communications* **2012,** *3*, 1241.

12. Yan, D.-X.; Pang, H.; Li, B.; Vajtai, R.; Xu, L.; Ren, P.-G.; Wang, J.-H.; Li, Z.-M., Structured Reduced Graphene Oxide/Polymer Composites for Ultra-Efficient Electromagnetic Interference Shielding. *Advanced Functional Materials* **2015,** *25* (4), 559-566.

13. Xu, Y.; Hong, W.; Bai, H.; Li, C.; Shi, G., Strong and ductile poly(vinyl alcohol)/graphene oxide composite films with a layered structure. *Carbon* **2009,** *47* (15), 3538-3543.

14. Liang, J.; Huang, Y.; Zhang, L.; Wang, Y.; Ma, Y.; Guo, T.; Chen, Y., Molecular-Level Dispersion of Graphene into Poly(vinyl alcohol) and Effective Reinforcement of their Nanocomposites. *Advanced Functional Materials* **2009,** *19* (14), 2297-2302.

15. Dreyer, D. R.; Park, S.; Bielawski, C. W.; Ruoff, R. S., The chemistry of graphene oxide. *Chemical Society Reviews* **2010,** *39* (1), 228-240.

16. Chi, C.; Dan, L., Solvated Graphenes: An Emerging Class of Functional Soft Materials. *Advanced Materials* **2013,** *25* (1), 13-30.

17. Hummers, W. S.; Offeman, R. E., Preparation of Graphitic Oxide. *Journal of the American Chemical Society* **1958,** *80* (6), 1339-1339.

18. Kovtyukhova, N. I.; Ollivier, P. J.; Martin, B. R.; Mallouk, T. E.; Chizhik, S. A.; Buzaneva, E. V.; Gorchinskiy, A. D., Layer-by-Layer Assembly of Ultrathin Composite Films

from Micron-Sized Graphite Oxide Sheets and Polycations. *Chemistry of Materials* **1999,** *11* (3), 771-778.

19. Marcano, D. C.; Kosynkin, D. V.; Berlin, J. M.; Sinitskii, A.; Sun, Z.; Slesarev, A.; Alemany, L. B.; Lu, W.; Tour, J. M., Improved Synthesis of Graphene Oxide. *ACS Nano* **2010,** *4* (8), 4806-4814.

20. Chen, H.; Li, C.; Qu, L., Solution electrochemical approach to functionalized graphene: History, progress and challenges. *Carbon* **2018,** *140*, 41-56.

21. Yang, S.; Lohe, M. R.; Müllen, K.; Feng, X., New-Generation Graphene from Electrochemical Approaches: Production and Applications. *Advanced Materials* **2016,** *28* (29), 6213-6221.

22. Su, C.-Y.; Lu, A.-Y.; Xu, Y.; Chen, F.-R.; Khlobystov, A. N.; Li, L.-J., High-Quality Thin Graphene Films from Fast Electrochemical Exfoliation. *ACS Nano* **2011,** *5* (3), 2332-2339.

23. Parvez, K.; Li, R.; Puniredd, S. R.; Hernandez, Y.; Hinkel, F.; Wang, S.; Feng, X.; Müllen, K., Electrochemically Exfoliated Graphene as Solution-Processable, Highly Conductive Electrodes for Organic Electronics. *ACS Nano* **2013,** *7* (4), 3598-3606.

24. Parvez, K.; Wu, Z.-S.; Li, R.; Liu, X.; Graf, R.; Feng, X.; Müllen, K., Exfoliation of Graphite into Graphene in Aqueous Solutions of Inorganic Salts. *Journal of the American Chemical Society* **2014,** *136* (16), 6083-6091.

25. Rao, K. S.; Senthilnathan, J.; Liu, Y.-F.; Yoshimura, M., Role of Peroxide Ions in Formation of Graphene Nanosheets by Electrochemical Exfoliation of Graphite. *Scientific Reports* **2014,** *4*, 4237.

26. Yang, S.; Brüller, S.; Wu, Z.-S.; Liu, Z.; Parvez, K.; Dong, R.; Richard, F.; Samorì, P.; Feng, X.; Müllen, K., Organic Radical-Assisted Electrochemical Exfoliation for the Scalable Production of High-Quality Graphene. *Journal of the American Chemical Society* **2015,** *137* (43), 13927-13932.

27. Ambrosi, A.; Pumera, M., Electrochemically Exfoliated Graphene and Graphene Oxide for Energy Storage and Electrochemistry Applications. *Chemistry – A European Journal* **2016,** *22* (1), 153-159.

28. Cao, J.; He, P.; Mohammed, M. A.; Zhao, X.; Young, R. J.; Derby, B.; Kinloch, I. A.; Dryfe, R. A. W., Two-Step Electrochemical Intercalation and Oxidation of Graphite for the Mass Production of Graphene Oxide. *Journal of the American Chemical Society* **2017,** *139* (48), 17446-17456.

29. Tian, Z.; Yu, P.; Lowe, S. E.; Pandolfo, A. G.; Gengenbach, T. R.; Nairn, K. M.; Song, J.; Wang, X.; Zhong, Y. L.; Li, D., Facile electrochemical approach for the production of graphite oxide with tunable chemistry. *Carbon* **2017,** *112*, 185-191.

30. Pei, S.; Wei, Q.; Huang, K.; Cheng, H.-M.; Ren, W., Green synthesis of graphene oxide by seconds timescale water electrolytic oxidation. *Nature Communications* **2018,** *9* (1), 145.

31. Noel, M.; Santhanam, R., Electrochemistry of graphite intercalation compounds. *Journal of Power Sources* **1998,** *72* (1), 53-65.

32. Beck, F.; Jiang, J.; Krohn, H., Potential oscillations during galvanostatic overoxidation of graphite in aqueous sulphuric acids. *Journal of Electroanalytical Chemistry* **1995,** *389* (1), 161-165.

33. Darling, H. E., Conductivity of Sulfuric Acid Solutions. *Journal of Chemical & Engineering Data* **1964,** *9* (3), 421-426.

34. Ionov, S. G.; Avdeev, V. V.; Kuvshinnikov, S. V.; Pavlova, E. P., Physical and Chemical Properties of Flexible Graphite Foils. *Molecular Crystals and Liquid Crystals Science and Technology. Section A. Molecular Crystals and Liquid Crystals* **2000,** *340* (1), 349-354.

Chapter 5. Microwave reduction of electrochemically-derived graphene oxide

5.1 Introduction

5.1.1 Reduction of graphene oxide

Graphene has extraordinary electronic properties, which makes it attractive for many applications such as energy storage[35] and catalysis[16]. The presence of high electrical conductivities of graphene is due to its perfectly flat sheet composed of sp^2 bonded carbon atoms[130-131]. To achieve such unique properties, it is necessary to produce graphene with minimal defects and sp^3 functional groups. High-quality graphene can be produced by chemical vapor deposition (CVD)[132], epitaxial growth[133], and micromechanical cleavage[28]. Even though high-quality materials can be achieved by these methods, scalability is another vital factor that should be considered. These methods have high cost with low yield of graphene[134]. Therefore, they are not suitable methods for high yield production of high-quality graphene. In comparison, graphene oxide (GO) can be used as a cheap and scalable precursor to graphene due to high yield production of GO by oxidation of graphite[134]. GO could be reduced to remove sp^3 oxygen functional groups and defects to form graphene with greatly enhanced electrical conductivity. The most commonly-used methods to reduce graphene oxide are chemical[134] and thermal reduction[135]. Chemical reduction of graphene oxide can be achieved using various reducing agents such as hydrazine, which is toxic and hazardous[136]. The chemically-reduced GO normally shows electrical conductivity of less than 1×10^4 S/m and C/O ratio of less than 15[136]. Thermal reduction of graphene oxide involves a heating process to reach a high temperature, which is time- and energy-consuming. Recently, microwave reduction appears to be another increasingly popular method to reduce graphene oxide due to its efficient and convenient heating process[16, 110-113, 137-138]. The reduction of graphene oxide can be achieved by microwave irradiation within seconds or minutes. Moreover, the method is very convenient and can easily be performed in a household microwave oven.

5.1.2 Challenges in microwave reduction of GO

Despite increasing attention, there are still challenges in the microwave reduction of graphene oxide. Firstly, the reduction efficiency of chemically-derived graphene oxide (CGO) via microwave is limited. Some previous work has reported microwave reduction of CGO, but the reduced graphene oxide is highly disordered[110, 138]. The Raman spectra show prominent and

broad D peaks which indicate large amounts of residual defects within the graphene structures[110, 138]. To solve the problem, it is necessary to partially reduce CGO before microwave irradiation and successfully achieved high-quality graphene after the two reduction processes[16]. However, partial reduction of CGO requires thermal annealing at 300 °C for 1 h, which costs time and energy. Even though high-quality graphene was produced, the complex method loses the advantages of convenience, high efficiency and low cost compared to the straight microwave reduction method. Some other research has tried adding graphite or reduced graphene oxide into the CGO as catalysts to improve the efficiency of microwave reduction, which reveal increased electrical conductivity[113] or aromatic domain size[114]. Previous reports have mainly involved microwave reduction of graphene oxide derived by chemical methods due to its high yield, high dispersibility, and processability. However, it was found that CGO shows limited microwave reduction efficiency if pre-treatment or catalysts are not involved, which will increase the complexity of the reduction method[16, 109-110, 113].

As in previous sections, electrochemical oxidation of graphite can be used to produce dispersible and processable graphene oxide. It is able to meet the demand for high scalability due to the use of graphite as source and high dispersibility with controllable and optimised electrochemical processes. As a promising candidate of GO, EGO could also be used as a precursor to graphene. As shown in Chapter 3, mechanically produced EGO shows a facile reduction ability with a high electrical conductivity after thermal reduction, which indicates a different structure of EGO compared to CGO. As highly dispersible EGO was produced in Chapter 4, it would be interesting to study whether the dispersible EGO shows high microwave reduction efficiency to produce high-quality graphene.

This chapter will study the microwave reduction of EGO to examine its efficiency and the quality of produced graphene. The reduced EGO by microwave will be characterized for its change of structure and chemistry, and compared with other microwave reductions of CGO for discussion of mechanisms.

5.2 Experimental Section

5.2.1 Production of EGO and CGO

EGO was produced by the Tee-cell electrochemical oxidation method described in Chapter 4. Graphite foil was used as a graphite source. During electrochemical oxidation, constant current 2 mA was applied to the 32 mg graphite foil pellet with 12 M H_2SO_4 for 22 hours. The product

was then washed to remove remaining H_2SO_4 and ultrasonicated by an ultrasonic probe (Branson Digital Sonifier S450D, 1/2" Horn, 500W, 30% amplitude, 30 min). The produced EGO dispersion (0.5 mg/ml) was filtered through a PVDF membrane (diameter 47 mm, pore size 0.22 μm) by vacuum to form an EGO membrane (mass loading 1.2 mg/cm^2). After the filtration, the membrane was dried in air for over 24 hours to remove water. The EGO membrane was then peeled from the PVDF filter for further microwave treatment.

CGO was also produced to make a comparison with EGO. It was synthesized by a modified Hummers method reported by Kovtyukhaova et al[46]. The method has been described in Chapter 4. To produce CGO with a relatively lower oxidation degree, 30 g $KMnO_4$ was used instead of 60 g to oxidise 20 g graphite. The resultant CGO was also ultrasonicated by the same process as EGO. The CGO dispersion (0.5 mg/ml) was formed into CGO membrane with the mass loading of 1.2 mg/cm^2.

5.2.2 Microwave irradiation of EGO and CGO

Microwave irradiations of EGO and CGO membranes were performed in the centre in a household microwave oven (Anko P70B20AP-ST, 700 W, 2450MHz). The EGO or CGO membrane was first put into a glass vial, which was then put into a N_2 glove box for overnight to fill the glass vial with N_2 gas. The cap was screwed tightly on glass vial to prevent gas exchanging with outside air. The glass vial with EGO or CGO membrane (diameter 35 mm, thickness 5 μm) and N_2 gas inside was then put into the microwave oven for the microwave irradiation. The microwave power could be adjusted from 10% to 100% (out of 700 W). The microwave time could also be set from 1 s to minutes. It was found that microwave time of 3 seconds could induce the microwave reaction of the EGO membrane with the observation of bright sparks. For the membranes to be microwave-treated in an air atmosphere, the glass vial holding the membrane would be put in the air for overnight and then taken for microwave irradiation.

The microwave-irradiated EGO or CGO is abbreviated to MwEGO or MwCGO.

5.2.3 Characterisations

Scanning electron microscopy (SEM) was used to characterise the morphology and structure change of the EGO membrane before and after microwave irradiation. SEM images were taken by FEI Nova NanoSEM 450 FEGSEM with an accelerating voltage of 5.00 kV. The samples

were prepared by cutting the membranes through their cross-section. Then the cross-section of the membrane was imaged by SEM.

Raman spectroscopy was used to characterise the chemical structure of the EGO before and after microwave reduction, which could also indicate the quality of the reduced EGO. The Raman spectra were measured by a Renishaw InVia Raman Microscope with a 532 nm laser wavelength and a 10 µm laser spot size.

X-ray Diffraction (XRD) was used as a tool to characterise the composition of the product and the crystalline structure of the EGO, MwEGO, CGO, and MwCGO membranes. To measure the XRD of the MwEGO membrane, the porous membrane was compressed under a pressure of 100 bar to compact the membrane. As a comparison, the original EGO membrane was also compressed by the same pressure, even though it was already a compact membrane. Both of CGO and MwCGO membranes kept a compact membrane before and after microwave irradiation, but they were also compressed as a comparison. Chemically-reduced CGO (CrCGO) and chemically-reduced EGO (CrEGO) were also used to compare with MwEGO. CrCGO or CrEGO were prepared by reducing the CGO or EGO dispersion (0.5 mg/ml) with a hydrazine solution with hydrazine to GO ratio of 7:10. Then the CrCGO or CrEGO dispersion was formed into membranes (mass loading 1.2 mg/cm2) by vacuum filtration through a PVDF filter. The membranes were also compressed to produce a comparable control.

Thermogravimetric analysis (TGA) was used to characterise the chemical structures of EGO, CGO, MwEGO, and MwCGO. It was measured by a Thermo thermogravimetry/differential thermal analyser (TG/DTA) 6300 from 25 °C to 700 °C with a heating rate of 1 °C/min. All samples were conducted in the air atmosphere. After measurement, the data of curves from 100 °C to 700 °C were examined, since weight loss below 100 °C were mainly due to evaporation of water molecules which mostly escaped above 100 °C. The weight (W) at each point was transformed into weight percentage (w%) by calculation of the equation 5.1.

$$w\% = (W_{point} - W_{100\,°C}) / W_{100\,°C} * 100\%. \qquad 5.1$$

X-ray photoelectron spectroscopy (XPS) was used to quantitatively characterise the composition of C, O elements and oxygen groups in EGO and CGO. It was conducted in a VG ESCALAB220i-XL spectrometer with a hemispherical analyser. After obtaining the data, the curves were analysed by the software CasaXPS. The background was removed first from the

curves for further fitting. The percentage of each type of atom was derived by having considered Relative Sensitivity Factors.

5.2.4 Measurement of electrical conductivity

The sheet resistance of the MwEGO and MwCGO membranes were measured using a Jandel four-point probe. The probe was connected to a linear arrayed head with 1 mm spacing. To accurately measure the sheet resistance of the expanded membranes, they were compressed under a pressure of 100 bar to transform the porous structure into a dense layer structure. The conductivity of the membrane could be calculated by the equation 5.2.

$$\text{Conductivity} = 1/\text{resistivity} = 1/(\text{sheet resistance}*\text{thickness}) \qquad 5.2$$

The thickness of the membranes was measured by Yuzuki electronic micrometer (resolution 0.001 mm). MwEGO and MwCGO produced under various microwave time, power and atmosphere were tested for their conductivities. In addition, the conductivity of MwEGO was also compared to that of reduced graphene oxide by other reduction methods. Thermally-reduced EGO (TrEGO) and CGO (TrCGO) were produced by thermally annealing EGO and CGO at 300 °C for 1 h. Microwave-irradiated TrEGO (MwTrEGO) and TrCGO (MwTrCGO) were produced by irradiating TrEGO and TrCGO with microwave at 700 W for 10 s in N_2 atmosphere. Chemically-reduced EGO (CrEGO) and CGO (CrCGO) were made by reducing EGO and CGO with hydrazine solution as described in section 5.2.3.

5.3 Results and discussion

To study the microwave reduction process of EGO, EGO dispersion was vacuum-filtered so as to form a laminated membrane with a mass loading of 1.2 mg/cm^2. The membrane was then placed in to a vial with an atmosphere of air or nitrogen (see details in experiment section above). The vial containing the EGO membrane was then placed in to the microwave oven for treatment. As a comparison, the CGO membrane was fabricated with the same process and mass loading. Upon microwave irradiation of EGO membranes for about 3 seconds, bright sparks were observed inside the vial, indicating violent reactions between EGO membranes and microwave. After microwave irradiation, the EGO membrane became an expanded membrane with larger thickness and porous layer structures. As a comparison, CGO membrane showed no sparking and expansion, even when the microwave irradiation lasts for 2 minutes.

Figure 1 shows the appearance of the EGO membrane before and after the microwave irradiation process. As shown in **Figure 1a**, the EGO membrane before microwave treatment ws a flat, smooth and thin membrane. However, after microwave treatment (**Figure 1b**), the membrane is expanded and bent. To further examine its microstructure change, SEM images of the cross-section of the membrane are taken before and after microwave treatment. From **Figure 1c, d**, a drastic change of the thickness and microstructure can be seen. Before microwave treatment, the EGO membrane shows densely packed laminated layers with a thickness of around 4.1 μm. However, the membrane after microwave treatment showed a porous microstructure, with the thickness increased to about 480 μm. The porous microstructure should be caused by the gas formation between EGO layers during the removal of oxygen functional groups, as often happened in thermal or chemical reduction of graphene oxide membranes.

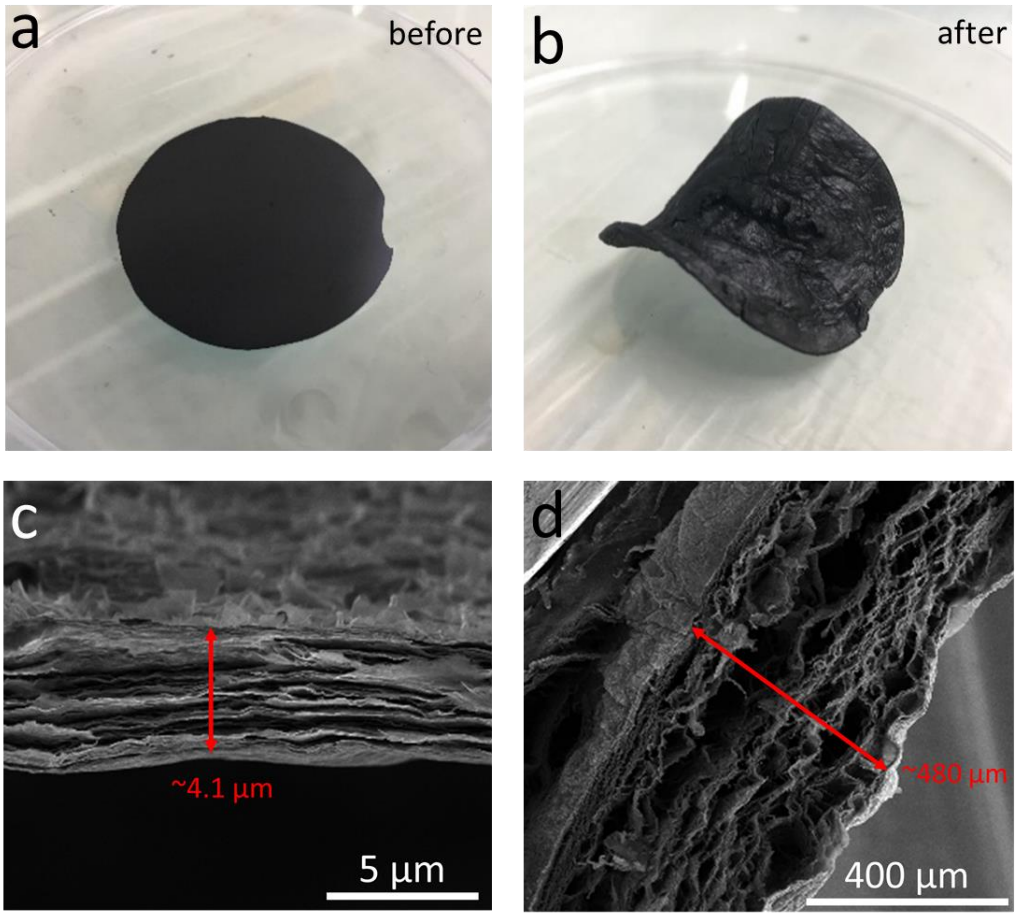

Figure 1. Digital image of EGO membrane (a) before and (b) after microwave treatment. SEM pictures showing the cross-section of EGO membrane (c) before and (d) after microwave. Scale bar in (c) is 5 μm and in (d) is 400 μm.

5.3.1 Structural characterization

In the first part of the study, structural and chemical characterisations of EGO after microwave irradiation were performed to reveal the quality of microwave-irradiated EGO (MwEGO) and change of structure and chemistry caused by microwave reduction.

Raman spectroscopy

Raman spectroscopy was used to investigate the atomic-scale structural change on EGO sheets and the intrinsic quality of the carbon material after microwave treatment. **Figure 2a, b** shows Raman spectra of EGO and CGO, respectively. Both of EGO and CGO consist of two prominent peaks in the range of 1000 – 1800 cm^{-1}: D peak and G peak. D peak is induced from disruption of sp^2 symmetry in sixfold aromatic rings. Therefore, high intensity of D peaks for both EGO and CGO indicate the presence of defects including sp^3 bonds and hole defects within the structure of graphene oxide. The G peak is attributed to the motion of sp^2 pair carbon atoms, and thus is related to the graphitic domains. After microwave irradiation of EGO and CGO, the Raman spectra were measured and are shown in **Figure 2c, d, e**. Raman spectrum (**Figure 2d**) of microwave-irradiated CGO (MwCGO) after microwave treatment in N_2 atmosphere shows almost no change compared to that of CGO (**Figure 2b**), which indicates no reduction and structural change of CGO subjected to the microwave treatment. In comparison, Raman spectra of MwEGO obtained from microwave treatment of EGO in N_2 and air atmosphere show obvious changes, as can be observed in **Figure 2c** and **Figure 2e** respectively. The main parameters of the D and G peaks from Raman spectra are displayed in **Table 1**.

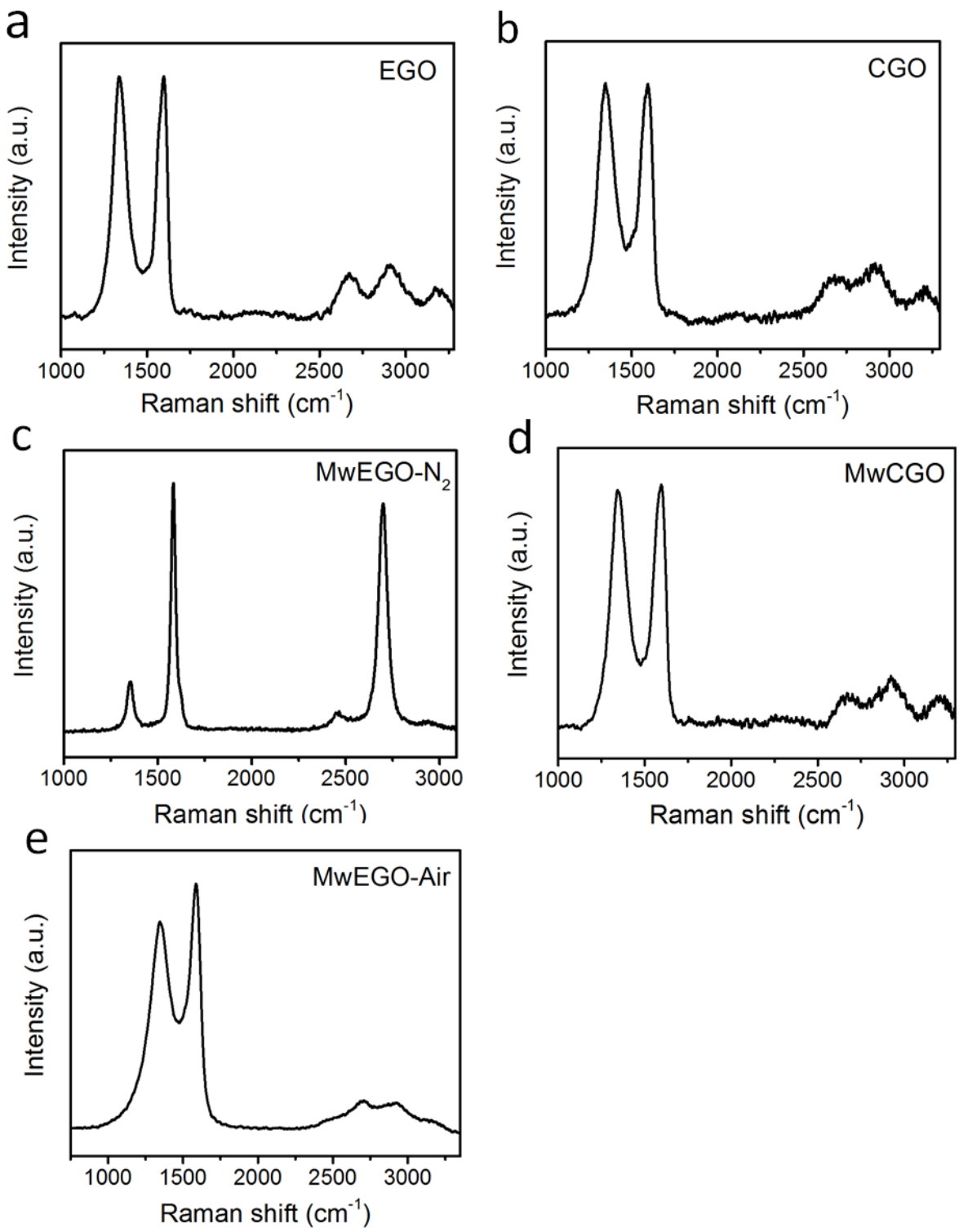

Figure 2. Raman spectra of (a) EGO and (b) CGO before microwave treatment, (c) MwEGO-N_2 and (d) MwCGO after microwave treatment in N_2, (e) MwEGO after microwave treatment in air.

Table 1. Comparison of the main peak parameters in Raman spectra of EGO, MwEGO-N_2, MwEGO-Air shown in Figure 2.

	Position (cm^{-1})	**FWHM (cm^{-1})**		**I_D/I_G**
	G	D	G	
EGO	1588.4	93.5	57.7	0.997
MwEGO-N2	1582.8	39.5	28.4	0.187
MwEGO-Air	1586.2	171.9	64.3	0.902

Significant changes in the position of G peak from EGO to MwEGO can be seen. The position of G peak is correlated with the lattice strain or doping in graphene sheets. Pristine graphene or graphite is reported to show a position of G peak at 1582 cm^{-1}. Oxidised graphene or graphite typically has a blue-shifted G peak due to the introduction of oxygen and defects into the lattice. As shown in **Table 1**, EGO shows a G peak position of 1588.4 cm^{-1} due to its oxidised structure. In contrast, MwEGO irradiated in the N_2 atmosphere shows a G peak position at 1582.8 cm^{-1}, which present a great red shift from EGO. The G position of MwEGO is close to that of pristine graphene at 1582 cm^{-1}, indicating significant loss of oxygen groups and formation of aromatic graphene domains. However, MwEGO produced in air atmosphere shows a G peak position at 1586.2 cm^{-1}, which is much higher than that of MwEGO from N_2. This reveals a higher amount of residual oxygen groups in MwEGO from the air than from N_2, which may be due to its inferior tendency of reduction or oxidation of residual carbon atoms in the air.

Another clear change is seen in the full width at half maximum (FWHM) of D and G peak. The broadening of D and G peaks results from the broader distribution of aromatic domain size and orientation, which is normally due to decreased aromatic domain size and the introduction of oxygen bonding and lattice strain. MwEGO irradiated in N_2 shows much decreased FWHM of D (39.5 cm^{-1}) and G peaks (28.4 cm^{-1}) compared to EGO, which has FWHM of 93.5 cm^{-1} and 57.7 cm^{-1} for D and G peak, respectively. The sharpening of D and G peaks for MwEGO from N_2 indicates a larger aromatic domain and reduced oxygen bonding after microwave reduction, contributing to increased order of sp^2 clusters. However, MwEGO irradiated in air demonstrates opposite change with a great increase in FWHM of D (171.9 cm^{-1}) and G (64.3

cm^{-1}) peak, indicating its increased disorder and decreased size of aromatic domains may be due to disruption of sp^2 domains during oxidation of the carbon structure in the air.

The most significant change is the intensity of D peak, which is correlated with the number of defects within graphene lattice. The D and G peak ratio I_D/I_G is an important parameter to quantitatively interpret the defects or aromatic domains. From **Table 1**, it can be seen that MwEGO irradiated in N_2 has a much lower I_D/I_G of 0.187 than EGO, which shows I_D/I_G of 0.997. The decreased I_D/I_G indicates a reduction in the number of defects and transformation of them into graphitic regions after microwave irradiation of EGO in N_2. The MwEGO produced in the air only shows a small decrease of I_D/I_G to 0.902, which represents large amounts of defects remaining in the structure.

The size of the aromatic domain (L_a) is correlated with the D and G peak ratio I_D/I_G. The Tuinstra and Koening (TK) relationship, which holds for carbons with aromatic domains size larger than 10 nm, can be applied to determine L_a of MwEGO irradiated in N_2. In the TK model, I_D/I_G is inversely proportional to L_a. To calculate the size of the aromatic domain L_a for the MwEGO in N_2, the equation 5.3 proposed by Cançado et al[86] is used.

$$L_a(nm) = (2.4 \times 10^{-10}) \times \lambda^4 \times (\frac{I_D}{I_G})^{-1} \qquad 5.3$$

where λ is the wavelength of incident light (532 nm). The calculated L_a is 102.8 nm for MwEGO that is reduced by microwave in N_2. This high value of L_a shows a large size of the aromatic domain in MwEGO irradiated in N_2. This L_a value is similar to the value reported in a previous work of microwave-reduced graphene oxide, where the graphene oxide is pre-treated by thermal heating at 300 °C for 1 h.[16] Nevertheless, no thermal treatment is required before microwave treatment to partially reduce EGO. EGO can be directly reduced by microwave radiation within 3 seconds to produce high-quality graphene.

Moreover, the valley between the D and G peaks almost disappears after microwave treatment of EGO in N_2, which represents greatly reduced oxygen functional groups since the valley is an indication of sp^3 bonding or doping[90]. In contrast, the valley between D and G peaks of MwEGO produced in air shows an obvious increase, which is even higher than that of CGO. This shows more sp^3 bonding formed during microwave treatment in air. It may be because oxidation of the sample happens during the microwave treatment process that there is a loss of sp^2 bonding and increase of sp^3 bonding. In addition to the D and G peaks, another

characteristic graphitic peak is the 2D peak at ~2700 cm^{-1}, which indicates highly-ordered π-bonding in graphene structure[139]. From **Figure 2c**, it can be seen that the intense 2D peak of MwEGO irradiated in N_2, which is greatly enhanced compared to that of EGO. This indicates a dramatic increase in interplanar coherence length that is resulted from uniformly stacked aromatic domains due to the removal of sp^3 bonding and strains after microwave treatment in N_2.

The above findings from Raman spectrums indicate the significant structural changes from EGO to MwEGO after microwave irradiation. For MwEGO irradiated in N_2, the removal of defects and oxygen functional groups and formation of aromatic domains have been shown from the changes of position, FWHM and intensity of the D, G, and 2D peaks. The quality of MwEGO in N_2 was examined by the calculation of aromatic domain size L_a (102.8 nm). However, the MwEGO irradiated in air shows different structural changes from MwEGO in N_2 with many defects and sp^3 bonding remaining in the structure, which is likely due to the oxidation of carbon structures in the air. Therefore, care must be taken about the atmosphere of EGO during microwave reduction, which will cause a great influence on the structure of the MwEGO products. In contrast, CGO shows little change in its Raman spectrum, exhibiting little activation of the structure during the microwave irradiation.

XRD

During microwave treatment of EGO membrane, the oxygen functional groups will be removed by reduction, causing the changes in interlayer structures such as the interlayer distance between two adjacent sheets. Therefore, XRD would be another useful tool to characterise the reduced structure after microwave treatment. Information can be obtained from XRD as to whether the GO structure is transformed into graphene/graphite structure and information of the aromatic region in the graphitic structure after microwave treatment. To remove the influence of the gas formation between sheets causing porous structure, the membrane after microwave treatment was compressed with a constant pressure, which is also performed in an original EGO membrane for XRD tests.

The XRD spectrums of EGO and CGO membrane before and after microwave treatment in N_2 are shown in **Figure 3**. As can be seen in **Figure 3a**, EGO shows a peak at around 12.2°, which corresponds to an interlayer distance of 0.72 nm between sheets. This indicates the presence of oxygen functional groups within the structure. After microwave treatment, MwEGO shows a

peak at 26.0°, indicating an interlayer distance of 0.34 nm. The decreased interlayer distance demonstrates the loss of oxygen groups between sheets. It is well-known that graphite has a characteristic peak at around 26.7°. This indicates the transformation of the graphene oxide structure into the graphitic structure with graphene sheets stacked together. By comparison, MwCGO shows a small right-shift in the XRD spectrum (**Figure 3b**) which may be due to a slight removal of the moisture between the graphene oxide sheets. No peaks could be found at around 26°, which indicates no reduction of CGO at all.

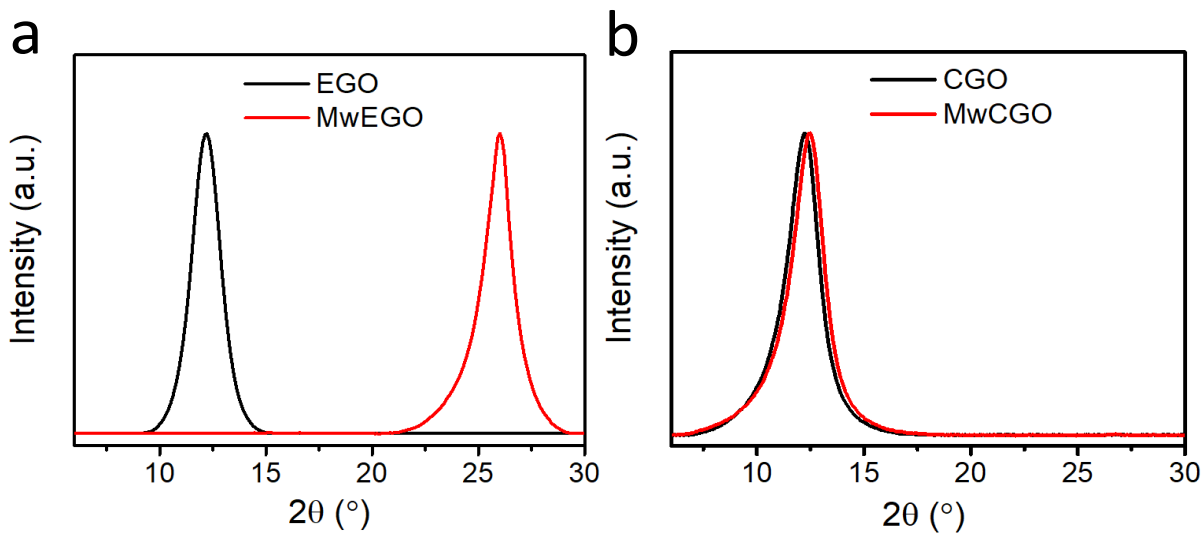

Figure 3. XRD change before and after microwave of (a) EGO membrane and (b) CGO membrane.

To further analyze the quality of MwEGO and assess the efficiency of microwave reduction, another frequently used reduction method, chemical reduction by hydrazine, was performed to make a comparison with microwave reduction. Chemically reduced CGO (CrCGO) and chemically reduced EGO (CrEGO) were produced by reduction of CGO and EGO with hydrazine solution. The hydrazine to GO ratio of 7:10 is used, which is reported to be an optimal ratio for producing highly conducting graphene sheets[47]. The XRD spectrums of MwEGO, CrEGO, and CrCGO are compared in **Figure 4**. The detailed information about the structural features can be obtained by analysing the XRD spectrums. Important peak parameters are listed in **Table 2**, which provide information about interlayer distance and coherence. As can be clearly observed from **Figure 4**, the three samples show different peak positions, with MwEGO exhibiting largest 2θ values of 26.0° that is closest to the peak position of graphite (26.7°). In contrast, CrEGO shows a peak position at 24.9°, which is smaller than that of MwEGO. Among the samples, CrCGO shows the smallest 2θ values of 23.4°. By

calculation of the interlayer distance (d) from the 2θ values, CrCGO shows largest d of 0.38 nm and CrEGO shows second largest d of 0.36 nm, both of which are larger than MwEGO (0.34 nm). The smaller interlayer distance of MwEGO shows that it contains the least amount of remaining oxygen groups or bonding within the structure, which is closest to the structure of graphite.

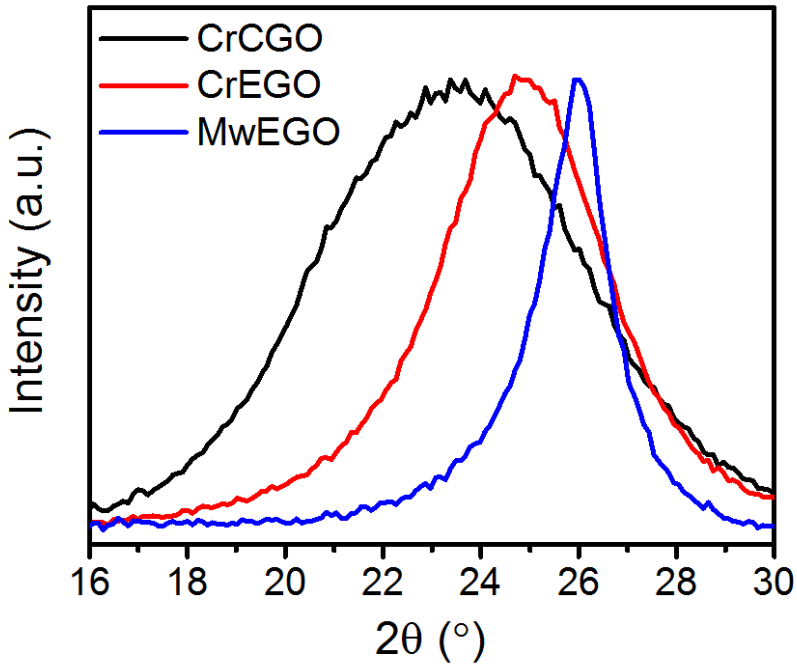

Figure 4. XRD (002) peak of MwEGO, CrEGO, and CrCGO with normalised intensity.

Table 2. Parameters from XRD (002) peaks in Figure 4.

	2θ (°)	d (nm)	$FWHM_{\pi}$ (°)	L_c (nm)	layers
MwEGO	26.0	0.34	1.60	5.04	15
CrEGO	24.9	0.36	3.92	2.05	6
CrCGO	23.4	0.38	6.37	1.26	3

The broadening of the diffraction peaks provides other important information, including information about coherence in aromatic regions. It can be seen from **Figure 4** that MwEGO shows the sharpest peak, with CrEGO showing a broader peak than it and CrCGO showing the broadest peak. This shows the most ordered structure of MwEGO and highest disorders within

CrCGO structures. To quantitatively analyse the broadening, full width at half maximum (FWHM) was measured from the XRD peaks. MwEGO, CrEGO and CrCGO show FWHM of 1.60°, 3.92°, and 6.37° respectively. According to the Scherrer equation (5.4) shown below, FWHM can be used to calculate the crystallite size or coherence length.

$$L_c = \frac{0.89\lambda}{\beta(2\theta)_{(00l)} cos\theta} \qquad 5.4$$

where L_c is the coherence length along (00l) inter-sheet directions, λ is the wavelength of incident X-ray (1.5405 Å), β(2θ) is line broadening in radians. As shown in **Table 2**, L_c is about 5.04 for MwEGO, which indicates an average of about 15 layers forming an aromatic coherence domain. Compared to MwEGO, CrCGO produced by chemical reduction shows a much smaller L_c value of 2.05, with an average 6 layers of π-bonds domain stacked together. CrCGO shows the smallest L_c value of 1.26, which means that only 3 layers of aromatic coherence domain exist in its reduced structure.

The structural information obtained from the XRD results shows that MwEGO contains the least residual oxygen groups and the largest aromatic coherence domains among the three reduced graphene oxide samples. It is clear from these findings that microwave reduction shows much higher reduction efficiency than chemical reduction by hydrazine, since not only higher-quality graphene is obtained from microwave reduction but also it also requires much shorter processing time (3 – 10 s) than chemical reduction (3 h). Higher quality of CrEGO than CrCGO demonstrates that EGO can be more easily reduced and transformed into aromatic coherence structures than CGO. This agrees with the observation that EGO can be more easily activated and reduced under microwave treatment than CGO.

TGA

Thermogravimetric analysis (TGA) has been utilised to analyse the change of chemical structure after microwave irradiation in N_2. **Figure 5** shows TGA curves of EGO, CGO and their microwave-treated counterparts, MwEGO and MwCGO, which were measured in an air atmosphere. TGA curves of EGO and CGO are similar, which contain two major weight losses in the whole temperature range. As can be observed in **Figure 5a**, both of EGO and CGO show the first major weight loss at around 150 – 210 °C and 140 – 200 °C, respectively, which is caused by decomposition of some oxygen groups. The weight loss % of EGO and CGO in this stage are about 29.9% and 29.6%, respectively, which indicates a similar degree of oxidation

of EGO and CGO. In the temperature region of around 200 – 450 °C before the next major weight drop, CGO loses weight at around 15.4%. In comparison, EGO loses less weight of around 11.5% in the temperature range of 210 – 500 °C. The weight loss in this range may be due to the decomposition of oxygen groups which are more thermally stable and requires higher thermal energy. The second major weight loss of CGO at around 450 °C is due to the loss of the remaining carbon in the air since the remaining weight drops to zero. In contrast, EGO shows such a carbon loss process at around 500 °C, which indicates better oxidative stability of EGO. This may be due to thermally reduced EGO showing a more aromatic structure like graphite, which makes it less oxidative in the air. From the TGA analysis of EGO and CGO, similarities and differences between the two graphene oxide structures can be seen, which exhibits similar amounts of thermally-unstable oxygen functional groups (which are lost at around 150 – 210 °C or 140 – 200 °C), different amounts of thermally-stable oxygen groups (degrading at around 200 – 450 °C or 210 – 500 °C) and different aromatic structures. These structural differences will provide insights into the different behaviors of EGO and CGO under microwave treatment.

The MwEGO and MwCGO were also tested by TGA to reveal their changes in chemical structures and their different chemical compositions. The TGA curves of MwEGO and MwCGO are shown in **Figure 5b**. MwCGO shows little change in TGA curves compared to CGO, which proves that no reduction process occurs in CGO. In contrast, MwEGO presents a significant change in the TGA curve compared to EGO, where there is mainly one dramatic weight loss at around 500 – 680 °C for MwEGO. Before 500 °C, a limited weight loss of MwEGO could be observed, which shows that limited oxygen functional groups are remaining in MwEGO after the microwave irradiation. This proves a reduction process happens with the removal of the majority of oxygen groups in EGO during the microwave treatment. Another feature of MwEGO is that it shows higher oxidative stability than EGO, which could be observed from its higher decomposition temperature (from 500 °C up to 680 °C) than EGO (from 500 °C up to 570 °C). This indicates a transition of defective/oxidative carbon structure into a highly-ordered graphene-like structure from EGO to MwEGO.

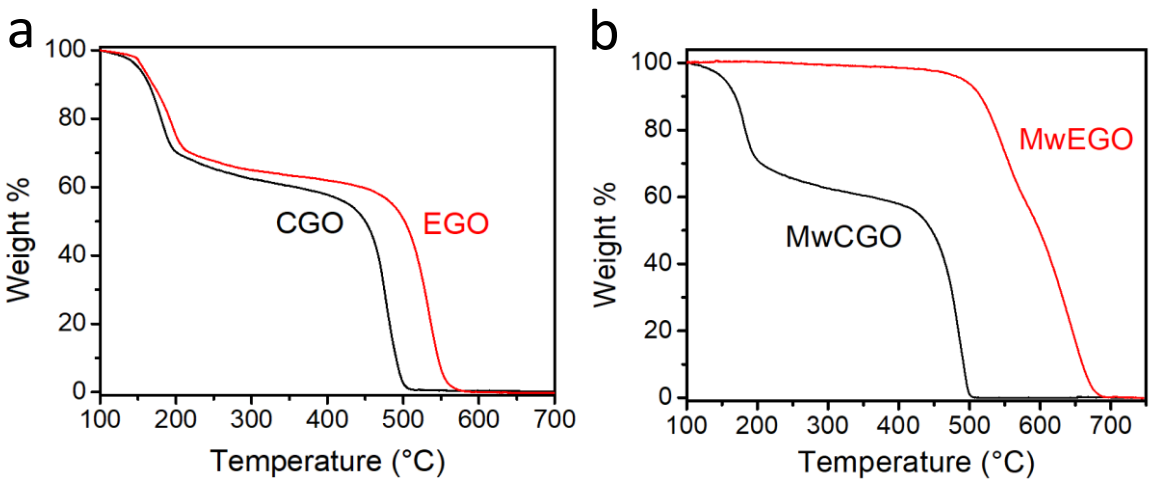

Figure 5. TGA curves of (a) EGO and CGO, (b) MwEGO and MwCGO, performed in air atmosphere.

XPS

To quantitatively analyse chemical compositions, X-ray photoelectron spectroscopy (XPS) was used to test EGO, CGO, and their microwave-treated counterparts. **Figure 6** shows the XPS survey spectra of the four samples, which contain two main peaks that are originated from carbon (284.4 eV) and oxygen (531.4 eV). Carbon and oxygen content of each sample has been calculated from the spectra and listed in **Table 3**. EGO contains approximately 74.4 at. % carbon content and 25.6 at. % oxygen content with a C/O ratio of 2.9. In comparison, CGO contains less carbon content of about 73.4 at. % and more oxygen content of about 26.6 at. % with a C/O ratio of 2.8. After microwave irradiation, MwEGO shows a significantly decreased oxygen content to about 2.9 at. % with an increased carbon content of 97.1 at. %, which results in a high C/O ratio of 33.6. As a comparison, CGO shows little change in carbon and oxygen content after microwave treatment.

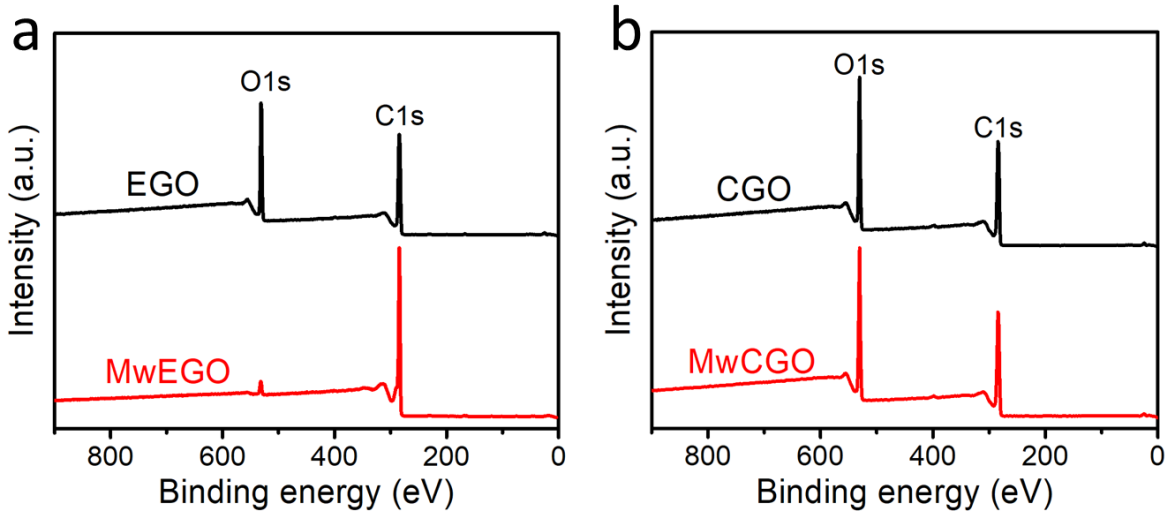

Figure 6. XPS survey spectra of (a) EGO and MwEGO, (b) CGO and MwCGO at room temperature.

Table 3. Carbon and oxygen content of EGO, MwEGO, CGO, and MwCGO.

Atom%	EGO	MwEGO	CGO	MwCGO
C	74.4	97.1	73.4	73.5
O	25.6	2.9	26.6	26.5

The high-resolution XPS C 1s spectra of EGO and MwEGO were scanned to reveal the carbon bonds. The C 1s signal of EGO (**Figure 7a**) can be fitted into three main components: sp^2 graphitic carbon at 284.4 eV, C=O/C-OH/C-O-C at 286.4 eV, COOH at 288.1 eV. The presence of strong carbon-oxygen peaks indicates their high oxidation. After microwave irradiation, the carbon-oxygen bonds were greatly removed with a main sharp peak at 284.4 eV, as shown in **Figure 7b**. The tail of sp^2 peak can be fitted with two weak carbon-oxygen peaks: C-OH peak at 285.5 eV and C=O peak at 287.1 eV. The C 1s spectrum of MwEGO is similar to that of graphite, which consists of a weak C-O peak due to atmospheric oxidation[108]. In addition to C-OH/C=O peaks, a π-π* satellite peak can be observed at around 290.6 eV in C 1s spectrum of MwEGO, which is resulted from delocalised π conjugation of aromatic carbon domain[108]. The comparison of MwEGO and EGO indicates the transformation of carbon-oxygen bonds and restoration of aromatic carbon structure in the MwEGO sample.

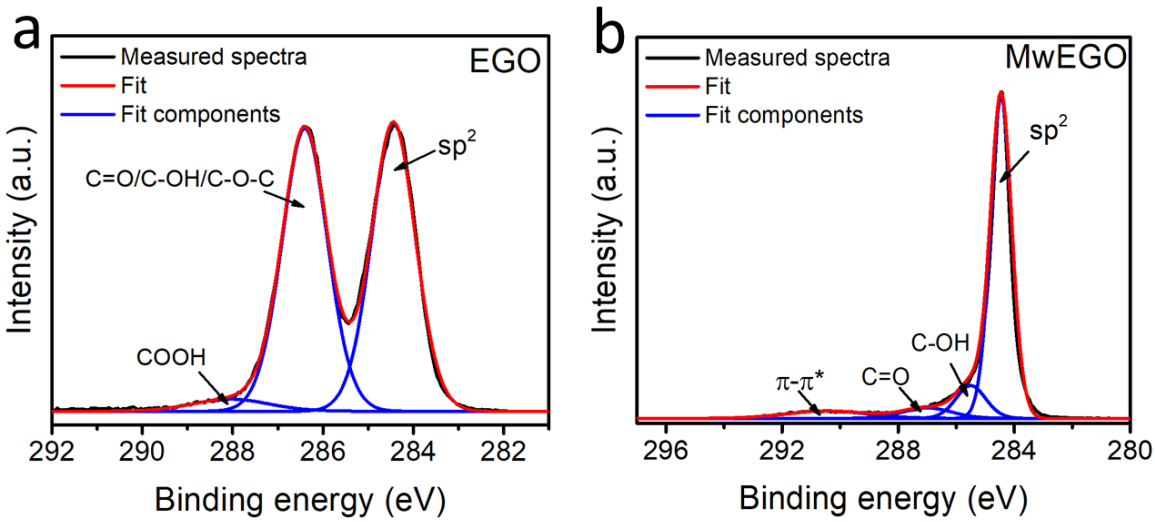

Figure 7. XPS C 1s spectra of (a) EGO and (b) MwEGO with fit components: sp^2, C=O/C-OH/C-O-C, COOH.

5.3.2 Electrical conductivity

In the next part, the electrical conductivity of EGO was measured the four-point probe conductivity test for different microwave conditions: microwave time, power and atmosphere. As an important parameter that increases with reduction degree due to the loss of oxygen functional groups and the formation of aromatic networks, electrical conductivity could be used to signify the reduction process and reduction efficiency during microwave treatment.

Influence of microwave time and power

The influence of microwave time was studied by measuring the electrical conductivity of the membrane after microwave time of 0, 1 s, 3 s, 6 s, and 10 s with a microwave power of 700 W in the atmosphere of N_2. The conductivity change of EGO and CGO with microwave time is shown in **Figure 8a**. As can be observed, EGO and CGO membrane shows a similar electrical conductivity of about 0.1 S/m due to their high oxidation degree and disrupted the conductive network. After 3 s of microwave treatment, the conductivity of EGO shows an abrupt increase to about 36000 S/m. In this short process, bright sparks from the EGO membrane in the vial can be seen inside the microwave oven. With further microwave treatment, the sparks continue along with a further increase of conductivity to about 49000 S/m after 10 seconds. However, CGO membrane shows no sparks during the whole process. Correspondingly, the conductivity of CGO membrane shows almost no change, which remains at around 0.1 S/m.

The influence of microwave power was studied by microwave irradiation of EGO under different irradiation powers (10% - 100% of 700W) for 10 s in N_2 atmosphere. The conductivity change with microwave power is shown in **Figure 8b**. The result shows that a minimum of 20% (140 W) of the highest microwave power (700 W) can achieve the rapid microwave reduction of EGO. When the microwave power is further increased from 20% (140 W) to 100% (700 W) as shown in the inset of **Figure 8b**, the conductivity will gradually increase to around 49000 S/m.

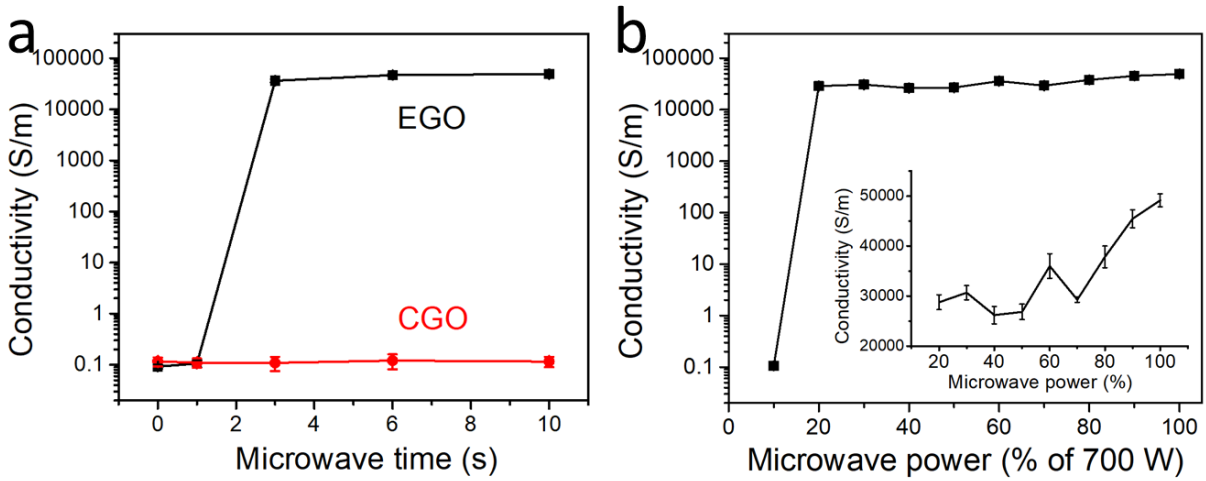

Figure 8. (a) Electrical conductivity of EGO and CGO with microwave time. (b) Conductivity change with microwave power for EGO. Inset: rescaled conductivity range for 20% - 100% microwave power.

Influence of atmosphere

Another important factor that influences the microwave reduction efficiency is the atmosphere surrounding the EGO membrane, as shown in the Raman results. A previous study has reported the influence of atmospheric gas on the product of microwave reduction[111]. Ar atmospheres show a far more effective reduction process than air atmosphere during microwave reaction of a mixture of GO and graphene nanosheets[111]. To study the influence of atmosphere on the microwave reduction efficiency of EGO membrane, the N_2 gas surrounding EGO inside the vial has been changed to air. During the microwave reaction in the air atmosphere (10 s, 700 W), the same phenomenon of bright sparks as in N_2 atmosphere can be observed. However, in that case, a majority part of the sample was burned and disappeared with only a small part of the membrane remaining. The weight of the EGO membrane was measured before and after the microwave treatment, as shown in **Figure 9a**. From the change of weight percentage, about

57% loss of the initial weight remains for microwave-treated EGO in the N_2 atmosphere. The lost weight is mainly due to the loss of oxygen moieties. However, in the air atmosphere, only 8% of the initial weight remains after microwave irradiation. This shows that most of the EGO is lost in the air, with the removal of not only oxygen functional groups but also large amounts of aromatic carbon atoms. By comparing the conductivities of microwave-treated EGO membranes in air and N_2 (**Figure 9b**), lower conductivities of MwEGO microwave-treated in the air are observed, than those treated in N_2. This shows the much lower efficiency of microwave reduction in air atmosphere than in inert N_2 gas, which agrees well with the Raman analysis.

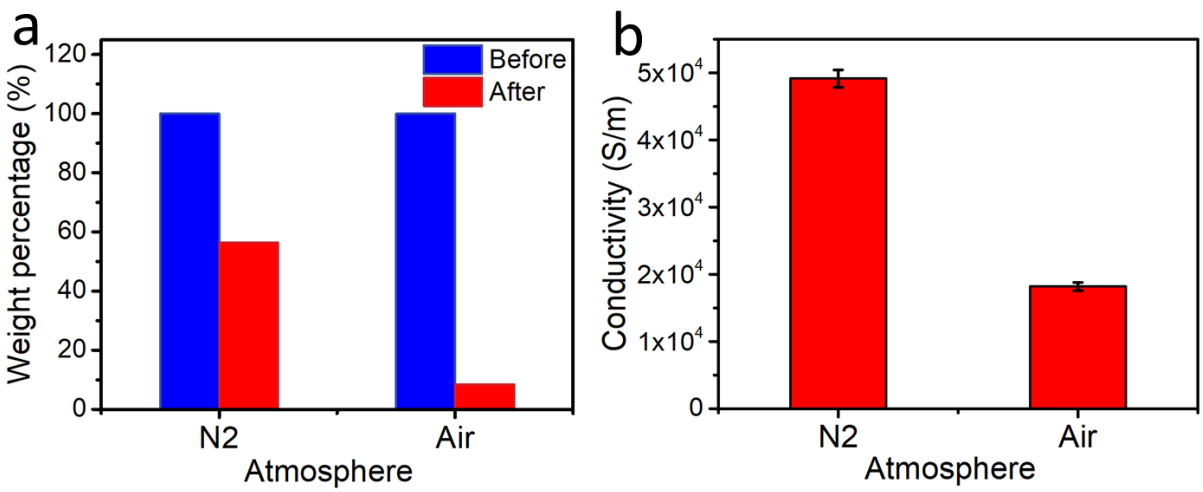

Figure 9. (a) Weight percentages of EGO membranes before and after microwave treatment. (b) Electrical conductivity of EGO membrane after microwave treatment in air and N_2.

Comparison of reduction methods

The efficiency of microwave reduction was compared further with other commonly-used reduction methods: thermal reduction, microwave reduction of thermally reduced GO, and chemical reduction. The conductivities of the reduced graphene oxide were compared and shown in **Figure 10**. As a traditional reduction method, thermal annealing of GO is often utilised to produce conductive graphene. Here, both EGO and CGO were thermally annealed in inert nitrogen atmosphere at 300 °C for 1 h. The electrical conductivity (1.8×10^4 S/m) of thermally-reduced EGO (TrEGO) is higher than that (9.4×10^2 S/m) of thermally-reduced CGO (TrCGO), which agrees well with the findings in Chapter 3 that EGO shows excellent conductivity after thermal reduction. It should be noted that the EGO used here are produced with a higher oxidation degree (C/O = 2.91) than EGO (C/O = 3.64) synthesised in Chapter 3,

thus making it less conductive (1.8 x 10^4 S/m) even after thermal annealing at 300 °C than EGO in chapter 3 (4.1 x 10^4 S/m) annealed at 200 °C. However, the conductivity of TrEGO is lower than that of MwEGO, indicating a higher efficiency of microwave reduction than the thermal reduction of 300 °C.

Another microwave reduction method has been reported by Voiry et al., showing that a pre-microwave step of thermal treatment of CGO at 300 °C for 1 h could result in high reduction efficiency of microwave irradiation on the sample[16]. To allow comparison, EGO and CGO was thermally heated at 300 °C for 1 h and then irradiated with microwave at 700W for 10 s to produce microwave-irradiated TrEGO (MwTrEGO) and TrCGO (MwTrCGO), respectively. The electrical conductivity of MwTrCGO (4.8 x 10^3 S/m) is higher than that of TrCGO (9.4 x 10^2 S/m), indicating activated reduction process under microwave irradiation of TrCGO. The much higher conductivity of MwTrCGO than MwCGO also confirmed the increase of microwave reduction efficiency after thermal pre-treatment of CGO. However, MwTrEGO shows similar conductivities to TrEGO (1.8 x 10^4 S/m) and lower conductivities than MwEGO, indicating no further reduction of TrEGO under microwave irradiation. This shows that partially reduced graphene oxide may exhibit a greater microwave reduction efficiency than the more completely reduced graphene oxide. This hypothesis requires future verification.

The XRD spectra of CrEGO and CrCGO have been compared with that of MwEGO in the previous section, which shows MwEGO contains less residual oxygen groups and larger aromatic coherence domains than CrEGO and CrCGO. The conductivities of CrEGO and CrCGO were also measured for further comparison with MwEGO. CrEGO shows conductivity of around 4.0 x 10^4 S/m, which is lower than 4.9 x 10^4 S/m of MwEGO. CrCGO exhibits a much lower conductivity of around 6.4 x 10^3 S/m, which agrees well with the XRD results. This shows a higher efficiency of microwave reduction of EGO, compared with chemical reduction of EGO or CGO.

As can be seen from the results, MwCGO shows the lowest conductivity whereas MwEGO shows the highest conductivity among the various reduction methods. The different microwave reduction abilities of EGO and CGO maybe resulted from their different structures. The facile microwave reduction of EGO demonstrates that it is more suitable than CGO to be used in the microwave route to reduce graphene oxide into conductive graphene.

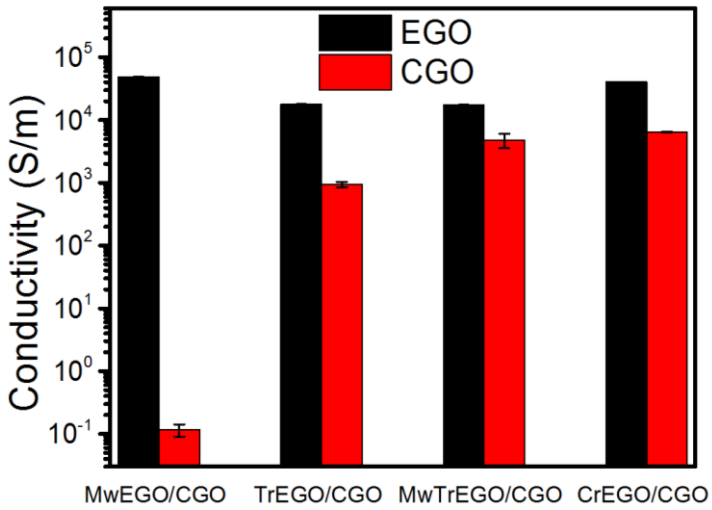

Figure 10. Electrical conductivities of MwEGO, MwCGO, TrEGO, TrCGO, MwTrEGO, MrTrCGO, CrEGO, CrCGO. (MwEGO/CGO: microwave-treated EGO/CGO at 700W for 10s; TrEGO/CGO: thermally-reduced EGO/CGO at 300 °C for 1 h; MwTrEGO/CGO: microwave-treated TrEGO/CGO; CrEGO/CGO: chemically-reduced EGO/CGO by hydrazine for 3h.)

5.3.3 Comparison of MwEGO with previous microwave work

Microwave reduction of EGO membrane and properties of MwEGO was also compared with previous works about microwave reductions of graphene oxide produced mainly from the modified Hummers method, as listed in **Table 4**. There are three main types of samples and microwave reduction processes: microwave reduction of pure CGO (No. 2, 3, 6), microwave reduction of a mixture of CGO and graphene/graphite (No. 4, 5, 8, 9), and microwave reduction of TrCGO (No. 7).

Table 4. Comparison of MwEGO with microwave-reduced GO in previous work

No.	Sample	Reduction process	I_D/I_G	L_a (nm)	Electrical conductivity	C/O ratio	Ref.
1	EGO membrane	Microwave, 3 s	0.187	102.8	49140 S/m	C/O = 33.6 (or 97.11% carbon)	This work
2	CGO dispersion (Hummers method)	Microwave, 10 min	0.96	17.5	200 S/m	C/O = 5.46	Wufeng Chen et al.[109]
3	CGO powders (modified Hummers method)	Microwave, air, 1 min	~ 1	~19.2	274 S/m	C/O = 2.75	Yanwu Zhu et al.[110]
4	Mixture of graphite oxide (modified Hummers method) and graphene powders	Microwave, H_2, 50 s (20 s on-time and 5 s off-time)	0.785	21.4	1250 S/m	C/O = 18.5	Sang-Hoon Park et al.[111]
5	Mixture of graphite oxide (Hummers method) and graphene	Microwave, 10 min	~1.7	~22.7	430 S/m	C/O = 16.99	Han Hu et al.[112]
6	Graphite oxide (Hummers method)	Microwave, 3 min	0.76	22.1	-	C/O = 11.6	Colin Hong An

							Wong et al.[138]
7	Graphene oxide (modified Hummers method)	Thermal annealing 1h at 300 °C + Microwave 1-2 s	<0.1	180±77	-	~ 93% carbon	Damien Voiry et al.[16]
8	Graphene oxide powder (modified Hummers method) + 1 mg flake graphite powder	Catalytic microwave, 2-3 s	0.88	21.8	48662–53180 S/m	C/O = 17.4	Runze Liu et al.[113]
9	Graphene oxide paper (modified Hummers method) + Reduced graphene oxide (RGO) paper	RGO paper triggered microwave, 3-5 s	~0.14	~100	~40 Ω/□ (thickness ≈ 35 – 45 µm for GO paper, ~714 S/m)	-	Wen-Shuai Jiang et al.[114]

By comparing with microwave reductions of pure CGO, I_D/I_G of EGO membrane (0.187) in this work is much lower than that of microwave-reduced pure CGO (0.96, ~1, 0.76). The calculated aromatic domain size L_a from I_D/I_G of MwEGO (102.8 nm) is also much larger than other MwCGOs (17.5 nm, ~19.2 nm, 22.1 nm). In addition to the aromatic domain, MwEGO also shows much higher electrical conductivity and C/O ratios than other MwCGOs. This agrees well with the results of CGO in this work, which shows a poor reduction efficiency under microwave irradiation.

Other studies found that adding a small number of graphite powders, graphene powders or reduced graphene oxide paper in contact with CGO can trigger microwave reduction of CGO, as listed in No. 4, 5, 8, 9 in **Table 4**. The triggered MwCGOs showed a much higher reduction

efficiency than pure MwCGOs, with the high electrical conductivity of around 48662–53180 S/m (No. 8) or high aromatic domain sizes of around 100 nm (No. 9). By comparison, the conductivity and aromatic domain size of MwEGO is also around 49140 S/m and 102.8 nm, at a similar level to the highest conductivity and L_a of triggered MwCGOs. In addition, MwCGO also shows the highest C/O ratio of 33.6 compared with all the previous works. This shows microwave reduction efficiency of pure EGO can reach the level of triggered microwave reduction of CGO with graphite/graphene.

Voiry et al.[16] (No.7 in **Table 4**) showed that microwave reduction of TrCGO in argon could greatly improve reduction efficiency. As discussed in the previous section, the conductivity of MwTrCGO was measured by using CGO with similar oxidation degree to EGO, which is one order of magnitude lower than MwEGO. In Voiry's work[16], a very high aromatic domain size of around 180 nm was achieved with around 93% carbon content. MwEGO in this work shows smaller aromatic domain size but higher carbon content (97.11%). However, the microwave reduction of EGO is much simpler than the microwave reduction of TrCGO which requires a thermal annealing step for 1 h at 300 °C.

5.3.4 Possible mechanisms

The above results have shown superior microwave reduction efficiency of EGO than CGO under the same conditions, which is the result of their different chemical structures. As have been discussed in previous works, pure CGO shows poor reduction efficiency due to its poor microwave absorption ability. Graphite has proven to be a good microwave absorber with abundant π electrons. It can efficiently absorb microwaves and dissipate them into thermal energy. Therefore, graphite powders have been used as catalysts in graphene oxide for efficient microwave reduction. Another possible catalyst is reduced graphene oxide (RGO), as have been previously reported in several works[111, 114]. RGO is a good absorber for microwaves due to its recovered π-π conjugated networks, which interact well with microwaves[111, 114]. The catalysts could transfer the absorbed microwave into thermal heat or arc, which can be emitted to adjacent graphene oxide. The microwave reduction of thermally-reduced CGO shows similar mechanisms. Slightly reduced CGO could produce conductive areas that easily absorb microwaves, which will result in rapid heating of the whole CGO, causing further reduction.

The structural difference of EGO and CGO could be observed in their Raman spectra (**Figure 2a and b**), which shows sharper D and G peaks of EGO than CGO. Smaller FWHM of EGO

indicates its larger aromatic domain size, as increasing FWHM (peak broadness) results from the disrupted sp^2 domains. Therefore, it can be speculated that effective microwave reduction of EGO is due to its larger aromatic domain sizes, which may form conjugated networks within EGO membranes. The delocalized electrons can freely move within the π-π network, absorbing microwaves and dissipate as thermal energy. The increased temperature can easily reduce more parts of the oxidised region and convert them into conjugated domains. The microwave absorption of larger aromatic domains will cause an "avalanche-like" increase in temperature, removing oxygen functional groups and rearranging carbon atoms. As a result, a less defective and highly conductive graphene structure can be formed.

5.4 Conclusion

This chapter has involved the study of EGO in an effective reduction method: microwave reduction. Microwave reduction processes of EGO membrane and properties of MwEGO membrane have been explored, which showed an efficient microwave reduction process of EGO membrane within 3 seconds and high-quality graphene developed in this rapid process. The Raman and XRD analysis showed a large aromatic domain size of 102.8 nm within the basal plane, and 15 layers of aromatic coherence domain along inter-sheet directions. Chemical analysis from TGA and XPS showed a significant loss of oxygen atoms in the microwave reduction process, with a high C/O ratio of 33.6. The electrical conductivity measurements showed that MwEGO can be reduced to conductive graphene, with a minimum microwave time of 3 seconds and power of 140 W, with a highest electrical conductivity of 49140 S/m achieved at 10 seconds and 700 W. By comparing the results of other reduction methods and previous microwave reductions of CGO, it was found that EGO shows the highest level of reduction efficiency under microwave irradiation with excellent qualities of MwEGO. A likely mechanism was proposed to explain the high microwave reduction efficiency of EGO, which was due to its larger aromatic regions that efficiently absorb microwave and dissipate them into heat, causing a rapid loss of oxygen atoms and rearrangements of carbon atoms.

This study makes progress in understanding the reduction properties and structures of EGO, which shows differences to CGO. EGO also shows a promising candidate for producing high-quality and highly conductive graphene with large domain sizes using the fast, effective and low-cost microwave reduction method.

5.5 References

1. Yang, X.; Zhu, J.; Qiu, L.; Li, D., Bioinspired Effective Prevention of Restacking in Multilayered Graphene Films: Towards the Next Generation of High-Performance Supercapacitors. *Advanced Materials* **2011,** *23* (25), 2833-2838.

2. Voiry, D.; Yang, J.; Kupferberg, J.; Fullon, R.; Lee, C.; Jeong, H. Y.; Shin, H. S.; Chhowalla, M., High-quality graphene via microwave reduction of solution-exfoliated graphene oxide. *Science* **2016**.

3. Li, D.; Kaner, R. B., Graphene-Based Materials. *Science* **2008,** *320* (5880), 1170-1171.

4. Rao, C. N. R.; Sood, A. K.; Subrahmanyam, K. S.; Govindaraj, A., Graphene: The New Two-Dimensional Nanomaterial. *Angewandte Chemie International Edition* **2009,** *48* (42), 7752-7777.

5. Kim, K. S.; Zhao, Y.; Jang, H.; Lee, S. Y.; Kim, J. M.; Kim, K. S.; Ahn, J.-H.; Kim, P.; Choi, J.-Y.; Hong, B. H., Large-scale pattern growth of graphene films for stretchable transparent electrodes. *Nature* **2009,** *457*, 706.

6. Berger, C.; Song, Z.; Li, X.; Wu, X.; Brown, N.; Naud, C.; Mayou, D.; Li, T.; Hass, J.; Marchenkov, A. N.; Conrad, E. H.; First, P. N.; de Heer, W. A., Electronic Confinement and Coherence in Patterned Epitaxial Graphene. *Science* **2006,** *312* (5777), 1191-1196.

7. Novoselov, K. S.; Geim, A. K.; Morozov, S. V.; Jiang, D.; Zhang, Y.; Dubonos, S. V.; Grigorieva, I. V.; Firsov, A. A., Electric Field Effect in Atomically Thin Carbon Films. *Science* **2004,** *306* (5696), 666-669.

8. Pei, S.; Cheng, H.-M., The reduction of graphene oxide. *Carbon* **2012,** *50* (9), 3210-3228.

9. Yang, D.; Velamakanni, A.; Bozoklu, G.; Park, S.; Stoller, M.; Piner, R. D.; Stankovich, S.; Jung, I.; Field, D. A.; Ventrice, C. A.; Ruoff, R. S., Chemical analysis of graphene oxide films after heat and chemical treatments by X-ray photoelectron and Micro-Raman spectroscopy. *Carbon* **2009,** *47* (1), 145-152.

10. Chua, C. K.; Pumera, M., Chemical reduction of graphene oxide: a synthetic chemistry viewpoint. *Chemical Society Reviews* **2014,** *43* (1), 291-312.

11. Zhu, Y.; Murali, S.; Stoller, M. D.; Velamakanni, A.; Piner, R. D.; Ruoff, R. S., Microwave assisted exfoliation and reduction of graphite oxide for ultracapacitors. *Carbon* **2010,** *48* (7), 2118-2122.

12. Park, S.-H.; Bak, S.-M.; Kim, K.-H.; Jegal, J.-P.; Lee, S.-I.; Lee, J.; Kim, K.-B., Solid-state microwave irradiation synthesis of high quality graphene nanosheets under hydrogen containing atmosphere. *Journal of Materials Chemistry* **2011,** *21* (3), 680-686.

13. Hu, H.; Zhao, Z.; Zhou, Q.; Gogotsi, Y.; Qiu, J., The role of microwave absorption on formation of graphene from graphite oxide. *Carbon* **2012,** *50* (9), 3267-3273.

14. Han, H. J.; Chen, Y. N.; Wang, Z. J., Effect of microwave irradiation on reduction of graphene oxide films. *RSC Advances* **2015,** *5* (113), 92940-92946.

15. Liu, R.; Zhang, Y.; Ning, Z.; Xu, Y., A Catalytic Microwave Process for Superfast Preparation of High-Quality Reduced Graphene Oxide. *Angewandte Chemie* **2017,** *129* (49), 15883-15888.

16. Wong, C. H. A.; Jankovský, O.; Sofer, Z.; Pumera, M., Vacuum-assisted microwave reduction/exfoliation of graphite oxide and the influence of precursor graphite oxide. *Carbon* **2014,** *77*, 508-517.

17. Jiang, W.; Yang, C.; Chen, G.-X.; Yan, X.-Q.; Chen, S.-N.; Su, B.-W.; Liu, Z.; Tian, J., Preparation of High-Quality Graphene Using Triggered Microwave Reduction Under Air Atmosphere. *Journal of Materials Chemistry C* **2018**.

18. Chen, W.; Yan, L.; Bangal, P. R., Preparation of graphene by the rapid and mild thermal reduction of graphene oxide induced by microwaves. *Carbon* **2010,** *48* (4), 1146-1152.

19. Kovtyukhova, N. I.; Ollivier, P. J.; Martin, B. R.; Mallouk, T. E.; Chizhik, S. A.; Buzaneva, E. V.; Gorchinskiy, A. D., Layer-by-Layer Assembly of Ultrathin Composite Films from Micron-Sized Graphite Oxide Sheets and Polycations. *Chemistry of Materials* **1999,** *11* (3), 771-778.

20. Cançado, L. G.; Takai, K.; Enoki, T.; Endo, M.; Kim, Y. A.; Mizusaki, H.; Jorio, A.; Coelho, L. N.; Magalhães-Paniago, R.; Pimenta, M. A., General equation for the determination of the crystallite size La of nanographite by Raman spectroscopy. *Applied Physics Letters* **2006,** *88* (16), 163106.

21. Claramunt, S.; Varea, A.; López-Díaz, D.; Velázquez, M. M.; Cornet, A.; Cirera, A., The Importance of Interbands on the Interpretation of the Raman Spectrum of Graphene Oxide. *The Journal of Physical Chemistry C* **2015,** *119* (18), 10123-10129.

22. Martins Ferreira, E. H.; Moutinho, M. V. O.; Stavale, F.; Lucchese, M. M.; Capaz, R. B.; Achete, C. A.; Jorio, A., Evolution of the Raman spectra from single-, few-, and many-layer graphene with increasing disorder. *Physical Review B* **2010,** *82* (12), 125429.

23. Li, D.; Muller, M. B.; Gilje, S.; Kaner, R. B.; Wallace, G. G., Processable aqueous dispersions of graphene nanosheets. *Nat Nano* **2008,** *3* (2), 101-105.

24. Ganguly, A.; Sharma, S.; Papakonstantinou, P.; Hamilton, J., Probing the Thermal Deoxygenation of Graphene Oxide Using High-Resolution In Situ X-ray-Based Spectroscopies. *The Journal of Physical Chemistry C* **2011,** *115* (34), 17009-17019.

Chapter 6. Electrochemically-derived graphene oxide membranes with high stability in aqueous solution

6.1 Introduction

6.1.1 Instability of CGO membrane in aqueous solution

Graphene oxide (GO) is a highly oxidized form of two-dimensional graphene sheet, which attracts wide interests in both research and industry fields due to its unique properties and scalable production[1-3]. With good processability of such homogeneous GO dispersions, GO sheets can be used as nano-building blocks for assembly of various macro-structures. For example, GO has been widely used to form laminated membranes by filtration or coating process[4]. GO membranes show characteristics of good flexibility, mechanical strength and tuneable chemistry, being relevant in many applications such as gas separation[5], batteries[6], water purification[7-8] and desalination[9]. GO membranes contain well-defined nanochannels between the GO sheets, which allow gas or liquid separation[5, 10], and the chemical groups in GO membranes make them selective with respect to ion permeation[11]. The majority of GO is synthesized from chemical methods such as the Hummers method using strong oxidants, which has the advantages of being scalable and allowing cheap production[12-13]. Chemically-derived graphene oxide (CGO) shows a high degree of oxidation with excellent dispersibility, which makes it an excellent platform for processing into hierarchical structures, and assembled CGO membranes have been widely studied[4, 10, 14-16]. However, pure graphene oxide membranes show very poor stability in aqueous solutions. When CGO membranes are used in aqueous solution, the adjacent GO sheets can be readily kept apart due to the repulsive electrostatic forces caused by the negatively charged oxygen groups such as carboxylic acid and hydroxyl groups[14].

Despite the intrinsic instability of graphene oxide membrane in water, some work has produced stable graphene oxide membrane by using aluminium oxide (AAO) filters[17]. Enhanced stability of the GO membranes is achieved by crosslinking of the Al^{3+} ions released from the AAO filters. However, interlayer Al^{3+} ions tend to be redispersed and removed in acid and NaCl solutions, causing disintegrations of the membrane[18]. This will limit their use in aqueous solutions containing H^+ or other monovalent cations. Moreover, the redispersed Al^{3+} will cause contamination of the aqueous solution, which is unfavourable in some applications such as ions separation. Other research has been attempting to increase the structural stability of GO membrane by crosslinking graphene oxide sheets with macromolecules or polymers[9, 19-20]. However, these large crosslinkers will change the structure of the GO membranes, such as their

well-defined nanochannels. Another common method to enhance stability is by partial reduction of GO membranes but it will compromise intrinsic properties of GO membrane[21-22]. For example, water flux will decrease due to decreased interlayer distance in the reduced parts of GO membrane.

6.1.2 Electrochemically-derived graphene oxide

As shown in previous sections, electrochemical oxidation of graphite is another promising and scalable method to produce graphene oxide. Increasing interest has been focused on electrochemical methods due to potential scalable production and the environmentally-friendly nature of the process[23-25]. Electrochemically-produced graphene oxide (EGO) sheets have been characterized for their chemistry and structure. It has been reported that EGO shows different chemical structures and properties compared with chemically oxidized graphene oxide (CGO)[26-28]. With a milder oxidation process, EGO exhibits fewer oxygen groups and less disrupted graphene structures than CGO. The chemical and structural differences of EGO compared to CGO render it highly conductive after reduction, affecting its applications such as electrochemical supercapacitors and transparent conducting films[28]. However, previous studies have mainly focused on the study of electrochemical process and characterization of the produced EGO sheets at the atomic scale. EGO sheets have rarely been assembled into macroscale membranes that have a broad range of potential applications, and knowledge gaps between the structure and properties of the EGO membranes remain. Therefore, to expand the applications of EGO, it is necessary to study the properties of EGO membranes and understand how the properties are affected by its atomic and membrane structure.

In this chapter, EGO membranes were fabricated using processable EGO dispersions as described in Chapter 4. Stability of EGO membrane in aqueous solution was investigated. The membranes were also characterized in detail for discussion of its stability. As a potential application, ionic sieving and water permeation properties of EGO membrane were tested. The structural and chemical characterization of EGO was also undertaken to understand the relationship between these properties.

6.2 Experimental section

6.2.1 Materials

Graphite foil was purchased from Sigma-Aldrich (Product No. GF82433538, thickness 0.2 mm) and used as the graphite source for the synthesis of electrochemically-derived graphene oxide (EGO). Reagent grade sulfuric acid H_2SO_4 (95% - 98%) was purchased from Sigma-Aldrich (Product No. 435589). Analytical reagent sodium chloride was purchased from Chem-Supply (Product No. SA046, 99.7%). Magnesium chloride hexahydrate was received from Merck. Rhodamin B and methylene blue were purchased from Sigma-Aldrich. Ultrapure water (from Millipore Direct-Q system) was used in all relevant experiments.

6.2.2 EGO preparation

EGO was synthesized by the electrochemical oxidation of graphite foil in a two-electrode Tee-cell[27]. The process used is the same as that described in Chapter 4. In the electrochemical oxidation process, a constant current (2 mA) was applied to the working electrode for 22 hours, with 12 M sulfuric acid solution was employed as the electrolyte. After the electrochemical oxidation of graphite foil for 22 hours, the samples were taken out and dispersed in water using agitation for a few minutes. The dispersion was washed by the centrifugation process repeatedly until the pH of the dispersion was around 7. After washing, EGO dispersion was subject to ultrasonication for 30 minutes via an ultrasonic probe (Branson Digital Sonifier S450D, 1/2" Horn, 500W, 30% amplitude). The ultrasonicated EGO dispersion was subsequently centrifuged at 4400 rpm. for 1 hour to remove large or non-exfoliated sheets. The weight percentage for remaining EGO after centrifugation was around 75%. CGO was produced by a modified Hummers method originally reported by Kovtyukhaova et al[13]. The purified CGO dispersion was subjected to the same ultrasonication and centrifugation procedure before further use.

6.2.3 Fabrication of EGO membrane

The EGO dispersion (0.5 mg/ml) was filtered through a polycarbonate membrane (Isopore, 0.1 µm pore size, Sigma-Aldrich) by vacuum filtration. When filtration was complete, the membrane was dried under vacuum conditions at room temperature for about 24 hours. Following this, the membrane was able to be peeled off the polycarbonate filter for further characterization. CGO membranes were fabricated using the same procedures.

6.2.4 Stability tests

To test the stability, EGO and CGO membranes were fabricated with the same mass loading of 0.6 mg/cm^2 and cut into round pieces with a diameter of 13 mm. Acidic (pH=1.5) or basic (pH=10.5) aqueous solutions were prepared by modifying ultrapure water (pH=6.8) with appropriate amounts of HCl or NaOH. During the stability test, both EGO and CGO membranes were immersed in acidic, neutral and basic aqueous solution for 1 week. After immersion for a certain time (e.g. 24 hours), the membranes in the solution were stirred by a vortex mixer (VELP Scientifica) at a speed of 400 rpm for 1 minute.

6.2.5 Characterization

The structures of EGO and CGO membranes in the dried and wet states, for different immersion times, were characterized by X-ray diffraction (XRD) measurements. XRD was performed in a Bruker D2 Phaser diffractometer with a Cu Kα radiation (k = 1.5418 Å). Raman spectroscopy was measured on a Renishaw InVia Raman Microscope with a laser wavelength of 532 nm and a laser spot size of 10 µm. X-ray photoelectron spectroscopy (XPS) was conducted on a VG ESCALAB220i-XL spectrometer which is equipped with a hemispherical analyser. For incident radiation, monochromatic Al Kα X-rays (1486.6 eV) was employed at 220 W (22 mA and 10kV). The surface charging effect was compensated by a low energy flood gun. Thermogravimetric analysis (TGA) of EGO or CGO was conducted by using a Thermo thermogravimetry/differential thermal analyser (TG/DTA) 6300 in the atmosphere of air using a heating rate of 1 °C/min. Zeta potential of the dispersion was performed by Malvern Zetasizer Nano ZS analyser. Atomic force microscopy (AFM) images of EGO sheets were taken by a Bruker Dimension Icon AFM in a tapping mode. For sample preparation, EGO dispersion with 0.01 mg/ml was drop-casted on a Si wafer and dried at 50 °C.

6.2.6 Permeation and nanofiltration test

EGO or CGO membranes were fabricated by a Sterlitech dead-end filtration cell with a compressed air and dried in air for overnight. For concentration-driven permeation tests, a device with a feed reservoir and a permeate reservoir on each side of a membrane clamp was used. EGO and CGO membranes (0.3 mg/cm^2) with a polycarbonate filter as a substrate were fabricated from 0.05 mg/ml EGO or CGO dispersions. The membrane was then assembled in the device using a membrane clamp with an exposure diameter of 4.9 mm. The feed reservoir was filled with 50 ml of feed solution (0.1 M NaCl, 0.1 M $MgCl_2$, 0.02 M methylene blue and

0.02 M Rhodamine B). The permeate reservoir was filled with 50 ml ultrapure water. Solution conductance change was monitored in the permeate reservoir to measure the diffusion of NaCl and $MgCl_2$. UV-Vis spectroscopy was used to monitor the concentration of methylene blue and Rhodamine B.

For nanofiltration testing, the Sterlitech dead-end filtration cell was used to monitor water filtration through EGO or CGO membrane with different mass loadings. For the rejection test, 1.0 M NaCl, 1.0 M $MgCl_2$, 0.04 mM MB and 0.04 mM RB were filtrated through the EGO or CGO membrane (0.02 mg/cm^2). The conductivities of NaCl and $MgCl_2$ permeates were measured to determine their rejections. Permeance was monitored by the weight increase of the permeate with time.

6.3 Results and discussion

EGO was prepared via electrochemical oxidation of graphite foil by using the Tee-cell setup, the same process as shown in Chapter 4. In this study, graphite was oxidized for 22 hours until the third stage (H_2O hydrolysis) was reached, by which time full electro-oxidation to EGO was achieved. EGO membranes can be fabricated via vacuum filtration of the EGO dispersion through a polymer filter membrane. After drying, free-standing EGO and CGO membranes with good consistency and uniformity could be obtained (**Figure 1**). This was consistent with the uniform EGO membrane fabricated in Chapter 4, which indicates good processability of EGO dispersion. The only distinct difference in appearance of the two membranes is that when the mass loading of the membrane is low (0.1 mg/cm^2), the CGO membrane is more yellow while EGO membrane has a brown colour. This may result from the lower oxidation degree of EGO than CGO as increasing oxidation will produce a more yellowish colour.

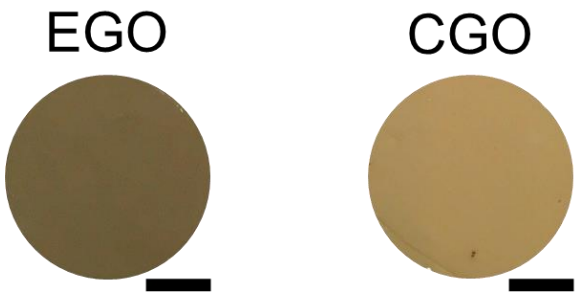

Figure 1. EGO and CGO membranes with the same areal mass of 0.1 mg/cm^2 (Scale bar: 4 mm).

6.3.1 Extraordinary stability to water

If they are to be used in water-based applications, the stability of graphene oxide membranes in different aqueous environment is important because it will directly affect the integrity and performance of the membranes. The stability of EGO and CGO membranes in acidic (pH=1.5), neutral (pH=6.8) and basic (pH=10.5) aqueous solutions was investigated. It should be noted that both EGO and CGO membranes were prepared by vacuum filtration of pure EGO and CGO dispersions through polycarbonate membranes, without any addition of external ions to strengthen the membranes by introduction of additional forces. The membranes after immersion and stirring in aqueous solution with various pH are shown in **Figure 2**. As in previous reports[17], CGO membranes showed poor integrity in aqueous solutions, and cleaved into pieces after one day of immersion due to the repulsion between the negatively charged sheets. After one week, CGO membranes were almost completely redispersed into the aqueous solution with pH=6.8 and pH=10.5. In the acid solution (pH=1.5), the CGO solution does not become yellowish due to relatively poor ionization of carboxylic acid groups with large amounts of H^+ in the solution. By comparison, EGO membranes were structurally very stable for at least one week of testing on the engineering scale. In acid and base solutions, EGO membranes also retained their integrity without any evident cracks after one-week of immersion.

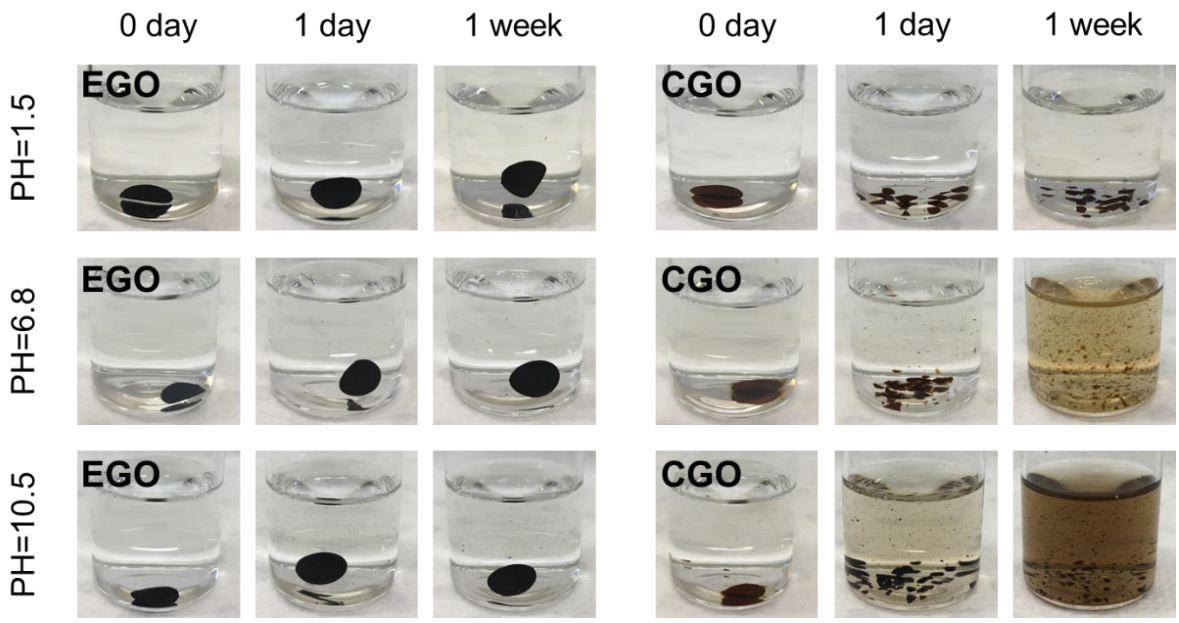

Figure 2. Stability of EGO and CGO membranes immersed in acid with pH=1.5 (top), neutral water with pH=6.8 (middle) and base solutions with pH=10.8 (bottom).

The structural changes of EGO and CGO membrane in water were studied via X-ray diffraction (XRD). As shown in **Figure 3a and 3b**, both EGO and CGO membranes showed an initial peak at around 12° in the dry state, corresponding to an interlayer GO sheet distance of about 0.74 nm. When EGO and CGO membranes were immersed in water, their XRD peaks shifted to a smaller 2θ value, showing an increase in interlayer distance due to the intercalation of water molecules into the both GO membranes. The changes in the interlayer distances of both the GO membranes with respect to their immersion time are shown in **Figure 3c**. Both CGO and EGO membranes showed an abrupt increase of interlayer distance after immersion in water for 1 min, demonstrating their fast response to humidity, which is known and has been used, for example, in humidity sensing[29-30]. The interlayer distance of EGO membrane increased very slightly from 1.12 nm to 1.17 nm after immersion in water for 1 hour and remained constant at 1.18 nm until a testing period of 7 days. For CGO membrane, its interlayer distance progressively increased with increased immersion time from 1.27 nm (1 min) to 1.40 nm (1 day). This behaviour is similar to previous reports where the interlayer distance of CGO membrane displayed a continuous increase for days until it reached around 6 nm[14]. Due to the limitations of XRD technique, the CGO peak cannot be detected after 1 day of immersion.

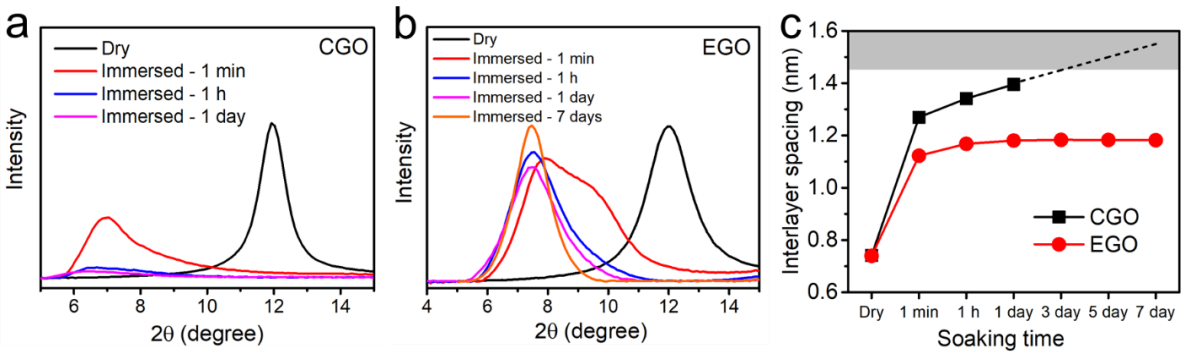

Figure 3. XRD patterns for (a) CGO membranes and (b) EGO membranes at different immersion times in water of neutral pH. (c) Interlayer spacing change with immersion time. The shaded grey area is beyond the detection limit.

Such swelling of GO membranes results from the insertion of water molecules between GO sheets, leading to increasing number of water layers[14-15, 31]. Previous research has correlated the number of intercalated water molecules between GO layers with the interlayer distance obtained by XRD, and it was found that a hydrated GO membrane with an interlayer distance of about 13 Å contained three layers of water molecules between the two GO sheets[15]. From the XRD patterns of EGO membrane immersed in water for 1 min, a non-symmetrical peak

can be observed which contains the transition states between fully dried and fully hydrated EGO membranes. The XRD patterns of EGO membrane (**Figure 4**) can be fitted with two component peaks: GO-1 and GO-2, centred on about 9.1° and 7.6°, respectively, corresponding to interlayer distances of 0.92 nm and 1.16 nm. Since the size of one water molecule is around 0.25 nm, the two fitting peaks represent EGO structure with one (0.92 nm – 0.74 nm = 0.18 nm) and two water monolayers between GO sheets (1.16 nm – 0.74 nm = 0.42 nm). The slightly smaller size of intercalated water molecules is due to their denser state in a confined environment compared with their existence in the bulk water environment[14]. For EGO membrane immersed for 1 min (**Figure 4a**), the GO-1 peak displayed a higher intensity than the GO-2 peak, indicating that majority part of structure was filled with one layer of water molecules. With increasing immersion time (**Figure 4b, c, d, e, f**), the intensity of GO-1 peak decreased while the intensity of GO-2 peak increased, showing that there is a driving force to establish a preferred two-layered water molecules intercalated EGO gallery.

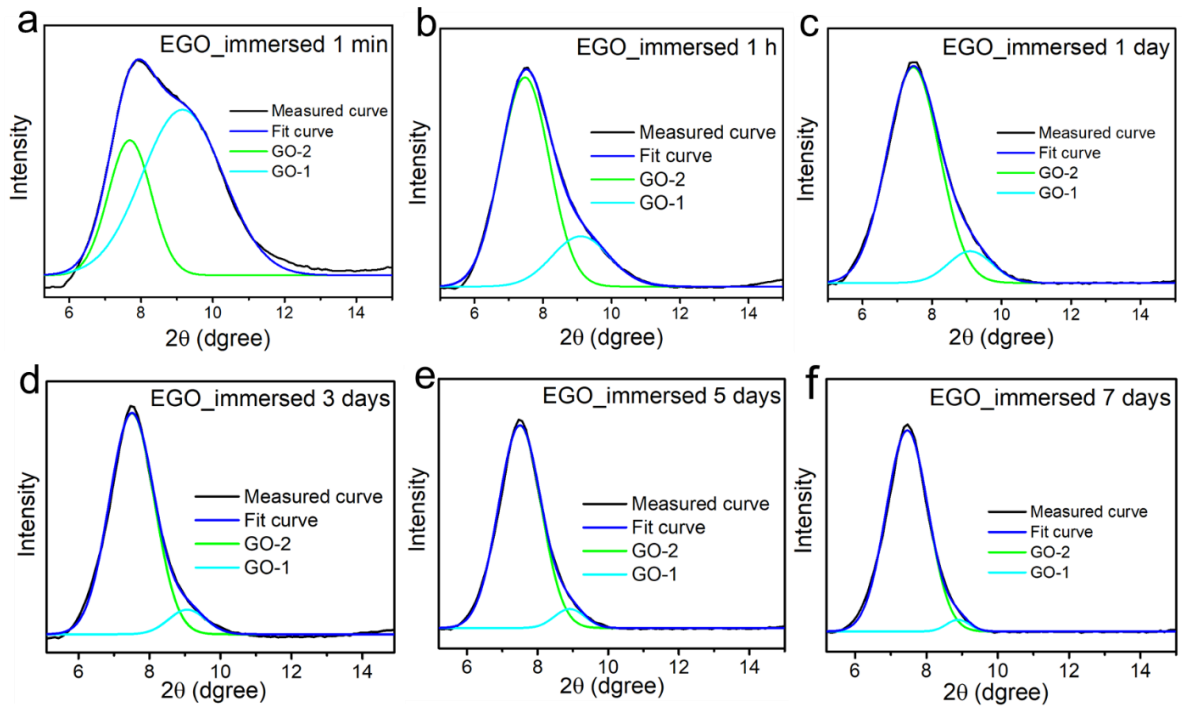

Figure 4. XRD patterns with fitting peaks: GO-1 (9.1°) and GO-2 (7.6°) for EGO membrane after immersion in neutral water for (a) 1 min, (b) 1 h, (c) 1 day, (d) 3 days, (e) 5 days and (f) 7 days.

As a comparison, XRD patterns of CGO membrane with fitted peaks are shown in **Figure 5**. The XRD peak of CGO membrane contains three fitted peaks: GO-1, GO-2, GO-3, where GO-

3 is centred on around 6.6° (interlayer spacing = 1.34 nm) which represents three layers of water molecules between CGO sheets. After immersion for 1 day, the XRD pattern changes to a combination of GO-2 and GO-3 peaks, indicating a mixed structure of two-layer and three-layer water structures. Due to the detection limits in the XRD technique, no peak with larger interlayer distance could be detected but from previous study, multiple layers of water molecules (up to 6 - 7 nm) can be intercalated between the GO sheets[14]. No GO-3 peak was observed in the XRD pattern of EGO membrane, even after immersion for 1 week (**Figure 4f**), indicating a stable two-layer water molecule structure within EGO membrane. This stable and consistent interlayer spacing of EGO represents an equilibrated state that is most likely determined by the interplay of attractive hydrogen bonding/sp^2 domains and repulsive negative ion charges (e.g. carboxylic acid).

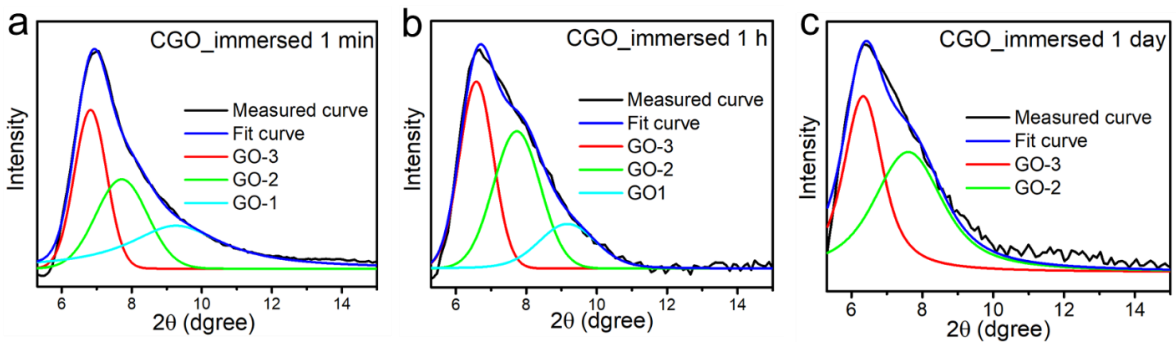

Figure 5. XRD patterns of CGO membrane after being immersed in neutral water for (a) 1 min, (b) 1 h, (c) 1 day, with fitting peaks: GO-1, GO-2, GO-3, centred at about 9.1°, 7.6° and 6.6°, respectively.

6.3.2 Ionic sieving and water permeation

GO membranes have been widely reported as promising separation membranes for nanofiltration and desalination, where high retentions and high permeance are required[7-9]. To be used as separation membranes with high performance, ionic sieving and water permeation are important properties to be considered. Moreover, such membrane performance is also a characteristic of GO membranes that can be used to probe the structure of nanochannels. Therefore, ionic sieving and water permeation properties of EGO membranes and used CGO membranes were investigated, to allow a comparison of structure. To measure the permeation of Na^+, a 0.1 M NaCl solution was used in the feed compartment. The amounts of Na^+ ions permeated through membranes with time were measured by monitoring electrical conductivity change of permeate compartments for every 10 seconds. It can be seen in **Figure 6a** that Na^+

ions concentration in permeate compartments increase with time for both EGO and CGO membranes. Specifically, EGO shows much reduced amounts of Na^+ ions permeating through the membrane, compared with CGO. In addition to the Na^+ ions permeation, the permeations rates of Mg^{2+}, MB and RB through the membranes were also tested, with the results shown in **Figure 6b**. As can be observed, permeation rate shows a significant drop above hydrated radius of about 4.5 Å, which agrees well with previous research[15]. MB and RB molecules show extremely low permeation, and no permeation has been detected for both EGO and CGO membranes. As for ions, EGO membrane shows about 8 times lower permeation rates for Na^+ and Mg^{2+} than CGO membranes. This shows higher rejections of EGO membranes for ions.

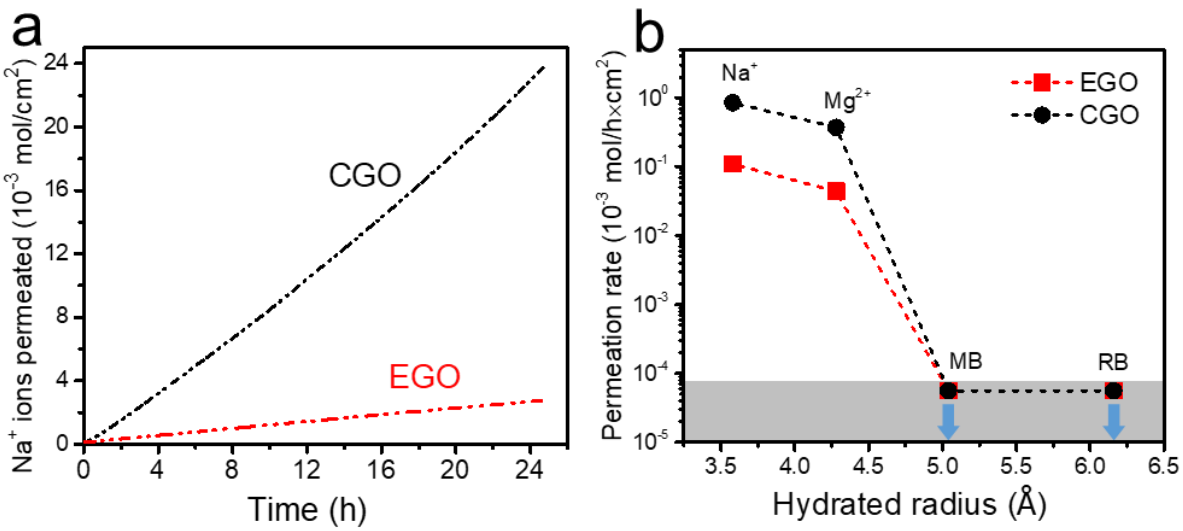

Figure 6. (a) Na^+ ions permeated through EGO and CGO membranes with time. (b) Permeation rates of Na^+, Mg^{2+}, Methylene blue (MB) and Rhodamine B (RB) through EGO and CGO membranes. Grey area is below our detection limit.

The stabilities of EGO and CGO membranes in the ionic sieving process were also examined by measuring permeation rates of Na^+ with prolonged permeation for up to 24 hours, as shown in **Figure 7**. Permeation rate of CGO membrane showed a significant increase from 0.3 x 10^{-3} to 0.85 x 10^{-3} mol/h×cm^2 in the first 3 hours, which is due to an abrupt increase of interlayer spacing when CGO membrane is swollen within the aqueous solution. It subsequently shows a gradual increase to 1.2 x 10^{-3} mol/h×cm^2 during the next 21 hours, which is caused by continuously increased interlayer distance within CGO membranes. The EGO membrane demonstrates a much lower permeation rate (~ 0.1 x 10^{-3} mol/h×cm^2) than CGO during the whole test period. There is a slight increase in the first two hours due to swelling of EGO

membrane in aqueous solution. However, after two hours, a very steady permeation rate for at least 24 hours is presented, demonstrating its stable structure in aqueous solution.

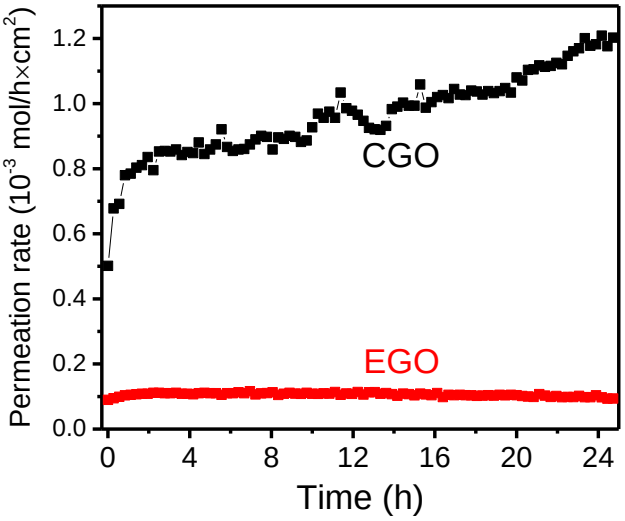

Figure 7. Na^+ permeation rate with permeation time through EGO and CGO membranes.

Water flux is another important factor other than rejection for filter membranes. Higher water flux is desired to achieve a higher filtration efficiency. Therefore, water flux of EGO and CGO membranes were also tested for comparison. Despite higher rejections for ions, water flux of EGO membranes was not reduced. From **Figure 8**, water flux of EGO membranes is much higher than that of CGO membranes at different mass loadings, which may be due to larger aromatic region of EGO exhibiting frictionless flow[15]. EGO membranes show around two times water flux of CGO membranes at a mass loading of 0.05, 0.1, and 0.15 mg/cm^2. However, the water flux of CGO membranes increased to more than half of EGO membranes at a mass loading of 0.02 mg/cm^2. The increased water flux may result from the poor stability of CGO membrane at a smaller thickness, which causes more holes or pathways in the membrane.

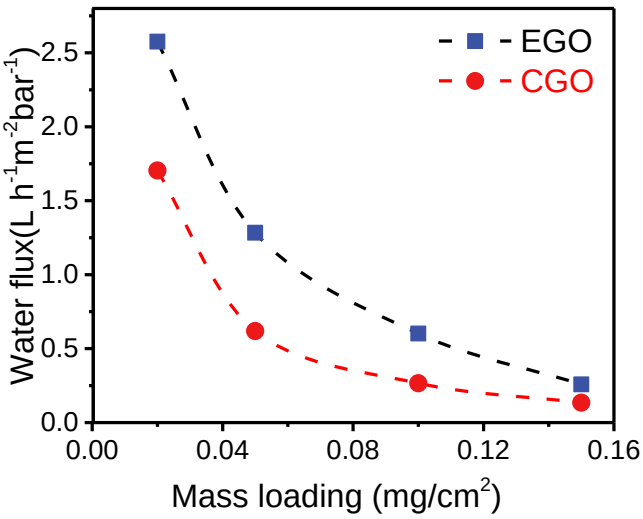

Figure 8. Water flux through EGO and CGO membranes at various mass loadings: 0.02, 0.05, 0.1, 0.15 mg/cm^2.

Nanofiltration performance of EGO and CGO membrane were evaluated for different ions and molecules by the pressure-drive filtration setup. Before measuring rejection of ions and molecules, they were stabilized by permeating RO water to reach a stable permeability. Rejection and permeance for NaCl, MgCl, MB and RB solutions were shown in **Figure 9a**. Rejection of ions were much smaller than that of probe molecules, which agrees well with the 4.5 Å cut-off radius reported previously. This shows size sieving effect for both EGO and CGO membranes. However, EGO membranes show around 8% and 7% higher rejection for NaCl and $MgCl_2$ respectively than CGO membranes. For molecules, EGO membranes show around 14% and 10% higher rejection for MB and RB than CGO membranes. In addition, EGO shows greater permeance than CGO membranes, similar to the comparison of pure water flux. To evaluate the rejection performance of EGO and CGO membranes in base solutions, 10 ml base solution with pH=10.8 were added on top of the membranes to soak them for one hour. Then RB solution with pH=10.8 was filtered through the membranes. As shown in **Figure 9b**, EGO membrane keeps 61.5% rejection for RB molecules, which is 22.8% higher than the rejection (38.7%) of CGO membrane. This difference is even higher than that in pH=6.8, which illustrates better stability of EGO in base solution than CGO membrane. In base solutions with pH=10.8, acid oxygen groups on graphene oxide such as carboxylic acid or hydroxyl groups will be more ionised and cause increased electrostatic repulsion between sheets, and thus an increased distance between layers. Increased pore size reduces the rejection of molecules. As

a stable graphene oxide membrane in aqueous solution, EGO membrane shows higher ion and molecular rejection, while simultaneously demonstrating a larger water flux than CGO membranes. This combination makes it a promising candidate to be used in water-based applications, such as ion sieving or desalination.

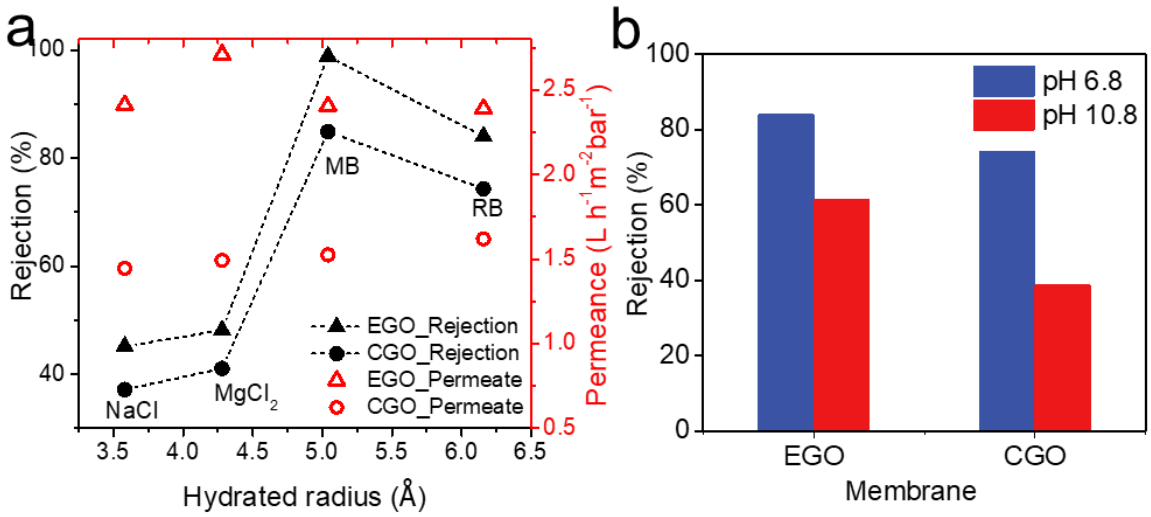

Figure 9. Nanofiltration test of EGO and CGO membrane. (a) Rejection and permeance of EGO and CGO membrane for ions and molecules of different hydrated radius in nanofiltration test. (b) Rejection of EGO and CGO membranes for RB molecules at pH= 6.8 and 10.8.

6.3.3 Structural and chemical characterization

To understand these membrane properties of EGO membranes, the structure and chemistry of EGO were characterized via Raman Spectroscopy, XPS and TGA. **Figure 10a** shows Raman spectra of EGO in the first-order region from 1000 cm^{-1} to 1900 cm^{-1}. The spectra were fitted with D peak, G peak and D'' peak in the valley between D and G peaks. In comparison, Raman spectra of CGO are shown in **Figure 10b**. The main parameters of the peaks are displayed in **Table 1**. The prominent peak at around 1590 cm^{-1} is G peak, which is directly related to the motion of sp^2 atoms in graphene. Another peak in the region of around 1350 cm^{-1} is D peak, which is dependent on the breathing modes of six-atom carbon rings near the defect regions. The D peak is often used to indicate the defects in graphene-based materials. The Full width at half maximum (FWHM) of D peak and G peak are also important parameters that reveal structures of carbon material. The broadening of D and G peaks in graphene oxide are related to disorder in the graphene plane, resulting from a decreasing size of sp^2 aromatic clusters[32-33]. By comparison of FWHM from **Table 1**, it can be seen that EGO shows a much smaller FWHM

of D peak and G peak than CGO. The smaller FWHM of EGO indicates much larger sp^2 domain size.

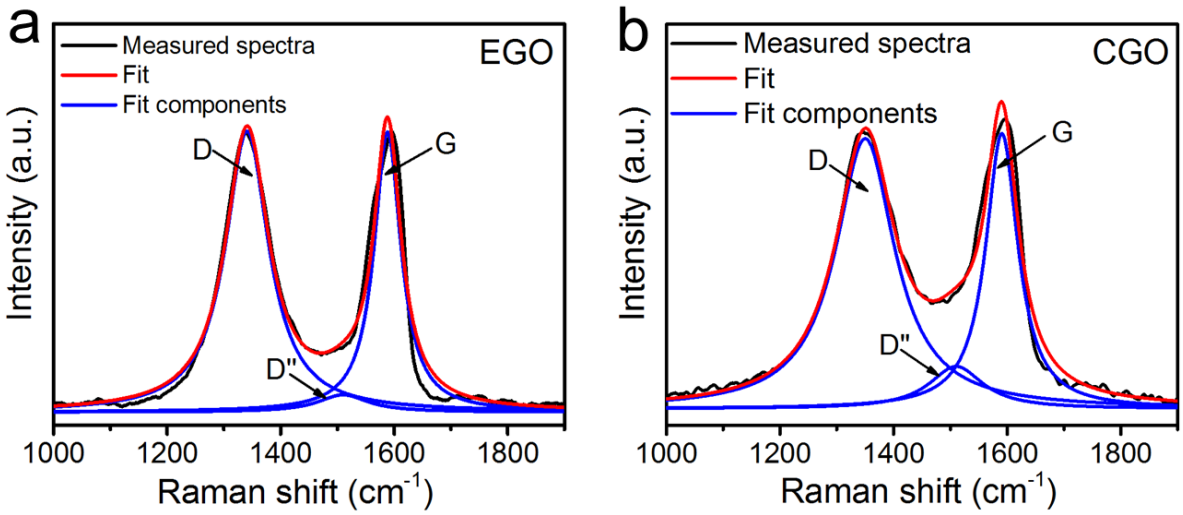

Figure 10. Raman spectrum of (a) EGO and (b) CGO in the first order region (1000 cm^{-1} – 1900 cm^{-1}).

Table 1. Comparison of the main peak parameters in Raman spectra for CGO and EGO.

	FWHM (cm^{-1})				
	D	G	**I_D/I_G**	**L_a (nm)**	**$I_{D''}/I_G$**
EGO	92.9	57.4	0.99	11.4	0.06
CGO	126.1	69.1	0.98	1.3	0.15

To quantitatively determine the aromatic domain size L_a for CGO and EGO, the intensity ratios of D and G peak I_D/I_G were measured and calculated, with the results presented in **Table 1**. CGO and EGO show almost the same value of I_D/I_G peak ratio. As proposed by Ferrari and Robertson[34], the Raman spectra of disordered carbon material are classified by a three-stage model. In Stage one, I_D/I_G will increase when aromatic domain size L_a decreases, which is similar to Tuinstra-Koenig (T-K) relation. When L_a further decreases and becomes stage two, the T-K relation will not be valid since there are decreased signals from sixfold aromatic rings near defects. As a result, the I_D/I_G peak ratio will decrease in stage two. By considering dramatic

difference of FWHM and almost same I_D/I_G peak ratio of CGO and EGO, it can be speculated that they are classified as different stages. EGO, with larger aromatic domain size, should be governed by Stage 1; while CGO should be in stage two due to its smaller aromatic domain size. The value of L_a can be calculated using a modified Lucchese equation (equation 6.1) as given below[33].

$$\frac{I_D}{I_G} = C_A \frac{(r_A^2 - r_S^2)}{(r_A^2 - 2r_S^2)} [e^{-\pi r_S^2/L_D^2} - e^{-\pi(r_A^2 - r_S^2)/L_D^2}] \qquad 6.1$$

where C_A = 5.43 for 532 nm laser, r_A = 3.1 nm, r_S = 1.0 nm. The calculated L_a for CGO and EGO are 1.3 nm and 11.4 nm, respectively. The larger L_a value of EGO indicates larger aromatic domain size and better long-range order. Another comparison that can be extracted from the Raman spectra of CGO and EGO is the D'' peak, the appearance of which is correlated to chemical doping or sp^3 bonding. $I_{D''}/I_G$ peak ratio for EGO is more than two times lower than that of CGO. This indicates much less sp^3 bonding in EGO, which is in agreement with the larger aromatic domain size we calculated. Much larger aromatic domains for EGO can form a more ordered and crystalline structure. When the membrane is immersed in aqueous solutions, the interactions of the aromatic domains will assist the membranes to retain a more ordered structure, with a stable interlayer distance. This will contribute to its high stability in water and good ionic sieving properties. Moreover, the larger aromatic region of EGO can also explain its higher water flux according to the model proposed by Joshi et al, which proposed that water shows frictionless flow in the pristine graphene regions[15].

Figure 11a shows XPS C1s spectra of EGO to analyse its chemical structure. In addition, XPS spectra of CGO is shown in **Figure 11b** as a comparison. The spectra were fitted with three peak components: sp^2 (284.4 eV), C=O/C-OH/C-O-C (286.4 eV) and COOH (288.0 eV). Percentages of each components for CGO and EGO were shown in **Table 2**. EGO showed larger percentage of sp^2 bonds (48.0 %) than CGO (44.7 %), which indicates a reduced oxidation degree of EGO. By comparing percentage of oxygen groups, it can be seen that EGO contains higher number of C=O/C-OH/C-O-C groups while much lesser percentage of COOH groups than CGO. EGO only shows 3.5 % of COOH groups compared to 8.4 % for CGO.

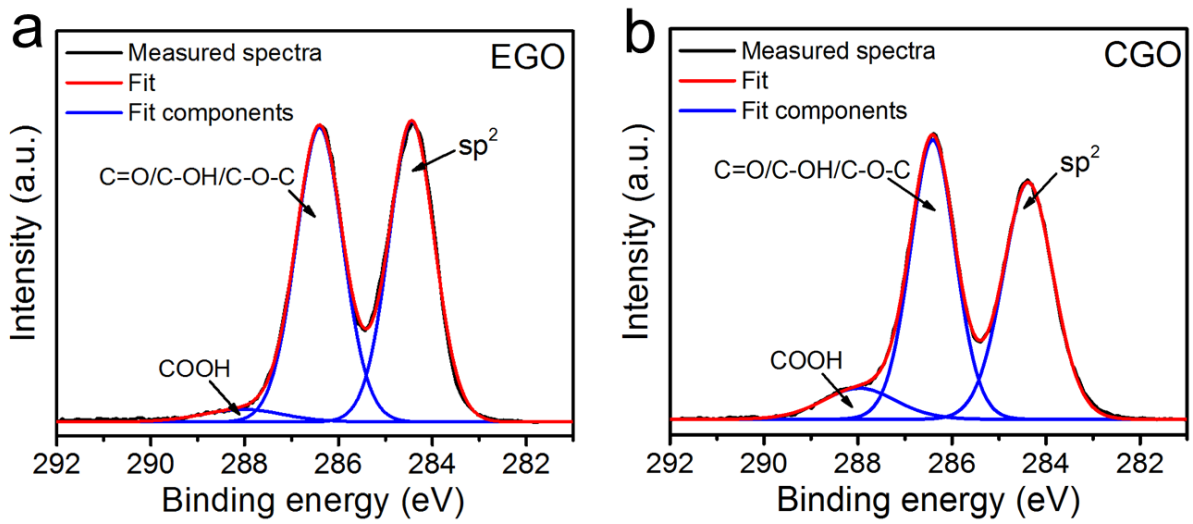

Figure 11. X-ray photoelectron (XPS) spectra of (a) EGO and (b) CGO in the C1s region (281 – 292 eV).

Table 2. Percentage of XPS C1s components for CGO and EGO.

	CGO	**EGO**
sp^2	44.7%	48.0%
C=O/C-OH/C-O-C	46.9%	48.5%
COOH	8.4%	3.5%

As shown in the thermogravimetric analysis (TGA) curves in **Figure 12**, EGO exhibits approx. 30% of weight loss at around 200 °C due to the removal of most oxygen groups, which is slightly less than for than CGO. EGO also shows less weight loss in the middle region between two significant weight losses (around 200 – 500 °C) than CGO (around 200 – 400 °C), likely due to less amount of thermally unstable C=O/COOH groups in EGO. The much higher carbon decomposition temperature for EGO indicates its higher thermal stability after reduction. From the above results, it can be seen most of the oxygen bonded to graphene plane during oxidation of EGO form epoxy, hydroxyl, or carbonyl groups, with only a small amount were further oxidized into carboxylic groups. These differences in chemical structure of CGO and EGO provide insight to their different stability in aqueous solution. It is well known that carboxylic

acid groups can be easily ionized in aqueous solution, especially in alkaline solution, and lead to electrostatic repulsive forces between graphene oxide sheets. This will cause an increase in the interlayer spacing between graphene oxide sheets, which leads to poor structural stability of graphene oxide laminated membranes. Hydroxyl groups, conversely, can form attractive hydrogen bonding between the sheets. Therefore, apart from the larger aromatic domains, lower carboxylic acid and higher hydroxyl content of EGO also contribute to membrane stability in water.

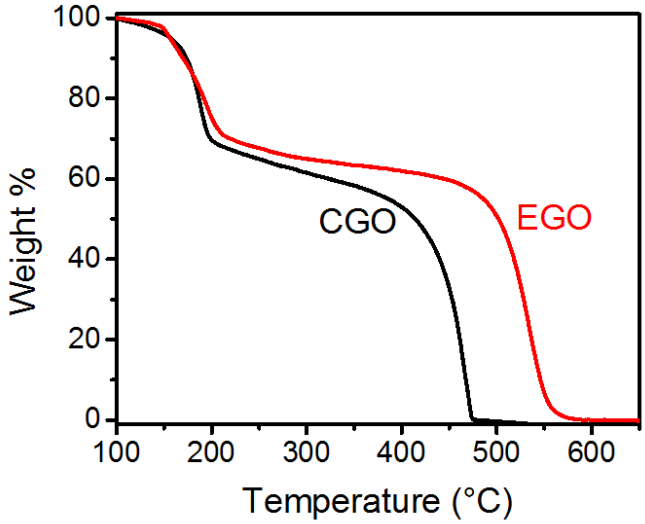

Figure 12. Thermogravimetric analysis (TGA) curves of EGO and CGO in air atmosphere.

6.4 Conclusions

The chemical properties and structures of graphene oxide membranes produced from electrochemically-derived graphene oxide have been investigated, and compared with those of chemically-derived graphene oxide. The EGO membrane was highly stable and maintained its intact structure after prolonged immersion in water and after being subjected to vigorous shaking. The interlayer distance between the hydrated EGO sheets was found to be very stable (at 1.18 nm) which is attributed to the formation of a stable two-layer water molecule between the EGO sheets at its equilibrium hydrated state. Furthermore, EGO membrane exhibited superior water filtration performance than CGO membranes with much higher stability, ionic rejections and water flux. From structural and chemical analysis, EGO showed larger aromatic domain size and lower carboxylic acid content, which contributes to its high stability and good ionic sieving performance. In contrast, CGO membrane disintegrated in less 24 hours in water

and showed poor stability with lower ionic rejections and water flux due to its smaller aromatic domain size and higher number of carboxylic groups.

Due to the robust properties of EGO membranes in aqueous condition over a broad pH range, the EGO membrane will be very useful for a broad range of aqueous solution-based applications such as water purification and chemical or biomolecule sensing. The work also highlights the importance of tuning and understanding the chemical and structural properties of graphene oxide to allow its optimal use in a range of applications.

6.5 Reference

1. Chen, D.; Feng, H.; Li, J., Graphene Oxide: Preparation, Functionalization, and Electrochemical Applications. *Chemical Reviews* **2012,** *112* (11), 6027-6053.
2. Zhu, Y.; Murali, S.; Cai, W.; Li, X.; Suk, J. W.; Potts, J. R.; Ruoff, R. S., Graphene and Graphene Oxide: Synthesis, Properties, and Applications. *Advanced Materials* **2010,** *22* (35), 3906-3924.
3. Dreyer, D. R.; Park, S.; Bielawski, C. W.; Ruoff, R. S., The chemistry of graphene oxide. *Chemical Society Reviews* **2010,** *39* (1), 228-240.
4. Yoon, H. W.; Cho, Y. H.; Park, H. B., Graphene-based membranes: status and prospects. *Philos. Trans. Royal Soc. A* **2016,** *374* (2060).
5. Kim, H. W.; Yoon, H. W.; Yoon, S.-M.; Yoo, B. M.; Ahn, B. K.; Cho, Y. H.; Shin, H. J.; Yang, H.; Paik, U.; Kwon, S.; Choi, J.-Y.; Park, H. B., Selective Gas Transport Through Few-Layered Graphene and Graphene Oxide Membranes. *Science* **2013,** *342* (6154), 91-95.
6. Huang, J.-Q.; Zhuang, T.-Z.; Zhang, Q.; Peng, H.-J.; Chen, C.-M.; Wei, F., Permselective Graphene Oxide Membrane for Highly Stable and Anti-Self-Discharge Lithium–Sulfur Batteries. *ACS Nano* **2015,** *9* (3), 3002-3011.
7. Huang, H.; Song, Z.; Wei, N.; Shi, L.; Mao, Y.; Ying, Y.; Sun, L.; Xu, Z.; Peng, X., Ultrafast viscous water flow through nanostrand-channelled graphene oxide membranes. *Nature Communications* **2013,** *4*, 2979.
8. Akbari, A.; Sheath, P.; Martin, S. T.; Shinde, D. B.; Shaibani, M.; Banerjee, P. C.; Tkacz, R.; Bhattacharyya, D.; Majumder, M., Large-area graphene-based nanofiltration membranes by shear alignment of discotic nematic liquid crystals of graphene oxide. *Nature Communications* **2016,** *7*, 10891.
9. Morelos-Gomez, A.; Cruz-Silva, R.; Muramatsu, H.; Ortiz-Medina, J.; Araki, T.; Fukuyo, T.; Tejima, S.; Takeuchi, K.; Hayashi, T.; Terrones, M.; Endo, M., Effective NaCl and dye rejection of hybrid graphene oxide/graphene layered membranes. *Nat Nano* **2017,** *advance online publication*.

10. Nair, R. R.; Wu, H. A.; Jayaram, P. N.; Grigorieva, I. V.; Geim, A. K., Unimpeded Permeation of Water Through Helium-Leak–Tight Graphene-Based Membranes. *Science* **2012,** *335* (6067), 442-444.

11. Hong, S.; Constans, C.; Surmani Martins, M. V.; Seow, Y. C.; Guevara Carrió, J. A.; Garaj, S., Scalable Graphene-Based Membranes for Ionic Sieving with Ultrahigh Charge Selectivity. *Nano Letters* **2017,** *17* (2), 728-732.

12. Hummers, W. S.; Offeman, R. E., Preparation of Graphitic Oxide. *Journal of the American Chemical Society* **1958,** *80* (6), 1339-1339.

13. Kovtyukhova, N. I.; Ollivier, P. J.; Martin, B. R.; Mallouk, T. E.; Chizhik, S. A.; Buzaneva, E. V.; Gorchinskiy, A. D., Layer-by-Layer Assembly of Ultrathin Composite Films from Micron-Sized Graphite Oxide Sheets and Polycations. *Chemistry of Materials* **1999,** *11* (3), 771-778.

14. Zheng, S.; Tu, Q.; Urban, J. J.; Li, S.; Mi, B., Swelling of Graphene Oxide Membranes in Aqueous Solution: Characterization of Interlayer Spacing and Insight into Water Transport Mechanisms. *ACS Nano* **2017,** *11* (6), 6440-6450.

15. Joshi, R. K.; Carbone, P.; Wang, F. C.; Kravets, V. G.; Su, Y.; Grigorieva, I. V.; Wu, H. A.; Geim, A. K.; Nair, R. R., Precise and Ultrafast Molecular Sieving Through Graphene Oxide Membranes. *Science* **2014,** *343* (6172), 752-754.

16. Dikin, D. A.; Stankovich, S.; Zimney, E. J.; Piner, R. D.; Dommett, G. H. B.; Evmenenko, G.; Nguyen, S. T.; Ruoff, R. S., Preparation and characterization of graphene oxide paper. *Nature* **2007,** *448*, 457.

17. Yeh, C.-N.; Raidongia, K.; Shao, J.; Yang, Q.-H.; Huang, J., On the origin of the stability of graphene oxide membranes in water. *Nat Chem* **2015,** *7* (2), 166-170.

18. Xi, Y.-H.; Hu, J.-Q.; Liu, Z.; Xie, R.; Ju, X.-J.; Wang, W.; Chu, L.-Y., Graphene Oxide Membranes with Strong Stability in Aqueous Solutions and Controllable Lamellar Spacing. *ACS Applied Materials & Interfaces* **2016,** *8* (24), 15557-15566.

19. Thebo, K. H.; Qian, X.; Zhang, Q.; Chen, L.; Cheng, H.-M.; Ren, W., Highly stable graphene-oxide-based membranes with superior permeability. *Nature Communications* **2018,** *9* (1), 1486.

20. Zhang, Y.; Zhang, S.; Chung, T.-S., Nanometric Graphene Oxide Framework Membranes with Enhanced Heavy Metal Removal via Nanofiltration. *Environmental Science & Technology* **2015,** *49* (16), 10235-10242.

21. Han, Y.; Xu, Z.; Gao, C., Ultrathin Graphene Nanofiltration Membrane for Water Purification. *Advanced Functional Materials* **2013,** *23* (29), 3693-3700.

22. Liu, H.; Wang, H.; Zhang, X., Facile Fabrication of Freestanding Ultrathin Reduced Graphene Oxide Membranes for Water Purification. *Advanced Materials* **2015,** *27* (2), 249-254.

23. Yu, P.; Lowe, S. E.; Simon, G. P.; Zhong, Y. L., Electrochemical exfoliation of graphite and production of functional graphene. *Current Opinion in Colloid & Interface Science* **2015,** *20* (5–6), 329-338.

24. Yang, S.; Lohe, M. R.; Müllen, K.; Feng, X., New-Generation Graphene from Electrochemical Approaches: Production and Applications. *Advanced Materials* **2016,** *28* (29), 6213-6221.

25. Chen, H.; Li, C.; Qu, L., Solution electrochemical approach to functionalized graphene: History, progress and challenges. *Carbon* **2018,** *140*, 41-56.

26. Yu, P.; Tian, Z.; Lowe, S. E.; Song, J.; Ma, Z.; Wang, X.; Han, Z. J.; Bao, Q.; Simon, G. P.; Li, D.; Zhong, Y. L., Mechanically-Assisted Electrochemical Production of Graphene Oxide. *Chemistry of Materials* **2016,** *28* (22), 8429-8438.

27. Tian, Z.; Yu, P.; Lowe, S. E.; Pandolfo, A. G.; Gengenbach, T. R.; Nairn, K. M.; Song, J.; Wang, X.; Zhong, Y. L.; Li, D., Facile electrochemical approach for the production of graphite oxide with tunable chemistry. *Carbon* **2017,** *112*, 185-191.

28. Cao, J.; He, P.; Mohammed, M. A.; Zhao, X.; Young, R. J.; Derby, B.; Kinloch, I. A.; Dryfe, R. A. W., Two-Step Electrochemical Intercalation and Oxidation of Graphite for the Mass Production of Graphene Oxide. *Journal of the American Chemical Society* **2017,** *139* (48), 17446-17456.

29. Bi, H.; Yin, K.; Xie, X.; Ji, J.; Wan, S.; Sun, L.; Terrones, M.; Dresselhaus, M. S., Ultrahigh humidity sensitivity of graphene oxide. *Scientific Reports* **2013,** *3*, 2714.

30. Borini, S.; White, R.; Wei, D.; Astley, M.; Haque, S.; Spigone, E.; Harris, N.; Kivioja, J.; Ryhänen, T., Ultrafast Graphene Oxide Humidity Sensors. *ACS Nano* **2013,** *7* (12), 11166-11173.

31. Talyzin, A. V.; Hausmaninger, T.; You, S.; Szabo, T., The structure of graphene oxide membranes in liquid water, ethanol and water-ethanol mixtures. *Nanoscale* **2014,** *6* (1), 272-281.

32. Ferrari, A. C.; Rodil, S. E.; Robertson, J., Interpretation of infrared and Raman spectra of amorphous carbon nitrides. *Physical Review B* **2003,** *67* (15), 155306.

33. Cançado, L. G.; Jorio, A.; Ferreira, E. H. M.; Stavale, F.; Achete, C. A.; Capaz, R. B.; Moutinho, M. V. O.; Lombardo, A.; Kulmala, T. S.; Ferrari, A. C., Quantifying Defects in Graphene via Raman Spectroscopy at Different Excitation Energies. *Nano Letters* **2011,** *11* (8), 3190-3196.

34. Ferrari, A. C.; Robertson, J., Interpretation of Raman spectra of disordered and amorphous carbon. *Physical Review B* **2000,** *61* (20), 14095-14107.

Chapter 7. Conclusions and future work

7.1 Conclusions

This thesis has focused on the investigation of electrochemically-derived graphene oxide (EGO) with a comprehensive study of its synthesis, characterization and structure/property relationships, and explored possible applications. With the challenges of incomplete oxidation and exfoliation from previous electrochemical oxidation methods, it presents the development of a novel electrochemical oxidation method that differs from conventional methods for continuous oxidation and exfoliation processes. In order to produce EGO with good processability, the influences of electrochemical conditions on the aqueous dispersibility was undertaken, with the aim of developing aqueous dispersible EGO. It also seeks to determine and understand the novel and advantageous properties of EGO, compared with chemically-derived graphene oxide (CGO). The properties of EGO-based multilayer membranes were also studied with regards to their stability in aqueous solution and ionic sieving properties. In terms of producing conductive graphene, the reduction process of GO was also investigated. In particular, the use of microwave reduction of EGO and CGO was studied, in terms of process efficiency and the quality of the output. A summary of the main contributions and findings of this thesis are as follows.

A novel mechanically-assisted electrochemical method has been developed to produce graphene oxide with a continuous oxidation and exfoliation process. The new electrochemical method utilises mechanical stirring to assist with the electrochemical oxidizing process, which allows the direct use of graphite flakes as the graphite source, instead of bulk graphite electrode that shows the problems of premature peeling of graphite pieces. The continuous stirring process provides centrifugal forces that push the graphite flakes towards the working electrode. This enabled repeated physical contact of the graphite flakes and working electrode, which allows the partially exfoliated graphite to take the continual oxidation and exfoliation. In addition, this novel method also shows the advantages of a green process without the use of hazardous chemical oxidants, simple purifications compared to conventional chemical processes, and recyclable electrolytes, all of which are desirable in the industrial production of graphene oxide. The resultant EGO is less oxidised and defective than conventional CGO. An interesting property is long-term stability of EGO in ethanol, which is better than CGO. In addition, EGO also shows facile thermal reduction ability and high conductivity after the

thermal reduction. This work has provided a promising solution for cost-effective and large-scale production of graphene oxide, which shows great potential for application in industries.

With the requirement of producing processable EGO for further assembly in applications, the next part of thesis investigated the influence of electrochemical oxidation processes on the aqueous dispersibility of EGO, which lead to the production of aqueous dispersible EGO with optimized electrochemical conditions. Electrochemical oxidation time, graphite sources and electrolyte concentrations were found to show significant influence on the aqueous dispersibility of resultant EGO. Longer oxidation times were favourable for producing EGO with high aqueous dispersibility. EGO produced from graphite foil shows much higher aqueous dispersibility than that produced from graphite flakes, which may be due to the greater concentration of pores and edge defects in graphite foil encouraging more oxidation processes. In addition, 12 M H_2SO_4 electrolyte were found to be optimum for producing aqueous dispersible EGO because higher concentrations led to inferior oxidation due to limited H_2O, whilst lower concentrations required very long oxidation times due to poor levels of intercalation. The EGO dispersion produced at optimised conditions was also characterised, and showed long-term stability and zeta potential of less than -30 mV. This indicates that there exist sufficient repulsive forces between EGO sheets in the dispersion. In addition, the fabrication of a uniform EGO membrane demonstrated the good processability of the EGO dispersion.

The manipulation of EGO was then focused on another intriguing property of graphene oxide, its ability to be reduced via microwaves. The microwave reduction ability of EGO was investigated and compared with its use on CGO. A significant finding is the rapid microwave reduction of EGO within seconds to produce very high-quality graphene with a large aromatic domain size of 102.8 nm and a high C/O ratio of 33.6. EGO reduced by microwave irradiation also showed high conductivity of about 49140 S/m. Conversely, CGO was not as efficiently reduced by microwave irradiation. A possible mechanism to explain the high reduction efficiency of EGO using microwaves is that large aromatic regions of EGO can more readily absorb the microwaves and dissipate them efficiently as heat.

The properties of EGO multilayer membranes were studied in the final part of the work, with a comparison with CGO membranes. EGO membranes show a high stability in aqueous solution, which is much better than CGO membranes that can easily swell and disintegrate in aqueous solutions. The interlayer distance of EGO membranes in water was found to be very

consistent at 1.18 nm with the formation of stable two water molecule layers between adjacent EGO sheets. The ionic sieving and nanofiltration performances were also characterized, and it was found that EGO shows better rejections to ions and molecules and higher permeance than CGO membranes. In addition, the structures of EGO were characterized to explain the possible mechanisms for the superior stability and ionic or molecular sieving performances of EGO membrane. The results show that EGO contain larger aromatic domain size and lower carboxylic acid groups, which contribute to a more ordered structure, with well-maintained interlayer distance. This study has thus demonstrated a potential application of EGO, where it can be used in nanofiltration applications. It also provides a deeper understanding on the structure of EGO and its membranes.

The findings of the thesis thus contribute the strategies related to synthesis of EGO and an understanding of its structure, chemistry, and properties. It is expected that this work will advance the development of electrochemical oxidation methods to produce graphene oxide in academic research and industry, and more applications of EGO based on such understanding of structures and properties should result.

7.2 Future work

This work has represented an investigation on the synthesis of EGO and studies of its properties, which requires further research. Following areas that are proposed for further investigation are:

1) Current studies on the novel mechanically-assisted electrochemical methods are only based on the small prototype setup, which requires further developments for industrial productions. A larger setup needs to be designed based on this prototype for large-scale production. Problems of lower oxidation and exfoliation may appear with larger setups because larger amounts of graphite flakes may make it harder for each graphite flake to get physical contact with working electrode. The effect of stirring could be reduced in a larger setup. Therefore, it requires further modifications of the setup design or electrochemical processes such as stirring speeds.

2) The second part has studied the influence of electrochemical processes on aqueous dispersibility. However, some proposed mechanisms to explain the influence of the electrochemical conditions still require verifications. For example, electrochemical oxidation process shows different oxidation voltages at various electrolyte concentrations

which may be due to the formation of different oxygen groups. To explain the change of oxygen groups and structures under the various electrochemical conditions, it is still necessary to investigate using characterizations such as X-ray photoelectron spectroscopy, X-ray diffraction, and Raman spectroscopy.

3) An intriguing property found in this study is the efficient reduction of EGO by thermal annealing and microwave irradiation. These properties demonstrate the potential use of EGO as a precursor for conductive graphene. More applications can be explored in future involving reduced EGO such as transparent conductive films, conductive fillers in polymer composites that can be thermally reduced at relatively lower temperatures than CGO, or EGO-inorganic composites that can be reduced by microwave irradiation to achieve high conductivities.

4) With a preliminary study of EGO membrane which shows high stability and superior ionic or molecular sieving performances, the EGO membrane can be further developed for various applications. It can be combined with intercalants to increase the interlayer spacing for precise nanofiltration of larger molecules. The EGO membrane can also be partially reduced to decrease the interlayer spacing to allow for desalinations and separation of smaller ions.